Foundations and Trends® in Systems and Control

Adaptive Internal Models in Neuroscience

Suggested Citation: Mireille Broucke (2021), "Adaptive Internal Models in Neuroscience", Foundations and Trends® in Systems and Control: Vol. xx, No. xx, pp 1–18. DOI: 10.1561/XXXXXXXXX.

Mireille E. Broucke
University of Toronto
broucke@control.utoronto.ca

now
the essence of knowledge
Boston — Delft

Contents

Acknowledgements

I am grateful to my graduate students Erin Battle, Ahmad Abdel Gawad, Mohamed Hafez, and Erick Mejia Uzeda, who have been dedicated and persevering collaborators on this research.

Neuroscience Acronyms

AOS Accessory Optic System

B Brainstem

C Cerebellum

CF Climbing Fiber

FC Floccular Complex

FTN Floccular Target Neurons

GH Gaze Holding

IO Inferior Olive

MF Mossy Fiber

MN Motoneuron

MVN Medial Vestibular Nuclei

NOT Nucleus of the Optic Tract

NPH Nucleus Prepositus Hypoglossi

NU Nodulus-Uvula

OKAN Optokinetic After-Nystagmus

OKN Optokinetic Nystagmus

OKR Optokinetic Reflex

OKS Optokinetic System

PC Purkinje Cell

SCC Semicircular Canals

SP Smooth Pursuit

VAN Vestibular After-Nystagmus

VN Vestibular Nuclei

VOR Vestibulo-Ocular Reflex

VSM Velocity Storage Mechanism

1

Introduction

This monograph makes contributions to the field of *systems neuroscience*. Systems neuroscience aims to understand the brain at a systems or behavioral level, particularly considering the interactions between different brain regions and the rest of the body. By way of contrast, *systems biology* regards the study of biological processes particularly at the cellular level.

When one peruses the literature on systems neuroscience one rather quickly stumbles upon terms such as *motor control*, *adaptation*, *learning*, *perception*, *consolidation*, and *internal models*, among others. All words that pique the curiosity of the control theorist. Questions that arise are: what control architectures does the brain use to solve problems of motor control and adaptation? Are these control architectures the same as the ones already employed in robotics and engineering? Where are these internal models in the brain? How does the brain deal with disturbances? What control problems has the brain already solved through its evolutionary advantage that control theorists with their engineering models and principles have not?

This monograph initiates an investigation into some of these questions.

We were particularly intrigued by the pervasiveness of discourse on internal models in the brain in the neuroscience literature, contrasted with a void regarding internal models of control theory. This dichotomy was highlighted in a session at the 2018 IEEE Conference on Decision and Control (Huang *et al.*, 2018), with the hope that the two research areas could be brought closer together.

Our working hypothesis is that the internal model principle of control theory is operating in one or more areas of the brain. This is not a wild conjecture since neuroscientists have been discussing internal models for at least 40 years. Rather it shifts the focus from the role of internal models to replicate the dynamics of a system to be controlled (Jordan and Rumelhart, 1992; Wolpert and Kawato, 1998) to a role of internal models to replicate exogenous signals (Francis and Wonham, 1975). This shift of interpretation brings into view developments in control theory on the design of internal models, developments which have, up to now, not been regarded as relevant to brain modeling by either research community.

Validating our hypothesis requires working both on the control theory side and on the neuroscience side. The task involves carefully examining the experimental record in neuroscience for any evidence of behavior that reflects the internal model principle. On the other side, we review developments in control theory to determine if available internal model designs are suitable for brain modeling (see Chapter 3). This monograph offers a curated and condensed view of two major thrusts of the last 50 years in control theory: *regulator theory*, discussed in Chapter 2, and *adaptive control*, discussed in Chapter 4. The synthesis of these two areas (a process still ongoing) has resulted in *adaptive internal models*, discussed in Chapter 5.

On the neuroscience side we have particularly focused on experimental results for the *oculomotor system*. Study of the oculomotor system proves to be immensely gratifying because the brain structures and the neural circuits are reasonably well known; the experimental record is thorough and unrelenting; the oculomotor research community has a history of outstanding modelers (Robinson, 1981; Zee, 2018); and fi-

nally, the oculomotor system is widely regarded to provide the blueprint for all other motor systems. Results for the oculomotor system as well as visuomotor adaptation are found in Chapters 6–9. These chapters draw upon our prior work (Battle and Broucke, 2021; Broucke, 2020; Broucke, 2021; Gawad and Broucke, 2020; Hafez *et al.*, 2021).

1.1 Internal Models in Control Theory

Regulator theory and the associated *regulator problem* regard a control specification to make an error signal of a control system tend to zero asymptotically, despite the presence of persistent, exogenous disturbance and reference signals entering the control loop. A key assumption is that the disturbance and reference signals can be modeled by a linear *exosystem*. A controller that satisfies the requirements of the regulator problem is called a *regulator*.

Starting from the 1970's, regulator designs progressed from multi-input multi-output (MIMO) linear time-invariant (LTI) systems with known plant and exosystem parameters, to uncertain nonlinear systems (Byrnes *et al.*, 1997), and finally to regulator designs when neither plant nor exosystem parameters are known. Of particular relevance are regulator designs based on *adaptive internal models*, which appeared in the control theory literature in the mid 1990's to early 2000's (Bodson *et al.*, 1994; Bodson and Douglas, 1997; Nikiforov, 1996; Nikiforov, 1997a; Marino and Tomei, 2000; Marino and Tomei, 2003a; Serrani and Isidori, 2000; Serrani *et al.*, 2001). We present highlights of this progression for linear systems.

Known Plant and Exosystem. When both the plant parameters and exosystem parameters are known, the solution is given in (Davison, 1976; Francis and Wonham, 1976; Francis, 1977), where necessary and sufficient conditions for regulation are provided. The solution relies on the design of an *observer* or a *servocompensator* that asymptotically reconstructs exogenous signals using an internal model. The internal model is not adaptive. These developments are reviewed in our Chapter 2.

Known Plant and Unknown Exosystem. In the case when the plant model is known and only the dimension of the exosystem is known, then the adaptive internal models in (Nikiforov, 1996; Marino and Tomei, 2003b) provide an asymptotic estimate of exogenous signals. If only an upper bound on the dimension of the exosystem is available, but the plant is minimum phase, asymptotically stable, and has known relative degree, then the adaptive internal model in (Marino and Tomei, 2007) asymptotically reconstructs exogenous signals. For this design, persistent excitation guarantees exponential convergence of observer and parameter estimation errors. Linear systems with known parameters but subject to unknown time delays in the control loop were studied in (Gerasimov *et al.*, 2020; Gerasimov *et al.*, 2019a; Gerasimov *et al.*, 2019b; Nikiforov *et al.*, 2020). In the case of discrete-time systems, a design based on averaging theory is developed in (Guo and Bodson, 2009). A different approach for discrete-time systems appears in (Fiorentini *et al.*, 2006) but requires the online solution of a Sylvester equation at each time-step.

Unknown Plant and Known Exosystem. It is possible that uncertainties are limited to the plant, while the exosystem is known perfectly. If the plant is stable, then an adaptive internal model design is given in (Marino and Tomei, 2015). It uses knowledge of the signs of the DC gain and either the real or imaginary part of the frequency response at the frequencies of the exosystem.

Unknown Plant and Unknown Disturbance. The most complex case is when both the plant model and the exosystem are uncertain. There are a number of results for this problem. *Kreisselmeier observers* and *backstepping* are proposed in (Nikiforov, 1997a) to design adaptive internal models to reconstruct exogenous signals assuming the order of the exosystem is known. More generally, novel techniques for designing internal models to reconstruct exogenous signals were presented in (Nikiforov, 2004a; Nikiforov, 2004b). The case of output tracking a measurable reference signal with unknown frequencies by an unknown single-input single-output (SISO) LTI system using output feedback was considered in (Nikiforov, 1997b).

If the plant is minimum phase with known relative degree and bounds on parameter uncertainties (for both the plant and exosystem) are known, then the design in (Marino and Tomei, 2011) may be used. In (Marino and Tomei, 2016), the design of (Marino and Tomei, 2015) was extended by estimating disturbance frequencies online. The design relies on averaging theory, and it is assumed that the plant is stable and the frequency response information previously mentioned is available. A discrete-time solution is given in (Tomei, 2017), also using averaging theory. An alternative design for discrete-time systems appeared in (Hoagg *et al.*, 2008) based on deadbeat control and employing a logarithmic Lyapunov function argument for stability and parameter convergence.

Uncertain plants and exosystems are considered in (Basturk and Krstic, 2012; Basturk and Krstic, 2014) when only state derivative feedback measurements are available to the internal model. Unknown time delays in the input or state are addressed in (Basturk and Krstic, 2015; Basturk, 2017). Finally (Yilmaz and Basturk, 2019) considers unknown minimum-phase LTI systems with known relative degree and system order. Again using Kreisselmeier observers and adaptive backstepping as in (Nikiforov, 1997a), the internal model design in (Yilmaz and Basturk, 2019) rejects unknown sinusoidal exogenous signals while making the system output track a given reference trajectory using only output feedback.

1.2 Internal Models in Neuroscience

Many parts of the brain have been implicated in motor control and motor learning including, but not limited to, the *basal ganglia*, the *motor cortex*, and the *cerebellum*. What is of greatest interest to us is that neuroscientists have posited that the cerebellum, in particular, contains internal models. Here we review relevant theories of cerebellar function. Our review is not complete, but highlights theoretical model development since the 1970's, focusing on those theories that interpret cerebellar function in terms of adaptive control, adaptive filters, and internal models; see (Barlow, 2002) for a detailed discussion and (Mont-

gomery and Bodznick, 2016) for a historical perspective.

In 1967, Eccles, Ito, and Szentagothai published a landmark book on the neuronal structure of the cerebellum (Eccles *et al.*, 1967). Their use of the term "neuronal machine" invited comparison with computer science and control theory. The striking uniformity of the cerebellum (see Section 3.2), despite the fact that it receives inputs from many parts of the cerebral cortex, inspired Marr (Marr, 1969) and Albus (Albus, 1971) to propose computational models of the cerebellar circuit as a spatial pattern classifier. The Marr-Albus theory provided significant detail concerning the neuronal circuitry and the specific wiring of the cerebellum, with a focus on modifiable synapses to account for learning. The Albus theory arguably provided the first neural network model of the cerebellum.

Following this, (Calvert and Meno, 1972) developed a spatio-temporal model of cortical activity and applied it to the cerebellum. They operated under the assumption that while the true input-output relationship is highly nonlinear (exhibiting such phenomena as saturation and refractory periods), the cerebellum may be modeled as a linear system since the ensemble behavior appears linear. To the best of our knowledge, this is the first attempt at using linear models to qualitatively describe cerebellar function and behavior, albeit at a neuronal level rather than at a higher behavioral level.

In (Hassul and Daniels, 1977), the authors observed discrepancies between experimental results and the predictions of (Calvert and Meno, 1972). They opted for a simpler model by treating the cerebellar cortex as a lumped linear system, bypassing the need to model the spatial structure of neuronal circuitry in the cerebellum. Their model predicted that the cerebellum implements a form of lead-lag compensation to maintain loop stability in spite of the substantial delays involved in signal paths to and from the cerebellum.

While the Marr-Albus model has been highly influential both on subsequent theory and experimentation, it did not account for the temporal aspect of adaptation and learning, considering that information in the central nervous system (CNS) is conveyed by continuous time (analog)

signals that are frequency-modulated by nerve impulses. To address this shortcoming, Fujita (Fujita, 1982) proposed an *adaptive filter* model inspired by the least mean square algorithm in adaptive signal processing (Widrow and Stearns, 1985). This model built on the work in (Hassul and Daniels, 1977) to provide a mechanism by which the lead-lag compensator could be made adaptive in order to account for the learning capabilities attributed to the cerebellum. If some performance metric is defined on the output of the cerebellum by way of some reference or target output, then the adaptive filter minimizes the mean square error of this performance metric. Using the adaptive filter model, Fujita was able to successfully simulate the vestibulo-ocular reflex (Fujita, 1982), a critical step in translating neuronal models to tangible motor behavior. A comprehensive review of this work can be found in (Ito, 1984). The adaptive filter model has been further developed by Dean, Porrill, and co-workers to account for experimental discoveries on synaptic plasticity and noise cancellation (Dean *et al.*, 2010); see below.

The idea that the cerebellum contains internal models appears to originate in the work of Ito and Kawato (Ito, 1970; Kawato *et al.*, 1987). Internal models are defined as neural mechanisms that can mimic the input-output characteristics (or their inverses) of the motor apparatus (Kawato, 1999; Miall and Wolpert, 1996; Wolpert *et al.*, 1998). *Forward internal models* predict sensory consequences from *efference copies* of issued motor commands, whereas *inverse internal models* calculate feedforward motor commands from desired reference trajectories.

The inverse model interpretation of the cerebellum was elaborated in (Gomi and Kawato, 1992; Kawato and Gomi, 1992) as *feedback error learning*, related to the *computed-torque method* in robotics (Spong *et al.*, 2005). The cerebellum builds an inverse model of the part of the motor system to be controlled. It takes desired reference trajectories which are assumed to be available as measurements and converts them to feedforward motor commands. The difference between actual motor commands (which include feedback terms) and feedforward motor commands generates a *motor error*, which drives the adaptation process to improve the estimate of the inverse model.

The forward model interpretation of the cerebellum has been elaborated over a series of papers in (Dean *et al.*, 2002; Porrill *et al.*, 2004; Dean and Porrill, 2008; Dean *et al.*, 2010). The forward model transforms motor commands (available as efference copies) to predictions of motor action. These predictions of motor action are compared to the actual system response to generate an output (sensory) error, which, in turn, is used to train the cerebellum to generate improved motor commands. Dean and Porrill further interpret the function of the cerebellum to decorrelate sensory signals from error signals. This interpretation fits well within the mathematical framework of regulator theory in which exogenous (sensory) signals must be removed or "rejected" from errors, if those errors are to be driven to zero.

Several other theories of cerebellar function have been proposed. A Smith predictor model of the cerebellum was suggested in (Miall *et al.*, 1993). A *Smith predictor* is a compensator that counteracts long delays in the feedback path (Smith, 1959). Such a control mechanism would allow to overcome the long transport delays from visual feedback to motor command, for instance. Other theories propose that the cerebellum is a *Kalman filter* (Paulin, 1989), an *optimal controller* (Jordan and Todorov, 2002) or a *Bayesian state estimator* (Paulin, 2005). Despite numerous proposals, there is no consensus, to date, on a computational model of the cerebellum.

This monograph describes a different approach to modeling the cerebellum. We delegate to the cerebellum a primary role of satisfying the internal model principle of control theory (Francis and Wonham, 1976). On this basis, we then apply adaptive internal models from the control literature on regulator theory. Despite a different angle of attack, our approach and resulting models may be regarded as an extension of the class of models that derive from the adaptive filter interpretation of cerebellar function.

1.3 Control Theory and Systems Neuroscience

Control theory has contributed to understanding many biological processes, but the application of control theory in system-level studies of the brain is a relatively new endeavor. One must grapple with what level in the hierarchy of neurological processes to focus for a specific modeling problem (Gernstner and W. Kistler, 2014). Single neurons or small groups of neurons are modeled using the Hodgkin-Huxley model of action potential propagation, or larger groups of neurons comprising neural circuits of modest size may be modeled using population dynamic models such as the Wilson-Cowan model. Next come studies of brain regions such as visual cortex, the hippocampus, the thalamus, which likewise draw upon neural network and population dynamic models. At the highest level is the study of networks of brain regions and their interaction with the body, as in the study of the motor systems, of Parkinson's disease, and so forth. See (Gernstner and W. Kistler, 2014; Dayan and Abbott, 2001) for further discussion on computational methods. The emerging interface between control theory and systems neuroscience is further discussed in (Madhav and Cowan, 2020; Schiff, 2009; Schiff, 2012).

This monograph attends to the highest level of the hierarchy by exploring the functional role of the cerebellum and how it contributes to motor systems in humans. However, a number of other themes are being explored at the interface between systems neuroscience and control theory.

- In addition to the work of David Robinson and others on the oculomotor system (Robinson, 1981), fundamental concepts of *linear system theory* such as feedback and controllability have been applied to clarify and understand the brain at a systems level. For example, (Gu *et al.*, 2015) explores the degree to which the network structure of the brain determines the level of brain activity in connected brain regions. To make precise their idea, the authors utilize a discrete-time linear system whose state vector captures neural activity in distinct brain regions. The controllability

Gramian is used to obtain quantitative predictions on brain activity based on network structure. Khalil and co-workers studied micro-stimulation of the *basal ganglia* and Parkinson's disease by using using ideas from MIMO linear system theory (Liu *et al.*, 2010; Liu *et al.*, 2011).

- *Optimal control theory* has been applied to clarify how the brain manages redundant degrees of freedom of the limbs to achieve repeatable, energy efficient movements (Jordan and Todorov, 2002). The interactions between the motor cortex (M1), basal ganglia, and motor periphery to produce multi-joint movements such as arm reaches have similarly been explored using optimal control theory (Scott, 2004). Optimal control theory was also applied in (Gu *et al.*, 2017) to understand how the brain makes transitions through different brain states - states of neural activity within discrete brain regions.

- *Dynamical system theory* has held a prominent place both in systems neuroscience and systems biology (Iglesias and Ingalls, 2009). For instance, Slotine and co-workers utilized nonlinear contraction analysis to model action selection by the basal ganglia (Girard *et al.*, 2008). Dynamical system theory has been applied to large scale models of the cerebral cortex, for instance, to model epileptic seizures, sleep, and anesthesia (Breakspear, 2017).

- *Network theory* is another key contributor to the study of the brain at a systems level, taking inspiration from the area of network biology (Barabasi and Oltvai, 2004). Hierarchically organized networks of neurons combined with linear threshhold population models were utilized in (Nozari and Cortes, 2021a; Nozari and Cortes, 2021b) to analyze the emergent behavior of selective attention. Many other works treat the brain from a network perspective.

Finally, it is worth mentioning that while this monograph focuses on the application of the internal model principle to understand the cerebellum, the principle has also found application in systems biology. Doyle

and co-workers (Yi *et al.*, 2000) applied the internal model principle to show robustness to disturbances in bacterial chemotaxis. Their analysis specifically regards disturbance rejection of constant exogenous signals using integral feedback.

1.4 Notation

Let $\mathbb{R}$ denote the real numbers, $\mathbb{R}^+$ denotes the non-negative real numbers, and $\mathbb{C}$ denotes the complex numbers. For a matrix $A \in \mathbb{R}^{n\times n}$, $\sigma(A)$ denotes its *spectrum*; the elements of $\sigma(A)$ are the eigenvalues of A. For a symmetric matrix $A \in \mathbb{R}^{n\times n}$, $\lambda_{max}(A)$ denotes the largest real eigenvalue of A. Also for symmetric $A \in \mathbb{R}^{n\times n}$, we write $A > 0$ if A is positive definite.

1.5 Corrections in this Version

This pdf version includes corrections to the published version.

- In Sections 4.2.2 - 4.2.4, and part of Section 4.3, tildes on the parameter vector ψ have been added.
- The formula for $\overline{e}$ in (4.2.10) has been corrected.
- The formula for w_f in Lemma 5.2.5 has been corrected.

2

Regulator Theory

Regulator theory deals with the question of how to regulate to zero an error or output of a control system, despite the presence of exogenous reference and disturbance signals entering the control loop. The *regulator problem* is one of the central problems of control theory dating to the work of James Clerk Maxwell on the regulation of flyball governors (Maxwell, 1868). It is a natural next step in a progression of control specifications of increasing complexity beyond stabilization to include rejection of exogenous signals.

Significant progress was made in the 1970's when the focus was to extend to the multi-input, multi-output (MIMO) setting results for single-input single-output (SISO) control systems (Davison, 1972; Davison, 1975; Davison, 1976; Francis, 1977; Francis and Wonham, 1975; Francis and Wonham, 1976; Johnson, 1971; Smith and Davison, 1972; Wonham and Pearson, 1974). For instance, the ubiquitous notion to place an integrator in the feedforward path of a unity feedback loop in order to achieve step tracking by a SISO open-loop stable plant is fully generalized to MIMO systems and general reference signals. The insights and tools of that period have largely supplanted prior thought on the SISO case due to their depth and clarity, and they form the

cornerstones of what we call *classical regulator theory*. In classical regulator theory both the plant parameters and the frequency content of reference and disturbance signals are assumed to be known.

2.1 Mathematical Background

We highlight several linear algebra results that are important in classical regulator theory.

Lemma 2.1.1. Given a matrix $S \in \mathbb{R}^{q\times q}$, there exist q independent solutions $\Sigma \in \mathbb{R}^{q\times q}$ of the matrix equation

$$\Sigma S = S\Sigma\,.$$

Definition 2.1.2. Given matrices $A \in \mathbb{R}^{n\times n}$, $S \in \mathbb{R}^{q\times q}$, and $X \in \mathbb{R}^{n\times q}$, a *Sylvester equation* in unknown $\Pi \in \mathbb{R}^{n\times q}$ is a matrix equation of the form

$$\Pi S = A\Pi + X\,. \tag{2.1.1}$$

Theorem 2.1.3 (Sylvester (Gantmacher, 1959))**.** The Sylvester equation (2.1.1) has a unique solution Π for any X if and only if $\sigma(A)\cap\sigma(S) = \emptyset$.

2.2 Regulator Problem

We consider a single-input single-output linear time-invariant (LTI) control system

$$\begin{aligned} \dot{x} &= Ax + Bu + Ew && \text{(2.2.1a)}\\ \dot{w} &= Sw && \text{(2.2.1b)}\\ e &= Cx + Dw\,, && \text{(2.2.1c)} \end{aligned}$$

where $x(t) \in \mathbb{R}^n$ is the *state*, $u(t) \in \mathbb{R}$ is the *input*, $e(t) \in \mathbb{R}$ is the *error*, $w(t) \in \mathbb{R}^q$ is the *exosystem state*, and $Dw(t) \in \mathbb{R}$ and $Ew(t) \in \mathbb{R}^n$ consist of *reference* and *disturbance signals*. We are interested to find a feedback controller called a *regulator* to make the error go to zero: $e(t) \longrightarrow 0$. Stabilization of the error encompasses both the *tracking problem*, to make the system output $y = Cx$ asymptotically track a

reference signal $r = -Dw$, and the *disturbance rejection problem*, to asymptotically reject disturbances Ew and Dw. Variants of the problem depend on what measurements and what information about the plant and exosystem are available to the regulator. For example, the simplest case is when all system parameters are known, and both $x(t)$ and $w(t)$ are measurable. Then we look for a *static state feedback*

$$u = Kx + Hw\,. \tag{2.2.2}$$

Ultimately, one would like to solve the problem when the measurement is e (and/or y), and the plant and exosystem parameters are unknown.

Problem 2.2.1 (Regulator Problem). Consider the system (2.2.1). Suppose the system parameters (A, B, C, D, E, S) are unknown. Find an *error feedback regulator*

$$\dot{x}_c = Fx_c + Ge \tag{2.2.3a}$$
$$u = Hx_c + Ke\,, \tag{2.2.3b}$$

with *regulator state* $x_c(t) \in \mathbb{R}^p$, such that the following conditions are met:

(AS) The equilibrium $(0, 0) \in \mathbb{R}^n \times \mathbb{R}^p$ of the *unforced closed-loop system*

$$\dot{x} = (A + BKC)x + BHx_c \tag{2.2.4a}$$
$$\dot{x}_c = Fx_c + GCx \tag{2.2.4b}$$

is asymptotically stable.

(R) The forced closed-loop system satisfies: for all $(x(0), x_c(0), w(0))$, $e(t) \longrightarrow 0$ as $t \longrightarrow \infty$. ◁

Assumption 2.2.1. Consider (2.2.1). We assume the following:

(A1) (A, B) is controllable.

(A2) (C, A) is observable.

(A3) S has simple eigenvalues on the imaginary axis.

The assumptions (A1)-(A2) (or the more relaxed requirements of stabilizable and detectable) are well-known conditions for the existence of matrices F, G, H, and K such that the unforced closed-loop system matrix

$$A_{cl} := \begin{bmatrix} A+BKC & BH \\ GC & F \end{bmatrix} . \tag{2.2.5}$$

is Hurwitz, thereby satisfying (AS) of Problem 2.2.1. Assumption (A3) ensures that the exosystem is capable to model persistent disturbance and reference signals, and it ensures those signals are bounded.

2.3 Regulator Equations

To develop a solution to Problem 2.2.1, we first address the simpler question of state feedback. Suppose $u = Kx + Hw$. The closed-loop system is

$$\dot{x} = (A+BK)x + (BH+E)w \tag{2.3.1a}$$
$$e = Cx + Dw\,. \tag{2.3.1b}$$

The unforced closed-loop system is $\dot{x} = (A+BK)x$, so to meet the requirement (AS), we choose K such that $A+BK$ is Hurwitz. Next, we notice that because of (A3), $\sigma(A+BK) \cap \sigma(S) = \emptyset$. By Theorem 2.1.3, there exists a unique matrix $\Pi \in \mathbb{R}^{n\times q}$ such that

$$\Pi S = (A+BK)\Pi + BH + E = A\Pi + B\Gamma + E\,, \tag{2.3.2}$$

where $\Gamma := H + K\Pi$. The form of (2.3.2) is reminiscent of a coordinate transformation. We define a new state

$$z := x - \Pi w\,.$$

Using (2.3.2), the closed-loop system becomes

$$\dot{z} = (A+BK)z \tag{2.3.3a}$$
$$e = Cz + (C\Pi + D)w\,. \tag{2.3.3b}$$

We see that disturbances have been removed from the first equation, and moreover $z(t) \longrightarrow 0$. Then to achieve $e(t) \longrightarrow 0$ for all initial conditions $w(0)$, we require that $C\Pi + D = 0$. These observations motivate the main result on state feedback.

Theorem 2.3.1. Consider the system (2.2.1) satisfying assumptions (A1) and (A3). Problem 2.2.1 is solvable by a state feedback (2.2.2) if and only if there exist matrices (Π, Γ) with $\Pi \in \mathbb{R}^{n\times q}$ and $\Gamma \in \mathbb{R}^{1\times q}$ such that

$$\Pi S = A\Pi + B\Gamma + E \tag{2.3.4a}$$
$$0 = C\Pi + D\,. \tag{2.3.4b}$$

Moreover, a state feedback solving the problem is

$$u = \Gamma w + K(x - \Pi w)\,, \tag{2.3.5}$$

where $K \in \mathbb{R}^{1\times n}$ is any row vector such that $(A + BK)$ is Hurwitz.

Proof. To prove sufficiency, suppose (A1),(A3), and (2.3.4) hold. By (A1) there exists K such that $A+BK$ is Hurwitz. Consider the feedback (2.3.5). Since the unforced system is $\dot{x} = (A + BK)x$, condition (AS) is satisfied. Next define $z = x - \Pi w$. Then using (2.3.4a) we obtain $\dot{z} = (A + BK)z$, so $z(t) \longrightarrow 0$. Finally, using (2.3.4b) we obtain $e(t) = Cz(t) \longrightarrow 0$, thus satisfying condition (R).

To prove necessity, suppose $u = Kx + Hw$ is a static state feedback solving the problem. The matrix $A+BK$ is Hurwitz according to (AS). Using (A3), we have $\sigma(S)\cap\sigma(A+BK) = \emptyset$, so applying Theorem 2.1.3 there exists a unique $\Pi \in \mathbb{R}^{n\times q}$ satisfying

$$\Pi S = (A + BK)\Pi + BH + E\,.$$

Letting $\Gamma := K\Pi + H$, we obtain (2.3.4a). As shown above, using (2.3.4a), $\dot{z} = (A+BK)z$. Also, $e = Cz+(C\Pi+D)w$. We know $z(t) \longrightarrow 0$, and by condition (R), $e(t) \longrightarrow 0$. Thus, $(C\Pi + D)w(t) \longrightarrow 0$ for all initial conditions $w(0)$. By (A3), we conclude (2.3.4b) holds. □

The equations (2.3.4) are called the *regulator equations* (Francis, 1977). Theorem 2.3.1 not only provides conditions for a solution by state feedback, but it also clarifies when zero steady-state error is achievable. Define $x_{ss}(t) := \Pi w(t)$ and $u_{ss}(t) := \Gamma w(t)$. Using (2.3.4), we find

$$\dot{x}_{ss}(t) = Ax_{ss}(t) + Bu_{ss}(t) + Ew(t) \tag{2.3.6a}$$
$$0 = Cx_{ss}(t) + Dw(t)\,. \tag{2.3.6b}$$

Thus, $x_{ss}(t)$ with input $u_{ss}(t)$ is a solution of (2.2.1a) that renders the error to be exactly zero. The existence of an open-loop control $u_{ss}(t)$ and a corresponding solution $x_{ss}(t)$ that hold the error exactly at zero is clearly a necessary condition to solve the regulator problem using state feedback. The proof of Theorem 2.3.1 shows that when the regulator equations hold and the unforced system is stable, then $x(t) \longrightarrow x_{ss}(t)$ and $u(t) \longrightarrow u_{ss}(t)$ using (2.3.5). Therefore, $x_{ss}(t)$ is the steady state response under the exogenous input $(B\Gamma + E)w(t)$.

The solution of the regulator equations depends on precise knowledge of the plant and exosystem parameters (A, B, C, D, E, S). The regulator problem is said to be *well-posedness* if it is solvable for some nominal plant and exosystem parameter values, and it remains solvable (by a possibly different controller) in a neighborhood of those nominal values. Theorem 2.3.1 suggests that well-posedness of the regulator problem will depend on solvability of the regulator equations for all parameter values close enough to the nominal values. This requirement can be shown to be equivalent to solvability of the regulator equations for nominal values of the plant and exosystem parameters, but arbitrary E and D in (2.3.4) (Saberi *et al.*, 2000); see also Lemma 1.4.2 in (Isidori *et al.*, 2003).

Lemma 2.3.2. Let (A, B, C, S) be fixed matrices. Consider the linear equations

$$\Pi S = A\Pi + B\Gamma + X \tag{2.3.7a}$$

$$0 = C\Pi + Y\,. \tag{2.3.7b}$$

For each (X, Y) there exists a solution (Π, Γ) if and only if

(A4) $\det \begin{bmatrix} A - \lambda I & B \\ C & 0 \end{bmatrix} \neq 0$ for all $\lambda \in \sigma(S)$.

This condition is called a *non-resonance condition* because it says that no eigenvalue of the exosystem is a *zero* of the plant.

2.4 The Internal Model Principle

We turn to the case when e is the only measurement, and we must use an error feedback regulator (2.2.3). Then a deep principle of control theory makes its first appearance: the *internal model principle*.

Theorem 2.4.1. Consider the system (2.2.1) satisfying assumption (A3). Let (2.2.3) be an error feedback regulator such that A_{cl} is Hurwitz. Then (2.2.3) solves Problem 2.2.1 if and only if there exist matrices (Π, Γ, Σ) with $\Pi \in \mathbb{R}^{n\times q}$, $\Gamma \in \mathbb{R}^{1\times q}$, and $\Sigma \in \mathbb{R}^{p\times q}$ such that

$$\begin{aligned} \Pi S &= A\Pi + B\Gamma + E && \text{(2.4.1a)}\\ 0 &= C\Pi + D && \text{(2.4.1b)}\\ \Sigma S &= F\Sigma && \text{(2.4.1c)}\\ \Gamma &= H\Sigma\,. && \text{(2.4.1d)} \end{aligned}$$

Proof. By assumption the regulator satisfies the stability requirement (AS). We will show that (R) is satisfied if and only if there exist (Π, Γ, Σ) satisfying (2.4.1). By (A3), $\sigma(A_{cl}) \cap \sigma(S) = \emptyset$. Then by Theorem 2.1.3 there exists a unique solution (Π, Σ) of the Sylvester equation

$$\begin{bmatrix}\Pi\\ \Sigma\end{bmatrix} S = \begin{bmatrix} A+BKC & BH \\ GC & F\end{bmatrix}\begin{bmatrix}\Pi\\ \Sigma\end{bmatrix} + \begin{bmatrix} E+BKD \\ GD\end{bmatrix}.$$

This equation splits into two equations

$$\begin{aligned} \Pi S &= A\Pi + BH\Sigma + E + BK(C\Pi + D) && \text{(2.4.2a)}\\ \Sigma S &= F\Sigma + G(C\Pi + D)\,. && \text{(2.4.2b)} \end{aligned}$$

Define $z = x - \Pi w$ and $\tilde{x}_c = x_c - \Sigma w$. Using (2.4.2), the closed-loop system is

$$\begin{aligned} \dot{z} &= (A+BKC)z + BH\tilde{x}_c + [A\Pi + BH\Sigma + E + BK(C\Pi + D) - \Pi S]\, w\\ &= (A+BKC)z + BH\tilde{x}_c\\ \dot{\tilde{x}}_c &= F\tilde{x}_c + GCz + [F\Sigma + G(C\Pi + D) - \Sigma S]\, w\\ &= GCz + F\tilde{x}_c\,. \end{aligned}$$

By the assumption on A_{cl}, this closed-loop system is stable, so $z(t) \longrightarrow 0$ and $\tilde{x}_c(t) \longrightarrow 0$. Now we have

$$e = Cx + Dw = Cz + (C\Pi + D)w\,.$$

Then $e(t) \longrightarrow 0$ if and only if $C\Pi + D = 0$. But $C\Pi + D = 0$ and (2.4.2) yield (2.4.1), where we have selected $\Gamma := H\Sigma$. This proves the result. □

Equation (2.4.1c) gives rise to the important *internal model principle* of control theory: any regulator solving Problem 2.2.1 contains an *internal model* of those dynamics of the exosystem that are observable through the error signal e for the composite system

$$\begin{aligned} \dot{x} &= Ax + Ew && \text{(2.4.3a)} \\ \dot{w} &= Sw && \text{(2.4.3b)} \\ e &= Cx + Dw\,. && \text{(2.4.3c)} \end{aligned}$$

Lemma 2.4.2. Consider the system (2.2.1) satisfying assumption (A3). Let (2.2.3) be an error feedback regulator solving Problem 2.2.1. Then every eigenvalue of S that is observable for the system (2.4.3) is an eigenvalue of F.

Proof. Let $v \neq 0$ be an eigenvector of S associated with eigenvalue $\lambda \in \sigma(S)$; i.e. $Sv = \lambda v$. Then from (2.4.1c) we have

$$\Sigma S v = \lambda(\Sigma v) = F(\Sigma v)\,.$$

If $\Sigma v \neq 0$, then Σv is an eigenvector of F and $\lambda \in \sigma(F)$. If $\Sigma v = 0$, then we must show λ is an unobservable eigenvalue of (2.4.3). Consider the vector $\overline{v} := \begin{bmatrix} \Pi v \\ v \end{bmatrix} \neq 0$. Using (2.4.1), we have

$$\begin{bmatrix} (A-\lambda I) & E \\ 0 & S-\lambda I \end{bmatrix} \begin{bmatrix} \Pi v \\ v \end{bmatrix} = \begin{bmatrix} (A-\lambda I)\Pi v + (\Pi S - A\Pi - BH\Sigma)v \\ (S-\lambda I)v \end{bmatrix} = 0$$

$$\begin{bmatrix} C & D \end{bmatrix} \begin{bmatrix} \Pi v \\ v \end{bmatrix} = (C\Pi + D)v = 0\,.$$

Therefore, $\lambda \in \sigma(S)$ is an unobservable eigenvalue of (2.4.3). □

So far we found algebraic conditions (2.3.4) called regulator equations that characterize the existence of a steady-state for the plant such that the error is exactly zero. And we found a necessary condition for any error feedback regulator that it must satisfy the internal model principle. But we have not yet proposed a solution to the regulator problem. Next we consider two classical regulator designs (Davison, 1976; Francis, 1977).

2.5 Regulator Design I

The first regulator design, proposed in (Francis, 1977), is suggested by the idea that only the eigenvalues of S observable through e for the composite system (2.4.3) are relevant. We therefore make an assumption that in addition to (A2), (2.4.3) is observable. We will see below this assumption is no loss of generality.

Assumption 2.5.1. Consider the open-loop system (2.2.1). We assume the following:

(A2′) The pair $\left(\begin{bmatrix} C & D \end{bmatrix}, \begin{bmatrix} A & E \\ 0 & S \end{bmatrix}\right)$ is observable.

With (A2′) we can employ the observer-based design in (Francis, 1977). Consider the observer

$$\dot{\hat{x}} = A\hat{x} + Bu + E\hat{w} + G_1(e - \hat{e}) \tag{2.5.1a}$$
$$\dot{\hat{w}} = S\hat{w} + G_2(e - \hat{e}) \tag{2.5.1b}$$
$$\hat{e} = C\hat{x} + D\hat{w}\,. \tag{2.5.1c}$$

Using (A2′) we can select G_1 and G_2 such that

$$\begin{bmatrix} A & E \\ 0 & S \end{bmatrix} - \begin{bmatrix} G_1 \\ G_2 \end{bmatrix} \begin{bmatrix} C & D \end{bmatrix} \tag{2.5.2}$$

is Hurwitz. Finally we choose the feedback

$$u = \Gamma\hat{w} + K(\hat{x} - \Pi\hat{w})\,, \tag{2.5.3}$$

where (Π, Γ) is the solution of the regulator equations (2.3.4), and K is selected such that $A + BK$ is Hurwitz.

Theorem 2.5.2. Consider the system (2.2.1) satisfying assumptions (A1)-(A4) and (A2′). The regulator (2.5.1)-(2.5.3) solves Problem 2.2.1.

Proof. Define the estimation errors $\widetilde{x} = x - \hat{x}$ and $\widetilde{w} = w - \hat{w}$. The unforced closed-loop system obtained by substituting (2.5.3) into (2.2.1) and setting $w(t) \equiv 0$ is

$$\begin{aligned} \dot{x} &= (A + BK)x - BK\widetilde{x} - B(\Gamma - K\Pi)\widetilde{w} \\ \dot{\widetilde{x}} &= (A - G_1C)\widetilde{x} + (E - G_1D)\widetilde{w} \\ \dot{\widetilde{w}} &= (-G_2C)\widetilde{x} + (S - G_2D)\widetilde{w}\,. \end{aligned}$$

Since $(A + BK)$ and (2.5.2) are Hurwitz, the equilibrium $(x, \widetilde{x}, \widetilde{w}) = (0, 0, 0)$ of the unforced closed-loop system is asymptotically stable. This proves condition (AS) of Problem 2.2.1.

Next define $z = x - \Pi w$. Then we have

$$\begin{aligned} \dot{z} &= (A + BK)z + [A\Pi + B\Gamma + E - \Pi S]w - BK\widetilde{x} + B(\Gamma - K\Pi)\widetilde{w} \\ e &= Cz + (C\Pi + D)w\,. \end{aligned}$$

Using (2.3.4), we obtain $z(t) \longrightarrow 0$ and $e(t) \longrightarrow 0$, which verifies (R) of Problem 2.2.1. □

The previous result was based on an observability assumption (A2′) that permits the use of observers for both x and w. This assumption is restrictive, but it is not a loss of generality. One can always perform a reduction to eliminate the part of the composite system (2.4.3) that is unobservable through e. In light of (A2), the reduced system will retain the full plant model, whereas the part of the exosystem model that is redundant with the plant is trimmed off.

Lemma 2.5.3. Consider the system (2.2.1). Suppose that conditions (A1) and (A2) hold but not (A2′). There exists a coordinate transformation such that in new coordinates the open-loop system is:

$$\dot{x}' = Ax' + Bu + E'w' \tag{2.5.4a}$$

$$\dot{w}' = S'w' \tag{2.5.4b}$$

$$e = Cx' + D'w'\,. \tag{2.5.4c}$$

where S', E', and D' have a partitioned structure

$$S' = \begin{bmatrix} S_1 & 0 \\ S_{21} & S_2 \end{bmatrix}, \qquad E' = \begin{bmatrix} E_1 & 0 \end{bmatrix}, \qquad D' = \begin{bmatrix} D_1 & 0 \end{bmatrix}.$$

Moreover, the pair $\left(\begin{bmatrix} C & D_1 \end{bmatrix}, \begin{bmatrix} A & E_1 \\ 0 & S_1 \end{bmatrix} \right)$ is observable.

Lemma 2.5.3 gives a procedure to resolve the problem of (A2′) failing for the original system. Apply the coordinate transformation suggested in the proof, the reduced system is

$$\begin{aligned} \dot{x}' &= Ax' + Bu + E_1 w_1 \\ \dot{w}_1 &= S_1 w_1 \\ e &= Cx' + D_1 w_1 . \end{aligned}$$

We see that the original plant is retained, but the exosystem has been trimmed. The resulting system satisfies (A2′) so we can apply Theorem 2.5.2 to design a regulator.

2.6 Regulator Design II

A second regulator design was proposed in (Davison, 1976). The theme of this design is to follow the steps one follows for unity feedback loops in the Laplace domain: first place the unstable poles of disturbance and reference signals inside the feedforward path of the control loop. Second, add a compensator to stabilize the augmented closed-loop system. Effectively the regulator design is split into a part to satisfy the internal model principle, called the *internal model*, and a part to stabilize the closed-loop system. Consider the internal model

$$\begin{aligned} \dot{\hat{w}} &= S\hat{w} + G_{im} e && \text{(2.6.1a)} \\ u_{im} &= H_{im}\hat{w} . && \text{(2.6.1b)} \end{aligned}$$

This is not an observer for the exosystem, and $\hat{w}$ is not an estimate of w, but we continue to use the variable $\hat{w}$ for consistency with other

regulator designs. The control input splits into a stabilizing controller u_s and the controller u_{im} to satisfy the internal model principle:

$$u = u_s + u_{im}\,. \tag{2.6.2}$$

When we combine (2.2.1a) with (2.6.1), we have an augmented system

$$\begin{aligned} \dot{x} &= Ax + BH_{im}\hat{w} + Bu_s + Ew && \text{(2.6.3a)}\\ \dot{\hat{w}} &= G_{im}Cx + S\hat{w} + G_{im}Dw && \text{(2.6.3b)}\\ e &= Cx + Dw\,. && \text{(2.6.3c)} \end{aligned}$$

Suppose that the system matrix for the unforced augmented system

$$A_{cl} = \begin{bmatrix} A & BH_{im} \\ G_{im}C & S \end{bmatrix} \tag{2.6.4}$$

is Hurwitz. Then we do not require a stabilizing controller, so let $u_s = 0$.

Theorem 2.6.1. Consider the system (2.2.1) satisfying assumption (A3). Consider the regulator (2.6.1), and suppose A_{cl} in (2.6.4) is Hurwitz. Then (2.6.1) solves Problem 2.2.1.

Proof. By the assumption on A_{cl}, (AS) is satisfied, so we must only verify the regulation requirement (R). By (A3), $\sigma(A_{cl}) \cap \sigma(S) = \emptyset$. Then by Theorem 2.1.3 there exists a unique solution (Π, Σ) of the Sylvester equation

$$\begin{bmatrix} \Pi \\ \Sigma \end{bmatrix} S = \begin{bmatrix} A & BH_{im} \\ G_{im}C & S \end{bmatrix} \begin{bmatrix} \Pi \\ \Sigma \end{bmatrix} + \begin{bmatrix} E \\ G_{im}D \end{bmatrix}.$$

This equation splits into two equations

$$\begin{aligned} \Pi S &= A\Pi + BH_{im}\Sigma + E && \text{(2.6.5a)}\\ \Sigma S &= S\Sigma + G_{im}(C\Pi + D)\,. && \text{(2.6.5b)} \end{aligned}$$

Considering the first equation, if we define $\Gamma := H_{im}\Sigma$, then (2.4.1a) and (2.4.1d) are satisfied. For the second equation, if we can show that (Π, Σ) satisfy $\Sigma S = S\Sigma$ and $C\Pi + D = 0$, then (Π, Σ, Γ) satisfy (2.4.1). Then by Theorem 2.4.1 we can conclude the proposed regulator solves Problem 2.2.1.

Define two linear operators: $\mathcal{L}_1 : \mathbb{R}^{q\times q} \to \mathbb{R}^{q\times q}$ and $\mathcal{L}_2 : \mathbb{R}^{1\times q} \to \mathbb{R}^{q\times q}$ by

$$\mathcal{L}_1(\Sigma) := S\Sigma - \Sigma S \tag{2.6.6}$$
$$\mathcal{L}_2(Z) := G_{im} Z\,. \tag{2.6.7}$$

First, we know $\dim(\text{Im }(\mathcal{L}_2)) \leq q$ since the dimension of the image of a linear map does not exceed the dimension of its domain. Second, by Lemma 2.1.1, the equation $\mathcal{L}_1(\Sigma) = 0$ has at least q independent solutions, so $\dim(\text{Ker}(\mathcal{L}_1)) \geq q$. Thus, $\dim(\text{Im }(\mathcal{L}_1)) \leq q^2 - q$.

Now consider the equations

$$\Pi S = A\Pi + BH_{im}\Sigma + X \tag{2.6.8a}$$
$$\Sigma S = S\Sigma + G_{im}C\Pi + Y\,. \tag{2.6.8b}$$

Since $\sigma(A_{cl}) \cap \sigma(S) = \emptyset$, Theorem 2.1.3 implies (2.6.8) has a solution (Π, Γ) for each (X, Y). The second equation can be written in terms of our two linear operators as:

$$\mathcal{L}_1(\Sigma) + \mathcal{L}_2(C\Pi) = -Y\,.$$

Since $Y \in \mathbb{R}^{q\times q}$ is arbitrary, this equation implies

$$\text{Im }(\mathcal{L}_1) + \text{Im }(\mathcal{L}_2) = \mathbb{R}^{q\times q}\,.$$

Based on the bounds on the dimensions of Im $(\mathcal{L}_1)$ and Im $(\mathcal{L}_2)$ obtained above, it must be that $\dim(\text{Im }(\mathcal{L}_1)) = q^2 - q$, $\dim(\text{Im }(\mathcal{L}_2)) = q$, $\dim(\text{Ker}(\mathcal{L}_2)) = 0$, and Im $(\mathcal{L}_1) \cap$ Im $(\mathcal{L}_2) = \{0\}$.

We return to (2.6.5b), which can be written as

$$\mathcal{L}_1(\Sigma) + \mathcal{L}_2(C\Pi + D) = 0\,.$$

Because Im $(\mathcal{L}_1) \cap$ Im $(\mathcal{L}_2) = \{0\}$, it must be that $\mathcal{L}_1(\Sigma) = 0$ and $\mathcal{L}_2(C\Pi + D) = 0$. The first equation yields (2.4.1c). Since $\dim(\text{Ker}(\mathcal{L}_2)) = 0$, the second equation gives $C\Pi + D = 0$, which is (2.4.1b). We have shown that (Π, Σ, Γ) satisfy (2.4.1), as desired. □

The previous design assumed we could select H_{im} and G_{im} such that A_{cl} is fortuitously Hurwitz. This will not always be possible, and we

may need to employ a dynamic compensator to stabilize the augmented system (2.6.3). We introduce a second part of the regulator, a stabilizing dynamic compensator of the form

$$\dot{x}_s = F_s x_s + G_s e \tag{2.6.9a}$$
$$u_s = H_s x_s \,. \tag{2.6.9b}$$

The augmented system can be stabilized by a dynamic compensator if it is controllable and observable. This can be shown by combining (A1)-(A4) with additional assumptions on G_{im} and H_{im}.

Lemma 2.6.2. Suppose (A1),(A2), and (A4) hold, $\sigma(F_{im}) \subset \sigma(S)$, (F_{im}, G_{im}) is controllable, and (H_{im}, F_{im}) is observable. Then

$$\left(\begin{bmatrix} C & 0 \end{bmatrix}, \begin{bmatrix} A & BH_{im} \\ G_{im}C & F_{im} \end{bmatrix}, \begin{bmatrix} B \\ 0 \end{bmatrix} \right) \tag{2.6.10}$$

is controllable and observable.

Proof. First we show $\left(\begin{bmatrix} A & 0 \\ G_{im}C & F_{im} \end{bmatrix}, \begin{bmatrix} B \\ 0 \end{bmatrix} \right)$ is controllable. Suppose not. By the PBH test, there exist $v_1 \in \mathbb{R}^n$ and $v_2 \in \mathbb{R}^q$ such that

$$v_1^{\mathrm{T}}(A - \lambda I) + v_2^{\mathrm{T}} G_{im} C = 0 \,, \quad v_1^{\mathrm{T}} B = 0 \,, \quad v_2^{\mathrm{T}}(F_{im} - \lambda I) = 0$$

for some $\lambda \in \mathbb{C}$. Notice that $v_2 \neq 0$, otherwise (A, B) is not controllable. Therefore, by the third equation $\lambda \in \sigma(F_{im}) \subset \sigma(S)$. Notice also that $v_2^{\mathrm{T}} G_{im} \neq 0$, otherwise (F_{im}, G_{im}) is not controllable. Then we have

$$\begin{bmatrix} v_1^{\mathrm{T}} & v_2^{\mathrm{T}} G_{im} \end{bmatrix} \begin{bmatrix} A - \lambda I & B \\ C & 0 \end{bmatrix} = 0$$

for some $\lambda \in \sigma(S)$. This contradicts (A4). Controllability of (2.6.10) follows because controllability is unaffected by state feedback.

Next we show $\left(\begin{bmatrix} C & 0 \end{bmatrix}, \begin{bmatrix} A & 0 \\ G_{im}C & F_{im} \end{bmatrix} \right)$ is observable. Suppose not. By the PBH test, there exist $v_1 \in \mathbb{R}^n$ and $v_2 \in \mathbb{R}^q$ such that

$$(A - \lambda I)v_1 + BH_{im}v_2 = 0 \,, \quad Cv_1 = 0 \,, \quad GCv_1 + (F_{im} - \lambda I)v_2 = 0 \,,$$

for some $\lambda \in \mathbb{C}$. Notice that $v_2 \neq 0$, otherwise (C, A) is not observable. Therefore, by the second and third equation $\lambda \in \sigma(F_{im}) \subset \sigma(S)$. Notice also that $H_{im}v_2 \neq 0$, otherwise (H_{im}, F_{im}) is not observable. Then we have

$$\begin{bmatrix} A - \lambda I & B \\ C & 0 \end{bmatrix} \begin{bmatrix} v_1 \\ H_{im}v_2 \end{bmatrix} = 0\,,$$

for some $\lambda \in \sigma(S)$. This contradicts (A4). □

The previous result suggests we should choose F_{im} such that $\sigma(F_{im}) \subset \sigma(S)$; G_{im} such that (F_{im}, G_{im}) is controllable; and H_{im} such that (H_{im}, F_{im}) is observable. One choice (in the SISO case) is $F_{im} = S$ with S in companion form, $G_{im} = \begin{bmatrix} 0 & \cdots & 0 & 1 \end{bmatrix}^{\mathrm{T}}$ and $H_{im} = \begin{bmatrix} 1 & 0 & \cdots & 0 \end{bmatrix}$. Assembling the two parts of the regulator (2.6.1) and (2.6.9) into one, we define:

$$F := \begin{bmatrix} S & 0 \\ 0 & F_s \end{bmatrix}\,, \quad G := \begin{bmatrix} G_{im} \\ G_s \end{bmatrix}\,, \quad H := \begin{bmatrix} H_{im} & H_s \end{bmatrix}\,. \tag{2.6.11}$$

The system matrix of the unforced closed-loop system is

$$A_{cl} = \begin{bmatrix} A & BH \\ GC & F \end{bmatrix}\,. \tag{2.6.12}$$

Theorem 2.6.3. Consider the system (2.2.1) satisfying assumption (A3). Consider a regulator (2.2.3) with F, G, and H as in (2.6.11), and $K = 0$. Suppose (F_s, G_s, H_s) are selected so that A_{cl} in (2.6.12) is Hurwitz. Then (2.2.3) solves Problem 2.2.1.

Proof. By the assumption on A_{cl}, (AS) is satisfied, so we must only verify the regulation requirement (R). The closed-loop system is

$$\begin{bmatrix} \dot{x} \\ \dot{x}_s \\ \dot{\hat{w}} \end{bmatrix} = \begin{bmatrix} A & BH_s & BH_{im} \\ G_sC & F_s & 0 \\ G_{im}C & 0 & S \end{bmatrix} \begin{bmatrix} x \\ x_s \\ \hat{w} \end{bmatrix} + \begin{bmatrix} E \\ G_sD \\ G_{im}D \end{bmatrix} w\,. \tag{2.6.13}$$

Define $\xi = (x, x_s)$ and the submatrices

$$\overline{A} = \begin{bmatrix} A & BH_s \\ G_sC & F_s \end{bmatrix}\,, \quad \overline{B} = \begin{bmatrix} B \\ 0 \end{bmatrix}\,, \quad \overline{C} = \begin{bmatrix} C & 0 \end{bmatrix}\,, \quad \overline{E} = \begin{bmatrix} E \\ G_sD \end{bmatrix}\,.$$

Then we can rewrite the closed-loop system as

$$\begin{bmatrix} \dot{\xi} \\ \dot{\hat{w}} \end{bmatrix} = \begin{bmatrix} \overline{A} & \overline{B}H_{im} \\ G_{im}\overline{C} & S \end{bmatrix} \begin{bmatrix} \xi \\ \hat{w} \end{bmatrix} + \begin{bmatrix} \overline{E} \\ G_{im}D \end{bmatrix} w \,. \tag{2.6.14}$$

By (A3), $\sigma(A_{cl}) \cap \sigma(S) = \emptyset$. Then by Theorem 2.1.3 there exists a unique solution (Π, Σ) of the Sylvester equation

$$\begin{bmatrix} \Pi \\ \Sigma \end{bmatrix} S = \begin{bmatrix} \overline{A} & \overline{B}H_{im} \\ G_{im}\overline{C} & S \end{bmatrix} \begin{bmatrix} \Pi \\ \Sigma \end{bmatrix} + \begin{bmatrix} \overline{E} \\ G_{im}D \end{bmatrix} .$$

The proof now proceeds exactly as in Theorem 2.6.1. We conclude (2.2.3) solves Problem 2.2.1. □

2.7 Final Remarks

This chapter presents an overview of some of the major findings of classical regulator theory: the regulator equations, the internal model principle, and two classical regulator designs. We focused on SISO linear systems, though most of the results are extendable to the multi-input multi-output (MIMO) setting; see (Isidori, 2017; Saberi *et al.*, 2000) for this development. An advanced treatment of regulator theory from a geometric viewpoint is presented in (Wonham, 1985).

With the aim to keep the discussion relatively simple, we did not discuss structurally stable regulators. A *structurally stable regulator* is a regulator that solves the regulator problem, for a fixed exosystem, over a range of plant parameter values near some nominal values, so long as closed-loop stability is preserved. A structurally stable regulator requires a more involved internal model design in the MIMO case which was not presented here; see (Saberi *et al.*, 2000; Isidori *et al.*, 2003; Isidori, 2017) for more discussion. Regulator Design I uses exact information about the plant and exosystem parameters to solve the regulator equations, but nevertheless can be shown to be structurally stable. Regulator Design II can also be shown to be structurally stable. In sum, classical regulator theory addresses uncertainty in the plant parameters, but not the exosystem parameters. Further comments on robustness are provided on Chapter 10.

One quickly discerns that classical regulator theory may not be well suited to model all control processes in neuroscience. The most immediate limitation is the requirement to know the frequency content of disturbance and reference signals. We discuss some limitations of classical regulator theory in the context of neuroscience in the next chapter.

3

Internal Models in Neuroscience

This chapter revisits classical regulator theory, examining how well it serves an endeavor of mathematically characterizing internal models in the brain. Limitations immediately present themselves; however, recent progress in control theory has filled important gaps, and this gives us hope that we are moving toward supplying the required theoretical tools. On the neuroscience side, we look at the architecture of the cerebellum. The pattern of connectivity suggests highly structured mathematical equations, which are given in Section 3.3. We will be looking for this structure in our internal model designs. The structural model does not consider individual neurons or neuron types, but describes their aggregate contribution. How to map the structural systems-level model to the neural microcircuit of the cerebellum is an interesting and important open problem.

3.1 Regulator Problem Revisited

Consider again the classical regulator problem formulated in Chapter 2. We have a single-input single-output LTI control system

$$\begin{aligned} \dot{x} &= Ax + Bu + Ew && \text{(3.1.1a)} \\ \dot{w} &= Sw && \text{(3.1.1b)} \\ e &= Cx + Dw\,, && \text{(3.1.1c)} \end{aligned}$$

with $x(t) \in \mathbb{R}^n$, $u(t) \in \mathbb{R}$, $e(t) \in \mathbb{R}$, $w(t) \in \mathbb{R}^q$, and $Dw(t) \in \mathbb{R}$ and $Ew(t) \in \mathbb{R}^n$ represent reference or disturbance signals.

We assume the plant parameters (A, B, C) are known, and we assume the parameters associated with the exosystem (E, D, S) are also known. We want to design a regulator

$$\begin{aligned} \dot{x}_c &= Fx_c + Ge && \text{(3.1.2a)} \\ u &= Hx_c + Ke\,, && \text{(3.1.2b)} \end{aligned}$$

to make the error e go to zero asymptotically. This is the regulation condition (R) in Problem 2.2.1. The second requirement (AS) is that the equilibrium of the *unforced closed-loop system*

$$\begin{aligned} \dot{x} &= (A + BKC)x + BHx_c && \text{(3.1.3a)} \\ \dot{x}_c &= Fx_c + GCx && \text{(3.1.3b)} \end{aligned}$$

is asymptotically stable.

Aspects of this problem must be revised or relaxed to address modeling of internal models in the brain. It's easy to identify the most immediate restrictions.

- The foremost restriction of classical regulator theory is that the exosystem parameters are assumed to be known. This restriction has been recognized in control theory as being too limiting for at least 25 years, leading to the development of *adaptive internal models*. An overview of this development was presented in Section 1.1, and it will be the focus of our Chapter 5. Adaptive internal models are the main tool we exploit to develop our neuroscience models, and many sophisticated designs are now available.

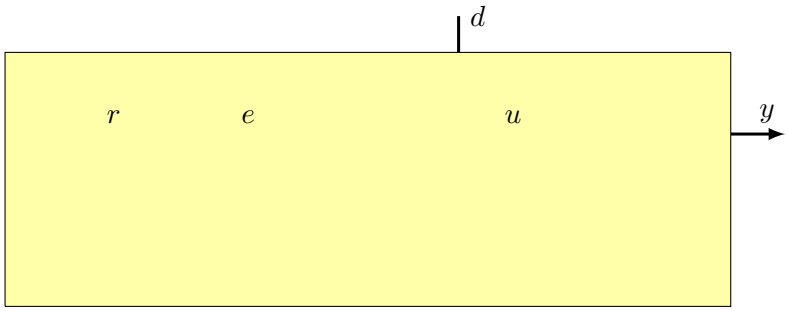

Figure 3.1: A unity feedback loop with a plant P and controller C. A persistent reference signal r is generated by a process R within the control system.

- The second most important restriction of classical regulator theory is the assumption that the plant parameters are known. A number of results in the control literature have addressed this restriction; see Section 1.1. There is one caveat. The brain utilizes a vast separation of time scales for parameter adaptation: some adaptive processes such as smooth pursuit eye movements take place over milliseconds; others such as adaptation to lesions of the eye muscles take place over weeks. Generally, we have found that experimental studies (particularly with the oculomotor system) show that adaptation to exogenous disturbances happens rapidly, while adaptation to model changes is very slow. Current regulator designs that deal with unknown plant and exosystem parameters combine plant and exosystem parameter adaptation as one process. A modular approach may better capture brain processes.

In sum, the main limitation of classical regulator theory is the well-known restriction of a priori knowledge of parameters. Another limitation regards an assumption on signals. Built into the (AS) requirement is an implicit understanding about what constitutes an "unforced system". Signals designated as *exogenous* are those entering the control system from the "outside" or the environment: disturbances and reference signals. The requirement (AS) ensures that if these signals entirely disappear, are dropped as measurements, or are nulled, then the control

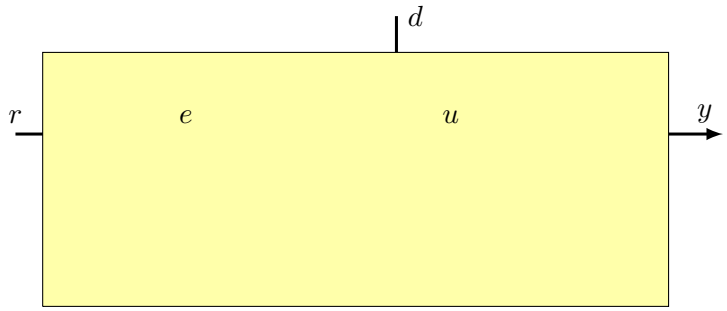

Figure 3.2: A unity feedback control system with exogenous signals r and d. The connection from y to e is persistent.

system gracefully "shuts down" to a stable state. Notably the connection from the plant output y to $e = r - y$ is regarded as immutable.

Consider, in particular, the possible interpretations of a classical unity feedback loop. Firstly, the reference signal r may be regarded as an endogenous signal, part of the system being controlled, and therefore persistent (if we assume no faults), as in Figure 3.1. For example in a temperature control system consisting of a house and a thermostat, the setpoint temperature of the thermostat is endogenous - it may always be assumed to be available, under nominal operation. The same may be said for temperature regulation or blood sugar regulation in the body: without a setpoint for blood sugar, there is no meaningful stability requirement. The measurement $y = Cx$ is also assumed to be endogenous and persistent. The controller utilizes e as its only input, since there is no realistic scenario in which y would be present without r.

A second interpretation, which is the most common in engineering applications, is that both the reference signal r and the disturbance d are exogenous, and therefore may not persist, but the connection from y to e is endogenous and persistent; see Figure 3.2. A paradox of this unity feedback loop is that the controller utilizes e as its only measurement, even though in this case a separate measurement of y may be available. When the reference signal disappears, the controller continues to require $e = -y$ for closed-loop stability, particularly if the open-loop

system has been made unstable by the insertion of an internal model in the feedforward path to satisfy the internal model principle. The regulator has no shut off mechanism since the internal model is built in permanently. Moreover, the classical design philosophy intertwines closed-loop stability with the choice of internal model. Undergraduates are taught to place the unstable poles of the exosystem in the feedforward path; then stabilize the resulting augmented system.

To summarize, if r is exogenous, but y is endogenous and therefore persistent as a measurement, the controller could make use of a pure measurement of y, for instance to achieve closed-loop stability. Yet the classical unity feedback loop does not permit such a measurement structure. The controller continues to be driven by e both for stability and regulation; for instance, as in Regulator Design II.

Regulator theory for MIMO systems has addressed several of the constraints of the classical unity feedback loop by allowing, for example, a separate measurement y for stabilization and e for regulation. Alternatively, a measurement y may be used both for stabilization and regulation, while the signal e is independently defined as the signal to be regulated. An assumption that e is "readable" from y" was introduced in (Francis and Wonham, 1976), such that the measurement e is recoverable from y. The text (Saberi *et al.*, 2000) has as one of its themes to extend classical regulator theory to allow separate measurements and regulated variables. These extensions may be relevant in a biological context, especially if a modular design approach is adopted: extra measurements in y may be dedicated to closed-loop stability, while the measurement of e through y is dedicated to regulation, and so forth. More commonly, regulator designs that allow additional measurements do not insist on such a partition of tasks.

Now consider the situation in Figure 3.3. The environment is outside the feedforward path, and the connection from y to e arises in the environment. The exogenous signals, which must be assumed to be unreliable, are e and d. For example, consider a self-driving car that must follow a lead car at a safe distance. If the lead car changes lanes, suddenly the error measurement is dropped. If the unforced closed-

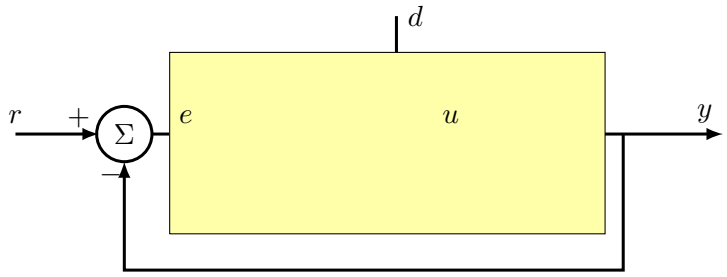

Figure 3.3: A unity feedback control system with exogenous signals e and d. The connection from y to e occurs in the environment.

loop system is taken to be the remaining system after removal of e and d, then the stability requirement (AS) would be in conflict with the regulation requirement (R): the unstable poles of the exosystem inserted in the feedforward path to achieve regulation would cause the closed-loop system to be unstable when e is dropped as a measurement.

Let's see how the two classical regulator designs we presented in Sections 2.5 and 2.6 behave in the new interpretation of unforced closed-loop system. Regulator design I utilized observers for both plant and exosystem:

$$\dot{\hat{x}} = A\hat{x} + Bu + E\hat{w} + G_1(e - \hat{e}) \tag{3.1.4a}$$
$$\dot{\hat{w}} = S\hat{w} + G_2(e - \hat{e}) \tag{3.1.4b}$$
$$\hat{e} = C\hat{x} + D\hat{w}\,. \tag{3.1.4c}$$

Based on an observability assumption, G_1 and G_2 could be selected so that

$$\begin{bmatrix} A - G_1C & E - G_1D \\ -G_2C & S - G_2D \end{bmatrix} \tag{3.1.5}$$

is Hurwitz. The controller is

$$u = \Gamma\hat{w} + K(\hat{x} - \Pi\hat{w})\,, \tag{3.1.6}$$

where (Π, Γ) is the solution of the regulator equations. We ignore for the moment that precise values of (Π, Γ) are not available to the controller and focus instead on what happens when the signals e and d are

dropped. We obtain

$$\begin{aligned} \dot{x} &= Ax + Bu && \text{(3.1.7a)} \\ \dot{\hat{x}} &= (A - G_1C)\hat{x} + (E - G_1D)\hat{w} + Bu && \text{(3.1.7b)} \\ \dot{\hat{w}} &= -G_2C\hat{x} + (S - G_2D)\hat{w}\,. && \text{(3.1.7c)} \end{aligned}$$

Suppose that A is already Hurwitz or it has been stabilized by an independent stability mechanism. Then we can see that a reasonable way to handle the loss of e in the measurement is to remove u from all the equations. The $(\hat{x}, \hat{w})$ dynamics become decoupled from the x dynamics, and by the assumption on (3.1.5), they are exponentially stable. For this scheme to work, the controller would require a technology that detects the loss of measurement e and is capable to instantaneously latch u.

Consider regulator design II, which takes the form:

$$\begin{aligned} \dot{\hat{w}} &= S\hat{w} + G_{im}e && \text{(3.1.8a)} \\ u &= H_{im}\hat{w}\,. && \text{(3.1.8b)} \end{aligned}$$

When the measurement e is dropped, then we have

$$\begin{aligned} \dot{x} &= Ax + Bu + Ew \\ \dot{\hat{w}} &= S\hat{w} \\ u &= H_{im}\hat{w}\,. \end{aligned}$$

Now the system includes the unstable $\hat{w}$ dynamics. In an engineering system, one could devise a latch to disable these unstable dynamics when the error is dropped. However, this would result in undesirable chattering in the input u in case the measurement is intermittent. In a biological system, the internal model with state $\hat{w}$ may not be so easily disabled, since the internal model is physically implemented in a neural circuit. A graceful shut off mechanism is needed. It seems that whatever brain region supplies internal models for motor control, it must be supported by dedicated brain infrastructure for closed-loop stability that functions reasonably with or without incoming sensory error measurements.

Several other issues related to the dichotomy between biological and engineering applications of regulator theory deserve mention.

- All parameters (or constants) are in flux in the brain. How does a regulator self-calibrate to counter its own varying parameters? For example, a common plant parametrization used in adaptive control consists of two stable filters:

$$\begin{aligned}\dot{w}_1 &= Fw_1 + Gy \\ \dot{w}_2 &= Fw_2 + Gu \\ \hat{y} &= \hat{\theta}_1 w_1 + \hat{\theta}_2 w_2 \,,\end{aligned}$$

  where $\hat{y}$ is an estimate of the plant output y, and $(\hat{\theta}_1, \hat{\theta}_2)$ are estimates of plant parameters. For this design to work, the two stable filters must have identical system matrices (F, G). Such a requirement is never achieved in a biological system, unless some further adaptive process is in operation.

  Because control theory primarily focuses on designs that are ultimately implemented on a digital computer or microprocessor, variation of parameters of the regulator itself is not incorporated in the design. Robustness results for such designs likewise do not exist.

- The brain liberally utilizes (noisy) feedfoward signals to assist with disturbance rejection tasks. For example, the brain uses a noisy measurement of head velocity from the ear's semicircular canals to stabilize the gaze while the head is moving. The interaction between noisy feedforward signals and internal models has not been widely studied in regulator theory, to our knowledge. We expect interesting ideas would come forth in this area.

3.2 Cerebellum

The locus of internal models in the brain is believed to be the *cerebellum*. The cerebellum is a major brain region positioned at the back of the head, partly covered by the *cerebral cortex*, and itself covering the *brainstem*. It consists of the *cerebellar cortex*, forming the outer layer, and the *deep cerebellar nuclei*. While the human brain contains roughly

86 billion nerve cells, 69 billion, or 80% of them are in the cerebellum. The cerebellar cortex unfolded is more than 2 meters long in humans.

In 1967 nobel prize winner John Eccles and his co-authors laid out all the neuron types and their interconnections comprising the *microcircuit* of the cerebellum (Eccles *et al.*, 1967). Their work showed that the cerebellum contains relatively few neuron types, that it has a laminated structure with a repeating architectural pattern pervading each layer or zone, unlike any other brain region. We will refer to zones as functional *modules* (not to be confused with cerebellar *lobules*, which may consist of multiple modules) (Apps *et al.*, 2018). Each module has only two input pathways and a single output pathway.

The *cerebellar cortex* is a folded sheet divided into three main layers: from outside to inside, the *molecular layer*, the *Purkinje cell* (PC) layer, and the *granular layer*. These three layers contain the main neuron types of the cerebellum. Each neuron type has a distinctive cell body shape, cellular processes, and input/output connections.

- The first of two input pathways to the cerebellum is via the *mossy fiber* (MF) inputs. The mossy fibers carry an extraordinarily rich flow of information into the cerebellum from many sources, including sensory inputs as well as the output of the cerebellum itself.

- The granular layer is formed by tens of billions of *granule cells*, the most common cell type of the brain. Granule cells receive their input from the mossy fibers, further expanding the richness of information flow through their numbers.

- The axons of the granule cells form the *parallel fibers* (PFs), so-called because they run parallel to each other within the molecular layer.

- The parallel fibers connect with the dendrites of the principal neuron type of the cerebellum, the *Purkinje cells*, which comprise the Purkinje cell layer. Each Purkinje cell receives synaptic connections from as many as 200,000 parallel fibers, themselves

receiving inputs from 4.6 million granule cells, and each parallel fiber synapses with many Purkinje cells as it passes along the molecular layer.

- The second input pathway to the cerebellum is via the *climbing fibers* (CFs), which are the axons of cells from part of the brainstem called the *inferior olive*. Each climbing fiber forms a powerful connection with a single Purkinje cell. This one-to-one relationship between Purkinje cells and their climbing fibers contrasts with the massive convergence of information from the parallel fibers to the Purkinje cells. Climbing fibers are capable to modify the strength of the synapse between parallel fiber inputs onto the Purkinje cells.
- The Purkinje cell axons project to the *deep cerebellar nuclei* and the *vestibular nuclei*, forming the only output pathway from the cerebellum. The deep cerebellar nuclei also receive direct inputs from mossy fibers and climbing fibers.

Several other cell types occur in the cerebellum:

- Within the granular layer are *inhibitory Golgi cells* that receive mossy fiber and parallel fiber input and project to granule cells.
- In some areas of the cerebellum, there are excitatory cells called *unipolar brush cells* that also receive mossy fiber input and project to granule cells. Golgi cells and unipolar brush cells assist to further expand the information arriving in mossy fibers into granule cells.
- The molecular layer includes *stellate cells* that receive input from many parallel fibers, and their axons run across the molecular layer to contact Purkinje cell dendrites.
- The Purkinje cell layer includes *basket cells* that receive Purkinje cell and parallel fiber input and project back to Purkinje cells.

For our present purposes, the notable features of the anatomical structure of the cerebellum are:

- The cerebellum has a purely feedforward structure. Information flows from the mossy fiber inputs to granule cells and then via the parallel fibers to the Purkinje cells. The Purkinje cells send their outputs to the deep cerebellar nuclei and vestibular nuclei.

- There is a massive fanout of information from the mossy fiber inputs to the granule cells and the parallel fibers, followed by a massive fan-in of information from the parallel fibers to the Purkinje cells.

- Each functional module of the cerebellum is identical to the others and performs the same neural computation. The only distinction between modules is in terms of the input and output connections to other regions of the brain.

- Each functional module of the cerebellum processes its own sensory error signal received via the climbing fiber inputs from a circumscribed region of the *inferior olive* (IO). Each module sends its output to a circumscribed region in the cerebellar nuclei.

- The adaptive capability of the cerebellum is provided by the climbing fiber input, which changes the strength of the synapse between the parallel fibers and the Purkinje cells.

- Mossy fibers projecting to a similar region of the cerebellar cortex encode similar information.

- Each of the deep cerebellar nuclei and the vestibular nuclei has a projection to the MF inputs of the cerebellum. This projection is termed the *nucleo-cortical pathway* and is regarded to provide an *efference copy* of the motor command issued by the cerebellum (Ruigrok, 2011; Houck and Person, 2014; Houck and Person, 2015).

3.3 A Structural Model

Informed by the cerebellar architecture, we explore the efficacy of a *structural model*

$$\begin{aligned}
\dot{x} &= Ax + Bu + Ew && \text{(3.3.1a)}\\
e &= Cx + Dw && \text{(3.3.1b)}\\
\dot{w}_0 &= F_0 w_0 + F_0 G_0 e && \text{(3.3.1c)}\\
\dot{w}_1 &= F_1 w_1 + G_1 u_{mf,1} && \text{(3.3.1d)}\\
&\vdots && \text{(3.3.1e)}\\
\dot{w}_k &= F_k w_k + G_k u_{mf,k} && \text{(3.3.1f)}\\
\dot{w}_{k+1} &= F_{k+1} w_{k+1} + G_{k+1} u_{im} && \text{(3.3.1g)}\\
\hat{w} &= (w_0, w_1, \ldots, w_{k+1}) && \text{(3.3.1h)}\\
\dot{\hat{\psi}} &= \gamma e \hat{w}^{\mathrm{T}} && \text{(3.3.1i)}\\
u_{im} &= \hat{\psi}\hat{w} && \text{(3.3.1j)}\\
u &= u_s + u_{im}\,. && \text{(3.3.1k)}
\end{aligned}$$

Equation (3.3.1a) represents the open-loop system. Signal e is the (sensory) error that the cerebellum is tasked with driving to zero. The distinct mossy fiber input signals are $u_{mf,1}, \ldots, u_{mf,k}$. The filters (3.3.1c)-(3.3.1g) may be likened to the lead-lag filters utilized in (Fujita, 1982) to model the mossy fiber-granule cell-Golgi cell network. Here rather than restricting to a lead-lag interpretation, we allow these filters to have a more general form. We assume each filter is stable, i.e. F_i is Hurwitz, so that if a mossy fiber input is dropped or intermittent, the filter remains stable. Also, each pair (F_i, G_i) is controllable. The filter (3.3.1g) models the nucleo-cortical pathway. The equation (3.3.1i) is the standard least-mean-squares (LMS) parameter adaptation law, presumed to model the modifiable synapses between parallel fibers and Purkinje cells. The error signal e in this equation is supplied by the climbing fiber inputs. The output of the cerebellum is u_{im}, and the motor command is u, which includes u_s for closed-loop stability, as needed.

In the chapters that follow we present internal model designs that we deem to be promising to fullful the requirements of internal models in the brain, including the architecture of the cerebellum. The foremost priority is to remove the assumption that the exosystem parameters are known. This involves a review of the relevant results from adaptive control, the subject of the next chapter, on which these adaptive designs are based.

The regulator designs we present are for SISO LTI systems, as these represent the class of open-loop models we have worked with so far (primarily the oculomotor system). How the brain deals with MIMO plants (such as the arm or leg) requires a dedicated study of the brain regions that are involved, especially the interconnections between the motor cortex and the cerebellum. We do not utilize nonlinear regulator theory, despite the proliferation of significant results in this area, again due to our choice of model systems.

The designs we consider generally allow for separate consideration of stabilization and regulation, thereby setting up a structure to handle measurement of exogenous (possibly intermittent) error signals. However, the problem of regulation with intermittent measurements is not addressed in this monograph and will require a separate theoretical development.

This monograph focused on behaviors associated with *short-term adaptation*. Our finding is that short term adaptation may be modeled as a disturbance rejection problem to unknown exogenous reference and disturbance signals. As such, our regulator designs assume that plant parameters are known. Adaptation to changing plant parameters is regarded to be part of *long-term adaptation*, requiring a separate study both in terms of control theory developments and in terms of interpreting experimental results in the neuroscience literature.

4

Adaptive Control

Adaptive control was developed starting in the 1950's and includes a large body of results covering system identification, adaptive observers, adaptive pole placement, and model reference adaptive control, among other subjects. Standard references for the area are (Anderson and al., 1986; Ioannou and Sun, 2012; Narendra and Annaswamy, 1989; Sastry and Bodson, 1989). See also (Slotine and Li, 1991) for the application of adaptive control to robotic manipulators. This chapter reviews techniques from adaptive control that are required to extend the regulator problem to the adaptive case. Model reference adaptive control is not discussed, although it was a main focus of adaptive control researchers in the 1970-80's.

Model reference adaptive control assumes that a desired reference model, typically a stable linear system driven by a known reference input, is given. The control objective is to make the plant output track the output of the reference model. Since we cannot assume a reference model is given or known in the regulator problem, this formulation is not directly useful. However, many tools and techniques of adaptive control are of great interest in extending regulator theory to the fully adaptive setting.

Inspired by the approach in (Narendra and Annaswamy, 1989), this chapter is organized around the notion of *error models*, a conceptually elegant framework for discussing parameter adaptation in terms of driving an error signal to zero. Error models with their associated parameter adaptation laws provide a general design tool which can be applied in a variety of control applications.

4.1 Mathematical Background

Let $x : \mathbb{R}^+ \to \mathbb{R}^n$. The $\mathcal{L}_\infty$ norm is defined as

$$\|x\|_\infty = \sup_{t \geq 0} \|x(t)\| .$$

We say $x \in \mathcal{L}_\infty$ if $\|x\|_\infty$ exists.

Definition 4.1.1. Consider a function $f : \mathbb{R}^+ \to \mathbb{R}$. We say f is *uniformly continuous* if for each $\epsilon > 0$, there exists $\delta > 0$ such that for every $x, y \in \mathbb{R}$, $|x - y| < \delta$ implies $|f(x) - f(y)| < \epsilon$.

An easily checkable sufficient condition for a function to be uniformly continuous is the following.

Lemma 4.1.2. Consider a differentiable function $f : \mathbb{R}^+ \to \mathbb{R}$. If $\dot{f} \in \mathcal{L}_\infty$, then f is *uniformly continuous*.

Lemma 4.1.3 (Barbalat)**.** Consider a differentiable function $f : \mathbb{R}^+ \to \mathbb{R}$, and suppose $\lim_{t\to\infty} f(t)$ exists. If $\dot{f}$ is uniformly continuous, then $\lim_{t\to\infty} \dot{f}(t) = 0$.

When we refer to a transfer function $H(s)$, we mean a proper rational function in the Laplace variable $s = \frac{d}{dt}$. A transfer function is *stable* if all its poles are in the open left-half complex plane. For a strictly proper transfer function $H(s)$, we write $H(s) = C(sI - A)^{-1}B$ to denote that the triple (A, B, C) constitutes a minimal realization of $H(s)$.

Consider a strictly proper transfer function $H(s) = C(sI - A)^{-1}B$, and let $\psi(t) \in \mathbb{R}^{1\times q}$ and $w(t) \in \mathbb{R}^q$ be time-varying signals. Consider a scalar error given by

$$e = H(s)\left[\psi w\right] . \tag{4.1.1}$$

This mixed time and Laplace domain notation is a shorthand for an equivalent state space model of the form

$$\dot{x} = Ax + B(\psi(t)w(t)) \tag{4.1.2a}$$
$$e = Cx\,, \tag{4.1.2b}$$

where the dimension of state $x \in \mathbb{R}^n$ is determined by the order of the denominator polynomial of $H(s)$, and the initial conditions $x(0)$ can take any value in $\mathbb{R}^n$. Typically this mixed notation is used when A is Hurwitz, so the contribution of initial conditions is exponentially vanishing. We also use the notation $H(s)I\,[w]$, where I is the $q \times q$ identity matrix, to denote the component-wise filtering by $H(s)$ of each component of signal $w(t)$. The dimension of I will generally be inferred from the context.

Concepts from network theory regarding dissipative networks play a role in certain stability results in adaptive control; see (Ioannou and Sun, 2012) for more discussion.

Definition 4.1.4. Consider a transfer function $H(s)$. We say $H(s)$ is *strictly positive real* (SPR) if there exists $\epsilon > 0$ such that

$$\Re\,[H(s-\epsilon)] \geq 0$$

for all $s \in \mathbb{C}$ with $\Re(s) \geq 0$. That is, $H(s)$ maps every point in the right half complex plane to the right half complex plane, with margin $\epsilon > 0$.

Theorem 4.1.5. A transfer function $H(s)$ is SPR if and only if $H(s)$ is stable and

$$\Re\,[H(j\omega)] > 0\,, \qquad \forall \omega \geq 0\,. \tag{4.1.3}$$

A famous result regarding SPR transfer functions is the *Kalman-Yakubovich-Popov lemma*.

Lemma 4.1.6 (KYP Lemma)**.** Consider a linear system

$$\dot{x} = Ax + Bu \tag{4.1.4}$$
$$y = Cx\,, \tag{4.1.5}$$

where A is Hurwitz and (A, B) is controllable. The transfer function $H(s) = C(sI - A)^{-1}B$ is SPR if and only if there exist symmetric, positive definite matrices P and Q such that

$$A^{\mathrm{T}}P + PA = -Q\,, \qquad PB = C^{\mathrm{T}}\,. \tag{4.1.6}$$

Finally, we review some results for linear time-varying systems. Consider the linear time-varying system $[C(t), A(t)]$ defined by

$$\dot{x}(t) = A(t)x(t) \tag{4.1.7a}$$

$$y(t) = C(t)x(t)\,, \tag{4.1.7b}$$

where $x(t) \in \mathbb{R}^n$ and $y(t) \in \mathbb{R}^m$. Also $A(t) \in \mathbb{R}^{n\times n}$ and $C(t) \in \mathbb{R}^{m\times n}$ are piecewise continuous functions of time. Let $\Phi(t, t_0) \in \mathbb{R}^{n\times n}$ be the state transition matrix associated with $A(t)$.

Definition 4.1.7. The system $[C(t), A(t)]$ is called *uniformly completely observable (UCO) if there exist constants* $\beta_1, \beta_2, \delta > 0$ *such that for all* $t_0 \geq 0$

$$\beta_1 I \leq W_o(t_0, t_0 + \delta) \leq \beta_2 I\,,$$

where $W_o(t_0, t_0 + \delta) \in \mathbb{R}^{n\times n}$ *is the observability Gramian*

$$W_o(t_0, t_0 + \delta) = \int_{t_0}^{t_0+\delta} \Phi^{\mathrm{T}}(\tau, t_0)C^{\mathrm{T}}(\tau)C(\tau)\Phi(\tau, t_0)d\tau\,.$$

The latter condition may be rewritten as

$$\beta_1\|x(t_0)\|^2 \leq \int_{t_0}^{t_0+\delta} |C(\tau)x(\tau)|^2 d\tau \leq \beta_2\|x(t_0)\|^2\,,$$

for all $x(t_0)$ *and* $t_0 \geq 0$*, where* $x(t)$ *is the solution of* (4.1.7) *starting at* $x(t_0)$*.*

Lemma 4.1.8. Consider a function $L : \mathbb{R}^+ \to \mathbb{R}^{n\times 1}$. Suppose that for all $\delta > 0$, there exists $c_\delta \geq 0$ such that for all $t_0 \geq 0$

$$\int_{t_0}^{t_0+\delta} ||L(\tau)||^2 d\tau \leq c_\delta\,.$$

Then, the system $[C(t), A(t)]$ is UCO if and only if the system $[C(t), A(t)+ L(t)C(t)]$ is UCO. Moreover, if the observability grammian of $[C(t), A(t)]$ satisfies

$$\beta_1 I \leq W_o(t_0, t_0 + \delta) \leq \beta_2 I\,,$$

then the observability grammian of $[C(t), A(t)+L(t)C(t)]$ satisfies these inequalities with the same δ and

$$\beta_1' = \frac{\beta_1}{(1+\sqrt{c_\delta \beta_2})^2}\,, \quad \beta_2' = \beta_2 e^{c_\delta \beta_2}\,.$$

4.2 Error Models

4.2.1 Error Model I

We start with the simplest setting of parameter adaptation. We have a scalar signal

$$y = \psi w$$

that depends linearly on a row vector of constant, unknown *parameters* $\psi \in \mathbb{R}^{1\times q}$. The known vector $w(t) \in \mathbb{R}^q$ is called the *regressor*. Let $\hat{\psi}(t)$ be an estimate of ψ and define the *parameter error* $\widetilde{\psi} := \psi - \hat{\psi}$. Also define the estimate

$$\hat{y} := \hat{\psi} w\,,$$

and the error

$$e := y - \hat{y} = \widetilde{\psi} w\,.$$

We consider a *parameter adaptation law*

$$\dot{\hat{\psi}} = \gamma e w^{\mathrm{T}}\,, \tag{4.2.1}$$

where $\gamma > 0$ is the *adaptation rate*. This adaptation law is called *gradient descent* since it corresponds to the gradient of the squared error; namely,

$$\frac{\partial e^2}{\partial \widetilde{\psi}} = 2e\frac{\partial e}{\partial \widetilde{\psi}} = 2ew^{\mathrm{T}}\,.$$

Theorem 4.2.1. Consider the error $e = \widetilde{\psi} w$ and the parameter adaptation law (4.2.1). Suppose $w, \dot{w} \in \mathcal{L}_\infty$. Then $\widetilde{\psi} \in \mathcal{L}_\infty$, $e(t) \longrightarrow 0$, and $\widetilde{\psi}(t)w(t) \longrightarrow 0$.

Proof. Define the Lyapunov function $V = \widetilde{\psi}\widetilde{\psi}^{\mathrm{T}}$. Noting $\dot{\widetilde{\psi}} = -\dot{\hat{\psi}}$, we have

$$\dot{V} = -2e(\gamma \widetilde{\psi} w) = -2\gamma e^2 \leq 0\,.$$

We conclude $V, \widetilde{\psi} \in \mathcal{L}_\infty$. Since $w \in \mathcal{L}_\infty$, in turn $e, \dot{\widetilde{\psi}} \in \mathcal{L}_\infty$. Now consider

$$\ddot{V} = -4\gamma e \left[\dot{\widetilde{\psi}} w + \widetilde{\psi} \dot{w} \right] .$$

Since all terms on the right are bounded, then $\ddot{V} \in \mathcal{L}_\infty$, and by Lemma 4.1.2, $\dot{V}$ is uniformly continuous. Since V is a decreasing function which is lower bounded, it has a finite limit. Therefore we can apply Lemma 4.1.3 to conclude $\dot{V}(t) \longrightarrow 0$. This implies $e(t) \longrightarrow 0$. Since $e = \widetilde{\psi} w$, we also have $\widetilde{\psi}(t) w(t) \longrightarrow 0$. □

Remark 4.1. We are not in a position to conclude that $\widetilde{\psi}(t) \longrightarrow 0$. This requires an extra condition called *persistency of excitation*, which we consider in Section 4.2.3 for the third error model.

A small but useful extension is to allow for some exponentially stable dynamics to enter into e. Consider the system

$$\begin{aligned} e &= \widetilde{\psi} w + \psi_2 w_2 && \text{(4.2.2a)} \\ \dot{w}_2 &= F_2 w_2 && \text{(4.2.2b)} \\ \dot{\widetilde{\psi}} &= -\gamma e w^{\mathrm{T}} , && \text{(4.2.2c)} \end{aligned}$$

where $w_2 \in \mathbb{R}^r$, $\psi_2 \in \mathbb{R}^{1 \times r}$ is constant, and F_2 is Hurwitz.

Corollary 4.2.2. Consider the system (4.2.2) with $\gamma > 0$ and F_2 Hurwitz. Let $w, \dot{w} \in \mathcal{L}_\infty$. Then $\widetilde{\psi} \in \mathcal{L}_\infty$, $e(t), w_2(t) \longrightarrow 0$, and $\widetilde{\psi}(t) w(t) \longrightarrow 0$.

Proof. It is obvious that $w_2(t) \longrightarrow 0$. Consider the Lyapunov function

$$V = \frac{1}{\gamma} \widetilde{\psi} \widetilde{\psi}^{\mathrm{T}} + c_2 w_2^{\mathrm{T}} P_2 w_2 ,$$

where $c_2 > 0$ is to be determined, and P_2 is the symmetric, positive definite solution of $F_2^{\mathrm{T}} P_2 + P_2 F_2 = -I$. Then we have

$$\dot{V} = -2e(\widetilde{\psi} w) - c_2 w_2^{\mathrm{T}} w_2 = -2e^2 + 2e\psi_2 w_2 - c_2 w_2^{\mathrm{T}} w_2 .$$

Recall *Young's Inequality*: for any $a, b \in \mathbb{R}$ and $\varepsilon > 0$,

$$ab \leq \frac{a^2}{2\varepsilon} + \frac{\varepsilon b^2}{2} . \qquad \text{(4.2.3)}$$

Let $a = e$, $b = \psi_2 w_2$, and $\varepsilon = 2$. Then

$$\dot{V} \leq -\frac{3}{2}e^2 + 2w_2^{\mathrm{T}}\psi_2^{\mathrm{T}}\psi_2 w_2 - c_2 w_2^{\mathrm{T}} w_2 \,.$$

We choose $c_2 = 4\lambda_{max}(\psi_2^{\mathrm{T}}\psi_2) > 0$. Then we obtain

$$\dot{V} \leq -\frac{3}{2}e^2 - \frac{c_2}{2}w_2^{\mathrm{T}} w_2 \leq 0 \,.$$

We conclude $V, \widetilde{\psi} \in \mathcal{L}_\infty$. Since $w, w_2 \in \mathcal{L}_\infty$, in turn $e, \dot{\widetilde{\psi}} \in \mathcal{L}_\infty$. Also, $\dot{e}, \dot{w} \in \mathcal{L}_\infty$. Now consider

$$\ddot{V} = -2\dot{e}(\widetilde{\psi}w) - 2e(\widetilde{\psi}\dot{w}) - 2c_2 w_2^{\mathrm{T}} F_2 w_2 \,.$$

Since all terms on the right are bounded, then $\ddot{V} \in \mathcal{L}_\infty$, and by Lemma 4.1.2, $\dot{V}$ is uniformly continuous. Since V is a decreasing function which is lower bounded, it has a finite limit. Therefore we can apply Lemma 4.1.3 to conclude $\dot{V}(t) \longrightarrow 0$. This implies $e(t) \longrightarrow 0$. Since $e = \widetilde{\psi}w + \psi_2 w_2$, we also have $\widetilde{\psi}(t)w(t) \longrightarrow 0$. □

4.2.2 Error Model II

A second simple scenario for parameter adaptation is one in which a stable linear system is driven by a parameter-dependent signal, and the system states are measurable. Consider the system

$$\dot{x} = Ax + B(\widetilde{\psi}w) \,, \tag{4.2.4}$$

where A is Hurwitz, (A, B) is controllable, and $\psi(t) = \psi - \hat{\psi} \in \mathbb{R}^{1\times q}$ is a row vector of time-varying parameter estimation errors. Suppose the state $x(t)$ and the regressor $w(t)$ are measurable. We propose a parameter adaptation law of the form

$$\dot{\widetilde{\psi}} = -\gamma \left(B^{\mathrm{T}} P x\right) w^{\mathrm{T}} \,, \tag{4.2.5}$$

where $\gamma > 0$ is the adaptation rate, and P is the symmetric, positive definite solution of the Lyapunov equation

$$A^{\mathrm{T}}P + PA = -Q$$

for a given symmetric, positive definite matrix Q.

Theorem 4.2.3. Consider the system (4.2.4) and the parameter adaptation law (4.2.5) with $\gamma > 0$. Suppose A is Hurwitz and $w \in \mathcal{L}_\infty$. Then $x, \widetilde{\psi} \in \mathcal{L}_\infty$, and $x(t) \longrightarrow 0$.

Proof. Consider the Lyapunov function $V = x^{\mathrm{T}}Px + \frac{1}{\gamma}\widetilde{\psi}\widetilde{\psi}^{\mathrm{T}}$. Then we have

$$\begin{aligned} \dot{V} = 2x^{\mathrm{T}}P\dot{x} + \frac{2}{\gamma}\widetilde{\psi}\dot{\widetilde{\psi}}^{\mathrm{T}} &= 2x^{\mathrm{T}}P(Ax + B\widetilde{\psi}w) - 2\widetilde{\psi}wB^{\mathrm{T}}Px \\ &= -x^{\mathrm{T}}Qx \leq 0\,. \end{aligned}$$

It follows that $V, x, \widetilde{\psi} \in \mathcal{L}_\infty$. Since also $w \in \mathcal{L}_\infty$, from (4.2.4), we get $\dot{x} \in \mathcal{L}_\infty$. Therefore, $\ddot{V} = -2x^{\mathrm{T}}Q\dot{x} \in \mathcal{L}_\infty$. This means $\dot{V}$ is uniformly continuous by Lemma 4.1.2. Then by Lemma 4.1.3, we get $\dot{V}(t) \longrightarrow 0$. Therefore, $x(t) \longrightarrow 0$, as desired. □

A small extension, as in Corollary 4.2.2, is to allow some exponentially stable dynamics to be appended. Consider the closed-loop system

$$\dot{x} = Ax + B(\widetilde{\psi}w) + E(\psi_2 w_2) \tag{4.2.6a}$$

$$\dot{w}_2 = F_2 w_2 \tag{4.2.6b}$$

$$\dot{\widetilde{\psi}} = -\gamma\left(B^{\mathrm{T}}Px\right)w^{\mathrm{T}}\,, \tag{4.2.6c}$$

where $x \in \mathbb{R}^n$, $w_2 \in \mathbb{R}^r$, and $\psi_2 \in \mathbb{R}^{1\times r}$ is a constant.

Corollary 4.2.4. Consider the system (4.2.6) with $\gamma > 0$. Suppose A and F_2 are Hurwitz and $w \in \mathcal{L}_\infty$. Then $x, w_2, \widetilde{\psi} \in \mathcal{L}_\infty$, and $x(t), w_2(t) \longrightarrow 0$.

4.2.3 Error Model III

Consider a transfer function $H(s) = C(sI - A)^{-1}B$ with minimal realization (A, B, C), let $\widetilde{\psi} = \psi - \hat{\psi} \in \mathbb{R}^{1\times q}$ be a time-varying parameter estimation error vector, and let $w(t) \in \mathbb{R}^q$ be a known regressor. Consider a scalar error signal given by

$$e = H(s)\left[\widetilde{\psi}w\right]\,. \tag{4.2.7}$$

Recall this error model is equivalent to a state space model

$$\dot{x} = Ax + B(\widetilde{\psi}w) \tag{4.2.8a}$$
$$e = Cx\,. \tag{4.2.8b}$$

Comparing to the second error model, now we assume the state x is not measurable, but the measurement is e. Suppose the parameter vector is updated according to the parameter adaptation law

$$\dot{\widetilde{\psi}} = -\gamma e w^{\mathrm{T}}\,, \tag{4.2.9}$$

where $\gamma > 0$ is the adaptation rate.

Theorem 4.2.5. Consider the error (4.2.7) and the parameter adaptation law (4.2.9). Suppose that $H(s)$ is SPR. Then $x, e, \widetilde{\psi} \in \mathcal{L}_\infty$. Moreover, if $w \in \mathcal{L}_\infty$, then $e(t) \longrightarrow 0$.

Proof. Since $H(s)$ is SPR, by Lemma 4.1.6, given Q symmetric and positive definite, there exists P symmetric and positive definite such that

$$A^{\mathrm{T}}P + PA = -Q\,, \qquad PB = C^{\mathrm{T}}\,.$$

Consider the Lyapunov function $V = x^{\mathrm{T}}Px + \frac{1}{\gamma}\widetilde{\psi}\widetilde{\psi}^{\mathrm{T}}$. We have

$$\begin{aligned}\dot{V} = 2x^{\mathrm{T}}P\dot{x} + \frac{2}{\gamma}\widetilde{\psi}\dot{\widetilde{\psi}}^{\mathrm{T}} &= 2x^{\mathrm{T}}P(Ax + B\widetilde{\psi}w) - 2\widetilde{\psi}we \\ &= -x^{\mathrm{T}}Qx + 2x^{\mathrm{T}}C^{\mathrm{T}}\widetilde{\psi}w - 2e\widetilde{\psi}w \\ &= -x^{\mathrm{T}}Qx \leq 0\,.\end{aligned}$$

Therefore, $V, x, \widetilde{\psi} \in \mathcal{L}_\infty$, and thus $e \in \mathcal{L}_\infty$. Suppose $w \in \mathcal{L}_\infty$. Then from (4.2.8), $\dot{x} \in \mathcal{L}_\infty$. Then we have $\ddot{V} = -2x^{\mathrm{T}}Q\dot{x} \in \mathcal{L}_\infty$, so by Lemma 4.1.2, $\dot{V}$ is uniformly continuous. Then by Lemma 4.1.3, $\dot{V} \longrightarrow 0$. Hence, $x(t) \longrightarrow 0$ and $e(t) \longrightarrow 0$. □

4.2.4 Error Model IV

Suppose we have an error model

$$e = H(s)\left[\widetilde{\psi}w\right]\,,$$

where $\widetilde{\psi} = \psi - \hat{\psi} \in \mathbb{R}^{1\times q}$ is a row vector of time-varying parameter estimation errors, $w(t) \in \mathbb{R}^q$ is a known, bounded regressor, and $H(s) = C(sI - A)^{-1}B$ is a known stable, strictly proper transfer function. If $H(s)$ is not SPR, then we cannot use results for the third error model. Instead, a modification of the error takes us back to the first error model. Consider the *augmented error*

$$\begin{aligned} \overline{e} &:= e + H(s)\left[\hat{\psi}w\right] - \hat{\psi}H(s)I\left[w\right] \\ &= H(s)\left[\widetilde{\psi}w\right] + H(s)\left[\hat{\psi}w\right] - \hat{\psi}H(s)I\left[w\right] \\ &= H(s)\left[\psi w\right] - \hat{\psi}\overline{w} + \epsilon\,, \end{aligned} \tag{4.2.10}$$

where I is the $q \times q$ identity matrix, $\overline{w} := H(s)I\left[w\right] \in \mathbb{R}^q$ is the *filtered regressor*, and ϵ is an exponentially vanishing term. A state space realization of $\overline{w}$ is

$$\begin{aligned} \dot{\eta} &= A\eta + Bw^{\mathrm{T}} \\ \overline{w} &= (C\eta)^{\mathrm{T}}\,, \end{aligned}$$

where $\eta \in \mathbb{R}^{n\times q}$ is the state matrix, $A \in \mathbb{R}^{n\times n}$, $B \in \mathbb{R}^{n\times 1}$, and $C \in \mathbb{R}^{1\times n}$. The initial condition $\eta(0)$ for the state space realization is arbitrary, but its contribution is exponentially vanishing since A is Hurwitz. It is useful to note already that for ψ constant, the following swapping lemma holds.

Lemma 4.2.6. Suppose $\psi \in \mathbb{R}^{1\times q}$ is a constant parameter vector, $w(t) \in \mathbb{R}^q$ is a known regressor, and $H(s) = C(sI - A)^{-1}B$ is a stable transfer function. Then $\left(\psi H(s)I\left[w\right] - H(s)\left[\psi w\right]\right)(t) \longrightarrow 0$ exponentially.

Using the lemma and ignoring exponentially vanishing terms, we see that

$$\overline{e} = \psi H(s)I\left[w\right] - \hat{\psi}\overline{w} = \widetilde{\psi}\overline{w}\,.$$

Consider the parameter adaptation law

$$\dot{\psi} = -\gamma\overline{e}\overline{w}^{\mathrm{T}}\,, \tag{4.2.11}$$

where $\gamma > 0$. The error model (4.2.10) and parameter adaptation law (4.2.11) now correspond to the model in Section 4.2.1.

Lemma 4.2.7. Suppose $H(s) = C(sI - A)^{-1}B$ is a stable transfer function. Consider the augmented error (4.2.10) and the parameter adaptation law (4.2.11). Let $w, \dot{w} \in \mathcal{L}_\infty$. Then $\widetilde{\psi} \in \mathcal{L}_\infty$, $\overline{e}(t) \longrightarrow 0$, and $\widetilde{\psi}(t)\overline{w}(t) \longrightarrow 0$.

Proof. Since by assumption $w, \dot{w} \in \mathcal{L}_\infty$, and $H(s)$ is stable, then $\overline{w}, \dot{\overline{w}} \in \mathcal{L}_\infty$. Now we can apply Theorem 4.2.1 to signals $(\overline{e}, \widetilde{\psi}, \overline{w})$ to conclude $\widetilde{\psi} \in \mathcal{L}_\infty$, and $\overline{e}(t) \longrightarrow 0$. It then follows that $\overline{e}(t) = \widetilde{\psi}(t)\overline{w}(t) \longrightarrow 0$. □

This result does not provide conclusions on the original error signal e. For this we require the so-called *swapping lemma*.

Lemma 4.2.8. Let $\widetilde{\psi}$ and w be signals with $\widetilde{\psi}$ differentiable. Let $H(s) = C(sI - A)^{-1}B$ be a stable transfer function. Then

$$\widetilde{\psi}H(s)I\left[w\right] - H(s)\left[\widetilde{\psi}w\right] = H_c(s)\left[\dot{\widetilde{\psi}}H_b(s)\left[w\right]\right],$$

where $H_b(s) = (sI - A)^{-1}B$ and $H_c(s) = C(sI - A)^{-1}$.

Proof. Consider the state space models

$$\begin{aligned} \dot{\eta}_1 &= A\eta_1 + Bw^{\mathrm{T}}, & y_1 &= C\eta_1\widetilde{\psi}^{\mathrm{T}} \\ \dot{\eta}_2 &= A\eta_2 + B(\widetilde{\psi}w), & y_2 &= C\eta_2, \end{aligned}$$

where $\eta_1 \in \mathbb{R}^{n\times q}$ and $\eta_2 \in \mathbb{R}^n$. Notice that $y_1 = \widetilde{\psi}H(s)I\left[w\right]$ and $y_2 = H(s)\left[\widetilde{\psi}w\right]$. Next we compute

$$\begin{aligned} \frac{d}{dt}\left(\eta_1\widetilde{\psi}^{\mathrm{T}} - \eta_2\right) &= (A\eta_1 + Bw^{\mathrm{T}})\widetilde{\psi}^{\mathrm{T}} + \eta_1\dot{\widetilde{\psi}}^{\mathrm{T}} - A\eta_2 - Bw^{\mathrm{T}}\widetilde{\psi}^{\mathrm{T}} \\ &= A(\eta_1\widetilde{\psi}^{\mathrm{T}} - \eta_2) + \eta_1\dot{\widetilde{\psi}}^{\mathrm{T}}. \end{aligned}$$

Putting it all together,

$$\begin{aligned} y_1 - y_2 = \widetilde{\psi}H(s)I\left[w\right] - H(s)\left[\widetilde{\psi}w\right] &= C(\eta_1\widetilde{\psi}^{\mathrm{T}} - \eta_2) \\ &= H_c\left[\eta_1\dot{\widetilde{\psi}}^{\mathrm{T}}\right] \\ &= H_c\left[H_b[w^{\mathrm{T}}]\dot{\widetilde{\psi}}^{\mathrm{T}}\right]. \end{aligned}$$

□

Theorem 4.2.9. Suppose $H(s) = C(sI - A)^{-1}B$ is a stable transfer function. Consider the augmented error (4.2.10) and the parameter adaptation law (4.2.11). Let $w, \dot{w} \in \mathcal{L}_\infty$. Then $\widetilde{\psi} \in \mathcal{L}_\infty$, $\overline{e}(t) \longrightarrow 0$, $e(t) \longrightarrow 0$, and $\widetilde{\psi}(t)\overline{w}(t) \longrightarrow 0$.

Proof. By Lemma 4.2.7 we know $\widetilde{\psi} \in \mathcal{L}_\infty$, $\overline{e}(t) \longrightarrow 0$, and $\widetilde{\psi}(t)\overline{w}(t) \longrightarrow 0$. Since $\overline{w} \in \mathcal{L}_\infty$, from (4.2.11) we have $\dot{\widetilde{\psi}}(t) \longrightarrow 0$. Since $H(s)$ is stable and applying Lemma 4.2.8, we obtain

$$\left(\widetilde{\psi}H(s)I\left[w\right] - H(s)\left[\widetilde{\psi}w\right]\right)(t) \longrightarrow 0\,.$$

We conclude $e(t) \longrightarrow 0$. □

4.3 Persistency of Excitation

Theorem 4.2.1 says that if $e = \widetilde{\psi}w$ and $\dot{\widetilde{\psi}} = -\gamma e w^{\mathrm{T}}$, then $e(t) \longrightarrow 0$. Still unresolved is the question of whether the parameters converge; that is, $\widetilde{\psi}(t) \longrightarrow 0$. There are generally two avenues to address this question; see (Sastry and Bodson, 1989) for more discussion.

The first avenue investigates the properties of w and $\widetilde{\psi}w$ directly. Suppose $\widetilde{\psi}(t)$ asymptotically approaches a constant row vector. We also know $\widetilde{\psi}(t)w(t) \longrightarrow 0$. If $w(t)$ rotates through all of $\mathbb{R}^q$ during any time interval $[t, t+T]$ for some $T > 0$, then intuitively the only constant vector $\widetilde{\psi}$ for which $\widetilde{\psi}w(t) \longrightarrow 0$ is the zero vector. This intuition applies even when $\widetilde{\psi}$ does not converge by noting that if $w \in \mathcal{L}_\infty$ and $e(t) \longrightarrow 0$, then $\dot{\widetilde{\psi}} = -\gamma e w^{\mathrm{T}} \longrightarrow 0$. This means that progressively in time $\widetilde{\psi}$ varies more slowly. By the vector-valued Mean Value Theorem (Rudin, 1976, p.113):

$$\|\widetilde{\psi}(t_1) - \widetilde{\psi}(t_2)\| \leq \|\dot{\widetilde{\psi}}(t)\||t_1 - t_2|\,,$$

for some $t \in [t_1, t_2]$. The lack of variation of $\widetilde{\psi}$ in a time interval contraposed with the change in $w(t)$ on the same time interval allows one to show that $\widetilde{\psi}(t) \longrightarrow 0$. First, we have to make mathematically precise what it means for a vector to rotate in its space over any time interval.

Definition 4.3.1. We say $w : \mathbb{R}^+ \to \mathbb{R}^q$ is *persistently exciting* (PE) if there exist $\alpha_1, \alpha_2, T > 0$ such that

$$\alpha_1 I \leq \int_t^{t+T} w(\tau) w^{\mathrm{T}}(\tau) d\tau \leq \alpha_2 I \,, \tag{4.3.1}$$

for all $t \geq 0$.

Some useful properties of persistently exciting signals are the following.

Lemma 4.3.2. Let $w, \varepsilon : \mathbb{R}^+ \to \mathbb{R}^q$. If w is PE and ε is an exponentially stable signal, then $w + \varepsilon$ is PE.

Lemma 4.3.3. Let $w : \mathbb{R}^+ \to \mathbb{R}^q$. Suppose w is PE and differentiable, and $w, \dot{w} \in \mathcal{L}_\infty$. Also suppose $H(s)$ is a stable, SPR transfer function. Then $H(s)I\,[w]$ is PE.

We also need a definition.

Definition 4.3.4. A signal $w : \mathbb{R}^+ \to \mathbb{R}^q$ is said to be *stationary* if the following limit exists, uniformly in t_0:

$$R_w(t) := \lim_{T \to \infty} \frac{1}{T} \int_{t_0}^{t_0+T} w(\tau) w^{\mathrm{T}}(t+\tau) d\tau \,.$$

The limit, if it exists, is called the *autocovariance* of w.

The relationship between autocovariance and PE is spelled out in the following.

Lemma 4.3.5. Let w be stationary. Then w is PE if and only if $R_w(0)$ is positive definite.

Now we return to our main problem to prove convergence of the parameter estimates.

Theorem 4.3.6. Consider the error $e = \widetilde{\psi} w$, where $\widetilde{\psi}$ is differentiable, and $w, \widetilde{\psi} \in \mathcal{L}_\infty$. Suppose $\widetilde{\psi}(t) w(t) \longrightarrow 0$ and $\dot{\widetilde{\psi}}(t) \longrightarrow 0$. If w is stationary and PE, then $\widetilde{\psi}(t) \longrightarrow 0$.

Proof. Since w is stationary and PE, it has an autocovariance $R_w(t)$ and by Lemma 4.3.5, $R_w(0)$ is positive definite. We will show

$$\widetilde{\psi}(t)R_w(0)\widetilde{\psi}^{\mathrm{T}}(t) \longrightarrow 0\,,$$

which implies $\widetilde{\psi}(t) \longrightarrow 0$.

Since $\widetilde{\psi}, w \in \mathcal{L}_\infty$, there exists $\kappa > 0$ such that

$$\|\widetilde{\psi}(t)\|\,, \|w\| < \kappa\,, \qquad \forall t \geq 0\,. \tag{4.3.2}$$

Fix $\varepsilon > 0$. We will show there exists $T_1 > 0$ such that for all $t \geq T_1$, $\widetilde{\psi}(t)R_w(0)\widetilde{\psi}^{\mathrm{T}}(t) < \varepsilon$. Since w has an autocovariance, there exists $T > 0$ such that for all $t_0 \geq 0$

$$\left\| R_w(0) - \frac{1}{T}\int_{t_0}^{t_0+T} w(\tau)w^{\mathrm{T}}(\tau)\,d\tau \right\| \leq \frac{\varepsilon}{3\kappa^2}\,. \tag{4.3.3}$$

Then using (4.3.2), we have

$$\left\| \widetilde{\psi}(t)R_w(0)\widetilde{\psi}^{\mathrm{T}}(t) - \widetilde{\psi}(t)\frac{1}{T}\int_{t_0}^{t_0+T} w(\tau)w^{\mathrm{T}}(\tau)\,d\tau\widetilde{\psi}^{\mathrm{T}}(t) \right\| \leq \frac{\varepsilon}{3}\,. \tag{4.3.4}$$

Since $\widetilde{\psi}(t)w(t) \longrightarrow 0$ and $\dot{\widetilde{\psi}}(t) \longrightarrow 0$, there exists $T_1 > 0$ such that for all $t > T_1$

$$\|\widetilde{\psi}(t)w(t)\|^2 \leq \frac{\varepsilon}{3}\,, \tag{4.3.5}$$

and

$$\|\dot{\widetilde{\psi}}(t)\| \leq \frac{\varepsilon}{6\kappa^3 T}\,. \tag{4.3.6}$$

Using (4.3.6) and the vector-valued Mean Value Theorem (stated above), we have

$$\|\widetilde{\psi}(t) - \widetilde{\psi}(\tau)\| \leq \frac{\varepsilon(\tau - t)}{6\kappa^3 T}\,,$$

for all $\tau > t > T_1$. Then, using (4.3.2) we have for all $t > T_1$

$$\begin{aligned}
&\left\| \widetilde{\psi}(t)\frac{1}{T}\int_t^{t+T} w(\tau)w^{\mathrm{T}}(\tau)\,d\tau\widetilde{\psi}^{\mathrm{T}}(t) - \frac{1}{T}\int_t^{t+T} \widetilde{\psi}(\tau)w(\tau)w^{\mathrm{T}}(\tau)\widetilde{\psi}^{\mathrm{T}}(\tau)\,d\tau \right\| \\
&= \left\| \frac{1}{T}\int_t^{t+T} w^{\mathrm{T}}(\tau)(\widetilde{\psi}^{\mathrm{T}}(t) - \widetilde{\psi}^{\mathrm{T}}(\tau))w^{\mathrm{T}}(\tau)(\widetilde{\psi}^{T}(t) + \widetilde{\psi}^{\mathrm{T}}(\tau))\,d\tau \right\| \\
&\leq \frac{\varepsilon}{3}\,.
\end{aligned} \tag{4.3.7}$$

Using (4.3.5), we have for all $t > T_1$

$$\|\frac{1}{T}\int_t^{t+T} \widetilde{\psi}(\tau)w(\tau)w^{\mathrm{T}}(\tau)\widetilde{\psi}^{\mathrm{T}}(\tau)\,d\tau\| \leq \frac{\varepsilon}{3}\,. \tag{4.3.8}$$

Finally, using (4.3.4), (4.3.7), and (4.3.8) we have for all $t > T_1$,

$$\widetilde{\psi}(t)R_w(0)\widetilde{\psi}^{\mathrm{T}}(t) \leq \varepsilon\,.$$

This proves the result. □

The second avenue for proving convergence of the parameter estimates is to study the properties of (4.2.1), which can be equivalently written as the linear time-varying differential equation

$$\dot{\widetilde{\psi}}^{\mathrm{T}} = -\gamma\left(w(t)w^{\mathrm{T}}(t)\right)\widetilde{\psi}^{\mathrm{T}}\,. \tag{4.3.9}$$

The main result is as follows.

Theorem 4.3.7. Suppose w is piecewise continuous and PE. Then the equilibrium of (4.3.9) is globally exponentially stable.

Finally, we consider the error model studied in Section 4.2.3

$$\dot{x} = Ax + B(\widetilde{\psi}w) \tag{4.3.10a}$$

$$e = Cx \tag{4.3.10b}$$

$$\dot{\widetilde{\psi}}^{\mathrm{T}} = -\gamma ew\,, \tag{4.3.10c}$$

where $\gamma > 0$ and (A, B, C) is a minimal realization of $H(s) = C(sI - A)^{-1}B$.

Theorem 4.3.8. Let $H(s)$ be SPR, and suppose w is PE and $w, \dot{w} \in \mathcal{L}_\infty$. Then the equilibrium $(x, \widetilde{\psi}^{\mathrm{T}}) = (0, 0)$ of (4.3.10) is globally exponentially stable.

Proof. Consider the Lyapunov function $V = x^{\mathrm{T}}Px + \frac{1}{\gamma}\widetilde{\psi}\widetilde{\psi}^{\mathrm{T}}$, where P satisfies (4.1.6). From the proof of Theorem 4.2.5, $\dot{V} \leq -x^{\mathrm{T}}Qx$. Therefore,

$$\begin{aligned}\int_{t_0}^{t_0+\delta} \dot{V}d\tau \leq -\int_{t_0}^{t_0+\delta} x(\tau)^{\mathrm{T}}Qx(\tau)d\tau &\leq -\int_{t_0}^{t_0+\delta} \lambda_{min}(Q)\|x(\tau)\|^2 d\tau \\ &\leq -\frac{\lambda_{min}(Q)}{\|C\|^2}\int_{t_0}^{t_0+\delta} e(\tau)^2 d\tau\,.\end{aligned}$$

Based on Theorem 1.5.2 in (Sastry and Bodson, 1989), exponential convergence is guaranteed if for some $k_0 > 0$,

$$\int_{t_0}^{t_0+\delta} e^2(\tau)d\tau \geq k_0 \left(\|x(t_0)\|^2 + \|\widetilde{\psi}(t_0)\|^2 \right), \tag{4.3.11}$$

for all $t_0 \geq 0$, $x(t_0)$, and $\widetilde{\psi}(t_0)$. This condition can be interpreted as a UCO condition on (4.3.10).

To that end, define $L(t) := \begin{bmatrix} 0 \\ \gamma w(t) \end{bmatrix}$. Notice L satisfies the condition of Lemma 4.1.8 because $w \in \mathcal{L}_\infty$. Then we can apply Lemma 4.1.8 to obtain that UCO of (4.3.10) is equivalent to UCO of a simpler system

$$\dot{x} = Ax + B\widetilde{\psi}w \tag{4.3.12a}$$

$$\dot{\widetilde{\psi}}^{\mathrm{T}} = 0 \tag{4.3.12b}$$

$$e = Cx\,. \tag{4.3.12c}$$

To show (4.3.12) is UCO, we must show

$$\begin{aligned} e(t) &= Ce^{A(t-t_0)}x(t_0) + \int_{t_0}^{t} Ce^{A(t-\tau)}Bw(\tau)^{\mathrm{T}}d\tau\widetilde{\psi}(t_0)^{\mathrm{T}} \\ &:= e_1(t) + e_2(t) \end{aligned}$$

satisfies, for some $\beta_1, \beta_2, \delta > 0$, and for all $t_0 \geq 0$, $x(t_0)$, and $\widetilde{\psi}(t_0)$,

$$\beta_1 \left(\|x(t_0)\|^2 + \|\widetilde{\psi}(t_0)\|^2 \right) \leq \int_{t_0}^{t_0+\delta} e^2(\tau)d\tau \leq \beta_2 \left(\|x(t_0)\|^2 + \|\widetilde{\psi}(t_0)\|^2 \right). \tag{4.3.13}$$

By assumption, w is PE, and $w, \dot{w} \in \mathcal{L}_\infty$. By Lemma 4.3.3, we have that for all $t_0 \geq 0$, the signal

$$w_f(t) := \int_{t_0}^{t} Ce^{A(t-\tau)}Bw(\tau)d\tau$$

is PE. This means that, for some $\alpha_1, \alpha_2, T_0 > 0$

$$\alpha_1 \|\widetilde{\psi}(t_0)\|^2 \leq \int_{t}^{t+T_0} |e_2(\tau)|^2 d\tau \leq \alpha_2 \|\widetilde{\psi}(t_0)\|^2, \tag{4.3.14}$$

for all $t \geq 0$ and $\widetilde{\psi}(t_0)$.

Next, since A is Hurwitz there exist $k_1, \gamma_1 > 0$ such that

$$\int_{t_0+n_0T_0}^{\infty} e_1^2(\tau)d\tau \leq k_1\|x(t_0)\|^2 e^{-\gamma_1 n_0 T_0}\,, \tag{4.3.15}$$

for all $t_0 \geq 0$, $x(t_0)$, and an integer $n_0 > 0$. Since $[C, A]$ is observable, there exists $k_2(n_0T_0) > 0$ with $k_2(n_0T_0)$ increasing with n_0T_0 such that

$$\int_{t_0}^{t_0+n_0T_0} e_1^2(\tau)d\tau \geq k_2(n_0T_0)\|x(t_0)\|^2\,,$$

for all $t_0 \geq 0$, $x(t_0)$, and $n_0 > 0$. Let $n_1 > 0$ be another integer and let $\delta = (n_0 + n_1)T_0$. Using the fact that for $a, b \in \mathbb{R}$, $(a+b)^2 \geq \frac{1}{2}a^2 - b^2$ and $(a+b)^2 \geq \frac{1}{2}b^2 - a^2$, we have

$$\begin{aligned}
\int_{t_0}^{t_0+\delta} e^2(\tau)d\tau &= \int_{t_0}^{t_0+\delta} (e_1(\tau) + e_2(\tau))^2 d\tau \\
&\geq \frac{1}{2}\int_{t_0}^{t_0+n_0T_0} e_1(\tau)^2 d\tau - \int_{t_0}^{t_0+n_0T_0} e_2(\tau)^2 d\tau \\
&\quad + \frac{1}{2}\int_{t_0+n_0T_0}^{t_0+\delta} e_2(\tau)^2 d\tau - \int_{t_0+n_0T_0}^{t_0+\delta} e_1(\tau)^2 d\tau \\
&\geq \frac{1}{2}k_2(n_0T_0)\|x(t_0)\|^2 - n_0\alpha_2\|\widetilde{\psi}(t_0)\|^2 \\
&\quad + \frac{1}{2}n_1\alpha_1\|\widetilde{\psi}(t_0)\|^2 - k_1 e^{-\gamma_1 n_0 T_0}\|x(t_0)\|^2\,.
\end{aligned} \tag{4.3.16}$$

Let n_0 be sufficiently large to satisfy

$$\frac{1}{2}k_2(n_0T_0) - k_1 e^{-\gamma_1 n_0 T_0} \geq \frac{1}{4}k_2(n_0T_0)\,,$$

and n_1 sufficiently large to obtain $\frac{1}{2}n_1\alpha_1 - n_0\alpha_2 \geq \alpha_1$. By (4.3.16), the lower inequality of (4.3.13) is achieved by defining

$$\beta_1 = \min\left\{\alpha_1, \frac{1}{4}k_2(n_0T_0)\right\}\,.$$

Using inequalities (4.3.14) and (4.3.15), it can be seen that the upper inequality of (4.3.13) is satisfied by defining

$$\beta_2 = \max\{k_1, (n_0+n_1)\alpha_2\}\,.$$

Therefore, (4.3.13) is satisfied, showing that system (4.3.12) is UCO. □

4.4 Final Remarks

This chapter presented an overview of some of the major concepts and findings of adaptive control. These include error models, gradient-based parameter adaptation laws, strictly positive real transfer functions, augmented errors, and persistently exciting signals. The benefit of error models in adaptive control is that they provide an organized treatment of available stability results, and they promote a modular design in which different parameter adaptation laws may be utilized. Here we focused on the popular gradient adaptation law, but other choices include least squares, gradient with projection, least squares with projection, and integral cost adaptation, among others; see (Ioannou and Sun, 2012) for an overview.

An important subject in adaptive control is that of robustness. Its relevance was exposed through a number of examples of the failure of standard algorithms in the presence of unmodeled plant dynamics and bounded exogenous disturbances (Rohrs *et al.*, 1985). It is known that the main source of non-robustness is the parameter adaptation law, which introduces nonlinear time-varying dynamics. A number of modifications have been proposed, including adding a dead zone, the use of projection operators to keep parameters in a bounded set, the so-called σ-modification, and the e_1-modification scheme. A comprehensive treatment of these modified adaptation laws is found in (Ioannou and Sun, 2012). See also (Anderson and al., 1986) for a thorough analysis of stability and robustness, (Ortega and Tang, 1989) for a survey on robustness, and (Ortega *et al.*, 2020) for recent results.

Finally, persistency of excitation plays a role in robustness. Theorem 4.3.8 gives a global exponential stability result for a nominal system under persistency of excitation of the regressor w. If unmodeled plant dynamics and/or exogeneous signals result in bounded disturbances, the perturbed system will have bounded states based on a linear system theory argument, so long as the disturbances do not destroy the PE property of the regressor. In other words, for the states to remain bounded, the level of persistent excitation must be high enough relative to bounded disturbances so that the PE property is not destroyed. See (Narendra

and Annaswamy, 1989) for further discussion on the relationship between robustness and persistency of excitation.

5

Adaptive Internal Models

This chapter studies the regulator problem in the case when the plant parameters are known but the exosystem parameters are unknown. Each of the presented designs highlights some feature regarding availability of feedforward signals or of state measurements. Regulator design III considers a disturbance rejection problem in which the disturbance enters only at the plant input and the state vector is measurable. Regulator design IV considers a tracking problem in which the reference signal is measurable but the state is not measurable. Regulator design V combines the previous two designs. These designs are somewhat more general than required for the applications presented in this monograph, but they are of independent interest and can provide a framework to investigate other motor systems.

5.1 Plant Representation

We saw in Chapter 2 that the regulator equations (2.3.4) provide an algebraic characterization of an error-zeroing steady state (x_{ss}, u_{ss}) for the open-loop system (2.2.1). Utilizing (2.3.4), we performed a coordinate transformation $z = x - \Pi w$ in order to express *error dynamics*

relative to this error-zeroing steady state. These have the form

$$\dot{z} = Az + Bu - B\Gamma w \tag{5.1.1a}$$
$$e = Cz\,. \tag{5.1.1b}$$

As we have discussed, the transformed system makes it transparent that the regulator problem is equivalently a problem of stabilization of $z(t)$. Generally, z is not measurable as a state vector. However, the idea of stabilizing z provides a path to achieve stabilization for the original system. Let us split the controller as we did before in (2.6.2):

$$u = u_s + u_{im}\,. \tag{5.1.2}$$

Under assumption 2.2.1(A1)-(A2), we can define an observer

$$\dot{\hat{z}} = A\hat{z} + Bu_s + L_s(e - \hat{e}) \tag{5.1.3a}$$
$$\hat{e} = C\hat{z}\,, \tag{5.1.3b}$$

where L_s is selected so that $(A - L_sC)$ is Hurwitz. Define the estimation error $\tilde{z} = z - \hat{z}$. Using (5.1.1a) and (5.1.3), we obtain

$$\dot{\tilde{z}} = (A - L_sC)\tilde{z} + B(u_{im} - \Gamma w)\,.$$

So long as u_{im} is designed to achieve $u_{im}(t) - \Gamma w(t) \longrightarrow 0$, then we achieve $\tilde{z}(t) \longrightarrow 0$. Then we select $u_s = K\hat{z}$ such that $(A + BK)$ is Hurwitz in order to stabilize the z dynamics. No information about the exosystem or the solution of the regulator equations (Π, Γ) is needed to achieve stabilization, in contrast with a classical design philosophy where one first inserts the internal model in the feedforward path, then stabilizes the augmented system.

5.2 Exosystem Representation

In this chapter we contend with the fact that the parameters associated with the exosystem, namely (S, E, D) in (2.2.1) are unknown. In fact, there is redundancy in these parameters, and in analogy with the controllable canonical form and observable canonical form, which provide parsimonious representations of the plant in terms of a fewest number

of parameters, it is likewise desirable to find a representation of the exosystem that reduces the burden of identifying its unknown parameters. Several techniques for eliminating redundancy in the unknown parameters of the exosystem were introduced in (Nikiforov, 1996); see also (Nikiforov, 2004a; Nikiforov, 2004b).

Lemma 5.2.1. Let $F \in \mathbb{R}^{q\times q}$, $G \in \mathbb{R}^{q}$, and $L \in \mathbb{R}^{1\times q}$ be such that (F, G) is a controllable pair, (L, S) is an observable pair, and $\sigma(F) \cap \sigma(S) = \emptyset$. Then there exists a nonsingular matrix $M \in \mathbb{R}^{q\times q}$ such that

$$MS = (F + G\psi)M\,, \qquad \psi = LM^{-1}\,.$$

Proof. Since $\sigma(F)\cap\sigma(S) = \emptyset$, by Theorem 2.1.3, the Sylvester equation

$$MS = FM + GL \tag{5.2.1}$$

has a unique solution $M \in \mathbb{R}^{q\times q}$. We prove M is nonsingular. Suppose by way of contradiction that $\mathrm{Ker}(M) \neq \mathbf{0}$. Let $\{v_1, \ldots, v_k\}$ be a basis for $\mathrm{Ker}(M)$. Utilizing (5.2.1), we have

$$MSv_j = GLv_j\,, \qquad j = 1, \ldots, k\,. \tag{5.2.2}$$

Since M is square, there exist row vectors $\{w_1, \ldots, w_k\}$ such that $w_iM = 0$, $i = 1, \ldots, k$. Then

$$w_iGLv_j = 0\,, \qquad i, j = 1, \ldots, k\,. \tag{5.2.3}$$

Suppose $Lv_j = 0$ for all j. Then (5.2.2) gives $MSv_j = 0$, $j = 1, \ldots, k$. This implies $Sv_j \in \mathrm{Ker}(M)$, $j = 1, \ldots, k$, so $\mathrm{Ker}(M)$ is S-invariant and contained in $\mathrm{Ker}(L)$. This contradicts that (L, S) is observable. Suppose instead $Lv_j \neq 0$ for some j. From (5.2.3) (note $w_iG \in \mathbb{R}$), we get $w_iG = 0$, for all $i = 1, \ldots, k$. Using a dual argument, we obtain a contradiction with controllability of (F, G). We conclude M is nonsingular. Finally, by setting $\psi := LM^{-1}$, the result is obtained. □

Remark 5.1. We note that ψ is the unique row vector that assigns to $F + G\psi$ a set of eigenvalues that coincide with the eigenvalues of S. ◁

The previous lemma immediately leads to the following result.

Lemma 5.2.2. Consider a linear exosystem $\dot{\zeta} = S\zeta$ generating a signal $d = L\zeta$, and suppose that (L, S) is an observable pair. Let (F, G) be a controllable pair such that $\sigma(F) \cap \sigma(S) = \emptyset$. Then there exists a coordinate transformation $w = M\zeta$ such that in new coordinates, the exosystem is

$$\dot{w} = Fw + Gd \tag{5.2.4a}$$
$$d = \psi w\,, \tag{5.2.4b}$$

where $\psi = LM^{-1}$.

Lemma 5.2.3. Consider a signal d generated by the exosystem (5.2.4). Let $N(s)$ be a polynomial in $s = \frac{d}{dt}$ and define the signal $d' = N(s)\,[d]$. Then d' can be represented as

$$\dot{w} = (F + G\psi)w \tag{5.2.5a}$$
$$d' = \psi' w\,, \tag{5.2.5b}$$

where $w \in \mathbb{R}^q$ is the state of (5.2.4), and $\psi' = N(F + G\psi) \in \mathbb{R}^{1\times q}$.

Proof. We observe that for any integer $k \geq 0$,

$$\frac{d^k}{dt^k}\,(\psi w) = \psi(F + G\psi)^k w\,.$$

The result follows immediately. □

Lemma 5.2.4. Consider a signal d generated by the exosystem (5.2.4). Define the *filtered signal* $d_f := H(s)\,[d]$, where $H(s) = C(sI - A)^{-1}B$ is a stable transfer function. Then d_f can be represented as

$$\dot{w}_f = Fw_f + Gd_f \tag{5.2.6a}$$
$$d_f = \psi w_f + \varepsilon\,, \tag{5.2.6b}$$

where $w_f \in \mathbb{R}^q$ and $\varepsilon(t) \longrightarrow 0$ exponentially.

Proof. Let $H_\psi(s) = \psi(sI - F)^{-1}G$. Then $d = H_\psi(s)[d]$. Since stable scalar transfer functions commute, modulo an exponentially stable

term, we have

$$\begin{aligned} d_f &= H(s)[H_\psi(s)[d]] \\ &= H_\psi(s)[H(s)[d]] + \varepsilon \\ &= H_\psi(s)[d_f] + \varepsilon\,. \end{aligned}$$

A realization of $H_\psi(s)[d_f]$ proves the result. □

Remark 5.2. Consider again the situation of Lemma 5.2.4. Let $H(s)$ be a stable transfer function, and w, w_f, d, d_f as given above. Let $H(s)I\,[w]$ denote the component-wise application of the filter $H(s)$ to w. Analogous to the proof of Lemma 5.2.4, we can derive

$$\begin{aligned} H(s)I\,[w] &= H(s)I\left[(sI-F)^{-1}G\,[d]\right] \\ &= (sI-F)^{-1}G\,[H(s)\,[d]] + \varepsilon \\ &= (sI-F)^{-1}G\,[d_f] + \varepsilon \\ &= w_f + \varepsilon\,. \end{aligned}$$

Based on this calculation, we call $w_f := H(s)I\,[w]$ the *filtered regressor*. ◁

Lemma 5.2.5. Consider a signal d generated by the exosystem (5.2.4). Let $H(s)$ be a stable transfer function. Consider the filtered signal $d_f := H(s)\,[d]$ and the filtered regressor w_f. Suppose that no zero of $H(s)$ is an eigenvalue of $S = F + G\psi$. Then there exists a nonsingular matrix T such that

$$w_f = Tw + \varepsilon\,.$$

Moreover,

$$d = \psi_f w_f + \varepsilon\,,$$

where $\psi_f := \psi T^{-1}$.

Proof. Let $H(s) = \frac{N(s)}{D(s)}$ with $N(s)$ and $D(s)$ coprime. By Remark 5.2, $w_f = H(s)I\,[w] + \varepsilon$. That is,

$$D(s)I\,[w_f] = N(s)I\,[w] + \varepsilon\,.$$

We know from (5.2.4) that $\dot{w} = (F+G\psi)w$ and from Lemma 5.2.4 that also $\dot{w}_f = (F+G\psi)w_f + \varepsilon$. It follows

$$D(S)w_f = N(S)w + \varepsilon\,.$$

We claim that $N(S)$ is invertible. For suppose not; that is, $0 \in \sigma(N(S))$. By the Spectral Mapping Theorem, $\sigma(N(S)) = N(\sigma(S))$. This implies there exists $\lambda \in \sigma(S)$ such that $N(\lambda) = 0$, a contradiction to the assumption on the zeros of $H(s)$. Similarly, $D(S)$ is invertible because $D(s)$ is a Hurwitz polynomial and S has eigenvalues on the imaginary axis. Define $T := D(S)^{-1}N(S)$ and $\psi_f := \psi T^{-1}$. Then we have

$$w_f = Tw + \varepsilon\,.$$

Moreover, $d = \psi w = \psi(T^{-1}w_f + \varepsilon) = \psi_f w_f + \varepsilon$. □

5.3 Regulator Design III: Disturbance Rejection

Consider the open-loop system

$$\begin{aligned} \dot{x} &= Ax + Bu + Bd && \text{(5.3.1a)}\\ \dot{w} &= (F+G\psi)w && \text{(5.3.1b)}\\ d &= \psi w && \text{(5.3.1c)}\\ & && \text{(5.3.1d)} \end{aligned}$$

where $x \in \mathbb{R}^n$, $w \in \mathbb{R}^q$, $u \in \mathbb{R}$, and $d \in \mathbb{R}$. Comparing to (2.2.1), the exosystem (5.3.1b) has already been transformed according to Lemma 5.2.2. Moreover, the vector coefficient B multiplying d in (5.3.1a) is matched to the input u. This is a standard *disturbance rejection problem* in which the disturbance d enters additively in the control input.

Assumption 5.3.1. We assume the open-loop system (5.3.1) satisfies:

(A1) (A, B) is controllable.

(A2) $S = F + G\psi$ has simple eigenvalues on the imaginary axis.

(A3) (F, G) is a controllable pair, F is Hurwitz, and (ψ, S) is an observable pair.

(A4) Dimension q is interpreted as a known upper bound on the exosystem order, but the parameters (ψ, S) are unknown.

(A5) The parameters (A, B) are known.

(A6) The measurement is x.

Remark 5.3. (A1) may be relaxed to (A, B) stabilizable. (A2) guarantees that reference and disturbance signals are bounded. In (A4) the assumption that (ψ, S) is observable is without loss of generality since one can trim off the unobservable part of the exosystem without affecting the plant. Also in (A4), the interpretation of q as an upper bound on the exosystem order means the exosystem may be overmodeled for a particular instance of the disturbance. ◁

Consider the control input (5.1.2). For stabilization, let $u_s = Kx$ such that $(A + BK)$ is Hurwitz. To satisfy the internal model principle, consider the internal model

$$\begin{aligned} \dot{\hat{w}} &= S\hat{w} + G(d - \psi\hat{w}) \\ &= F\hat{w} + Gd\,. \end{aligned}$$

Define the estimation error $\tilde{w} = w - \hat{w}$. Then $\dot{\tilde{w}} = F\tilde{w}$, and since F is Hurwitz, $\tilde{w}(t) \longrightarrow 0$ exponentially. This internal model cannot be built as $d = \psi w$ is unavailable for measurement. Instead, we consider an internal model based on a *minimal order observer* proposed in (Nikiforov, 2004a) given by

$$\begin{aligned} \dot{w}_0 &= Fw_0 + (FN - NA)x - NBu && \text{(5.3.2a)} \\ \hat{w} &= w_0 + Nx && \text{(5.3.2b)} \\ u_{im} &= -\hat{\psi}\hat{w}\,, && \text{(5.3.2c)} \end{aligned}$$

where N is selected such that $NB = G$, and $\hat{\psi}$ is an estimate of ψ. Then we have

$$\begin{aligned} \dot{\hat{w}} &= Fw_0 + (FN - NA)x - NBu + N(Ax + Bu + Bd) \\ &= F(w_0 + Nx) + Gd \\ &= F\hat{w} + Gd\,. && \text{(5.3.3)} \end{aligned}$$

The *parameter adaptation law* is

$$\dot{\hat{\psi}} = \gamma(B^{\mathrm{T}}Px)\hat{w}^{\mathrm{T}}\,, \tag{5.3.4}$$

where $\gamma > 0$ is the adaptation rate, and $P \in \mathbb{R}^{n\times n}$ is the symmetric, positive definite solution of the Lyapunov equation

$$(A+BK)^{\mathrm{T}}P + P(A+BK) = -Q\,,$$

with $Q \in \mathbb{R}^{n\times n}$ symmetric and positive definite. Finally, the controller is

$$u = Kx - \hat{\psi}\hat{w}\,. \tag{5.3.5}$$

Define the *parameter estimation error* $\widetilde{\psi} := \psi - \hat{\psi}$.

Theorem 5.3.2. Consider the system (5.3.1) satisfying assumption 5.3.1, and consider the regulator (5.3.2), (5.3.4), and (5.3.5). Suppose $A+BK$ is Hurwitz. Then $x, \hat{\psi}, \hat{w} \in \mathcal{L}_\infty$, $x(t) \longrightarrow 0$, and $\widetilde{\psi}(t)\hat{w}(t) \longrightarrow 0$.

Proof. Applying input (5.3.5), the closed loop system is

$$\dot{x} = (A+BK)x + B\widetilde{\psi}\hat{w} + B\psi\widetilde{w} \tag{5.3.6a}$$

$$\dot{\widetilde{w}} = F\widetilde{w} \tag{5.3.6b}$$

$$\dot{\widetilde{\psi}} = -\gamma(B^{\mathrm{T}}Px)\hat{w}^{\mathrm{T}}\,. \tag{5.3.6c}$$

Since F is Hurwitz, from (5.3.6b) we get $\widetilde{w}(t) \longrightarrow 0$. By assumption (A2), $w \in \mathcal{L}_\infty$, so $\hat{w} \in \mathcal{L}_\infty$. Hence, the system satisfies all the assumptions of Corollary 4.2.4. We conclude $x, \widetilde{\psi} \in \mathcal{L}_\infty$, and $x(t) \longrightarrow 0$.

From (5.3.6a) we know $\dot{x} \in \mathcal{L}_\infty$; from (5.3.6c) we know $\dot{\widetilde{\psi}} \in \mathcal{L}_\infty$; and from (5.3.3), $\dot{\hat{w}} \in \mathcal{L}_\infty$. Then considering

$$\ddot{x} = (A+BK)\dot{x} + B\dot{\widetilde{\psi}}\hat{w} + B\widetilde{\psi}\dot{\hat{w}} + B\psi F\widetilde{w}\,,$$

we deduce that $\ddot{x} \in \mathcal{L}_\infty$, so by Lemma 4.1.2, $\dot{x}$ is uniformly continuous. Then by Lemma 4.1.3, $\dot{x}(t) \longrightarrow 0$. Using (5.3.6a), we conclude that $\widetilde{\psi}(t)\hat{w}(t) \longrightarrow 0$. □

Remark 5.4. Theorem 5.3.2 (as well as the rest of the theorems of this chapter) regards only the regulation requirement (R) of Problem 2.2.1.

The asymptotic stability requirement (AS) is not present in the theorem statement because Regulator Design III no longer achieves asymptotic stability. The unforced system with $w(0) = 0$ is stable based on a Lyapunov argument, and $\hat{w}(t)$ and $x(t)$ converge to zero, but $\hat{\psi}$ does not, as can be seen from (5.3.4). ◁

5.3.1 Extended Form

The internal model (5.3.2) is based on a minimal order observer, but an extended form provides an indication of how unknown plant parameters may be incorporated in the parameter adaptation process.

Suppose the system matrices (A, B) of plant (5.3.1a) take the special form

$$A = A_0 + B_0 a^{\mathrm{T}}, \qquad B = bB_0,$$

where

$$A_0 := \begin{bmatrix} 0 & 1 & \cdots & 0 \\ & & \ddots & 1 \\ 0 & & \cdots & 0 \end{bmatrix}, \qquad B_0 := \begin{bmatrix} 0 \\ \vdots \\ 0 \\ 1 \end{bmatrix}. \tag{5.3.7}$$

Vectors $a = (a_1, \ldots, a_n) \in \mathbb{R}^n$ and $b \in \mathbb{R}$ represent unknown plant parameters. Consider the extended internal model

$$\begin{aligned} \dot{w}_0 &= Fw_0 + (FN - NA_0)x && \text{(5.3.8a)} \\ \dot{w}_1 &= Fw_1 - NB_0 x_1 && \text{(5.3.8b)} \\ &\vdots && \text{(5.3.8c)} \\ \dot{w}_n &= Fw_n - NB_0 x_n && \text{(5.3.8d)} \\ \dot{w}_{n+1} &= Fw_{n+1} - NB_0 u && \text{(5.3.8e)} \\ \hat{w} &= w_0 + Nx + a_1 w_1 + \ldots + a_n w_n + b w_{n+1}, && \text{(5.3.8f)} \end{aligned}$$

where N is selected such that $NB_0 = G$. We can verify that once again

$$\dot{\hat{w}} = F\hat{w} + Gd,$$

so (5.3.8) does indeed provide an internal model of the disturbance d. Define the estimation error $\tilde{w} = w - \hat{w}$. Then $\dot{\tilde{w}} = F\tilde{w}$ and $\hat{w}(t) \longrightarrow w(t)$.

Next define the extended parameters ψ_d and regressor $\hat{w}_d$ as

$$\begin{aligned}\psi_d &:= \begin{bmatrix}\psi & a_1\psi & \cdots & a_n\psi & b\psi\end{bmatrix}\\ \hat{w}_d &:= (w_0 + Nx, w_1, \ldots, w_n, w_{n+1})\,.\end{aligned}$$

Then

$$d = \psi w = \psi\hat{w} + \varepsilon = \psi_d\hat{w}_d + \varepsilon\,,$$

where $\varepsilon = \psi\tilde{w}$ vanishes exponentially.

5.4 Regulator Design IV: Tracking

Consider the open-loop system

$$\begin{aligned}\dot{x} &= Ax + Bu && \text{(5.4.1a)}\\ \dot{w} &= (F + G\psi)w && \text{(5.4.1b)}\\ e &= r - y = \psi w - Cx\,, && \text{(5.4.1c)}\end{aligned}$$

where $x \in \mathbb{R}^n$, $w \in \mathbb{R}^q$, $u \in \mathbb{R}$ and $e \in \mathbb{R}$. Comparing to (2.2.1), the disturbance has been removed from (5.4.1a), and the exosystem (5.4.1b) has already been transformed according to Lemma 5.2.2. Further, $r = \psi w$ is a reference signal whose frequency content is unknown. Regarding $y = Cx$ as the system output, this is a standard *tracking problem*.

Assumption 5.4.1. We assume the open-loop system (5.4.1) satisfies:

(A1) (A, B) is controllable.

(A2) (C, A) is observable.

(A3) $S = F + G\psi$ has simple eigenvalues on the imaginary axis.

(A4) $\det \begin{bmatrix} A - \lambda I & B \\ C & 0 \end{bmatrix} \neq 0$ for all $\lambda \in \sigma(S)$.

(A5) (F, G) is a controllable pair, F is Hurwitz, and (ψ, S) is w.l.o.g. an observable pair.

(A6) Dimension q is interpreted as a known upper bound on the exosystem order, but the parameters (ψ, S) are unknown.

(A7) The parameters (A, B, C) are known.

(A8) The measurements are r and y.

We examine the information provided by the regulator equations. By (A4) and Lemma 2.3.2, there exist (Π, Γ) such that

$$\Pi S = A\Pi + B\Gamma \tag{5.4.2a}$$
$$0 = \psi - C\Pi\,. \tag{5.4.2b}$$

These equations have no particular structure other than that the feedforward control $u_{ss} = \Gamma w$ needed to achieve zero steady state error relies on parameters Γ that generally differ from the parameters ψ of the exosystem.

As usual we split the regulator design into a part for stabilization and a part to satisfy the internal model principle. If the state x is measurable $(C = I)$, then for stabilization we utilize $u_s = Kx$ such that $(A + BK)$ is Hurwitz. Otherwise we utilize a Luenberger observer

$$\dot{\hat{x}}_s = A\hat{x}_s + Bu + L_s(y - C\hat{x}_s) \tag{5.4.3a}$$
$$u_s = K\hat{x}_s\,, \tag{5.4.3b}$$

where L_s is such that $(A - L_sC)$ is Hurwitz and K is such that $(A + BK)$ is Hurwitz. If we define $\widetilde{x} = x - \hat{x}_s$, then we have $\dot{\widetilde{x}} = (A - L_sC)\widetilde{x}$, so $\widetilde{x}(t) \longrightarrow 0$ exponentially.

To satisfy the internal model principle, we consider the regulator design in (Nikiforov, 2004a). The internal model is

$$\dot{\hat{w}} = F\hat{w} + Gr \tag{5.4.4a}$$
$$u_{im} = \hat{\Gamma}\hat{w}\,, \tag{5.4.4b}$$

where $\hat{\Gamma} \in \mathbb{R}^{1\times q}$ is an estimate of Γ. Define $\widetilde{w} = w - \hat{w}$. Then $\dot{\widetilde{w}} = F\widetilde{w}$, and since F is Hurwitz, $\widetilde{w}(t) \longrightarrow 0$ exponentially.

Next we must design the parameter adaptation process. To that end, define the *augmented error*

$$\overline{e} := e + H(s)\left[\hat{\Gamma}\hat{w}\right] - \hat{\Gamma}H(s)I\left[\hat{w}\right]\,,$$

where $I \in q \times q$ is the identity matrix, and $H(s) := C(sI - (A + BK))^{-1}B$ is a stable transfer function. This formula is motivated by the fact that

$$\hat{e} := \hat{\Gamma} H(s) I\left[\hat{w}\right] - H(s)\left[\hat{\Gamma}\hat{w}\right]$$

will be seen in the proof of Theorem 5.4.2 to provide an estimate of e. Therefore, the augmented error

$$\overline{e} = e - \hat{e}$$

measures the difference between the true and estimated errors.

We define the *filtered regressor* to be

$$\overline{w} := H(s) I\left[\hat{w}\right] .$$

A realization of $\overline{w} \in \mathbb{R}^q$ is given by

$$\begin{aligned}
\dot{\eta}_1 &= (A + BK)\eta_1 + B\hat{w}_1 && \text{(5.4.5a)}\\
&\vdots && \text{(5.4.5b)}\\
\dot{\eta}_q &= (A + BK)\eta_q + B\hat{w}_q && \text{(5.4.5c)}\\
\overline{w} &= (C\eta_1, \ldots, C\eta_q) , && \text{(5.4.5d)}
\end{aligned}$$

where $\hat{w} = (\hat{w}_1, \ldots, \hat{w}_q) \in \mathbb{R}^q$, $\eta_1, \ldots, \eta_q \in \mathbb{R}^n$, and initial conditions are arbitrary. Then we define the parameter adaptation law to be

$$\dot{\hat{\Gamma}} = \gamma \overline{ew}^{\mathrm{T}} , \tag{5.4.6}$$

where $\gamma > 0$ is the adaptation rate. The overall controller is

$$u = K\hat{x}_s + \hat{\Gamma}\hat{w} . \tag{5.4.7}$$

Finally, define the parameter estimation error $\widetilde{\Gamma} := \Gamma - \hat{\Gamma}$.

Theorem 5.4.2. Consider the system (5.4.1) satisfying assumption 5.4.1, and consider the regulator consisting of (5.4.3), (5.4.4), (5.4.5), (5.4.6), and (5.4.7). Suppose $A+BK$ and $A-L_sC$ are Hurwitz. Then $x, \hat{\Gamma}, \hat{w} \in \mathcal{L}_\infty$, $e(t) \longrightarrow 0$, and $\widetilde{\Gamma}(t)\hat{w}(t) \longrightarrow 0$.

Proof. By (A4) and Lemma 2.3.2 there exist matrices (Π, Γ) satisfying the regulator equations (5.4.2). Define $z = x - \Pi w$. Then using (5.4.7)

we obtain

$$\begin{aligned}\dot{z} &= (A+BK)z - B\widetilde{\Gamma}\hat{w} - BK\widetilde{x} - B\Gamma\widetilde{w}\\ \dot{\widetilde{x}} &= (A-L_sC)\widetilde{x}\\ \dot{\widetilde{w}} &= F\widetilde{w}\\ e &= -Cz\,.\end{aligned}$$

Therefore, we can equivalently write

$$e = H(s)\left[\widetilde{\Gamma}\hat{w} + K\widetilde{x} + \Gamma\widetilde{w}\right] = H(s)\left[\widetilde{\Gamma}\hat{w}\right] + \varepsilon_1\,,$$

where $H(s) = C(sI-(A+BK))^{-1}B$ is a stable transfer function, and $\varepsilon_1(t) \longrightarrow 0$ exponentially. Now consider the augmented error

$$\begin{aligned}\overline{e} &= e + H(s)\left[\hat{\Gamma}\hat{w}\right] - \hat{\Gamma}H(s)I\left[\hat{w}\right]\\ &= H(s)\left[(\Gamma-\hat{\Gamma})\hat{w} + \varepsilon_1\right] + H(s)\left[\hat{\Gamma}\hat{w}\right] - \hat{\Gamma}H(s)I[\hat{w}]\\ &= H(s)\left[\Gamma\hat{w}\right] - \hat{\Gamma}H(s)I[\hat{w}] + \varepsilon_2\\ &= \widetilde{\Gamma}H(s)I\left[\hat{w}\right] + H(s)\left[\Gamma\hat{w}\right] - \Gamma H(s)I[\hat{w}] + \varepsilon_2 =: \widetilde{\Gamma}\overline{w} + \varepsilon_2\,,\end{aligned}$$

where we applied Lemma 4.2.6 in one of the steps.

Now we have

$$\begin{aligned}e &= H(s)\left[\widetilde{\Gamma}\hat{w}\right] + \varepsilon_1 && \text{(5.4.8a)}\\ \overline{w} &= H(s)I\left[\hat{w}\right] && \text{(5.4.8b)}\\ \overline{e} &= \widetilde{\Gamma}\overline{w} + \varepsilon_2 && \text{(5.4.8c)}\\ \dot{\widetilde{\Gamma}} &= -\gamma\overline{ew}^{\mathrm{T}}\,, && \text{(5.4.8d)}\end{aligned}$$

where $\varepsilon_1(t), \varepsilon_2(t) \longrightarrow 0$ exponentially. Since $r \in \mathcal{L}_\infty$, then using (5.4.4), $\hat{w}, \dot{\hat{w}} \in \mathcal{L}_\infty$. Since $H(s)$ is a stable transfer function, $\overline{w}, \dot{\overline{w}} \in \mathcal{L}_\infty$. All conditions are in place to apply Corollary 4.2.1. We conclude that $\widetilde{\Gamma}, \hat{\Gamma} \in \mathcal{L}_\infty$, $\overline{e}(t) \longrightarrow 0$, and $\widetilde{\Gamma}(t)\overline{w}(t) \longrightarrow 0$.

Since $\overline{w} \in \mathcal{L}_\infty$, from (5.4.8), $\dot{\widetilde{\Gamma}}(t) \longrightarrow 0$. Since $H(s)$ is stable, we can apply Lemma 4.2.8 to obtain

$$\left(\hat{\Gamma}H(s)I\left[\hat{w}\right] - H(s)\left[\hat{\Gamma}\hat{w}\right]\right)(t) \longrightarrow 0\,.$$

It follows that $e(t) \longrightarrow 0$. Finally, since $\widetilde{x}(t) \longrightarrow 0$ and $\widetilde{w}(t) \longrightarrow 0$ exponentially, and $(A + BK)$ is Hurwitz, also $z(t) \longrightarrow 0$. Hence $x \in \mathcal{L}_\infty$. □

5.5 Regulator Design V

We study a design that combines tracking and disturbance rejection. Consider the open-loop system

$$\begin{aligned} \dot{x} &= Ax + Bu + Bd && \text{(5.5.1a)} \\ \dot{w}_1 &= (F_1 + G_1\psi_1)w_1 && \text{(5.5.1b)} \\ \dot{w}_2 &= (F_2 + G_2\psi_2)w_2 && \text{(5.5.1c)} \\ d &= \psi_1 w_1 && \text{(5.5.1d)} \\ r &= \psi_2 w_2 && \text{(5.5.1e)} \\ y &= Cx && \text{(5.5.1f)} \\ e &= r - y\,, && \text{(5.5.1g)} \end{aligned}$$

where $x \in \mathbb{R}^n$, $w_1 \in \mathbb{R}^{q_1}$, $w_2 \in \mathbb{R}^{q_2}$, $u \in \mathbb{R}$, $d, r \in \mathbb{R}$, and $y \in \mathbb{R}$. Here r is a reference signal to be tracked by the system output y, while d is a disturbance that enters additively at the plant input.

Assumption 5.5.1. We assume the open-loop system (5.5.1) satisfies:

(A1) (A, B) is controllable.

(A2) (C, A) is observable.

(A3) $S = \operatorname{diag}(S_1, S_2)$ has simple eigenvalues on the imaginary axis, where $S_1 = F_1 + G_1\psi_1$, and $S_2 = F_2 + G_2\psi_2$;

(A4) $\det \begin{bmatrix} A - \lambda I & B \\ C & 0 \end{bmatrix} \neq 0$ for all $\lambda \in \sigma(S)$.

(A5) Each F_i is Hurwitz, (F_i, G_i) is a controllable pair, and (ψ_i, S_i) is w.l.o.g. an observable pair, for $i = 1, 2$.

(A6) Upper bounds on q_1 and q_2 are known, but the parameters of (ψ_1, S_1) and (ψ_2, S_2) are unknown.

(A7) The parameters (A, B, C) are known.

(A8) The measurements are r and y.

The diagonal structure of S permits a partition of the regulator equations in a natural way. By (A4) and Lemma 2.3.2, there exist (Π_1, Γ_1) and (Π_2, Γ_2) such that

$$\begin{aligned} \Pi_1 S_1 &= A\Pi_1 + B\Gamma_1 + B\psi_1 && \text{(5.5.2a)} \\ 0 &= -C\Pi_1 && \text{(5.5.2b)} \\ \Pi_2 S_2 &= A\Pi_2 + B\Gamma_2 && \text{(5.5.2c)} \\ 0 &= \psi_2 - C\Pi_2 \,. && \text{(5.5.2d)} \end{aligned}$$

The solution of the first set of equations is $\Pi_1 = 0$ and $\Gamma_1 = -\psi_1$, returning to the situation in Section 5.3. The second set has no particular structure.

We develop a controller of the form

$$u = u_s + u_{im,1} + u_{im,2} \,. \tag{5.5.3}$$

First we design u_s for closed-loop stability. Define $z := x - \Pi_2 w_2$. Using (5.5.2) we obtain the error model

$$\begin{aligned} \dot{z} &= Az + Bu - B\Gamma_1 w_1 - B\Gamma_2 w_2 && \text{(5.5.4a)} \\ e &= -Cz \,. && \text{(5.5.4b)} \end{aligned}$$

Under assumption 2.2.1(A1)-(A2), we can define an observer of the form:

$$\dot{\hat{z}}_s = A\hat{z}_s + Bu_s + L_s(e + C\hat{z}_s) \tag{5.5.5}$$

where L_s is selected so that $(A + L_s C)$ is Hurwitz. Define the estimation error $\tilde{z}_s = z - \hat{z}_s$. Using (5.5.3), we obtain

$$\dot{\tilde{z}}_s = (A + L_s C)\tilde{z}_s + Bu_{im,1} + Bu_{im,2} - B\Gamma_1 w_1 - B\Gamma_2 w_2 \,.$$

Assuming we can design $u_{im,1}$ and $u_{im,2}$ such that $(u_{im,1} - \Gamma_1 w_1)(t) \longrightarrow 0$ and $(u_{im,2} - \Gamma_2 w_2)(t) \longrightarrow 0$, independently of the $\tilde{z}_s$ error dynamics, then $\tilde{z}_s(t) \longrightarrow 0$. Therefore, we choose

$$u_s = K\hat{z}_s \,,$$

such that $(A + BK)$ is Hurwitz in order to stabilize the z dynamics.

Next we design $u_{im,1}$. Consider the internal model

$$\dot{\hat{x}}_d = A\hat{x}_d + Bu + L_d(y - C\hat{x}_d) \tag{5.5.6a}$$
$$\dot{\hat{w}}_f = F_1\hat{w}_f + G_1(y - C\hat{x}_d)\,, \tag{5.5.6b}$$

where we choose L_d such that $A_d := A - L_dC$ is Hurwitz. Define $\widetilde{x}_d := x - \hat{x}_d$. Then we have

$$\dot{\widetilde{x}}_d = A_d\widetilde{x}_d + Bd \tag{5.5.7a}$$
$$d_f := C\widetilde{x}_d\,. \tag{5.5.7b}$$

Define the stable transfer function $H_d(s) := C(sI - A_d)^{-1}B$. Then $d_f = H_d(s)\,[d]$ is the *filtered disturbance*. Recall from Lemma 5.2.4 that d_f can be represented as

$$\dot{w}_f = F_1w_f + G_1d_f \tag{5.5.8a}$$
$$d_f = \psi_1w_f + \varepsilon\,, \tag{5.5.8b}$$

where $w_f = H_d(s)I\,[w_1]$ is the *filtered regressor*. Define the estimation error $\widetilde{w}_f := w_f - \hat{w}_f$. Using (5.5.6b), we have $\dot{\widetilde{w}}_f = F_1\widetilde{w}_f$. Since F_1 is Hurwitz, we obtain $\widetilde{w}_f(t) \longrightarrow 0$. Now we have a regressor $\hat{w}_f$ for the filtered disturbance, but we require a regressor for d. This is provided by Lemma 5.2.5; namely, there exists $\Gamma_f \in \mathbb{R}^{1\times q_1}$ such that

$$d = \psi_1w_1 = \Gamma_fw_f + \varepsilon\,. \tag{5.5.9}$$

Finally, we define

$$u_{im,1} = \hat{\Gamma}_f\hat{w}_f\,, \tag{5.5.10}$$

where $\hat{\Gamma}_f \in \mathbb{R}^{1\times q_1}$ is an estimate of Γ_f.

Next we consider the design of $u_{im,2}$. The second internal model is

$$\dot{\hat{w}}_2 = F_2\hat{w}_2 + G_2r \tag{5.5.11a}$$
$$u_{im,2} = \hat{\Gamma}_2\hat{w}_2\,, \tag{5.5.11b}$$

where $\hat{\Gamma}_2 \in \mathbb{R}^{1\times q_2}$ is an estimate of Γ_2. Define $\widetilde{w}_2 := w_2 - \hat{w}_2$. Using (5.5.1c), we have $\dot{\widetilde{w}}_2 = F_2\widetilde{w}_2$, and since F_2 is Hurwitz, $\widetilde{w}_2(t) \longrightarrow 0$.

Let's summarize the design so far. We have an error model

$$\dot{z} = Az + Bu - B\Gamma_f w_f - B\Gamma_2 w_2 \tag{5.5.12a}$$
$$e = -Cz\,, \tag{5.5.12b}$$

and we have a controller

$$u = K\hat{z}_s + \hat{\Gamma}_f \hat{w}_f + \hat{\Gamma}_2 \hat{w}_2$$

where $(\hat{w}_f, \hat{w}_2)$ are known regressors, and $(\hat{\Gamma}_f, \hat{\Gamma}_2)$ are parameter estimates. We write this model more compactly by defining a composite parameter vector, regressor, and their estimates:

$$\Gamma := \begin{bmatrix} \Gamma_f & \Gamma_2 \end{bmatrix} \in \mathbb{R}^{1\times q}\,, \qquad w := (w_f, w_2) \in \mathbb{R}^q\,, \tag{5.5.13a}$$
$$\hat{\Gamma} := \begin{bmatrix} \hat{\Gamma}_f & \hat{\Gamma}_2 \end{bmatrix} \in \mathbb{R}^{1\times q}\,, \qquad \hat{w} := (\hat{w}_f, \hat{w}_2) \in \mathbb{R}^q\,, \tag{5.5.13b}$$

where $q = q_1 + q_2$. Define $\widetilde{w} := w - \hat{w}$. Then $\dot{\widetilde{w}} = F\widetilde{w}$, where $F = \operatorname{diag}(F_1, F_2)$. The error model becomes

$$\dot{z} = Az + Bu - B\Gamma w \tag{5.5.14a}$$
$$e = -Cz\,. \tag{5.5.14b}$$

Unfortunately this error model can not be used to design the parameter adaptation process following the steps in Section 4.2.4 because A may be unstable. To overcome this impasse, we consider an observer

$$\dot{\hat{z}}_p = A\hat{z}_p + Bu + L_p(e + C\hat{z}_p)\,, \tag{5.5.15}$$

where L_p is selected so that $A_p := (A + L_pC)$ is Hurwitz. Define the estimation error $\widetilde{z}_p := z - \hat{z}_p$. Then we obtain

$$\dot{\widetilde{z}}_p = A_p\widetilde{z}_p - B\Gamma w\,.$$

Notice that

$$e + C\hat{z}_p = -C\widetilde{z}_p = H_p(s)\left[\Gamma w\right]\,,$$

where $H_p(s) := C(sI - A_p)^{-1}B$ is a stable transfer function. This error model now recalls the one in Section 4.2.4. Thus, we define the *augmented error*

$$\overline{e} := e + C\hat{z}_p - \hat{\Gamma}H_p(s)I\left[\hat{w}\right]\,,$$

where I is the $q \times q$ identity matrix. The regressor for parameter adaptation is

$$\overline{w} := H_p(s) I\left[\hat{w}\right] .$$

A realization of $\overline{w} \in \mathbb{R}^q$ is

$$\begin{aligned}
\dot{\eta}_1 &= A_p \eta_1 + B\hat{w}^1 && \text{(5.5.16a)}\\
&\vdots && \text{(5.5.16b)}\\
\dot{\eta}_q &= A_p \eta_q + B\hat{w}^q && \text{(5.5.16c)}\\
\overline{w} &= \left(C\eta_1, \ldots, C\eta_q\right), && \text{(5.5.16d)}
\end{aligned}$$

where $\hat{w} = (\hat{w}^1, \ldots, \hat{w}^q) \in \mathbb{R}^q$ and $\eta_1, \ldots, \eta_q \in \mathbb{R}^n$.

Remark 5.5. We remark that $\hat{w}$ and $\overline{w}$ evolve according to identical dynamics, modulo exponentially vanishing terms. For recall that, by assumption, $\dot{w}_1 = S_1 w_1$ and $\dot{w}_2 = S_2 w_2$. Using (5.5.6b), (5.5.7b), (5.5.8), and (5.5.11), we obtain

$$\begin{aligned}
\dot{\hat{w}}_f &= S_1 \hat{w}_f + \varepsilon\\
\dot{\hat{w}}_2 &= S_2 \hat{w}_2 + \varepsilon\,,
\end{aligned}$$

where (abusing notation) ε captures any exponentially vanishing terms. Recall $S = \operatorname{diag}(S_1, S_2)$. Overall we obtain

$$\dot{\hat{w}} = S\hat{w} + \varepsilon\,.$$

Now consider $\overline{w} = H_p(s) I\left[\hat{w}\right]$. We have

$$\begin{aligned}
\dot{\overline{w}} &= sH_p(s) I\left[\hat{w}\right]\\
&= H_p(s) I\left[\dot{\hat{w}}\right]\\
&= H_p(s) I\left[S\hat{w}\right] + \varepsilon\\
&= SH_p(s) I\left[\hat{w}\right] + \varepsilon\\
&= S\overline{w} + \varepsilon\,.
\end{aligned}$$

◁

Using Lemma 5.2.5 we can extract an algebraic relationship between $\hat{w}$ and $\overline{w}$.

Lemma 5.5.2. Consider w, $\hat{w}$, and $\overline{w}$ as above. Suppose Assumption 5.5.1 holds. Then there exists a nonsingular matrix $T \in \mathbb{R}^{q\times q}$ such that

$$\overline{w} = T\hat{w} + \varepsilon\,.$$

Proof. Consider $H(s) = C(sI - A)^{-1}B$. By assumption (A4), no zero of $H(s)$ is an eigenvalue of S. Since $H_p(s) = C(sI - (A + CL_p))B$, also no zero of $N_p(s)$ is an eigenvalue of S (Brockett, 1965). Then we can apply Lemma 5.2.5 to obtain that there exists a nonsingular matrix $T = D_p(S)^{-1}N_p(S)$ such that

$$\overline{w} = T\hat{w} + \varepsilon\,.$$

□

Finally, we choose the parameter adaptation law

$$\dot{\hat{\Gamma}} = \gamma \overline{e}\overline{w}^{\mathrm{T}}\,,$$

where $\gamma > 0$ is the adaptation rate.

We summarize the overall design:

$$\begin{aligned}
\dot{\hat{z}}_s &= (A + BK)\hat{z}_s + L_s(e + C\hat{z}_s) && \text{(5.5.17a)}\\
\dot{\hat{x}}_d &= A\hat{x}_d + Bu + L_d(y - C\hat{x}_d) && \text{(5.5.17b)}\\
\dot{\hat{z}}_p &= A\hat{z}_p + Bu + L_p(e + C\hat{z}_p) && \text{(5.5.17c)}\\
\dot{\hat{w}}_f &= F_1\hat{w}_f + G_1(y - C\hat{x}_d) && \text{(5.5.17d)}\\
\dot{\hat{w}}_2 &= F_2\hat{w}_2 + G_2 r && \text{(5.5.17e)}\\
\hat{w} &= (\hat{w}_f, \hat{w}_2) && \text{(5.5.17f)}\\
\overline{w} &= H_p(s)I\,[\hat{w}] && \text{(5.5.17g)}\\
\overline{e} &= e + C\hat{z}_p - \hat{\Gamma}\overline{w} && \text{(5.5.17h)}\\
\dot{\hat{\Gamma}} &= \gamma \overline{e}\overline{w}^{\mathrm{T}} && \text{(5.5.17i)}\\
u &= K\hat{z}_s + \hat{\Gamma}\hat{w}\,. && \text{(5.5.17j)}
\end{aligned}$$

Define $\widetilde{\Gamma} := \Gamma - \hat{\Gamma}$ and $\widetilde{w} := w - \hat{w}$.

Theorem 5.5.3. Consider the system (5.5.1) satisfying assumption 5.5.1, and consider the regulator given in (5.5.17). Suppose $A + BK$, $A_s =$

$A + L_sC$, $A_d = A - L_dC$, and $A_p = A + L_pC$ are Hurwitz. Then $\hat{\Gamma}, \hat{w} \in \mathcal{L}_\infty$, $e(t) \longrightarrow 0$, and $\widetilde{\Gamma}(t)\hat{w}(t) \longrightarrow 0$.

Proof. Define $\widetilde{z}_s = z - \hat{z}_s$, $\widetilde{z}_p = z - \hat{z}_p$. Then using (5.5.17), we have

$$\begin{aligned}
\dot{z} &= (A + BK)z - B\widetilde{\Gamma}\hat{w} - B\Gamma\widetilde{w} - BK\widetilde{z}_s && \text{(5.5.18a)}\\
\dot{\widetilde{z}}_s &= A_s\widetilde{z}_s - B\widetilde{\Gamma}\hat{w} - B\Gamma\widetilde{w} && \text{(5.5.18b)}\\
\dot{\widetilde{z}}_p &= A_p\widetilde{z}_p - B\Gamma w && \text{(5.5.18c)}\\
\dot{\widetilde{w}} &= F\widetilde{w} && \text{(5.5.18d)}\\
e &= -Cz\,. && \text{(5.5.18e)}
\end{aligned}$$

Now consider the augmented error

$$\begin{aligned}
\overline{e} &= -C\widetilde{z}_p - \hat{\Gamma}H_p(s)I\left[\hat{w}\right]\\
&= H_p(s)\left[\Gamma w\right] - \hat{\Gamma}H_p(s)I\left[\hat{w}\right]\\
&= \widetilde{\Gamma}H_p(s)I\left[\hat{w}\right] + H_p(s)\left[\Gamma(\widetilde{w} + \hat{w})\right] - \Gamma H_p(s)I\left[\hat{w}\right]\\
&= \widetilde{\Gamma}\overline{w} + \varepsilon\,,
\end{aligned}$$

where $\varepsilon(t) \longrightarrow 0$ exponentially due to Lemma 4.2.6 and the exponential stability of $\widetilde{w}$.

Now we can study the system

$$\begin{aligned}
\overline{e} &= \widetilde{\Gamma}\overline{w} + \varepsilon\\
\dot{\widetilde{\Gamma}} &= -\gamma\overline{e}\overline{w}^{\mathrm{T}}\,.
\end{aligned}$$

Because $w, \dot{w} \in \mathcal{L}_\infty$, then $\hat{w}, \dot{\hat{w}}, \overline{w}, \dot{\overline{w}} \in \mathcal{L}_\infty$. Therefore, we can apply Corollary 4.2.2 to conclude that $\hat{\Gamma} \in \mathcal{L}_\infty$, $\overline{e}(t) \longrightarrow 0$, and $\widetilde{\Gamma}(t)\overline{w}(t) \longrightarrow 0$. Since $\overline{w} \in \mathcal{L}_\infty$ and $\overline{e}(t) \longrightarrow 0$, we have $\dot{\widetilde{\Gamma}}(t) \longrightarrow 0$. Then by Lemma 4.2.8,

$$\left(\widetilde{\Gamma}H_p(s)I\left[\hat{w}\right] - H_p(s)\left[\widetilde{\Gamma}\hat{w}\right]\right)(t) \longrightarrow 0\,.$$

Therefore, $H_p(s)\left[\widetilde{\Gamma}\hat{w}\right] \longrightarrow 0$.

Since $\hat{w}(t) \to w(t)$ exponentially and w is the state of an LTI system satisfying assumption (A3), there exist matrix $M \in \mathbb{R}^{q\times(2s+1)}$ and vector $\hat{w}_r(t)$ such that $\hat{w}(t) = M\hat{w}_r(t)$ and

$$\hat{w}_r(t) = (1, \cos(\omega_1 t), \sin(\omega_1 t), \ldots, \cos(\omega_s t), \sin(\omega_s t))$$

with $\omega_i \neq \omega_j$ for $i \neq j$ and $2s+1 \leq q$. Then we have

$$\overline{w} = H_p(s)I\,[\hat{w}] + \varepsilon = H_p(s)I\,[M\hat{w}_r] + \varepsilon = MH_p(s)I\,[\hat{w}] + \varepsilon =: M\overline{w}_r + \varepsilon\,.$$

Since $H_p(s)$ is a stable transfer function,

$$\begin{aligned}\overline{w}_r = (&H_p(0), |H_p(j\omega_1)|\cos(\omega_1 t + \phi(\omega_1)), |H_p(j\omega_1)|\sin(\omega_1 t + \phi(\omega_1)), \ldots,\\ &|H_p(j\omega_s)|\cos(\omega_s t + \phi(\omega_s)), |H_p(j\omega_s)|\sin(\omega_s t + \phi(\omega_s))) + \varepsilon\,.\end{aligned}$$

The zeros of $H_p(s)$ are the same as those of the plant $C(sI - A)^{-1}B$ (Brockett, 1965), and by (A4), $H_p(0) \neq 0$ and $|H_p(j\omega_k)| \neq 0$, for $k = 1, \ldots, s$. One can verify by direct calculation that $\overline{w}_r$ is stationary and its autocovariance is positive definite. By Lemma 4.3.5, $\overline{w}_r$ is PE.

We have $\overline{e} = \widetilde{\Gamma}\overline{w} + \varepsilon = \widetilde{\Gamma}M\overline{w}_r + \varepsilon$. Let $\widetilde{\Gamma}_r := \widetilde{\Gamma}M$. We have established that $\widetilde{\Gamma}_r(t)\overline{w}_r(t) \longrightarrow 0$, $\dot{\widetilde{\Gamma}}_r = \dot{\widetilde{\Gamma}}M \longrightarrow 0$, and $\overline{w}_r$ is PE, so we can apply Theorem 4.3.6 to conclude that $\widetilde{\Gamma}_r(t) \longrightarrow 0$. This implies $\widetilde{\Gamma}(t)\hat{w}(t) = \widetilde{\Gamma}_r(t)\hat{w}_r(t) \longrightarrow 0$. Observing (5.5.18) we also have $\widetilde{z}_s(t), z(t) \longrightarrow 0$. Finally, we conclude $e(t) \longrightarrow 0$. □

5.6 Final Remarks

In this chapter we presented several regulator designs inspired by the disturbance observer approach in (Nikiforov, 2004a) that incorporate adaptation in the internal model, thus removing the requirement that the frequency content of exogenous reference and disturbance signals must be known a priori. In all the designs the plant parameters are assumed to be known. While this assumption is not realistic in neuroscience applications, as we discussed before, the brain utilizes a separation of timescales to handle adaptation of disturbance parameters v.s. plant parameters. Rather than mix these two processes in one design, incurring a risk of introducing spurious processes in our models, we have opted for these simpler designs. We included the extended design in Section 5.3.1 to give some indication of how the assumption of known plant parameters may be removed. The extended design proved to be helpful in developing our model of the optokinetic system, presented in Chapter 7.

The first regulator design regards disturbance rejection for disturbances entering at the plant input. This design is relevant in modeling the slow eye movement systems and the optokinetic system. The second regulator design regards a tracking problem where the reference signal is assumed to be measurable. This design is evocative in neuroscience applications as the cerebellum appears to process a massive amount of feedforward sensory measurements. The final regulator design is the least directly relevant as a physiologically inspired model of the cerebellum. It includes a number of observers whose placements in the brain are, at present, simply possibilities or conjectures. Nevertheless, this design has found application in modeling visuomotor adaptation (Hafez *et al.*, 2021). At this time it is not known if the cerebellum utilizes state feedback or output feedback for motor control tasks, though given the amount of sensory information the cerebellum receives, the use of state feedback can certainly not be ruled out at this stage. Finally, we mention that all the regulator designs presented in this chapter can be made robust to plant parameter uncertainty and unmodeled, bounded disturbances using techniques from robust adaptive control, as mentioned in Section 4.4.

6

Slow Eye Movement Systems

The *slow eye movement systems* quite literally refer to those motor control systems that move the eyes slowly, in contrast with the *saccadic system* which produces one of the fastest movements of the body, a *saccade*. A part of the *oculomotor system*, the slow eye movement systems comprise several subsystems: the *vestibulo-ocular reflex* (VOR), *optokinetic system* (OKS), the *gaze fixation system*, the *smooth pursuit system*, and the *vergence system*. This chapter concentrates on modeling the VOR, smooth pursuit, and gaze fixation. The OKR will be discussed in Chapter 7 and the saccadic system in Chapter 9.

Our focus on the oculomotor system is motivated by the fact that it serves as an exemplar among motor control systems. As we discussed in Chapter 3, the structure and computations of the cerebellum are identical across all the systems it regulates, differences arising only in the input/output connections to each cerebellar module. The oculomotor system has a very simple plant (the eyeball), is phylogenetically the oldest motor system, and is believed to provide the blueprint for all other motor systems (Leigh and Zee, 2015).

The idea that the brain provides internal models of exogenous signals

specifically with regard to the oculomotor system has been suggested in the oculomotor literature, making this system a promising point of departure (Cerminara *et al.*, 2009; Churchland *et al.*, 2003; Lisberger, 2009). First, there is the so-called predictive capability of the smooth pursuit system - to track moving targets with zero steady-state error (Bahill and McDonald, 1983a; Deno *et al.*, 1995; Wyatt and Pola, 1988). Second, it has been shown experimentally that exogenous signals that can be modeled by low-order linear exosystems are easily tracked by the eyes, while unpredictable signals are not (Bahill and McDonald, 1983b; Collewijn and Tamminga, 1984; Deno *et al.*, 1995; Michael and Jones, 1966). Third, in an experiment called *target blanking*, a moving target is temporarily occluded, yet the eye continues to move (Cerminara *et al.*, 2009; Churchland *et al.*, 2003); researchers postulate the brain has an internal model of the motion of the target. In a fourth experiment called the *error clamp*, the retinal error is artificially clamped at zero using an experimental apparatus that places the target image on the fovea (Barnes *et al.*, 1995; Morris and Lisberger, 1987; Stone and Lisberger, 1990). Despite zero retinal error, the eye continues to track the target, suggesting that so called *extra-retinal signals* drive the smooth pursuit system.

6.1 Control Architecture

The oculomotor system anatomy includes the *oculomotor plant* consisting of the eyeball, muscles moving the eye, and *oculomotor neurons* that stimulate the muscles; the *brainstem* which provides the main feedback loop by receiving the retinal and vestibular (from the semicircular canals of the ear) signals and issuing the oculomotor command to the eye muscles; and the *cerebellum* which provides fine regulation of eye movements as a top up to the main control loop through the brainstem.

The control architecture may be abstractly represented by the block diagram in Figure 6.1, based on the neural circuit of the oculomotor system (Leigh and Zee, 2015); see also Section 3.2. A visual error signal encoding the difference between target and gaze angles is transmitted from the *visual cortex* to the *inferior olive* (IO), where it is relayed to ap-

propriate *climbing fiber* inputs (CFs) of the *cerebellum* (C) (specifically, the *floccular complex*). The cerebellum also receives *mossy fiber* inputs (MFs) containing a mixture of visual, eye movement, and vestibular information from the *medial vestibular nuclei* (MVN) in the *brainstem* (B) (Lisberger, 2009). The sole output of the cerebellum is transmitted via its *Purkinje cells* (PCs) to *floccular target neurons* (FTNs) in the MVN (Ramanchandran and Lisberger, 2008). The MVN also receives a head velocity signal from the semicircular canals of the ear. The output of the MVN is sent both to the *neural integrator* (NI) in the brainstem *nucleus prepositus hypoglossi* (NPH) and directly to the *oculomotor neurons* (MNs) of the oculomotor plant (P). Salient features of this architecture include:

(i) The cerebellum forms a side loop to the main feedback loop between the plant and the brainstem;

(ii) The brainstem has a direct feedthrough from the vestibular system to the plant to cancel measurable disturbance signals from head movement;

(iii) The CF cerebellar input is a sensory error signal carrying visual information; and

(iv) The cerebellum has only one output which acts as a top up to the control command generated by a brainstem-only pathway.

6.2 Oculomotor Plant

The horizontal motion of the eye is modeled by considering the eyeball as a sphere that is suspended in fluid and subjected to viscous drag, elastic restoring forces, and the pulling of two muscles. A reasonable approximation is obtained by assuming that the inertia of the eyeball is insignificant (Leigh and Zee, 2015; Robinson, 1981; Sylvestre and Cullen, 1999). Letting x be the horizontal eye angle and u be the net torque imparted by the two muscles, we obtain a first order model

$$\dot{x} = -K_x x + u\,. \tag{6.2.1}$$

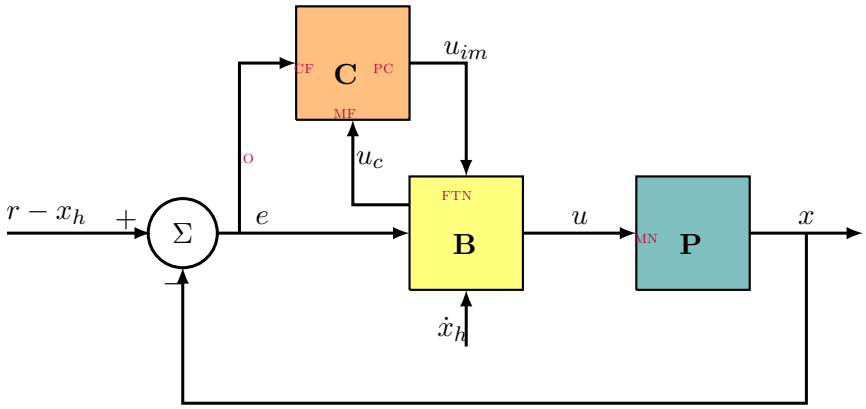

Figure 6.1: Control architecture for the VOR, gaze holding and smooth pursuit systems.

The parameter $K_x > 0$ is constant (or very slowly varying) such that the time constant of the eye is $\tau_x := 1/K_x \simeq 0.2$s (Robinson, 1981).

Consider a reference signal r representing the angle of a target moving in the horizontal plane. Let x_h and $\dot{x}_h$ denote the horizontal head angular position and angular velocity, respectively. The *retinal error* is defined to be

$$e := \alpha_e(r - x_h - x)\,. \tag{6.2.2}$$

Notice that $r - x_h - x$ is the target angle r relative to the *gaze angle* $x_h + x$. For sufficiently distant targets, this relative angle is proportional (through the scale factor $\alpha_e \in \mathbb{R}$) to a linear displacement on the retina from the fovea to the target image on the retina. The goal of the oculomotor system is to drive e to zero. As such, we can make a simplifying assumption that $\alpha_e = 1$ without sacrificing the plausibility of the model.

Our modeling assumptions are as follows. The eye position x is assumed to be unavailable for direct measurement (Guthrie *et al.*, 1983). The retinal error signal e (or a scaled version of it) is assumed to be available as a measurement to the brainstem and to both MF and CF inputs of the cerebellum (Blohm *et al.*, 2005; Krauzlis *et al.*, 1997). The reference signal r is unmeasurable. The vestibular system provides a measurement of the head angular velocity $\dot{x}_h$ to the brainstem but not

directly to the cerebellum (Gerrits *et al.*, 1989; Robinson, 1981), and it does not provide the head position x_h (Robinson, 1981).

Remark 6.1. Each of the eye movement systems has driving signals, signals required for computation of ongoing eye movement. Head velocity is a driving signal for the VOR. *Retinal error*, the difference between the target and fovea positions on the retina, drives the saccadic system (Pola, 2002). *Retinal slip velocity*, the time derivative of retinal error, is often taken to be the driving signal in models of the smooth pursuit system.

Here we have chosen the retinal error to be the driving signal of the VOR, gaze holding, and smooth pursuit. Experimental evidence supporting this assumption was obtained in several studies (Berthoz, 1988; Eggers *et al.*, 2003; Shelhamer *et al.*, 1995; Shelhamer *et al.*, 1994). Further, a series of studies by Pola and Wyatt (Pola and Wyatt, 1980; Wyatt and Pola, 1981; Wyatt and Pola, 1983b) showed that retinal slip velocity is inadequate to explain all the behaviors of the smooth pursuit system. Other studies used strobe-reared cats, who never experience retinal slip velocity (Mandl *et al.*, 1981; Jones and Mandl, 1979). Finally, direct experimental evidence that retinal errors drive the smooth pursuit system was given in (Blohm *et al.*, 2005); they used a flashing visual target for which no velocity information could be perceived directly.

It is known that in primates, the VOR, gaze holding, and smooth pursuit systems share the same neural pathways in the brainstem and cerebellum (in this chapter when we use the term "cerebellum", we refer more specifically to the *floccular complex*, comprising the flocculus and the ventral paraflocculus (Lisberger, 2009).), so it is plausible these systems share certain driving signals (Büttner and Waespe, 1984; Lisberger, 2015). For the model presented here, we assume the common visual driving signal shared by the VOR, gaze holding, and smooth pursuit systems is the retinal error. ◁

6.3 Brainstem

The brainstem provides two functions (among others) to the eye movement systems: a direct feedthrough of the head velocity signal for the VOR, and an estimate of the eye position used by all eye movement systems. The latter function has been the subject of a long-standing debate in the neuroscience community regarding how the eye position information is obtained. One theory dating to the 1800's proposed that the brain receives an *efference copy* of an internal signal carrying eye position information. An opposing theory argued that *proprioception* of eye muscle activity provides eye movement information, obviating the need for an efference copy. In the 1950's, the term *corollary discharge* was coined to characterize a copy of the motor command that informs the brain of ongoing eye movement. The debate between corollary discharge and proprioception has been largely settled, with experiments showing that proprioception from the eye muscles plays a negligible role in eye movement (Carpenter, 1972; Guthrie *et al.*, 1983; Keller and Robinson, 1971). Based on the experimental evidence, one can construct the eye position estimate using a standard observer.

We start from Robinson's *parallel pathway model* (Skavenski and Robinson, 1973) consisting of two parallel pathways in the brainstem that combine to form the oculomotor command; that is,

$$u = u_v + u_n \,,$$

where u_v is carried on the direct pathway from the MVN to the MNs; and u_n corresponds to an indirect pathway from MVN to NPH to MNs. The signal u_n is the output of the *brainstem neural integrator* in the NPH. Invoking equation (3) in (Robinson, 1974), the neural integrator is modeled as a leaky integrator:

$$\dot{\hat{x}} = -\widetilde{K}_x \hat{x} + u_v \,, \quad u_n = \alpha_x \hat{x} \,, \tag{6.3.1}$$

where α_x and $\widetilde{K}_x$ are constants (or very slowly varying). Using the fact that $u_v = u - \alpha_x \hat{x}$, this model can be re-expressed as

$$\dot{\hat{x}} = -\widehat{K}_x \hat{x} + u \,, \tag{6.3.2}$$

where $\widehat{K}_x := \widetilde{K}_x + \alpha_{\text{x}}$. Finally, we incorporate the idea from (Galiana and Outerbridge, 1984) that $\widehat{K}_x = K_x$ (henceforth we drop the hat); see also (Dale and Cullen, 2015; Green *et al.*, 2004). In sum, we deduce that the brainstem neural integrator forms an *observer* of the oculomotor plant. If we define the estimation error $\widetilde{x} := x - \hat{x}$, then $\widetilde{x}$ evolves according to $\dot{\widetilde{x}} = -K_x\widetilde{x}$, implying that $\hat{x}(t)$ converges exponentially to $x(t)$. Aside from a momentary perturbation (a push on the eyeball), $\hat{x}(t)$ well approximates $x(t)$.

Remark 6.2. The major variants of the brainstem model can be derived from (6.3.1). When $\hat{K}_x = K_x$, the model is called a *forward model* in the neuroscience literature. With the choice $\widehat{K}_x = 0$ and $\alpha_{\text{x}} = K_x$, the model is called an *inverse model*, because it cancels the stable pole of the oculomotor plant. The inverse model is not accurate since the neural integrator is leaky (Robinson, 1974); nevertheless, it finds use in models of the saccadic system (Pola, 2002) to allow modelers to account for gaze holding at the end of a saccade without explicitly modeling the contribution from the cerebellum. In control theoretic terms, the inverse model inserts a pole at zero to allow the eye to track an exosystem $R(s) = 1/s$. ◁

Remark 6.3. Our assumption that $\widehat{K}_x = K_x$ implicitly relies on the existence of two additional brain processes. First we assume that the brain is capable of *long-term adaptation* (over days and weeks) to changes in model parameters (e.g. weakening of the muscles of the eye) (Leigh and Zee, 2015). Second, we assume the brain is capable of *learning transfer*, a process by which adapted parameter values can be transferred from one brain region to another (cerebellum to brainstem) (Shutoh *et al.*, 2006; Kassardjian *et al.*, 2005). ◁

As a final step in modeling the brainstem, we identify the components of the signal u_v:

$$u_v = u_s + u_{im} - \alpha_{\text{VOR}}\dot{x}_h \,.$$

The signal $\alpha_{\text{VOR}}\dot{x}_h$ is the vestibular measurement of head angular velocity representing the direct feedthrough from the semicircular canals to the MNs for the VOR; the signal u_s carries visual information only and it

improves the closed-loop stability of the system; and the signal u_{im} is the output from the PCs of the cerebellum which is required to satisfy the internal model principle. Of course our choice to use the notation u_s and u_{im} is intended to recall the regulator designs in Chapter 5; these will be used to model the cerebellum.

To summarize, the brainstem processes a *brainstem-only* signal given by

$$u_b = \alpha_{\text{x}}\hat{x} - \alpha_{\text{VOR}}\dot{x}_h \,. \tag{6.3.3}$$

This signal can be interpreted as the first line of defense in rejecting disturbances in the retinal error signal. The term $\alpha_{\text{VOR}}\dot{x}_h$ represents a partial cancellation of the head velocity to improve the quality of vision. The term $\alpha_{\text{x}}\hat{x}$ represents a partial cancellation of the *drift term* of the oculomotor plant; without such cancellation, the eye would constantly drift to center, particularly without the support of the cerebellum, again diminishing the quality of vision.

The brainstem also processes signals that are part of a loop with the cerebellum. These signals are combined to form a *cerebellar signal* in the brainstem:

$$u_c = u_s + u_{im} \,.$$

When we compare these signals with the signals in the parallel pathway model we see that the overall motor command is

$$u = u_v + u_n = u_b + u_c \,.$$

6.4 Cerebellum

It has long been hypothesized that the cerebellum provides a top up to the disturbance supression activities of the brainstem. For example, the *flocculus central vestibular neuron complementary hypothesis* of (Büttner and Waespe, 1984) postulated that the cerebellum will be modulated if the signal provided by MVN neurons (in the brainstem) is not sufficient to achieve the objectives of the VOR, OKR, or smooth pursuit. This role of the cerebellum can be mathematically characterized in terms of regulation of e. A modeling problem transforms into

a synthesis problem: to design a regulator, consistent with the neural architecture, to make $e(t) \longrightarrow 0$.

The open-loop model we developed in the previous section is

$$\begin{aligned} \dot{x} &= -K_x x + u \\ \dot{\hat{x}} &= -K_x \hat{x} + u \\ e &= r - x_h - x \\ u_b &= \alpha_{\text{x}} \hat{x} - \alpha_{\text{VOR}} \dot{x}_h \\ u &= u_b + u_s + u_{im} \,. \end{aligned}$$

Assuming that $\hat{x}(t) \equiv x(t)$ for $t \geq 0$, we obtain the *error model*

$$\dot{e} = -\widetilde{K}_x e - u_s - u_{im} + \dot{r} + \widetilde{K}_x r - (1 - \alpha_{\text{VOR}}) \dot{x}_h - \widetilde{K}_x x_h \,, \qquad (6.4.2)$$

where $\widetilde{K}_x := K_x - \alpha_{\text{x}}$. We assume the reference signal r as well as the head position x_h are modeled as the outputs of a linear exosystem. Let $\eta(t) \in \mathbb{R}^q$ be the exosystem state and define the exosystem

$$\begin{aligned} \dot{\zeta} &= S\zeta \\ r &= D_1 \zeta \\ x_h &= D_2 \zeta \,, \end{aligned}$$

where $S \in \mathbb{R}^{q \times q}$, $D_1 \in \mathbb{R}^{1 \times q}$, and $D_2 \in \mathbb{R}^{1 \times q}$. Then (6.4.2) takes the form

$$\dot{e} = -\widetilde{K}_x e - u_s - u_{im} + E\eta \qquad (6.4.3)$$

where

$$E := D_1 S + \widetilde{K}_x D_1 - (1 - \alpha_{\text{VOR}}) D_2 S - \widetilde{K}_x D_2 \in \mathbb{R}^{1 \times q} \,.$$

Next we transform the exosystem according to Lemma 5.2.2. Let (F, G) be a controllable pair with F Hurwitz. The exosystem becomes

$$\dot{w} = (F + G\psi) w \,.$$

According to Lemma 5.2.2, $E\eta = \psi w$, so we can rewrite the error dynamics (6.4.3) in terms of the new exosystem state:

$$\dot{e} = -\widetilde{K}_x e - u_s - u_{im} + d \,, \qquad (6.4.4)$$

where $d = \psi w$ is the disturbance to be rejected. The parameters $(\widetilde{K}_x, \psi^{\mathrm{T}}) \in \mathbb{R}^{q+1}$ capture all unknown model and disturbance parameters.

Now we follow the design steps in Section 5.3. We select u_s to improve closed-loop stability (note the plant is already open-loop stable):

$$u_s = K_e e\,,$$

where $K_e > 0$. To generate u_{im}, we employ the adaptive internal model of Section 5.3.1:

$$\begin{aligned}
\dot{w}_0 &= Fw_0 + FGe && \text{(6.4.5a)}\\
\dot{w}_1 &= Fw_1 - Ge && \text{(6.4.5b)}\\
\dot{w}_2 &= Fw_2 - Gu_s && \text{(6.4.5c)}\\
\dot{w}_3 &= Fw_3 - Gu_{im} && \text{(6.4.5d)}\\
\hat{w} &= w_0 + Ge - \widetilde{K}_x w_1 - w_2 - w_3\,. && \text{(6.4.5e)}
\end{aligned}$$

We can verify that $\dot{\hat{w}} = F\hat{w} + Gd$, so (6.4.5) provides an internal model of disturbance d. Define the estimation error $\widetilde{w} = w - \hat{w}$. Then $\dot{\widetilde{w}} = F\widetilde{w}$ and $\hat{w}(t) \longrightarrow w(t)$.

Since the plant parameter $\widetilde{K}_x$ is not known, we may use the extended parameter vector and regressor of Section 5.3.1 in the adaptation process:

$$\begin{aligned}
\psi_d &:= \begin{bmatrix} \psi & -\widetilde{K}_x\psi & \psi & \psi \end{bmatrix}\\
\hat{w}_d &:= (w_0 + Ge, w_1, w_2, w_3)\,.
\end{aligned}$$

Then

$$d = \psi w = \psi\hat{w} + \psi\widetilde{w} = \psi_d\hat{w}_d + \varepsilon\,,$$

where $\varepsilon = \psi\widetilde{w}$ vanishes exponentially. Therefore we choose

$$u_{im} = \hat{\psi}_d\hat{w}_d\,,$$

where $\hat{\psi}_d$ is an estimate of ψ_d. Finally, the parameter adaptation rule is

$$\dot{\hat{\psi}}_d = e\hat{w}_d^{\mathrm{T}}\,.$$

By Theorem 5.3.2, this design achieves regulation of e.

Remark 6.4. Notice that the adaptive internal model only receives visual information in the signal e, so ongoing eye movement information, namely x or $\hat{x}$, is not directly supplied to it. However, since eye movement affects e, the output of the internal model indirectly reflects eye movement. Also, we assume that when the visual driving signal e is removed, as in darkness or when the eyes close, the cerebellum (specifically the floccular complex) falls inactive (Lisberger, 2015). However, we have not fully modeled how this inactivity takes place - whether it is instantaneous or gradual. ◁

The overall model of the slow eye movement systems that we have derived is:

$$\begin{aligned}
\dot{\hat{x}} &= -K_x\hat{x} + u && \text{(6.4.6a)}\\
\dot{w}_0 &= Fw_0 + FGe && \text{(6.4.6b)}\\
\dot{w}_1 &= Fw_1 - Ge && \text{(6.4.6c)}\\
\dot{w}_2 &= Fw_2 - Gu_s && \text{(6.4.6d)}\\
\dot{w}_3 &= Fw_2 - Gu_{im} && \text{(6.4.6e)}\\
\hat{w}_d &:= (w_0 + Ge, w_1, w_2, w_3) && \text{(6.4.6f)}\\
\dot{\hat{\psi}}_d &= e\hat{w}_d^{\mathrm{T}} && \text{(6.4.6g)}\\
u_b &= \alpha_{\text{x}}\hat{x} - \alpha_{\text{vor}}\dot{x}_h && \text{(6.4.6h)}\\
u_s &= K_e e && \text{(6.4.6i)}\\
u_{im} &= \hat{\psi}_d\hat{w}_d && \text{(6.4.6j)}\\
u &= u_b + u_s + u_{im}\,. && \text{(6.4.6k)}
\end{aligned}$$

One may arrive at somewhat different models by using other adaptive internal model designs in the control literature. In (Broucke, 2020; Broucke, 2021) we used an internal model design from (Serrani and

Isidori, 2000; Serrani *et al.*, 2001). The overall model is:

$$\begin{aligned}
\dot{\hat{x}} &= -K_x\hat{x} + u && \text{(6.4.7a)}\\
\dot{\hat{w}} &= F\hat{w} + G(u_s + u_{im}) && \text{(6.4.7b)}\\
\dot{\hat{\psi}} &= e\hat{w}^{\mathrm{T}} && \text{(6.4.7c)}\\
u_b &= \alpha_{\text{x}}\hat{x} - \alpha_{\text{VOR}}\dot{x}_h && \text{(6.4.7d)}\\
u_s &= K_e e && \text{(6.4.7e)}\\
u_{im} &= \hat{\psi}\hat{w} && \text{(6.4.7f)}\\
u &= u_b + u_s + u_{im}\,. && \text{(6.4.7g)}
\end{aligned}$$

The internal model is now given by a single equation (6.4.7b). This model provides less detail on specific mossy fiber inputs and due to its parsimony may be less directly related to the neural circuit. On the other hand, it's stability proof (given in (Serrani and Isidori, 2000; Serrani *et al.*, 2001)) does not require that the exosystem states are bounded, unlike the results in Chapter 5. Either model may be used for the slow eye movement systems, with differences showing up in their transient responses.

6.5 Neural Circuit

We want to verify that the model (6.4.6) is consistent with the neural architecture. Particularly, a mapping between brain projections and signals in our model must be identified. We refer to details about the neural circuit in (Büttner and Büttner-Ennever, 2006).

The retinal error signal e descends from the visual cortex and is utilized in our model in three forms: as the projection from the IO to the CF input in (6.4.6g); as a visual MF input u_s; and again as a visual signal u_s in the MVN. Note that u_s may be distinct in the MVN v.s. the MFs; here it is the same signal only for the sake of mathematical parsimony. Next, the projection from the PCs to the MVN corresponds to the signal u_{im}. From the MVN this signal then projects to the MF input of the cerebellum and to the MNs. The direct projection from the vestibular system to the MVN and thence to the MNs is modeled by $\alpha_{\text{VOR}}\dot{x}_h$. The eye position signal $\alpha_{\text{x}}\hat{x}$ nominally corresponds to the

projection from the NPH to the MNs; however, we do not make precise statements about its location as the neural substrate of the NPH is still under investigation (Dale and Cullen, 2015; Green *et al.*, 2004; Green *et al.*, 2007). The MF inputs to the flocculus have been classified as visual, vestibular, and eye movement MFs (Lisberger, 2009). In our model u_{im} carries an estimate of all persistent disturbances acting on the retinal error, so this signal alone may account for the mixture of signals observed on the MF inputs of the cerebellum.

While we have not provided a detailed mapping to cell types in the MVN, our model may be amenable to such a mapping. For example, consider the EH neurons, a class of FTNs thought to be involved in long-term adaptation of the VOR gain (Roy and Cullen, 2003). These cells receive inputs from the PCs and the vestibular system; that is,

$$u_{eh} = u_{im} + \alpha_{eh}\dot{x}_h \,.$$

During steady-state smooth pursuit with passive head rotation, our model predicts

$$u_{im} \simeq \dot{r} + \widetilde{K}_x r - (1 - \alpha_{\text{VOR}})\dot{x}_h - \widetilde{K}_x x_h \,.$$

Since $x(t) \simeq r(t) - x_h(t)$, this becomes

$$u_{im} \simeq \dot{x} + \widetilde{K}_x x + \alpha_{\text{VOR}}\dot{x}_h \,.$$

Therefore, our model predicts

$$u_{eh} \simeq \dot{x} + \widetilde{K}_x x + (\alpha_{\text{VOR}} + \alpha_{eh})\dot{x}_h \,,$$

which is the formula obtained experimentally in (Roy and Cullen, 2003, Fig. 14).

Our neural circuit has a few distinctions from some circuits in the literature. First, our model does not included a pure head velocity MF input. Not only are there no primary afferents (Gerrits *et al.*, 1989), but all secondary afferents in the MVN carry other signals as well (Robinson, 1981). Additionally, the resting rate of vestibular only MF inputs does not match that of vestibular nerve fibers, whereas they have resting rates comparable to vestibular only neurons in the MVN (Langer *et al.*, 0185; Lisberger and Fuchs, 1978b). Finally, the smooth pursuit

system, which relies in the cerebellum, is fully functional without any vestibular signal (Waterston *et al.*, 1992).

Second, our model does not make use of the projection from the NPH to the flocculus, presumed to provide an efference copy of the motor command u as an MF input, as doing so leads to inconsistencies with lesion experiments. If the NPH (but not the MVN) is lesioned, it is known that the VOR and smooth pursuit systems are still functional, showing minor changes in their transient responses (Cannon and Robinson, 1987; Kaneko, 1999; Kim *et al.*, 2016). It is also known that smooth pursuit is abolished after ablation of the flocculus (Zee *et al.*, 1981). If we assumed the projection from the NPH to the flocculus were u, we would arrive at a paradox that the smooth pursuit system can still function without an MF input to the cerebellum when the NPH is lesioned. In contrast, after lesioning the MVN, the VOR, the OKR, gaze holding, and smooth pursuit are all disabled or strongly modified, consistent with the idea that damage to the MVN effectively disables the flocculus (Cannon and Robinson, 1987).

6.6 Simulations

The simulations presented are taken from (Broucke, 2020; Broucke, 2021) for the model (6.4.7). The parameter values in the simulations are: $K_x = 5$, $\alpha_{\text{x}} = 0.95K_x$, $\alpha_{\text{VOR}} = 0.65$, $K_e = 5$, $q = 2$,

$$F = \begin{bmatrix} 0 & 1 \\ -1 & -1 \end{bmatrix}, \qquad G = \begin{bmatrix} 0 \\ 1 \end{bmatrix}.$$

These values were selected according to the following criteria. First, K_x is selected to match the known time constant $\tau_x = 1/K_x = 0.2$s of the human oculomotor plant. Second, α_{x} is selected so that $\widetilde{K}_x = K_x - \alpha_{\text{x}} = 0.25$ gives a time constant of $\tilde{\tau}_x = 1/\widetilde{K}_x = 4$s, in the range of the known time constant of the combined oculomotor plant and neural integrator (Glasauer, 2003). The final top-up to this time constant is provided by the cerebellum; see the discussion on gaze fixation below. We have chosen α_{VOR} called the VOR gain (see below) somewhat arbitrarily; it may range from 0.6 to 0.9 under natural conditions and is

highly adaptable. The parameter $K_e = 5$ has been selected to match the transient response of the smooth pursuit system (see Figure 6.14); however, it too appears to be adjustable (Broucke, 2020). The parameter q which sets the order of the internal model is of great interest and may vary according to which module of the cerebellum is under study. For the floccular complex, we have selected $q = 2$ based on the performance of the human smooth pursuit system; we have selected F so the adaptive internal model has stable complex conjugate poles. This choice is informed by the damped oscillations of the smooth pursuit system when initiating tracking of a constant speed target (Robinson *et al.*, 1986).

6.6.1 Vestibulo-Ocular Reflex

The purpose of the vestibulo-ocular reflex (VOR) is to stabilize the gaze (sum of eye and head angles) when the head is moving. This system has been intensively studied over the last 60 years, and experiments may be classified as follows.

(a) The standard *behavioral experiment* with the VOR involves involuntary sinusoidal rotation of the subject's head in darkness. The ratio of peak eye velocity to peak head velocity in steady-state is called the *VOR gain*. Another behavioral experiment involves involuntary sinusoidal rotation of the subject's head in the light, while the subject fixates on a stationary target. In this case, the *effective VOR gain* jumps to close to unity in human subjects.

(b) *VOR cancellation* is an experiment in which the subject's head is moved involuntarily while the subject must track a target that moves with the head. The experiment is called VOR cancellation because the brain must suppress its own (brainstem) reflex to move the eyes opposite to the head.

(c) *VOR adaptation experiments* involve experimental adaptation of the VOR gain.

(d) *Neurological experiments* typically record from the cells of the MVN or the Purkinje cells of the cerebellum.

(e) *Lesion experiments* involve total cerebellectomy, lesions of the flocculus only, the MVN, the NPH, or some combination thereof.

First we consider the standard experiment of measuring the VOR gain. This gain is measured in darkness when the cerebellum is relatively inactive, so in our model we assume $u_c = 0$. Then the eye dynamics evolve according to a brainstem-only control input. Assuming that $x(t) \simeq \hat{x}(t)$, we have

$$\dot{x} = -\widetilde{K}_x x - \alpha_{\text{VOR}} \dot{x}_h \,. \tag{6.6.1}$$

Suppose $x_h(t) = a_h \sin(\beta_h t)$. Assuming $\widetilde{K}_x > 0$, then the steady-state response of (6.6.1) has the form

$$x_{ss}(t) = -\alpha_{\text{VOR}} a_h \frac{\beta_h}{\widetilde{K}_x^2 + \beta_h^2} \Big(\beta_h \sin(\beta_h t) - \widetilde{K}_x \cos(\beta_h t) \Big) \,.$$

Generally $\widetilde{K}_x \ll \beta_h$, so

$$x_{ss}(t) \simeq -\alpha_{\text{VOR}} a_h \sin(\beta_h t) = -\alpha_{\text{VOR}} x_h(t) \,.$$

That is, the eye moves relative to the head with a scale factor of -α_{VOR}. The parameter α_{VOR} is called the *VOR gain* since it well approximates the ratio of head velocity to eye velocity measured in darkness. Our model predicts that the VOR in the dark is unaffected by disabling the cerebellum, as reported experimentally (Robinson, 1981; Zee *et al.*, 1981).

The second standard experiment with the VOR is to measure the VOR gain in the light while applying an involuntary sinusoidal head rotation $x_h(t) = a_h \sin(\beta_h t)$, where $a_h, \beta_h > 0$. Figure 6.2 shows simulation results for the values $a_h = 15$, $\beta_h = 0.1$Hz for $t \in [0, 10]$, and $\beta_h = 0.2$Hz for $t \in [10, 20]$. The initial condition on all states is zero except the eye angle, which starts at $x(0) = -10°$. We also plot the retinal error e, the cerebellar output u_{im}, the brainstem component u_b, and the parameter estimates $\hat{\psi}_1$ and $\hat{\psi}_2$. As expected, the eye moves opposite to the head rotation, and it adapts to the frequency of the sinusoidal disturbance.

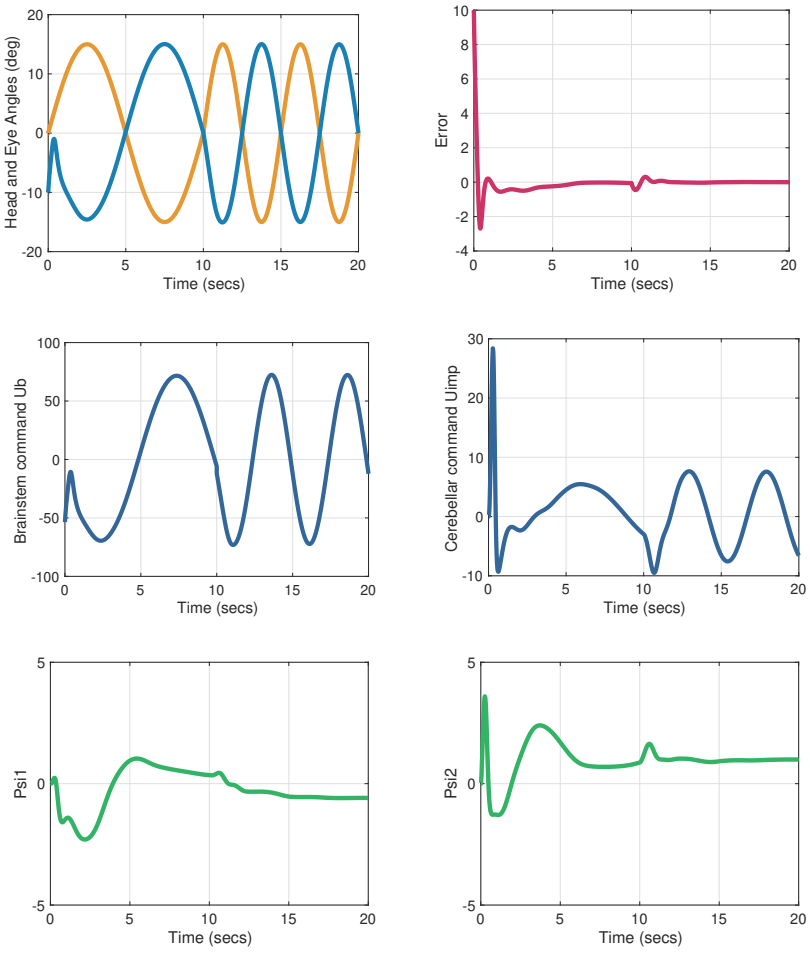

Figure 6.2: VOR with a sinusoidal head rotation. The top left figure shows the head (yellow) and eye (blue) angles; the eye moves opposite to the head for a properly functioning VOR. The top right figure shows the retinal error (red), which tends to zero. The middle figures are u_b and u_{im}, and the bottom figures are the parameter estimates $\hat{\psi}_1$ and $\hat{\psi}_2$. During $t \in [10, 20]$, the frequency of sinusoidal oscillation of the head is $\beta_h = 0.1$Hz and during $t \in [10, 20]$ it is $\beta_h = 0.2$Hz. We see that the cerebellar output u_{im} adapts to the change in frequency of the head disturbance.

A third standard experiment evokes *short-term adaptation* of the VOR. For example, suppose an involuntary sinusoidal head rotation is applied, given by $x_h(t) = a_h \sin(\beta_h t)$, where $a_h, \beta_h > 0$, while at the same time

the subject must track a target $r(t) = \alpha_r x_h(t)$, where α_r is a constant. Figure 6.3 shows simulation results for $\alpha_r = 0.5$, $a_h = 15$, $\beta_h = 0.1$Hz for $t \in [0, 10]$, and $\beta_h = 0.2$Hz for $t \in [10, 20]$. The initial condition on all states is zero except the eye angle, which starts at $x(0) = -10°$. We also plot the retinal error e, the cerebellar output u_{im}, the brainstem component u_b, and the parameter estimates $\hat{\psi}_1$ and $\hat{\psi}_2$. The eye moves opposite to the head rotation, but only with half the amplitude.

In an experiment called *VOR cancellation*, the head is rotated involuntarily while the eyes must track a head-fixed target (Büttner and Waespe, 1984). Suppose the head angle is $x_h(t) = a_h \sin(\beta_h t)$ with $a_h, \beta_h > 0$, and the target angle is $r(t) = x_h(t)$. Then the error is given by $e = -x$. The role of u_{im} in this case is to cancel the disturbance $\alpha_{\text{VOR}} \dot{x}_h$ introduced by the brainstem component u_b. Figure 6.4 illustrates the results for VOR cancellation using our model. Particularly, we note that the response amplitude of the brainstem component is not reduced during VOR cancellation, as experimentally confirmed in (Buettner and U. Buttner, 1979; Keller and Daniels, 1975).

Next we consider experiments involving an adapted VOR gain. The VOR gain α_{VOR} is subject to an adaptive brain process called long-term adaptation. While we do not include this process in our model (α_{VOR} is treated as a constant), we can consider how an adapted VOR gain affects short-term behavior of the oculomotor system. Such an experiment was reported in (Lisberger and Pavelko, 1986) in which the effect of the VOR gain on the transient response of the oculomotor system was investigated. It was discovered that the overshoot in the eye velocity to a sudden rotation of the head was larger when the VOR gain is smaller. In the experiment, a light spot at $r = 0$ on which the monkey fixates (in another otherwise dark room) is strobed. Here we assume the subject attempts to continuously fixate the eyes on a target at $r = 0$, even when the light spot is extinguished. The head position is a ramp function: $x_h(t) = 0$ for $t \in [0, 1]$ and $x_h(t) = -30t$ for $t \in [1, 5]$, resulting in a head angular velocity of -30°/s. Figure 6.5 illustrates the behavior observed in the experiments in (Lisberger and Pavelko, 1986). The blue curve is the eye angular velocity for $\alpha_{\text{VOR}} = 0.3$, red is with $\alpha_{\text{VOR}} = 0.5$, and yellow is with $\alpha_{\text{VOR}} = 0.8$. We see clearly that smaller

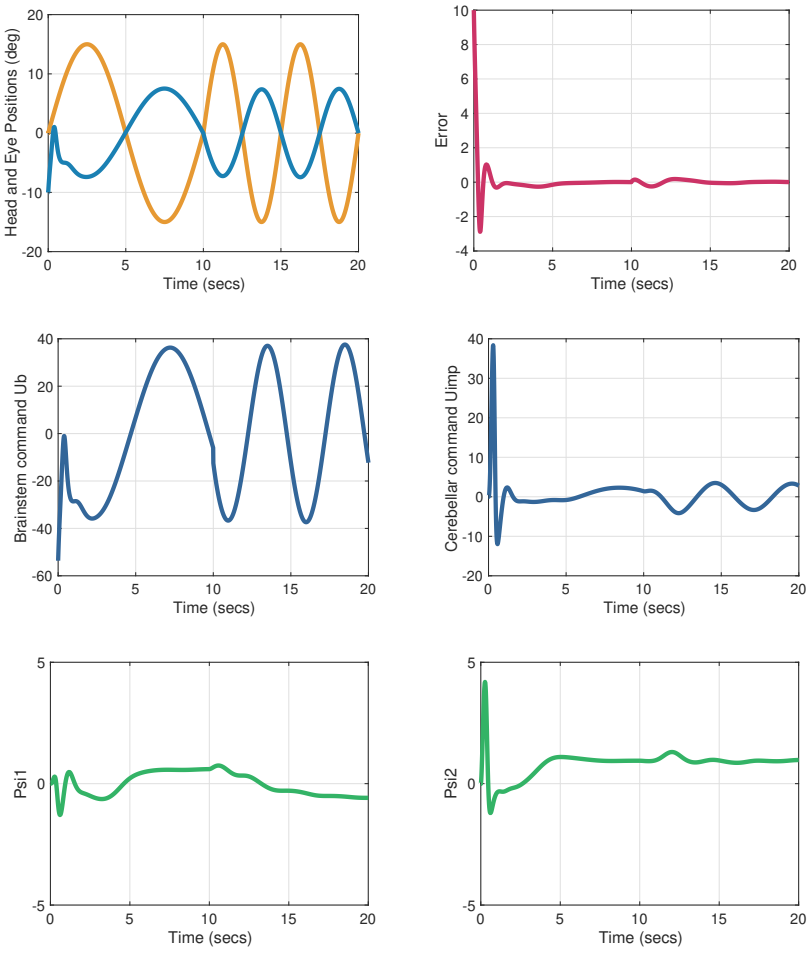

Figure 6.3: VOR while tracking a target moving relative to the head rotation. The top left figure shows the head (yellow) and eye (blue) angles, showing that the eye no longer moves opposite to the head because the subject is tracking a target with the same frequency but different amplitude as the head movement. The left figure shows that the retinal error (red) tends to zero. The middle figures are u_b and u_{im}, showing the cerebellar output u_{im} is reduced corresponding to the reduced eye movement. The brainstem component u_b of the VOR is unchanged compared to a standard VOR experiment, as expected. The bottom figures are the parameter estimates $\hat{\psi}_1$ and $\hat{\psi}_2$.

VOR gains result in larger overshoots.

A second experiment involving an adapted VOR gain was documented

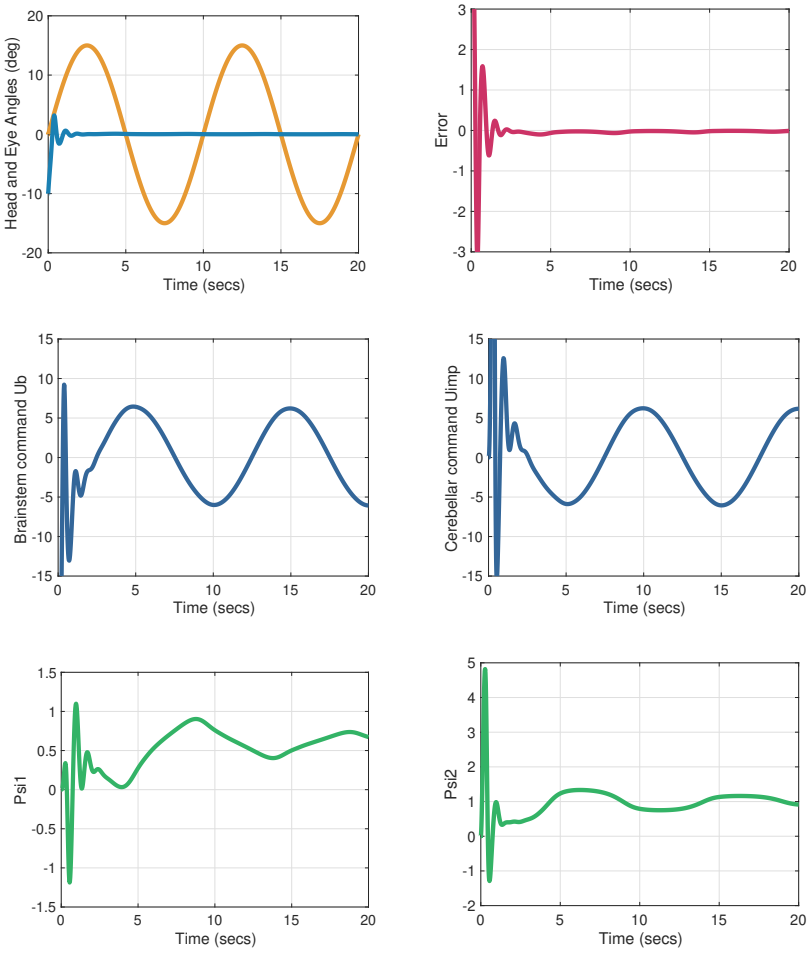

Figure 6.4: VOR cancellation. The top left figure shows the head (yellow) and eye (blue) angles, showing that the eye remains stationary as it tracks a head fixed target. The left figure shows that the retinal error (red) tends to zero. The middle figures are u_b and u_{im}, showing the cerebellar output u_{im} now fully compensates for the brainstem VOR signal to keep the eye stationary. The brainstem component u_b of the VOR is unchanged by the tracking task. The bottom figures are the parameter estimates $\hat{\psi}_1$ and $\hat{\psi}_2$.

in (Lisberger, 1994). Monkeys were adapted to a new VOR gain by wearing goggles in their cages. It was found that changes in the VOR gain had no affect on the monkey's ability to track a moving target. This

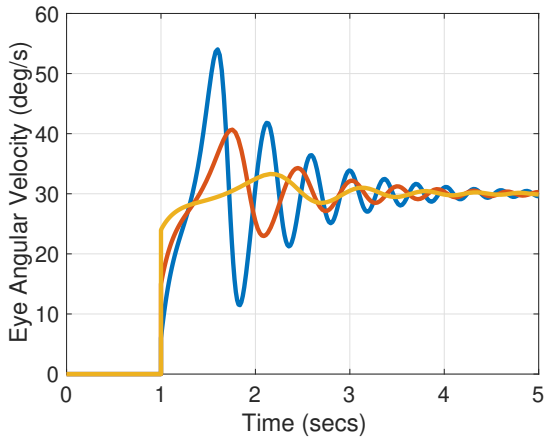

Figure 6.5: VOR with a step input in head velocity for the values $\alpha_{\text{VOR}} = 0.3, 0.5, 0.8$ (blue, red, yellow). The size of the overshoot in the eye velocity is inversely proportional to the value of α_{VOR}.

behavior is explained in our model when we consider that the cerebellar component u_{im} compensates for whatever fraction of the vestibular signal entering the error is not already cancelled by the brainstem component $-\alpha_{\text{VOR}}\dot{x}_h$.

In a third experiment involving an adapted VOR gain, it has been demonstrated that the VOR in the light is unaffected by changes in the VOR gain (Miles and Eighmy, 1980). Figure 6.6 shows this experimental behavior with our model, where $\alpha_{\text{VOR}} = 2$ for $t \in [0, 15]$ and $\alpha_{\text{VOR}} = -1$ for $t \in [15, 30]$. It is clear from the left figure in Figure 6.6 that our model predicts that in steady-state, the VOR in the light is unaffected by changes in the VOR gain.

Next we consider neurological experiments with the VOR. An experiment reported in (Lisberger and Fuchs, 1978a) demonstrated that the depth of firing rate of the output of the cerebellum increases with the frequency of sinusoidal head rotation while the subject fixates on a stationary target. In this case, $r = 0$ and $x_h = a_h \sin(\beta_h t)$. Considering the error model (6.4.2), the cerebellum must reject a disturbance signal with the form $-(1 - \alpha_{\text{VOR}})\dot{x}_h - \widetilde{K}_x x_h$. In particular, the term $\dot{x}_h = a_h \beta_h \cos(\beta_h t)$ is proportional to β_h. Figure 6.7 shows the simu-

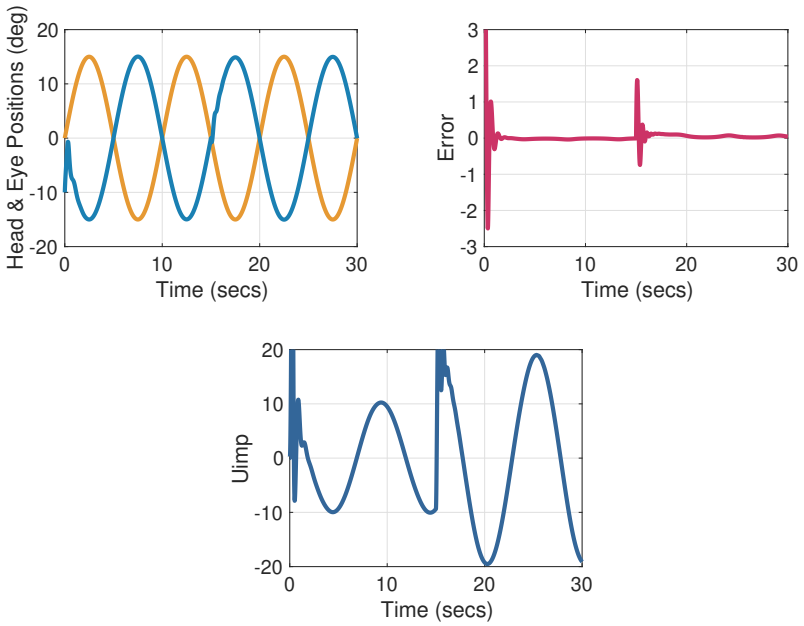

Figure 6.6: Effect of α_{VOR} on the VOR. The top left figure shows the head (yellow) and eye (blue) angles. During $t \in [0, 15]$, $\alpha_{\text{VOR}} = 2$ and during $t \in [15, 30]$, $\alpha_{\text{VOR}} = -1$. We observe that the abrupt change in VOR gain only mildly affects the eye movement during VOR, which continues to move opposite the head in this standard VOR experiment. The top right figure shows that the retinal error e tends to zero, irrespective of the VOR gain. The bottom figure shows that the cerebellar output u_{im} compensates for the change in VOR gain.

lation results for $a_h = 15$, $\beta_h = 0.1$Hz for $t \in [0, 20]$; $\beta_h = 0.2$Hz for $t \in [20, 40]$; and $\beta_h = 0.5$Hz for $t \in [40, 60]$. We see in the right figure that the amplitude of u_{im} increases as the frequency of the head rotation increases.

Finally, we consider lesion experiments with the VOR. A number of researchers have studied the VOR in the situation when the cerebellum is disabled either due to disease or cerebellectomy (Zee *et al.*, 1981). We illustrate this effect for *VOR cancellation*, in which the eyes must track a head fixed target; that is, the target position is mechanically coupled to the head position by an experimental apparatus so that $r(t) = x_h(t)$. Simulation results are shown in Figure 6.8 with $u_c = 0$ to disable the cerebellum. We observe in the left figure that the subject is no longer

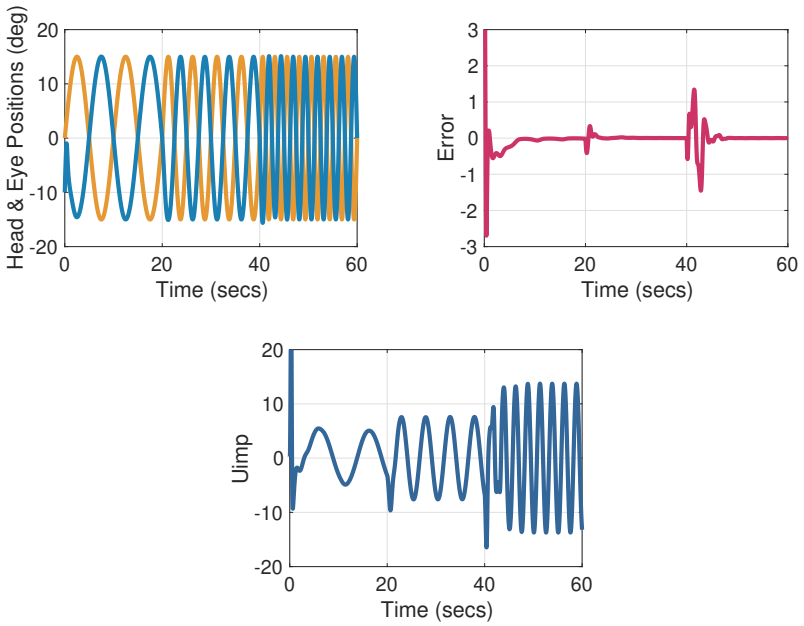

Figure 6.7: Effect of the frequency of oscillations of the head on the depth of modulation of the cerebellar component u_{im}. The top left figure shows the head (yellow) and eye (blue) angles, with the eye moving opposite to the head in this standard VOR experiment with three different frequencies of sinusoidal head movement. The left figure shows that the retinal error (red) tends to zero, with some transients occurring when the frequency of sinusoidal head oscillation changes. The bottom figure shows that the cerebellar output u_{im} has an amplitude that increases with increasing frequency of the sinusoidal head oscillation, as observed in experiments.

able to suppress the VOR - the blue curve shows that the eye position is not stabilized, despite a head-fixed target. This result corroborates many experimental findings (Zee *et al.*, 1981).

In a second lesion experiment, a careful study of the effects of disabling the neural integrator on the VOR, OKR, gazing holding, and smooth pursuit appeared in (Cannon and Robinson, 1987). In our model, disabling the neural integrator corresponds to removing the observer (6.4.6a) and setting $u_b = -\alpha_{\text{VOR}}\dot{x}_h$. For experiments conducted in total darkness, also $u_c = 0$. Therefore, in darkness the eye evolves according to dynamics $\dot{x} = -K_x x - \alpha_{\text{VOR}}\dot{x}_h$. Comparing with the normal eye dynamics in darkness: $\dot{x} = -\widetilde{K}_x x - \alpha_{\text{VOR}}\dot{x}_h$, we notice the change is

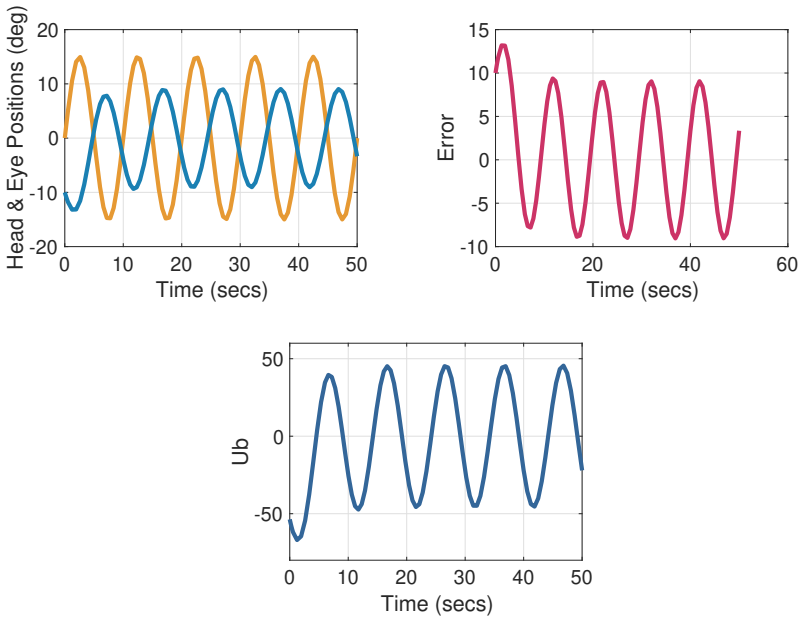

Figure 6.8: VOR cancellation with the cerebellum disabled. The top left figure shows the head (yellow) and eye (blue) angles. The eye no longer remains stationary in order to track a head fixed target because the cerebellar output that cancels the effect of the brainstem component of the VOR has been removed. The top right figure shows that the retinal error e does not go to zero. The bottom figure shows the brainstem component u_b, which drives the eye to move sinusoidally opposite to the head.

in the constant $\widetilde{K}_x = 0.05K_x \ll K_x$, where $\widetilde{K}_x$ was selected to approximate the known time constant of the combined oculomotor plant and neural integrator. For instance, for gaze holding with the head stationary, the eye drifts back to center with the time constant of the oculomotor plant. If the head angular velocity is a constant $\dot{x}_h = v$, then the eye position converges exponentially to $\overline{x} = -\alpha_{\text{VOR}} v/K_x$, rather than approximately tracking a ramp (with a very slow exponential decay). This is the behavior recovered in experiments (Cannon and Robinson, 1987): a step of constant head velocity in total darkness evokes a step change in eye position, not in eye velocity.

A further study of the effects of disabling the neural integrator on the VOR, OKR, and smooth pursuit in monkeys appeared in (Kaneko,

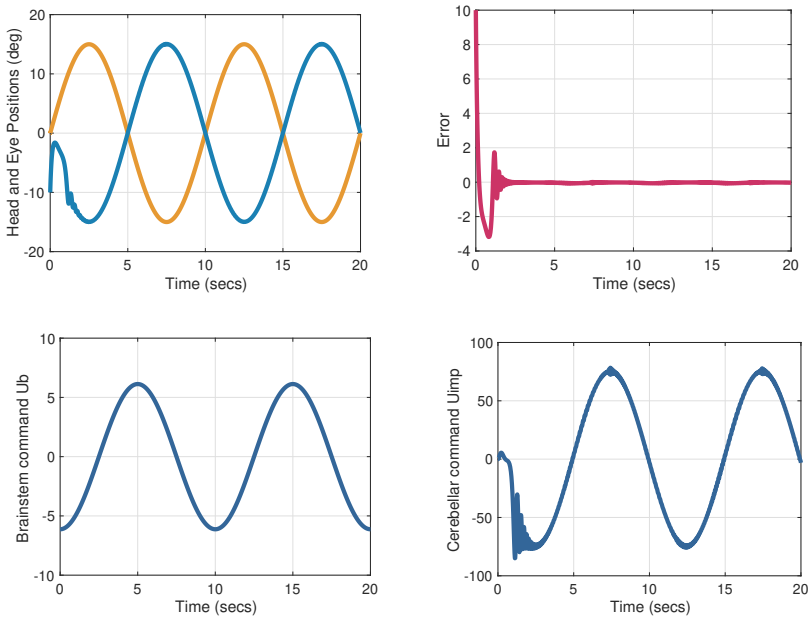

Figure 6.9: VOR with the neural integrator disabled. The top left figure shows the head (yellow) and eye (blue) angles, with the eye moving opposite to the head in this standard VOR experiment. The neural integrator has been disabled, so there is no signal $\alpha_x \hat{x}$ in the brainstem component u_b. Nevertheless the VOR operators as normal, modulo some possibly different transient behavior. The top right figure shows the error tends to zero. The bottom figures are u_b and u_{im}. The brainstem component u_b is unaffected by removing the neural integrator, while the cerebellar component u_{im} must now compensate for the change in disturbances affecting the system caused by removal of the neural integrator.

1999). They found these systems are minimally affected after a recovery period. Our model predicts that in the light, the cerebellum will compensate for the additional disturbances arising from the removal of the term $-\alpha_x \hat{x}$, such that the VOR is only mildly affected, as reported in (Kaneko, 1999). Figure 6.9 shows the behavior of the VOR in the light with the neural integrator disabled, with $x_h(t) = a_h \sin(\beta_h t)$, $a_h = 15$, and $\beta_h = 0.1$Hz for $t \in [0, 20]$. We observe the eye moves opposite to the head rotation, as expected.

We conclude the discussion of the VOR with experiments that blur the boundaries between the different eye movement systems. The optoki-

netic reflex is elicited by movement of large objects in the visual field or movement of the visual surround; it operates in tandem with the VOR. The driving signal of the OKR is different than the VOR, so strictly speaking it requires a separate model, developed in Chapter 7. However, OKR experiments may invoke the VOR, gaze holding, or smooth pursuit.

In many OKR experiments, the eyes must track a drum-fixed light slit with the head stationary and the optical drum rotating sinusoidally. In this case the error is $e = r - x$, where $r(t) = a_h \sin(\beta_h t)$. We treat this situation as being the same as smooth pursuit, to be discussed below. In an experiment called *OKR cancellation*, a light spot at $r = 0$ is placed in front of a moving striped optical drum. In this case, the pursuit system appears to override the OKR, as the eyes fixate on the fixed light spot, and the error is $e = -x$. If there is no head rotation, then this situation is the same as gaze holding, discussed in the next subsection.

In an experiment called *visual-vestibular conflict* the head and the optokinetic drum are mechanically coupled so that they rotate together, and the eyes must track a light strip on the drum (Baarsma and Collewijn, 1974). Therefore, we have $r(t) = x_h(t) = a_h \sin(\beta_h t)$, so $e = r - x_h - x = -x$. From the point of view of our mathematical model, this situation is no different than VOR cancellation. It has been reported that under such stimulation, the modulation of the firing rate of the cerebellum is larger than when the drum is not rotated (Waespe and Henn, 1978a); that is, when $r(t) = 0$, $x_h(t) = a_h \sin(\beta_h t)$, and $e = -x_h - x$.

In the context of our model, this finding makes sense. In the first case, the role of u_{im} is to cancel the term $\alpha_{\text{VOR}} \dot{x}_h$. In the second case, the role of u_{im} is to cancel the term $-(1 - \alpha_{\text{VOR}})\dot{x}_h - \widetilde{K}_x x_h$. Assuming that α_{VOR} is not close to 0.5 and that $\widetilde{K}_x$ is close to zero, the amplitude of the latter term is larger than the amplitude of the former. Figure 6.10 illustrates this comparison for values $\alpha_{\text{VOR}} = 0.9$; $a_h = 15$; $\beta_h = 0.2$Hz; $r = x_h = a_h \sin(\beta_h t)$ for $t \in [0, 15]$; and $r = 0$, $x_h = a_h \sin(\beta_h t)$ for $t \in [15, 30]$.

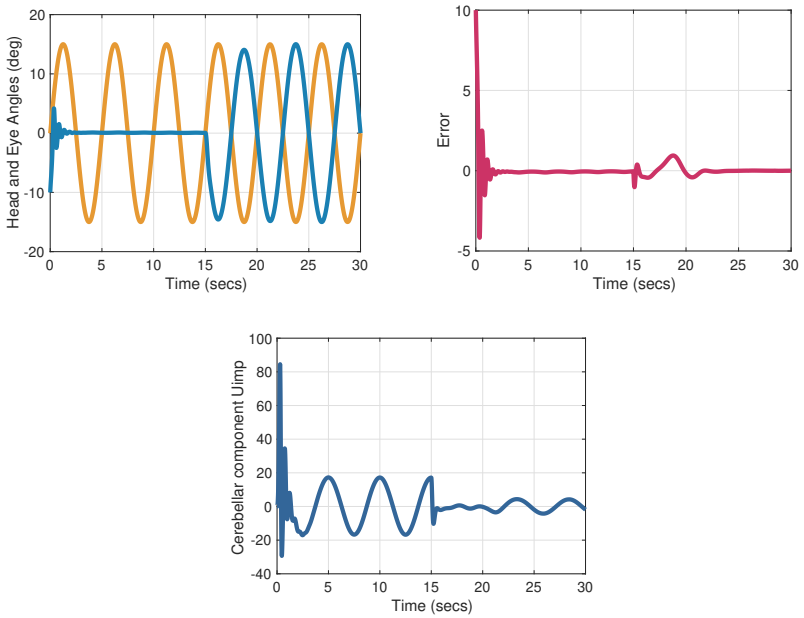

Figure 6.10: Visuo-vestibular conflict in the OKR and its effect on the depth of modulation of the cerebellar output u_{im}. The top left figure shows the head (yellow) and eye (blue) angles. The top right figure shows the retinal error (red). The bottom figures are u_b and u_{im}. During $t \in [0, 15]$, the eye must track a head fixed sinusoidally rotating target (a light strip on an optical drum), while during $t \in [15, 30]$, the eye must track a stationary target while the head is sinusoidally rotating. The bottom figure shows that the depth of modulation of the cerebellar output u_{im} is larger when the eye must track a head fixed target, even though the eye is not moving, than during the standard VOR experiment, when the eye does move. This behavior corresponds to experimental findings.

6.6.2 Gaze Fixation

The purpose of the *gaze fixation* or *gaze holding system* is to stabilize the gaze on a stationary object. Gaze holding has been described as a distributed brain function, involving the oculomotor plant, the brainstem, and the cerebellum, and consisting of three time constants (Leigh and Zee, 2015; Glasauer, 2003). The first time constant may be measured in darkness with the eye in an eccentric position at lights out, in an animal whose NPH has been lesioned (Cannon and Robinson, 1987). With the head stationary, $u_b = 0$. Also $u_c = 0$ because the cerebellum

(flocculus) is inactive in darkness. Then the eye evolves according to the dynamics $\dot{x} = -K_x x$, so the first time constant of gaze holding is $\tau_x = 1/K_x$, the time constant of the oculomotor plant itself. The second time constant is measured in normal (un-lesioned) subjects with the lights out. Then $u_b = \alpha_x \hat{x}$ and $u_c = 0$. Assuming $\hat{x}(t) \simeq x(t)$, the eye evolves according to dynamics $\dot{x} = -\widetilde{K}_x x$, so the second time constant of gaze holding is $\tilde{\tau}_x := 1/\widetilde{K}_x$, the time constant of the combined oculomotor plant and neural integrator.

The third time constant is measured in the light while the subject fixates on a stationary target at an eccentric position. Suppose $r \neq 0$ is constant and $x_h = 0$. Assuming that $\hat{x}(t) \simeq x(t)$, the error dynamics (6.4.2) take the form

$$\dot{e} = -\widetilde{K}_x e - u_c + \widetilde{K}_x r \,. \tag{6.6.2}$$

We see that to make the error go to zero it is necessary that $u_{im} \simeq \widetilde{K}_x r$. Then the eye will evolve according to the dynamics $\dot{x} = -\widetilde{K}_x (x - r) + K_e e$. In particular, the steady-state value of x is r, so our model predicts an infinite time constant for gaze holding in the light. In practice, this time constant is closer to 25s, potentially depending on the subject's fatigue.

Because the cerebellar component u_{im} must cancel a disturbance $\widetilde{K}_x r$ for gazing holding, the output of the PCs will be proportional to the eye position. This behavior is observed experimentally in many studies (Noda and Suzuki, 1979). Figure 6.11 shows the behavior for three target angles: $r(t) = 5^\circ$ for $t \in [0, 15]$; $r(t) = 10^\circ$ for $t \in [15, 30]$, and $r(t) = 15^\circ$ for $t \geq 30$.

Further evidence that $\widetilde{K}_x \neq 0$ comes from studies in which the cerebellum is disabled, either through ablation or disease. It is well known that in this case, in the light the eye has a slow drift back to the central position $x = 0$ (Carpenter, 1972; Noda and Suzuki, 1979; Robinson, 1974; Skavenski and Robinson, 1973; Zee *et al.*, 1976). In this case, $x_h = 0$, $u_c = 0$, and $u = u_b = \alpha_x \hat{x}$. Assuming $\hat{x}(t) \simeq x(t)$, the eye position evolves according to the dynamics $\dot{x} = -\widetilde{K}_x x$, the same model as in the dark, discussed above. Thus, the eye drifts back to center at an exponential rate determined by $\widetilde{K}_x$. Figure 6.12 depicts this behavior

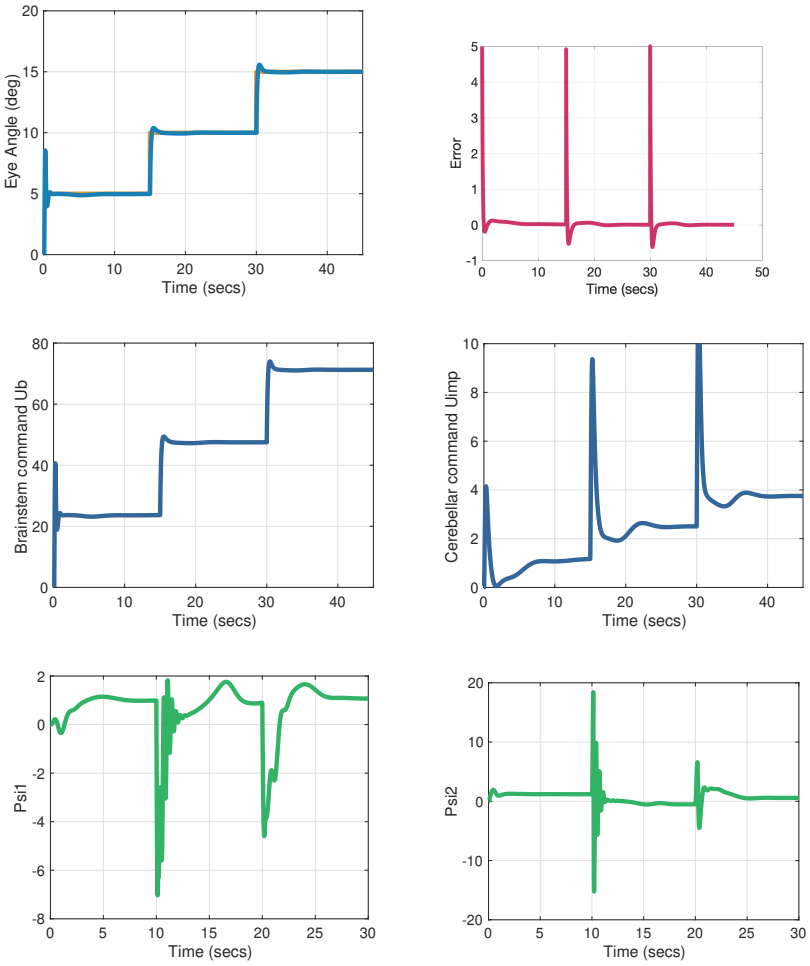

Figure 6.11: Gaze holding. The top left figure shows the head (yellow) and eye (blue) angles, with the eye holding three different eccentric positions. The top right figure shows the error tends to zero after each gaze shift. The middle figures are u_b and u_{im}. The brainstem component is $u_b = \alpha_x \hat{x}$, since there is no head movement, so its value is proportional to the eye angle. The cerebellar component u_{im} is also proportional to the eye angle, consistent with experimental findings. The bottom figures are the parameter estimates $\hat{\psi}_1$ and $\hat{\psi}_2$.

for the same target angles as in Figure 6.11.

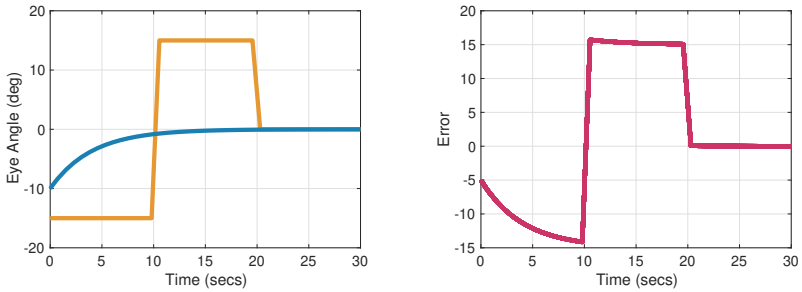

Figure 6.12: Gaze holding with the cerebellum disabled. The left figure shows the target (yellow) and eye (blue) angles, with the target in three different positions. We observe that without the cerebellum, the eye drifts back to center and is not able to hold the gaze on eccentric targets. The right figure shows the error does not tend to zero following a gaze shift to an eccentric target.

6.6.3 Smooth Pursuit

The purpose of the *smooth pursuit system* is to keep a moving object centered on the fovea. Experiments with the smooth pursuit system may be categorized, analogously with the VOR, as behavioral, neurological, and lesion experiments.

Figure 6.13 depicts a standard behavioral experiment for smooth pursuit of a sinusoidal target $r(t) = a_h \sin(\beta_h t)$, with $a_h = 15$, $\beta_h = 0.1$Hz for $t \in [0, 10]$ and $\beta_h = 0.2$Hz for $t \in [10, 20]$. We see that the cerebellar output u_{im} is strongly modulated during tracking of a sinusoidal target, as observed experimentally (Lisberger, 2009). Figure 6.14 depicts the transient response for smooth pursuit of a ramp target $r(t) = vt$ with $v = 5, 10, 20, 30$. This transient response matches that reported in Figure 3 in (Robinson *et al.*, 1986). Similar behavior is reported in (Wyatt and Pola, 1983a).

The perfect tracking capability of the smooth pursuit system has been well documented over the years; a small sampling includes (Bahill and McDonald, 1983a; Collewijn and Tamminga, 1984; Deno *et al.*, 1995; Wyatt and Pola, 1988). This tracking capability improves as the target motion becomes more predictable (Bahill and McDonald, 1983b). Figure 6.15 depicts the behavior of our model for smooth pursuit of a target $r(t) = a_1 \sin(2\pi\beta_1 t) + a_2 \sin(2\pi\beta_2 t)$, with $a_1 = 4.85$, $\beta_1 = 0.22$Hz,

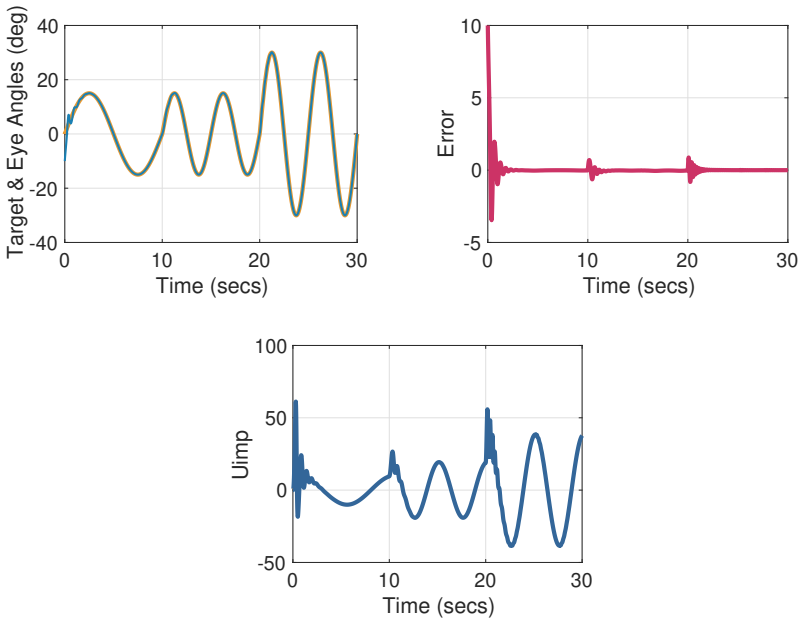

Figure 6.13: Smooth pursuit of a sinusoidal target. The top left figure shows the target (yellow) and the eye (blue) angles, for three frequencies of sinusoidal motion of the target. The blue and yellow plots are almost overlayed due to the near perfect tracking capability of the human eye. The top right figure shows the error, with transients introduced each time the frequency of the sinusoidal tracking signal is changed. The bottom figure shows the output of the cerebellum, which modulates according to the frequency of the target motion.

$a_2 = 0.853$ and $\beta_2 = 1.25$Hz. The time interval $t \in [9, 18]$ was chosen to match the data in Figure 1 of (Barnes *et al.*, 1987). This simulated behavior reproduces what is observed in experiments; namely, that while humans are not capable of perfect tracking of a sum of two or more sinusoids, nevertheless the smooth pursuit system performs reasonably well. The non-zero error displayed in the center of Figure 6.15 is corroborated by experimental findings in (Barnes *et al.*, 1987).

Figure 6.16 depicts the behavior of our model for smooth pursuit of a target $r(t) = a_1 \sin(2\pi\beta_1 t) + \cdots + a_4 \sin(2\pi\beta_4 t)$, with $a_1 = 6.94$, $\beta_1 = 0.214$Hz, $a_2 = 2.86$, $\beta_2 = 0.519$Hz, $a_3 = 2.11$, $\beta_3 = 0.702$Hz, $a_4 = 1.57$, and $\beta_4 = 0.946$Hz. The results are comparable to those obtained experimentally as shown in Figure 2 of (Collewijn and Tam-

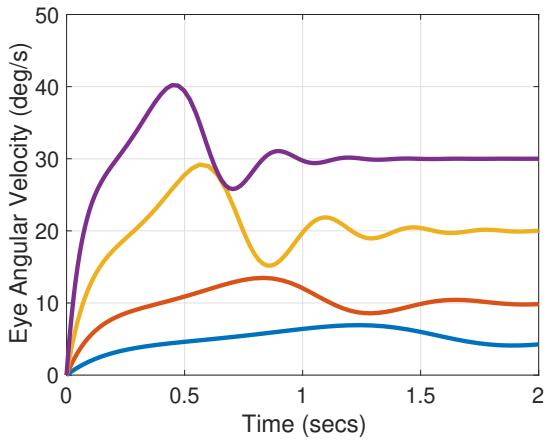

Figure 6.14: Smooth pursuit of a ramp target with velocity $v = 5, 10, 20, 30$ (blue, red, yellow, purple). The figure shows the characteristic transients associated with the onset of smooth pursuit, as recorded in experiments.

minga, 1984).

It is known that the processing delay for the retinal error to arrive at the cerebellum is on the order of 100ms. Nevertheless, the smooth pursuit system achieves nearly perfect tracking capability; its ability to do so in the face of this delay has been interpreted as a predictive capabability (Deno *et al.*, 1995). Our model does not impart any prediction to the smooth pursuit system, but the presence of the adaptive internal model aids in overcoming delays. Figure 6.17 depicts the behavior when tracking a sinusoidal target $r(t) = a\sin(2\pi\beta t)$ with $a = 10$ and $\beta = 0.1$Hz. The error e has been replaced by $e(t - \tau)$ with a time delay of $\tau = 107$ms. The other parameter values are the same as before but we set $K_e = 8$ for closed-loop stability. We observe there is little degradation in the system's tracking capability.

The choice of K_e to achieve closed-loop stability is tied to the time delay and the magnitude of the reference $r(t)$. Figure 6.18 depicts the largest delay attained with the smallest K_e for varying frequencies and amplitudes of reference signals of the form $r(t) = a\sin(2\pi\beta t)$. With $a = 10$ and $\beta = \{0.1, 0.2\}$Hz, delays of 107ms and 67ms were achieved with K_e equal to 8 and 13, respectively. Holding $\beta = 0.1$Hz but with

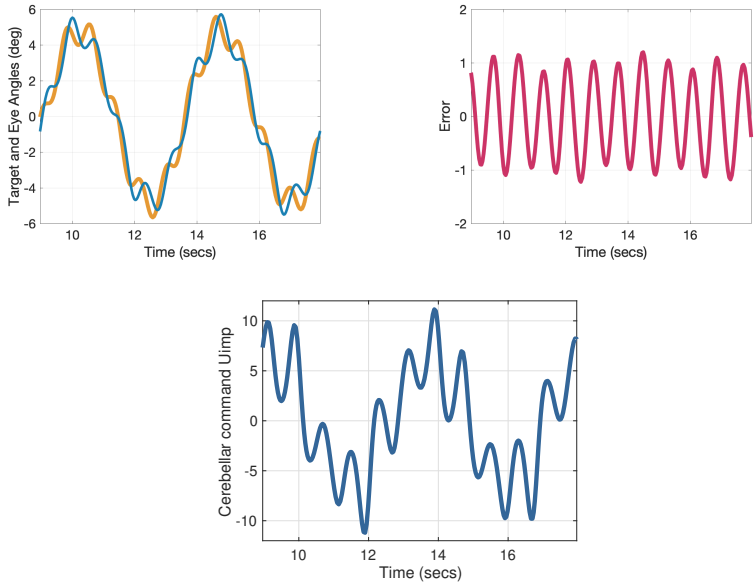

Figure 6.15: Smooth pursuit of a sum of two sinusoids. The top left figure shows the target (yellow) and the eye (blue) angles, as the eye tracks a target whose motion is the sum of two sinusoids. We observe that the eye is no longer able to achieve perfect tracking. The error in the top right figure does not tend to zero asymptotically. The cerebellar output u_{im} is shown in the bottom figure.

$a = \{5, 10, 20\}$, the model overcomes delays of 197ms, 107ms, and 56ms with K_e equal to 5, 8 and 15, respectively.

The *error clamp* experiment explores the role of the error signal using a technique called *retinal stabilization* (Barnes *et al.*, 1995; Morris and Lisberger, 1987; Stone and Lisberger, 1990). A monkey is trained to track a visual target moving at constant speed. After reaching steady-state, the retinal error is optically clamped at zero using an experimental apparatus that places the target image on the fovea. In experiments it is observed that the eye continues to track the target for some time after. Figure 6.19 depicts the error clamp behavior with our model, showing that the eye continues to track the target despite the error being clamped at $e \equiv 0$ during the time interval $t \in [5, 6]$.

In another series of experiments researchers explored the difference be-

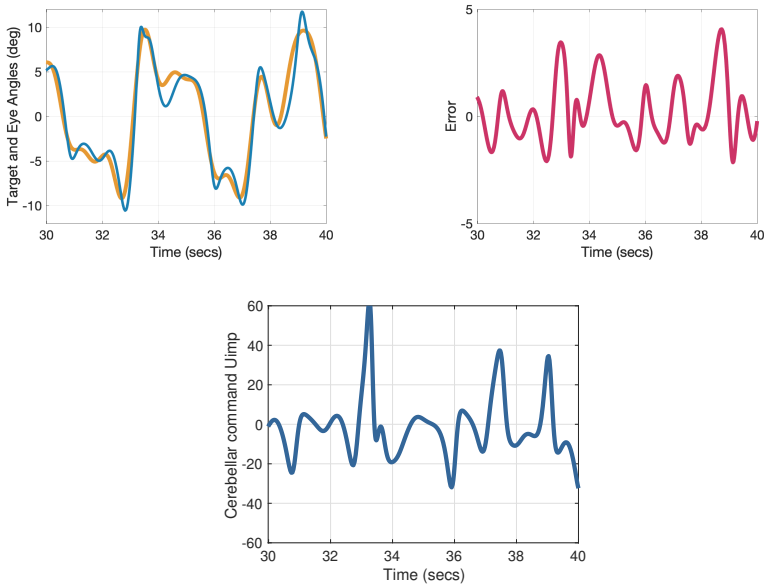

Figure 6.16: Smooth pursuit of a sum of four sinusoids. The top left figure shows the target (yellow) and eye (blue) angle, as the eye tracks a target whose motion is the sum of four sinusoids. The eye is no longer able to achieve perfect tracking, and the error in the top right figure does not go to zero asymptotically. The cerebellar output u_{im} is shown in the bottom figure.

tween *target stopping* and *target blanking*. In target stopping, a target with a ramp position is abruptly stopped. It is demonstrated experimentally that during target stopping, the oculomotor system switches from smooth pursuit to gaze holding (Krauzlis and Miles, 1996; Luebke and Robinson, 1988; Robinson *et al.*, 1986). In target blanking the target is blanked out or occluded, so that it is no longer visible. It is shown experimentally that with target blanking the eye continues to track for some time (Cerminara *et al.*, 2009; Churchland *et al.*, 2003).

Figure 6.20 depicts target stopping, in which $r(t) = 10t$ for $t \in [0, 2]$, and $r(t) = 20^\circ$ for $t \geq 2$. We observe that the error decays to zero with an exponential envelope after target stopping, as expected for the gaze holding system. Target blanking may be interpreted in our model as a zero error signal. As we have seen from the results of the error clamp experiment, depicted in Figure 6.19, the smooth pursuit system

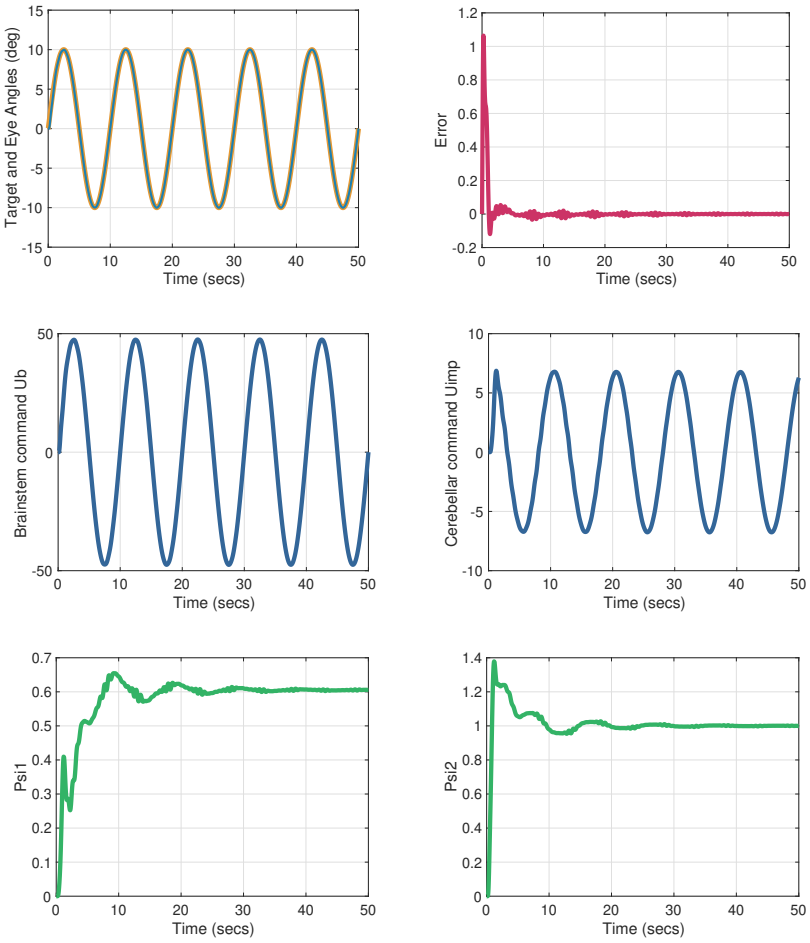

Figure 6.17: Smooth pursuit of a sinusoidal target with a time delay of 107ms in the retinal error signal. The top left figure shows the target (yellow) and eye (blue) angle, as the eye tracks a sinusoidally moving target. A time delay of 107ms is introduced in the measurement of the retinal error. The top right figure shows that the retinal error tends to zero, despite some additional transients. The middle figures show u_b and u_{im}. The brainstem component u_b is modulated according to the eye position (the head is stationary), while the cerebellar component is modulated according to the target movement. The bottom figures are the parameter estimates $\hat{\psi}_1$ and $\hat{\psi}_2$.

continues to track for some time.

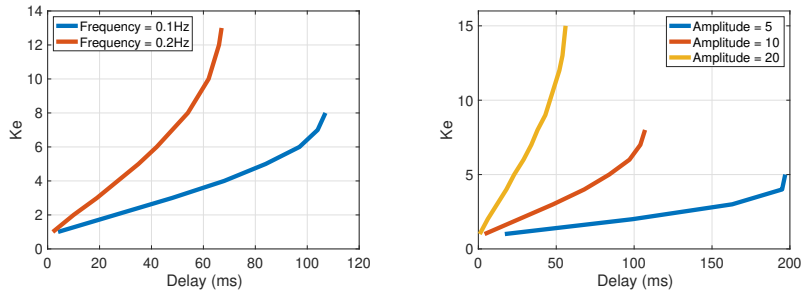

Figure 6.18: Maximum time delay as a function of K_e. The figures show the relationship between the feedback gain K_e and the time delays that can be tolerated in the closed-loop system. The left figure shows the smallest value of K_e required to maintain closed-loop stability as a function of the time delay in the retinal error for two different frequencies of a sinusoidally moving target. The right figure shows the smallest value of K_e required to maintain closed-loop stability as a function of the time delay in the retinal error and as a function of the amplitude of the sinusoidal target motion.

6.7 Final Remarks

We presented a model of the slow eye movement systems, specifically the VOR, smooth pursuit, and gaze holding, along with proposed computations for the cerebellum. Despite being fairly simple, the model captures many of the behaviors of these eye movement systems in a unified framework.

Two internal model designs were presented in (6.4.6b)-(6.4.6g) and (6.4.7b)-(6.4.7c). An important open problem is to determine which model (if either) is more accurate in terms of the cerebellar microcircuit. If it is the first model, then an open problem is to discover the adaptive brain process that allows the filters (6.4.6b) - (6.4.6e) to *synchronize* to identical parameter values in the pair (F, G).

Our current model of the slow eye movement systems does not account for *long term adaptation* of relevant parameters. Parameters that are subject to long-term adaptation are the VOR gain α_{VOR} and the gain associated with the neural integrator α_{x}. Similiarly, the model does not capture how the brainstem neural integrator parameters in (6.4.6a) are adapted to match the parameters of the oculomotor plant. Investigating

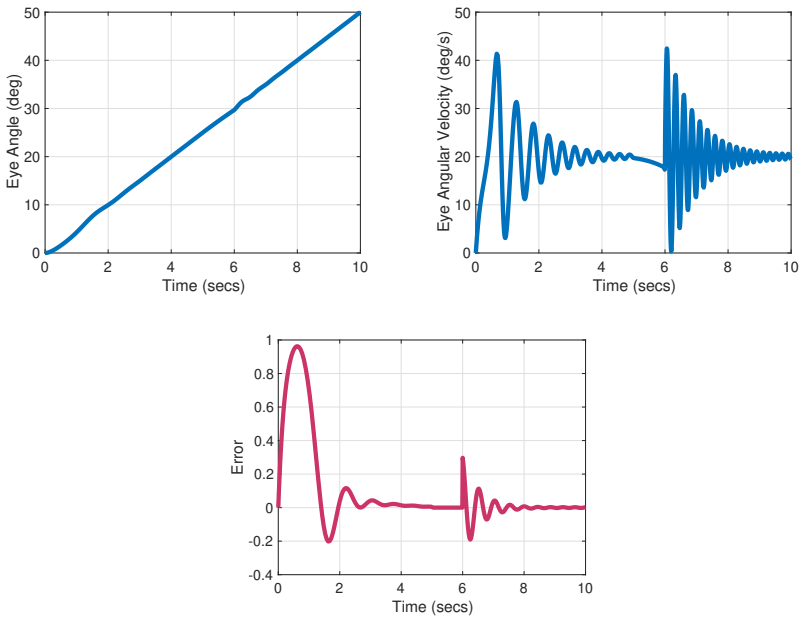

Figure 6.19: Smooth pursuit with an error clamp during $t \in [5, 6]$s. The top left figure shows the eye angle as the eye tracks a constant velocity target. During $t \in [5, 6]$s, the error is artificially clamped at zero by the experimental apparatus, yet the eye continues to track the target. The effect is observed in the bottom figure, which shows the error (difference between target and eye angles for the true target position). The top left figure shows some disturbance in the eye velocity when the error clamp is removed at $t = 6$s.

the adaptive brain processes by which these parameters are calibrated is an interesting avenue of future avenue of future work.

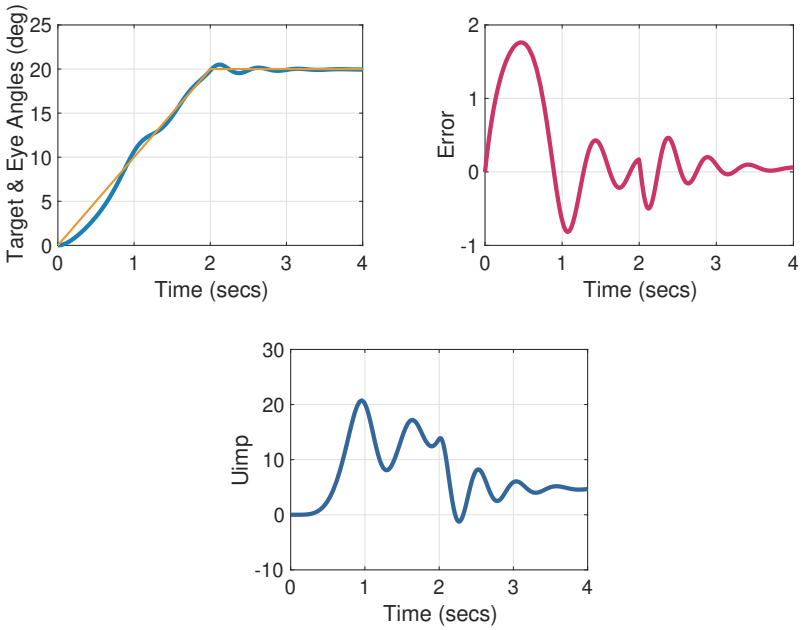

Figure 6.20: Smooth pursuit with target stopping at $t = 2$s. The top left figure shows the target (yellow) and eye (blue) angle. During $t \in [0, 2]$s, the eye tracks a constant velocity target. The target then stops, and the oculomotor system switches to gaze holding. Such behavior is not observed if the target is removed at $t = 2$s. The top left figure shows the error (red). The bottom figure is the cerebellar output u_{im}.

7

Optokinetic System

In the previous chapter we considered a model of a part of the cerebellum, the floccular complex (FC), involved in regulation of the vestibulo-ocular reflex, smooth pursuit, and gazing hold eye movement systems. This chapter examines a second functional module of the cerebellum, the nodulus-uvula (NU) which is responsible for regulating *the optokinetic system*.

The optokinetic system is an eye movement system to stabilize vision on a full-field moving visual surround. This eye movement system contrasts with the eye movement systems of the previous chapter whose goal is to stabilize on object on the fovea. The optokinetic system utilizes visual information impinging not only near the fovea but also on the periphery of the retina (Leigh and Zee, 2015). How the optokinetic system interacts with the other eye movement systems is of great interest scientifically, but also theoretically from the perspective of control theory: can parallel adaptive internal models work collaboratively to regulate the same error? Or does the brain utilize a switching mechanism to switch from one adaptive internal model to the other, reminiscent of switched system architectures for adaptive control (Narendra and Annaswamy, 1989)? Before such interesting questions can be ad-

dressed, we require a model of the optokinetic system that specifically takes account of the computations of the cerebellum.

Pioneering experimental work in the 1970's on the optokinetic system (Cohen *et al.*, 1977; Raphan *et al.*, 1979; Waespe and Henn, 1978a; Waespe and Henn, 1978b) lead to the discovery of the *velocity storage mechanism* (VSM), a behavior in which eye velocity is stored while following a constant velocity visual surround, even with intervening *saccades* (a fast reset of eye position) in a behavior called *nystagmus*. A striking feature of the VSM is that it partially fulfills the requirements of the internal model principle, as if evolution made a primitive attempt at architecting a neural internal model for this motor system.

Despite a comprehensive experimental record exposing all major behaviors of the optokinetic system, to this day, the two most important models of the optokinetic system (Cohen *et al.*, 1977; Robinson, 1981) do not incorporate the computations of the cerebellum. This chapter develops a model of the optokinetic system for horizontal eye motion based on regulator design III.

7.1 Oculomotor Plant and Brainstem

In Chapter 6 we presented an open-loop model of the oculomotor plant and brainstem

$$\begin{aligned} \dot{x} &= -K_x x + u \\ \dot{\hat{x}} &= -K_x \hat{x} + u \\ u_b &= \alpha_{\text{x}} \hat{x} - \alpha_{\text{VOR}} \dot{x}_h \,, \end{aligned}$$

where $x \in \mathbb{R}$ is the horizontal eye angle, $\hat{x}$ is the estimate of x provided by the neural integrator (6.3.2), and $\dot{x}_h$ is the horizontal head angular velocity. The signal u_b is the brainstem-only contribution to the motor command u. The parameter α_{VOR} is called the *VOR gain*.

This open-loop model must be extended to include aspects of the optokinetic system. First, the optokinetic system includes behaviors such as *nystagmus*, consisting of both fast and slow phases of eye motion, so a more suitable model of the oculomotor plant is a second-order model

(Sylvestre and Cullen, 1999). Second, the optokinetic system is known to be supported by a so-called *velocity storage integrator*, which can be modeled as a leaky integrator (Cohen *et al.*, 1977; Raphan *et al.*, 1979). Third, to support the *optokinetic reflex*, the brainstem-only pathway has a feedforward component of the *retinal slip velocity*, given by

$$e := \dot{x}_w - \dot{x}_h - \dot{x}\,.$$

Signal $\dot{x}_w(t) \in \mathbb{R}$ is the horizontal angular velocity of the visual field, and $\dot{x}$ is the horizontal angular eye velocity. A non-zero $\dot{x}_w$ is induced in experiments when a subject is seated inside a rotating optical drum.

Taken together, the open-loop model of the oculomotor plant and brainstem for the optokinetic system is

$$\begin{aligned}
\dot{x}_1 &= x_2 && \text{(7.1.2a)}\\
\dot{x}_2 &= \alpha_2(-x_2 - K_x x_1 + u) && \text{(7.1.2b)}\\
\dot{\hat{x}} &= -K_x\hat{x} + u && \text{(7.1.2c)}\\
\dot{v} &= -K_v v + K_v e && \text{(7.1.2d)}\\
u_b &= \alpha_{\text{x}}\hat{x} - \alpha_{\text{VOR}}\dot{x}_h + \alpha_{\text{OK}} e + \alpha_{\text{v}} v\,. && \text{(7.1.2e)}
\end{aligned}$$

Equations (7.1.2a)-(7.1.2b) comprise the second-order model of the oculomotor plant. Equation (7.1.2c) is the brainstem neural integrator. Equation (7.1.2d) is the *velocity storage integrator*. Signal $x_1 = x$ is the eye angle; $x_2 = \dot{x}$ is the eye angular velocity; u is the motor command, now regarded as an acceleration input; v is the state of the velocity storage integrator; $\alpha_{\text{OK}} e$ captures the drive provided by the optokinetic reflex, where α_{OK} is the called the *optokinetic gain*; the vestibulo-ocular reflex is modeled by $\alpha_{\text{VOR}}\dot{x}_h$, where α_{VOR} is the VOR gain; and $\alpha_{\text{v}} v$ captures the drive provided by the velocity storage integrator. The brainstem-only component of the motor command is u_b. Nominal parameter values are $K_x \simeq 5$, $\alpha_{\text{x}} \simeq 0.95 K_x$, $K_v \simeq 0.05$, $\alpha_2 \simeq 250$, $\alpha_{\text{OK}} = 1$, $\alpha_{\text{v}} = 10$, and $\alpha_{\text{VOR}} = 0.65$.

7.2 Cerebellum

Next we model the cerebellar contribution to the optokinetic system. Experimental and physiological evidence supports the idea that the

driving signal of the optokinetic system is the retinal slip velocity (Robinson, 1981). Moreover, this is the error signal that the cerebellum regulates to zero. This choice of error signal partitions the work of the cerebellum so that the nodulus/uvula (NU) regulates a velocity error, while the floccular complex (FC) regulates a positional error. This neat division is likely an oversimplification; however, the underlying philosophy that each cerebellar module is dedicated to one type of error signal is well supported by anatomical findings in which the topographic layout of the inferior olive is matched to the topography of the cerebellum (Apps *et al.*, 2018; Houck and Person, 2014; Houck and Person, 2015).

The error model associated with the NU is

$$\dot{e} = -\alpha_2 e - \alpha_2 u + \alpha_2 K_x x_1 + \ddot{x}_w - \ddot{x}_h + \alpha_2 \dot{x}_w - \alpha_2 \dot{x}_h \,.$$

The motor command is split as

$$u = u_b + u_s + u_{im} \,,$$

where u_s is a component for closed-loop stability, and u_{im} is the output of the NU. Because the error model is already highly stable due to the large value of α_2, we assume $u_s = 0$. Substituting u_b in the error model and assuming $\hat{x}(t) \equiv x_1(t)$, we have

$$\begin{aligned} \dot{e} \;\; = \;\; & -\alpha_2(1+\alpha_{\text{OK}})e - \alpha_2 u_{im} + \alpha_2 \widetilde{K}_x \hat{x} \\ & - \alpha_2(1-\alpha_{\text{VOR}})\dot{x}_h - \alpha_2 \alpha_{\text{V}} v + \alpha_2 d \,, \end{aligned} \tag{7.2.1}$$

where

$$d := \frac{1}{\alpha_2}[\ddot{x}_w - \ddot{x}_h] + \dot{x}_w$$

is the disturbance that must be rejected. This model may be regarded as a first-order model of velocity error dynamics, despite the fact that it includes a positional term $\alpha_2 \widetilde{K}_x \hat{x}$ arising from an incomplete cancellation of the drift term $K_x x_1$ of the oculomotor plant by the neural integrator (7.1.2c). Because the eye position is constantly reset during nystagmus, x_1 remains small. We therefore treat the positional term as a bounded disturbance acting on the velocity error dynamics. We assume this extra disturbance is not rejected by the cerebellum, so some

small steady-state errors will remain and a modified stability analysis will be required.

Remark 7.1. When we wrote the error model (7.2.1) a decision was taken about what disturbances the cerebellum cancels. An alternative error model is

$$\dot{e} = -\alpha_2(1+\alpha_{\text{ok}})e - \alpha_2 u_{im} + \alpha_2 \widetilde{K}_x \hat{x} - \alpha_2 \alpha_{\text{v}} v + \alpha_2 d\,.$$

Now the disturbance to be cancelled is

$$d := \frac{1}{\alpha_2}[\ddot{x}_w - \ddot{x}_h] + \dot{x}_w + (1-\alpha_{\text{vor}})\dot{x}_h\,,$$

so the NU picks up more disturbance rejection work by canceling the part of the head velocity signal not already rejected by the brainstem VOR. Either error model may be used, with neglible effect on the design of the regulator. The choice of error model will ultimately depend on how the FC and the NU share the task of rejecting the head velocity disturbance. We choose to work with (7.2.1) due to considerations about the neural circuit, to be discussed below. ◁

Experimental evidence supports the idea that the NU is dedicated to constant velocity disturbances (Heinen and Keller, 1996); whereas the FC handles sinusoidal disturbances as well. Thus, we assume the exosystem associated with the NU is first order:

$$\dot{w} = Fw + Gd \tag{7.2.2}$$
$$d = \psi w\,, \tag{7.2.3}$$

where $w \in \mathbb{R}$, F is Hurwitz, and (F, G) is a controllable pair.

For the internal model we use a modification of the extended design in

Section 5.3

$$\begin{aligned}
\dot{w}_0 &= Fw_0 + FGe && \text{(7.2.4a)}\\
\dot{w}_1 &= Fw_1 - Ge && \text{(7.2.4b)}\\
\dot{w}_2 &= Fw_2 - Gu_{im} && \text{(7.2.4c)}\\
\dot{w}_3 &= Fw_3 - G\hat{x} && \text{(7.2.4d)}\\
\dot{w}_4 &= Fw_4 - G\dot{x}_h && \text{(7.2.4e)}\\
\dot{w}_5 &= Fw_5 - Gv && \text{(7.2.4f)}\\
\hat{w} &= \frac{1}{\alpha_2}w_0 + \frac{1}{\alpha_2}Ge - (1+\alpha_{\text{ok}})w_1 - w_2 && \text{(7.2.4g)}\\
&\quad + \widetilde{K}_x w_3 - (1-\alpha_{\text{vor}})w_4 - \alpha_{\text{v}} w_5\,.
\end{aligned}$$

This model includes several additional filters (7.2.4d)-(7.2.4f) to account for feedforward measurements $\hat{x}$, $\dot{x}_h$, and v, in order that their effect not be cancelled by the internal model. Taking the derivative of $\hat{w}$ and utilizing (7.2.1), we verify again

$$\dot{\hat{w}} = F\hat{w} + Gd\,.$$

Define the estimation error $\tilde{w} := w - \hat{w}$. Then $\dot{\tilde{w}} = F\tilde{w}$, and since F is Hurwitz, $\tilde{w}(t) \longrightarrow 0$. If the plant parameters were known, then $\hat{w}$ would provide a regressor for parameter adaptation. Since these parameters are not known, we used the extended regressor $\hat{w}_d$ and extended parameter vector ψ_d as in Section 5.3.1:

$$\begin{aligned}
\psi_d &:= \begin{bmatrix} \frac{1}{\alpha_2}\psi & -(1+\alpha_{\text{ok}})\psi & -\psi & \widetilde{K}_x\psi & -(1-\alpha_{\text{vor}})\psi & -\alpha_{\text{v}}\psi \end{bmatrix}\\
\hat{w}_d &:= (w_0 + Ge, w_1, w_2, w_3, w_4, w_5)\,.
\end{aligned}$$

Then

$$d = \psi w = \psi\hat{w} + \psi\tilde{w} = \psi_d\hat{w}_d + \varepsilon\,,$$

where $\varepsilon = \psi\tilde{w}$ vanishes exponentially. Then we choose

$$u_{im} = \hat{\psi}_d\hat{w}_d\,, \qquad \text{(7.2.5)}$$

where $\hat{\psi}_d$ is an estimate of the unknown parameters ψ_d. The parameter adaptation rule is

$$\dot{\hat{\psi}}_d = \gamma e\hat{w}_d^{\mathrm{T}}\,, \qquad \text{(7.2.6)}$$

where $\gamma > 0$ is the adaptation rate.

7.3 Stability Analysis

The stability analysis focuses on the case when there is no head movement, $\dot{x}_h = 0$. Also we only study the envelope behavior of the eye velocity (see Figure 7.2) by ignoring the velocity resets caused by saccades. This assumption is reasonable due to the very fast initial rise of velocity in the slow phases of nystagmus following a saccade due to the optokinetic reflex. While a full hybrid stability analysis would increase the rigor of our analysis, we believe it would not necessary add significantly to the plausibility of the model, which is our primary concern here.

We begin the analysis with a nominal case when $\widetilde{K}_x = 0$, meaning there is no perturbation due to eye position. Define the parameter estimation error $\widetilde{\psi}_d = \psi_d - \hat{\psi}_d$. Then the closed-loop system is

$$\dot{e} = -\alpha_2(1 + \alpha_{\text{ok}})e - \alpha_2\alpha_{\text{v}}v + \alpha_2\widetilde{\psi}_d\hat{w}_d \tag{7.3.1a}$$

$$\dot{v} = -K_v v + K_v e \tag{7.3.1b}$$

$$\dot{\widetilde{\psi}}_d = -\gamma e\hat{w}_d^{\mathrm{T}} . \tag{7.3.1c}$$

Note that we omitted the exponentially stable $\widetilde{w}$ dynamics, which do not affect the stability outcome. Define the state $\xi := (e, v) \in \mathbb{R}^2$. Then we can write (7.3.1) as

$$\dot{\xi} = A\xi + B\widetilde{\psi}_d\hat{w}_d \tag{7.3.2a}$$

$$e = C\xi \tag{7.3.2b}$$

$$\dot{\widetilde{\psi}}_d = -\gamma e\hat{w}_d^{\mathrm{T}} , \tag{7.3.2c}$$

where

$$A = \begin{bmatrix} -\alpha_2(1 + \alpha_{ok}) & -\alpha_2\alpha_{\text{v}} \\ K_v & -K_v \end{bmatrix} , \quad B = \begin{bmatrix} \alpha_2 \\ 0 \end{bmatrix} , \quad C = \begin{bmatrix} 1 & 0 \end{bmatrix} .$$

This model matches the standard error model (4.2.7) or (4.3.10), so it makes sense to explore if our model is SPR in order to apply stability results from Section 4.3.

Lemma 7.3.1. Consider the error model (7.3.2) with α_2, α_{ok}, α_{v}, $K_v > 0$. Then $H(s) = C(sI - A)^{-1}B$ is SPR.

Proof. According to Theorem 4.1.5, we must first verify A is Hurwitz. The characteristic polynomial is $\det(sI-A) = s^2+(K_v+\alpha_2(1+\alpha_{\text{ок}}))s+\alpha_2 K_v(1+\alpha_{\text{ок}}+\alpha_{\text{v}})$. Since the coefficients of this second-order polynomial are strictly positive, A is Hurwitz. Second, we verify condition (4.1.3). We compute

$$H(j\omega) = \frac{\alpha_2(j\omega + K_v)}{(\alpha_2 K_v(1+\alpha_{\text{ок}}+\alpha_{\text{v}}) - \omega^2) + j\omega(K_v + \alpha_2(1+\alpha_{\text{ок}}))}\,.$$

Then we have

$$\Re\left[H(j\omega)\right] = \frac{\alpha_2^2 K_v^2(1+\alpha_{\text{ок}}+\alpha_{\text{v}}) + \alpha_2^2\omega^2(1+\alpha_{\text{ок}})}{(\alpha_2 K_v(1+\alpha_{\text{ок}}+\alpha_{\text{v}}) - \omega^2)^2 + \omega^2(K_v+\alpha_2(1+\alpha_{\text{ок}}))^2} > 0\,,$$

where we use $\alpha_2, \alpha_{\text{ок}}, \alpha_{\text{v}}, K_v > 0$, by assumption. Finally, it is easily verified that (A, B) is controllable. By Theorem 4.1.5, $H(s)$ is SPR. □

Theorem 7.3.2. Consider the closed-loop system (7.3.2) with α_2, $\alpha_{\text{ок}}$, α_{v}, $K_v > 0$. Suppose $d \neq 0$ is a constant disturbance. Then the equilibrium $(\xi, \widetilde{\psi}_d) = (0, 0)$ is locally exponentially stable.

Proof. By Lemma 7.3.1, $H(s)$ is SPR. Since d is a non-zero constant disturbance, w is also constant and non-zero, so it trivially satisfies the PE condition (4.3.1), and $w, \dot{w} \in \mathcal{L}_\infty$. Also, $\hat{w}_d$ is PE by Lemma 4.3.3. By Theorem 4.3.8, the equilibrium $(\xi, \widetilde{\psi}_d) = (0, 0)$ is locally exponentially stable. □

Next we consider the closed-loop system

$$\dot{\xi} = A\xi + B\widetilde{\psi}_d\hat{w}_d + B\nu \tag{7.3.3a}$$

$$e = C\xi \tag{7.3.3b}$$

$$\dot{\widetilde{\psi}}_d = -\gamma e\hat{w}_d^{\mathrm{T}}\,, \tag{7.3.3c}$$

where $\nu := \widetilde{K}_x\hat{x}$ is regarded as a bounded, unmodeled disturbance.

The system (7.3.3) is said to be *input-to-state stable* (ISS) if there exists a class $\mathcal{KL}$ function $\beta_1(\cdot)$ and a class $\mathcal{K}$ function $\beta_2(\cdot)$ such that for any $(\xi(0), \widetilde{\psi}_d(0))$ and any $\widetilde{K}_x\hat{x} \in \mathcal{L}_\infty$,

$$\|\xi(t)\| \leq \beta_1\left(\|\xi(0)\|, t) + \beta_2(\sup_{0\leq\tau\leq t}\|\nu(\tau)\|\right)\,.$$

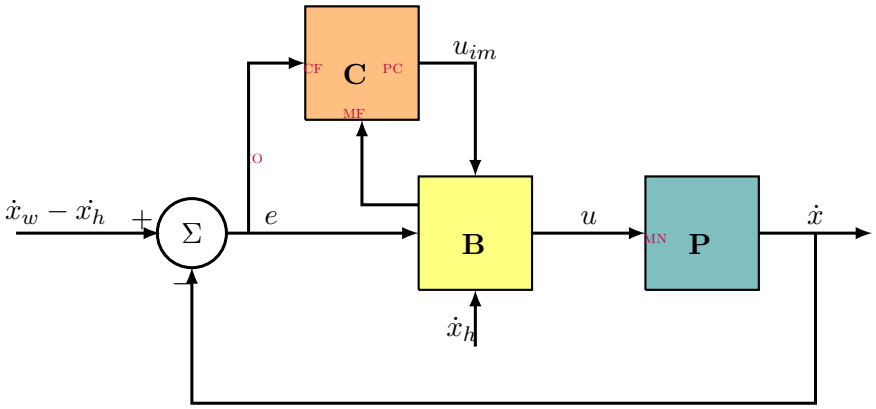

Figure 7.1: Control architecture for the optokinetic system consisting of the oculomotor plant (P), the brainstem (B), and the cerebellum (C). The retinal slip velocity e is the error signal to be regulated.

The following is an immediate application of Lemma 4.6 of (Khalil, 2001).

Theorem 7.3.3. Consider the closed-loop system (7.3.3) with α_2, α_{ok}, α_{v}, $K_v > 0$. Suppose $d \neq 0$ is a constant disturbance. Then (7.3.3) is ISS.

7.4 Neural Circuit

A high-level block diagram of the neural circuit of the optokinetic system is seen in Figure 7.1. The *visual cortex* processes visual signals arrriving from the retina by way of the optic nerve. The *nucleus of the optic tract* (NOT) projects to the *vestibular nuclei* (VN) of the *brainstem* (B). In particular, the NOT sends a measurement of *retinal slip velocity* to the VN (Büttner-Ennever and Horn, 1997). The brainstem comprises several regions (or functions) relevant to the optokinetic system: the VN, the *brainstem neural integrator* (NI), and the *velocity storage mechanism* (VSM). The VN act as hubs for signals to and from the cerebellum (see below). The NI provides an eye position signal (Kaneko, 1999). The VSM, also believed to be located in the VN (Robinson, 1981), provides "velocity storage" of a constant velocity vi-

sual surround - in essence approximating a pure integrator to track constant disturbances. Finally, the VN output is sent to the oculomotor neurons (MN) to stimulate the muscles and control eye movements (Leigh and Zee, 2015).

As already discussed, all modules of the cerebellum have two types of inputs: *mossy fiber* (MF) inputs and *climbing fiber* (CF) inputs. MF inputs to the NU include: primary afferents from the vestibular nerve (carrying a head velocity signal) (Barmack *et al.*, 1993); a signal from the VN; and a signal from the NI. The CF input to the NU comes from the NOT by way of the *inferior olive* (IO) (Barmack, 2006). Finally, the NU projects its sole output via its Purkinke cells (PCs) to the VN (Büttner and Büttner-Ennever, 2006).

A mapping between the neural circuit and signals in our model is as follows. Referring to (7.1.2e), the output of the neural integrator is the signal $\alpha_{\text{x}}\hat{x}$; the direct feedthrough of the retinal slip velocity to support the optokinetic reflex is the signal $\alpha_{\text{ok}}e$; and the output of the VSM is $\alpha_{\text{v}}v$. Signal e in (7.2.6) is the projection from the IO to the CF input of the cerebellum. Signals e, u_{im}, $\hat{x}$, $\dot{x}_h$, and v in (7.2.4) are the MF inputs to the cerebellum. The PC output of the cerebellum is u_{im}.

7.5 Simulations

The simulations include four basic behaviors of the optokinetic system: (i) OKN with constant stimulus velocity, both untrained and trained conditions; (ii) OKAN I in the dark, both untrained and trained conditions; (iii) OKAN suppression; and (iv) OKN suppression. An additional behavior called OKAN II is thought to arise from a process of long-term adaptation which, strictly speaking, lies outside our modeling work. Nevertheless, we provide a plausible argument to explain OKAN II. Therefore, we include a fifth behavior: (v) OKAN II.

Our simulations only account for the contribution of the NU, which is sufficient to elicit the main characteristics of the optokinetic system. The floccular complex also contributes lightly to the optokinetic system, so the simulations are to be interpreted as behavior with a lesioned

flocculus. Generally, lesion studies show that ablation of the flocculus and portions of the paraflocculus only tend to reduce OKN slow-phase eye velocities and leave OKAN unchanged (Zee *et al.*, 1981; Waespe *et al.*, 1983).

The parameter values used in the simulations are: $\alpha_2 = 250$, $K_x = 5$, $K_v = 0.05$, $\alpha_{\text{v}} = 10$, $\alpha_{\text{OK}} = 1$, $\alpha_{\text{VOR}} = 0.65$, $\alpha_{\text{x}} = K_x$, $F = -0.01$, $G = 0.01$, and $\gamma = 1e - 12$. The parameters α_2, K_x, and K_v were selected according to the known time constants of the oculomotor plant and the VSM. Parameters $\alpha_{\text{v}} = 10$, $\alpha_{\text{OK}} = 1$, and $\alpha_{\text{VOR}} = 0.65$ are all highly adaptable (through a process of long-term adaptation) and can be selected fairly arbitrarily. The choice $\alpha_{\text{x}} = K_x$ implies that eye position is not a disturbance in these simulations (this is not a requirement however). Parameters F and G were selected to give a reasonable time constant for the NU. The choice of γ reflects the relatively longer time (on the order of, say, 30 minutes) for the NU to go from trained to untrained conditions. Finally, in order to make the figures easier to view, we display saccades only every 5s. In reality they typically occur roughly every 0.5s (Büttner *et al.*, 1976). However, for the plot of u_b, we show the true interval of saccades otherwise the estimate $\alpha_{\text{x}}\hat{x}$ (and therefore u_b) would be unnaturally large.

7.5.1 OKN and OKAN I

Optokinetic nystagmus (OKN) is perhaps the signature behavior of the optokinetic system. It is an eye movement in which the eye tracks the velocity of a (full-field) moving visual surround during the so-called *slow phase*, followed by a saccade to rapidly reset the eye position to zero in the *fast phase*. OKN is characterized by a fast initial rise in slow-phase eye velocity, followed by a slower rise to a steady-state velocity that nearly matches the velocity of the surround (Cohen *et al.*, 1977, Fig. 3A), (Raphan *et al.*, 1979, Fig. 3B, 4B).

The second signature behavior of the optokinetic system is *optokinetic after-nystagmus I* (OKAN I), a behavior following OKN when the lights are turned off. During OKAN I nystagmus continues in the same direction as OKN, even though there is no visual stimulation. After a

quick initial drop, the slow-phase velocity slowly decays to zero during OKAN I (Cohen *et al.*, 1977, Fig 2), (Büttner *et al.*, 1976, Fig 1); also (Raphan *et al.*, 1979; Zee *et al.*, 1981; Waespe *et al.*, 1984).

Figure 7.2 shows simulation results for OKN and OKAN I using our model, with the optokinetic drum rotating at a constant velocity of 60 deg/s for 60s. At the start of OKN, the slow-phase velocity jumps to about 55% of the steady-state value, then rises more slowly and stabilizes around $55°/s$. These characteristics can be attributed to the large retinal slip velocity at the onset of the experiment and the charging of the VSM, respectively. The non-zero steady-state error during OKN is observed because the NU internal model is *untrained*, meaning this is the first time the experiment is run with a specific subject.

Once the lights are extinguished at $t = 60$s, visual signals are no longer present and the cerebellum is effectively inactive, so the signal e is unavailable and $u_{im} = 0$. This causes the slow-phase eye velocity to rely on the dynamics from the VSM, which slowly dissipates its stored velocity, creating OKAN I. The slow-phase velocity experiences a 10% drop, then decays with a time constant of about 18s.

If the subject is involved in repeated trials of the same experiment eliciting OKN and OKAN I, the NU is trained over time. Consequently, the OKN steady-state slow-phase eye velocity increases (Miki *et al.*, 2020, Fig 1), the OKAN I time constant decreases (Cohen *et al.*, 1977, Fig 7), and the OKAN I duration decreases (Waespe and Henn, 1978b, Fig 2, 3). Compared to the untrained case in Figure 7.2, the steady-state velocity during OKN is about 8% higher, the OKAN I time constant is about 40% lower, and the OKAN I duration is about 36% lower. These results are shown in Figure 7.3.

It is possible to extract some additional relationships from our simulation results. For the OKN, the steady-state slow-phase eye velocity increases linearly with increasing stimulus velocity (Figure 4B in (Cohen *et al.*, 1977)). This is shown for our model with stimulus velocities of 60, 100, 120 and 180 deg/s in the left figure of Figure 7.4. For OKAN I, the peak slow-phase eye velocity is linearly related to stimulus velocity (Figures 2 and 4C in (Cohen *et al.*, 1977) and Figure 5 in (Koenig and

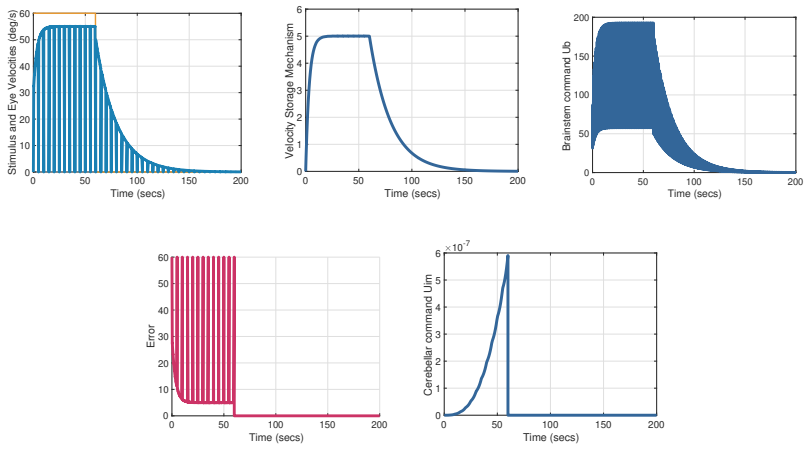

Figure 7.2: Untrained OKN and OKAN I. The untrained response during OKN is characterized by a fast rise in the slow phase eye velocity, followed by a slower rise to a steady-state eye velocity that nearly matches the velocity of the visual surround. We note a persistent steady-state error in the eye velocity because the NU internal model is untrained. During OKAN I, the lights are turned off and the cerebellum shuts off, but the eye continues to move in the same direction as during nystagmus. OKAN I is due to the discharge of the velocity storage mechanism when there is no visual stimulus. During OKAN I, after a quick initial drop, the eye velocity decays to zero at a slow exponential rate.

Dichgans, 1981)). This is shown for our model with stimulus velocities of 60, 100, 120 and 180 deg/s in the right figure of Figure 7.4.

7.5.2 OKAN Suppression

OKAN suppression or fixation suppression is an experiment in which the lights are turned on for a brief period of time during OKAN, revealing a stationary optokinetic drum on which the subject fixates. Figure 7.5 shows the results of our model when the lights are turned on 2s after the onset of OKAN I. The lights are left on for 5s, then turned off again. During fixation, the slow-phase eye velocity drops rapidly, as shown between the dashed red lines. This is due to the visual signal e and cerebellar output u_{im} returning during fixation, so the large error causes the velocity signal to drop along with the inhibitory effects of the cerebellum which cause the VSM time constant to drop (Waespe

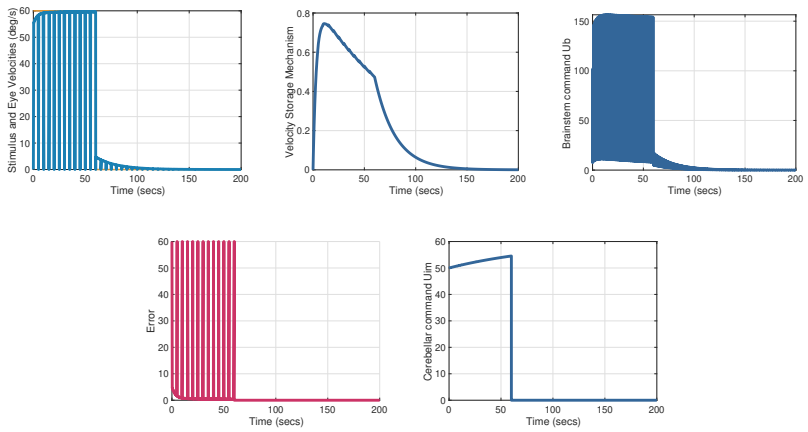

Figure 7.3: Trained OKN and OKAN I. The trained response during OKN is characterized by a decrease in steady-state error, suggesting that the NU internal model is now trained. The trained response during OKAN I shows a decrease in its duration and the exponential time constant, because the velocity storage mechanism has drained its state due to the smaller steady-state error during OKN.

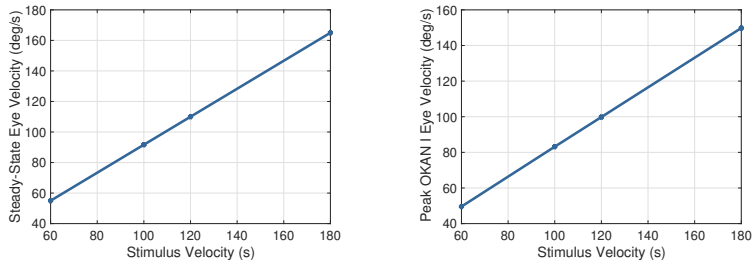

Figure 7.4: The left figure shows the linear relationship between stimulus velocity and steady-state velocity during OKN. The right figure shows the linear relationship between stimulus velocity and peak OKAN I velocity.

et al., 1984). Once the lights are turned off again, the velocity is able to recover at a depressed value due to the VSM having not dissipated all of its stored activity and continues its decay. This same behavior is reported in animal studies (Cohen *et al.*, 1977, Fig 8) and (Raphan *et al.*, 1979, Fig 7B)).

Longer fixation periods are known to inhibit the slow-phase velocity so that it cannot recover when the lights are turned off again (Cohen *et*

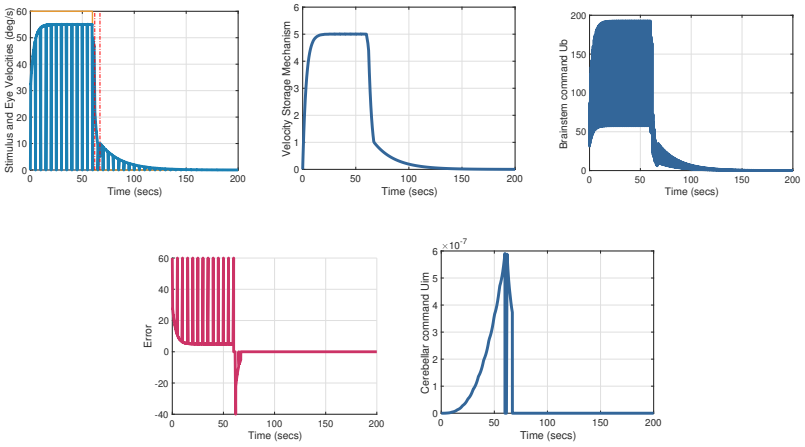

Figure 7.5: OKAN suppression with a 5s interval of gaze fixation. In an OKAN suppression experiment, the lights are turned on for a brief period during OKAN, revealing a stationary optokinetic drum. During fixation, the eye velocity drops rapidly, as the gaze fixation system takes over. When the lights are turned off again, OKAN I continues due to the remaining charge of the velocity storage mechanism.

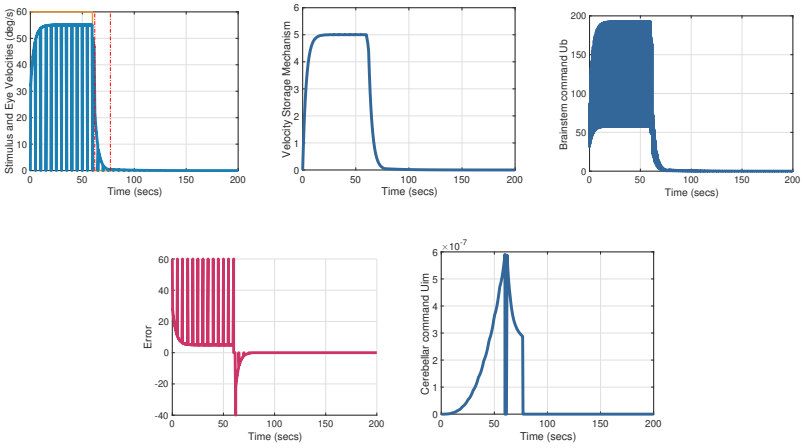

Figure 7.6: OKAN suppression with a 5s interval of gaze fixation. If the period of fixation is increased to 15s then the velocity storage mechanism further discharges its state, so that when the lights are turned off again, OKAN I is significantly reduced.

al., 1977, Fig 8). For example, with a fixation period of 15s introduced 2s after the onset of OKAN I, the slow-phase eye velocity is completely inhibited, as is shown in Figure 7.6.

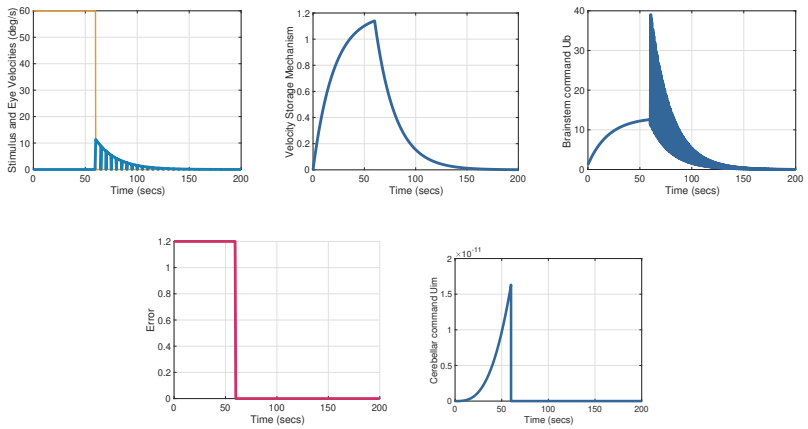

Figure 7.7: In an OKN suppression experiment, the subject fixates on a stationary target while the optical drum rotates in teh background. The effect of the rotating optical drum is to charge the velocity storage mechanism, even though hte eye is not moving. Thus, when the lights are turned off, OKAN I is elicited, though the response is reduced compared to the OKAN I response following OKN.

7.5.3 OKN Suppression

OKN suppression is an experiment in which the subject fixates on a target straight ahead while the illuminated optokinetic drum is rotating. Although nystagmus is not elicited, the VSM still charges while the drum is moving due to a reduced visual signal e, but to a lesser extent than without a fixation target. This causes a small velocity jump at the start of OKAN I when the lights are turned off, followed by a decay to zero (Waespe and Schwarz, 1986, Fig 8). This behaviour is replicated by our model as seen in Figure 7.7. Although the eye velocity is unchanged during the stimulation period, the VSM is still storing activity. The stored activity causes the slow-phase velocity to rise just past $10°/s$ once the lights turn off to elicit OKAN I.

7.5.4 OKAN II

OKAN II is a second phase of OKAN that arises only after a subject has become habituated to unidirectional optokinetic stimulation. That is, the optokinetic drum only spins in the positive or negative sense. The

presence of OKAN II depends on the duration of the optokinetic stimulation. After potentially many hours of stimulation (lasting 24 hours to 8 days in some experiments (Pettorossi *et al.*, 1999)), it is observed that the eye velocity in the slow phase of nystagmus reverses direction from the original stimulus direction (Waespe and Henn, 1978b). OKAN II is believed to arise from a process of long-term adaptation (Maioli, 1988; Pettorossi *et al.*, 1999; Waespe and Henn, 1978b) as a compensatory behavior to offset a natural condition called *gaze-evoked nystagmus* in which weakening of the muscles of the eye on one side causes the eye to slip in one direction only, resulting in repeated corrective saccades to maintain steady gaze.

OKAN II may be explained in our model by considering that weakening of the eye muscles in one direction would correspond to a reduction in the parameter K_x for stimulus in the positive sense. We posit that the long-term adaptation process that is activated by prolonged unidirectional nystagmus is a process that calibrates the time constant of the neural integrator via a parameter $\hat{K}_x$ to match the time constant of the oculomotor plant determined by K_x. Instead of utilizing (7.1.2c) in which time constants are matched, to elicit OKAN II we utilize the neural integrator model

$$\dot{\hat{x}} = -\hat{K}_x \hat{x} + u\,. \tag{7.5.1}$$

To model that the muscles have been weakened, we assume $\hat{K}_x \ll K_x$. Define the parameter mismatch

$$\Delta K_x := K_x - \hat{K}_x > 0\,.$$

Also define the estimation error $\widetilde{x} = x - \hat{x}$. Based on the first-order model of the oculomotor plant, a reasonable approximation of the estimation error dynamics is:

$$\dot{\widetilde{x}} = -\hat{K}_x \widetilde{x} - \Delta K_x x_1\,.$$

If the optokinetic experiment involves a slow phase in the positive sense, then $x_1(t) \geq 0$ (or on average $x_1(t)$ is positive). Since $\Delta K_x > 0$, $\widetilde{x}(t)$ will progressively drift with more negative values.

The oculomotor plant model during OKAN when the lights are off is

$$\begin{aligned}\dot{x}_1 &= x_2 \\ \dot{x}_2 &= \alpha_2(-x_2 - K_x x_1 + \alpha_{\text{x}}\hat{x} + \alpha_{\text{v}} v) \\ &= \alpha_2(-x_2 - \widetilde{K}_x x_1 - \alpha_{\text{x}}\widetilde{x} + \alpha_{\text{v}} v)\,.\end{aligned}$$

We see that the effect of the mismatch between plant and neural integrator is to introduce a term $\alpha_{\text{x}}\widetilde{x}$. The neural integrator generally works to cancel the eye position term $-K_x x_1$ via its contribution $\alpha_x \hat{x}$. Since we now have a parameter mismatch in which $\hat{K}_x \ll K_x$, we would expect α_x to be greatly reduced as well. We posit that $\alpha_x < 0$ so that the residual signal causes the slow-phase velocity to drift in the negative sense. In summary, OKAN II arises during OKAN when the cerebellum is inactive and when the velocity storage integrator has depleted its contribution, so $\alpha_{\text{v}} v \simeq 0$. What remains is the negative drive supplied by the drift term $\alpha_{\text{x}}\widetilde{x}$.

Our model generates OKAN II with parameter values of $K_x = 5$, $\hat{K}_x = 0.001$, $\alpha_{\text{x}} = -0.002 K_x$. Because the results are now dependent on the eye position, the simulations use a small saccade interval to demonstrate more realistic values. Figure 7.8 shows an experiment starting with 60s of unidirectional optokinetic stimulation before the lights are extinguished. OKAN I proceeds for about 53s as it decays to zero. Now the appearance of OKAN II is observed as the slow-phase velocity increases in the negative sense. The velocity reaches a peak value of about $-3.5°/s$, and eventually decays to zero (not pictured). These characteristics are very comparable to behavioral studies where the optokinetic stimulation is applied in one direction for 60s (Figure 1 in (Büttner *et al.*, 1976)).

With repeated trials or a longer stimulus duration, OKAN I is known to decrease in duration while OKAN II is known to increase in peak velocity and in duration (Waespe and Henn, 1978b, Fig 2), (Büttner *et al.*, 1976, Fig 2). Figure 7.9 shows results with our model over 100s of optokinetic stimulation in the positive sense. Comparing to Figure 7.8, the duration of OKAN I has decreased and the peak velocity of OKAN II has indeed increased with a longer stimulation duration.

7.6 Final Remarks

We presented a model of the optokinetic system that captures the main behaviors during constant velocity optokinetic nystagmus. The model proposes that the computations of the cerebellum, specifically the NU, comprise an adaptive internal model to realize the internal model principle of control theory.

The modeling and analysis may be extended in several directions. First, because of the relatively longer time required experimentally (up to 30 minutes) to go from an untrained to trained NU, we did not carry out the full simulation, but rather set the initial conditions consistent with the two states of the NU. The theoretical analysis proves that this transition from untrained to trained occurs; nevertheless, this aspect of the simulations is worth revisiting. Another extension of the analysis would be to include saccades by treating the model as a *hybrid system* with state dependent guard and reset conditions (Goebel *et al.*, 2009).

In Remark 7.1 we discussed that an alternative error model including the head velocity as a disturbance may be attributed to the NU. This highlights the issue that the proper choice of error model must be ascribed to each cerebellar module in order to fully characterize its role in disturbance rejection. If the alternative error model is correct, then an open problem is to determine how the FC shares the workload with the NU to suppress the disturbance on vision induced by head movement.

Analogous to the situation with the flocculus and the VOR gain α_{VOR}, no account is given of long-term adaptation of the optokinetic reflex gain α_{OK}. Finally, more research is needed to fully elucidate the adaptive mechanisms underlying OKAN II.

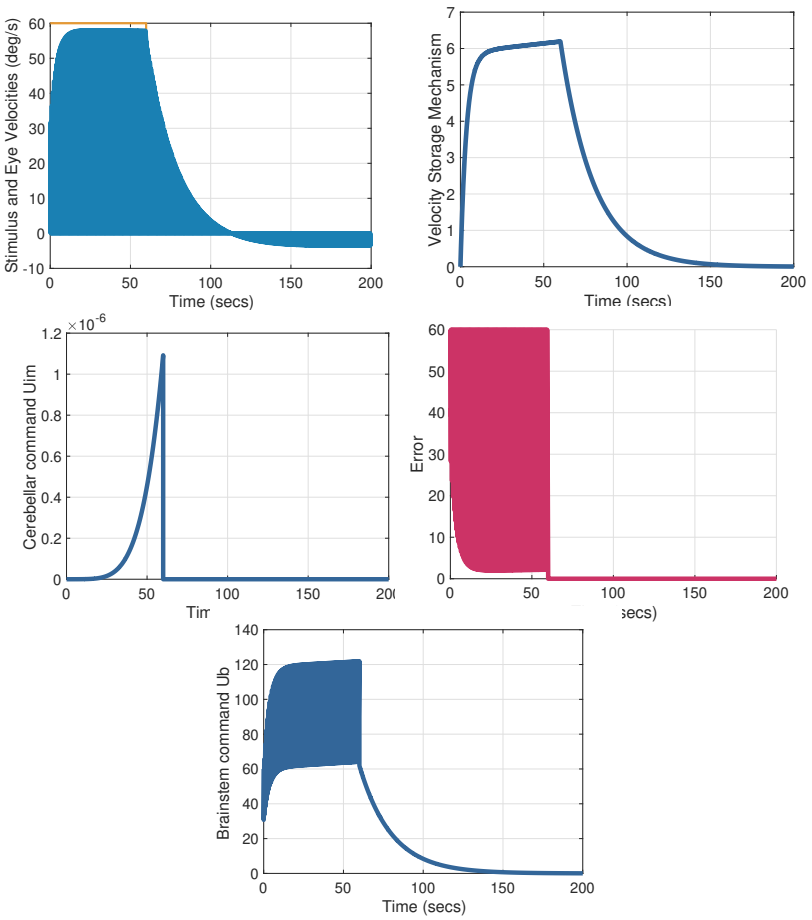

Figure 7.8: OKN followed by OKAN I and OKAN II. OKAN II is characterized by a reversal of the direction of eye movement relative to OKN and OKAN I. The effect is amplified when the duration of OKN is extended by many hours.

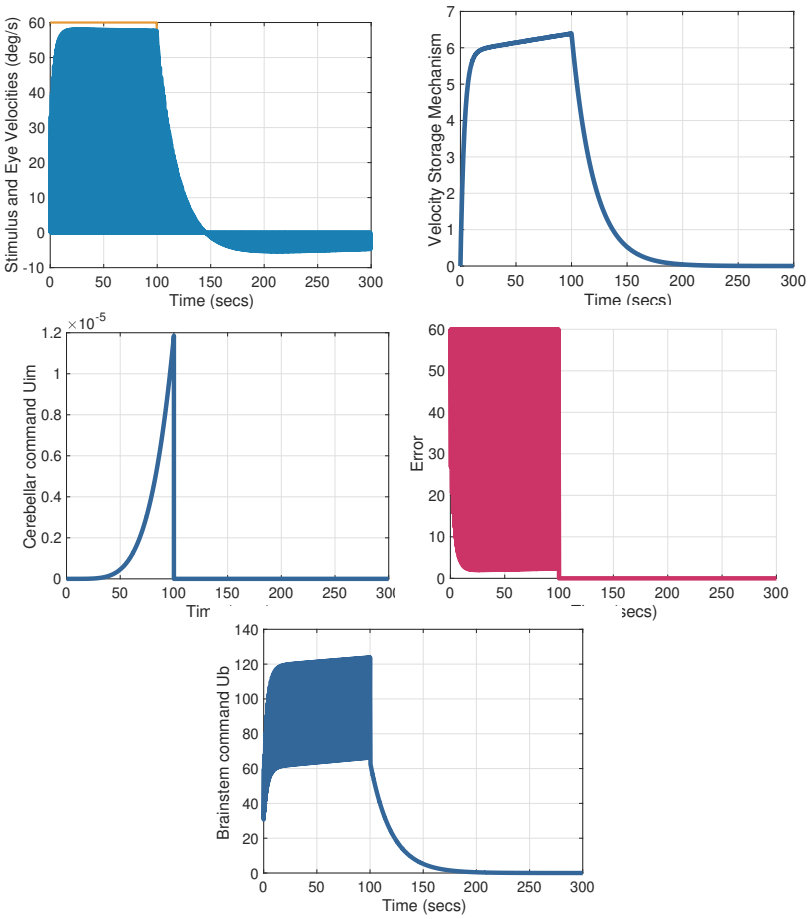

Figure 7.9: Longer duration of OKN, followed by OKAN I and OKAN II. The effect of a longer duration of OKN is to prolong the time of OKAN II (compare to the previous figure) during which the eye moves in the opposite direction to its initial direction during OKN.

8

Adaptive Internal Models in Discrete-Time

This chapter prepares the theoretical background for studying visuomotor adaptation and the saccadic system, subjects of Chapter 9. We present a regulator design that is more general than what is required for those models. By giving a more general treatment it becomes possible to appreciate that visuomotor adaptation and saccade adaptation sit in a general framework of disturbance rejection, and therefore they are driven by the same underlying mathematical principles as the oculomotor system.

The discrete-time regulator design is closest to the continuous-time regulator design V of Section 5.5. The motivation for giving a separate treatment of the discrete-time case is twofold. First, most researchers working in the area of visuomotor adaptation deal only with discrete-time models, so there is value to use a mathematical language that is familiar to them. Second, while it is possible to move seamlessly between discrete-time and continuous-time models in classical regulator theory, this is not so when dealing with adaptive internal models due to the nonlinear, time-varying nature of parameter adaptation laws. As such, a comparison between Section 5.5 and this chapter reveals that the discrete-time design of the regulator follows verbatim the

continuous-time design. Lemmas 8.1.2-8.1.4 are the direct analogues of Lemmas 5.2.2-5.2.5. Differences begin to appear in the parameter adaptation law (8.1.14), and particularly in the Lyapunov arguments of the proof of the main result Theorem 8.2. Futher comments on working in discrete-time v.s. continuous-time are found in the concluding chapter.

8.1 Regulator Design VI

Consider the discrete-time system

$$\begin{aligned} x(k+1) &= Ax(k) + Bu(k) + E\zeta(k) && \text{(8.1.1a)} \\ \zeta(k+1) &= S\zeta(k) && \text{(8.1.1b)} \\ e(k) &= Cx(k) + D\zeta(k)\,, && \text{(8.1.1c)} \end{aligned}$$

where $x(k) \in \mathbb{R}^n$ is the state, $\zeta(k) \in \mathbb{R}^q$ is the exosystem state, $u(k) \in \mathbb{R}$ in the input, and $e(k) \in \mathbb{R}$ is the error to be regulated. Here $D\zeta(k)$ is a disturbance that enters additively in the error, and $E\zeta(k)$ is a disturbance that enters in the state equation.

Assumption 8.1.1. We assume the system (8.1.1) satisfies the following assumptions:

(A1) (A, B) is a controllable pair.

(A2) (C, A) is an observable pair.

(A3) S has simple eigenvalues on the unit circle in the complex plane.

(A4) $\det \begin{bmatrix} A - \lambda I & B \\ C & 0 \end{bmatrix} \neq 0$ for all $\lambda \in \sigma(S)$. Then by Lemma 2.3.2, there exist (Π, Γ) such that

$$\begin{aligned} \Pi S &= A\Pi + B\Gamma + E && \text{(8.1.2a)} \\ 0 &= C\Pi + D\,. && \text{(8.1.2b)} \end{aligned}$$

(A5) (Γ, S) is an observable pair.

(A6) Dimension q is interpreted as a known upper bound on the order of the exosystem, while parameters (S, D, E) are unknown.

(A7) The parameters (A, B, C) are known.

(A8) The measurement is e.

Remark 8.1. Assumptions (A1) and (A2) may be relaxed; for instance, we may replace (A1) by (A, B) is stabilizable. (A3) guarantees that reference and disturbance signals are bounded. In (A4), the solution (Π, Γ) is unknown, but we assume it exists. (A5) is without loss of generality since one can trim off the unobservable part of the exosystem without affecting the plant. In (A6), the interpretation of q as an upper bound on the exosystem order means the exosystem may be overmodeled for a given disturbance. ◁

In the sequel, let $\varepsilon(k)$ represent any *arbitrary* exponentially stable term. We say the SISO transfer function $H(z)$ is *stable* if its poles lie inside the unit circle in the complex plane.

We develop a controller of the form

$$u(k) = u_s(k) + u_{im}(k)\,. \tag{8.1.3}$$

First we design u_s for closed-loop stability. Define $z(k) = x(k) - \Pi\zeta(k)$. Using (8.1.2) we obtain the error model

$$z(k+1) = Az(k) + Bu(k) - B\Gamma\zeta(k) \tag{8.1.4a}$$

$$e(k) = Cz(k)\,. \tag{8.1.4b}$$

Under Assumptions (A1)-(A2), we can define an observer of the form:

$$\hat{z}_s(k+1) = A\hat{z}_s(k) + Bu_s(k) + L_s(e(k) - C\hat{z}_s(k))\,, \tag{8.1.5}$$

where L_s is selected so that $(A - L_sC)$ is Schur stable. Define the estimation error $\widetilde{z}_s(k) := z(k) - \hat{z}_s(k)$. Using (8.1.3), we obtain

$$\widetilde{z}_s(k+1) = (A - L_sC)\widetilde{z}_s(k) + Bu_{im}(k) - B\Gamma\zeta(k)\,.$$

Assuming we can design u_{im} such that $(u_{im}(k) - \Gamma\zeta(k)) \longrightarrow 0$ independently of the $\widetilde{z}_s$ error dynamics, then $\widetilde{z}_s(k) \longrightarrow 0$. Therefore, we choose $u_s(k) = K\hat{z}_s(k)$ such that $(A + BK)$ is Schur stable in order to stabilize the z dynamics.

Next we design u_{im}. First, we transform the exosystem using the methods in Section 5.2. The proof of the next result is analogous to that of Lemma 5.2.2, so it is omitted.

Lemma 8.1.2. Consider a linear exosystem $\zeta(k+1) = S\zeta(k)$ generating a discrete-time signal $d(k) = \Gamma\zeta(k)$, and suppose that (Γ, S) is an observable pair. Let (F, G) be a controllable pair such that $\sigma(F) \cap \sigma(S) = \emptyset$. Then there exists a coordinate transformation $w(k) = M\zeta(k)$ such that in new coordinates, the exosystem is

$$w(k+1) = Fw(k) + Gd(k) \tag{8.1.6a}$$
$$d(k) := \psi w(k)\,, \tag{8.1.6b}$$

where $\psi = \Gamma M^{-1}$.

Applying Lemma 8.1.2, we obtain an error model

$$z(k+1) = Az(k) + Bu(k) - B\psi w(k) \tag{8.1.7a}$$
$$e(k) = Cz(k)\,, \tag{8.1.7b}$$

where $d(k) = \psi w(k)$ is the disturbance modeled by the exosystem (8.1.6). We build the internal model in two stages, beginning with the state observer

$$\hat{z}_d(k+1) = A\hat{z}_d(k) + Bu(k) + L_d(e(k) - C\hat{z}_d(k)) \tag{8.1.8}$$

where we choose L_d such that $A_d := A - L_dC$ is Schur stable. Next, define $\widetilde{z}_d(k) := z(k) - \hat{z}_d(k)$. Then

$$\widetilde{z}_d(k+1) = A_d\widetilde{z}_d(k) - Bd(k) \tag{8.1.9a}$$
$$d_f(k) := C\widetilde{z}_d(k)\,, \tag{8.1.9b}$$

where d_f is the *filtered disturbance*. Define the stable transfer function $H_d(z) := -C(zI - A_d)^{-1}B$. Then we can write $d_f = H_d(z)\,[d]$. The next result provides an alternative representation of d_f, analogous to Lemma 5.2.4 for the continuous-time case.

Lemma 8.1.3. Consider a discrete-time signal d generated by the exosystem (8.1.6). Define the *filtered signal* $d_f := H_d(z)\,[d]$, where $H_d(z)$

is a stable transfer function. Then d_f can be expressed as

$$w_f(k+1) = Fw_f(k) + Gd_f(k) \tag{8.1.10a}$$
$$d_f(k) = \psi w_f(k) + \varepsilon(k)\,, \tag{8.1.10b}$$

where $w_f(k) \in \mathbb{R}^q$.

Proof. Let $H_\psi(z) = \psi(zI - F)^{-1}G$. Then $d = H_\psi(z)[d]$. Since stable scalar transfer functions commute, modulo an exponentially stable term, we have

$$\begin{aligned} d_f &= H_d(z)[H_\psi(z)[d]] \\ &= H_\psi(z)[H_d(z)[d]] + \varepsilon \\ &= H_\psi(z)[d_f] + \varepsilon\,. \end{aligned}$$

A realization of $H_\psi(z)[d_f]$ proves the result. □

Remark 8.2. Consider again the situation of Lemma 8.1.3. Let $H(z)$ be a stable transfer function, and w, w_f, d, d_f as given above. Let $H(z)I\,[w]$ denote the component-wise application of the filter $H(z)$ to w. Analogous to the proof of Lemma 8.1.3, we can derive

$$\begin{aligned} H(z)I\,[w] &= H(z)I\left[(zI - F)^{-1}G\,[d]\right] \\ &= (zI - F)^{-1}G\,[H(z)\,[d]] + \varepsilon \\ &= (zI - F)^{-1}G\,[d_f] + \varepsilon \\ &= w_f + \varepsilon\,. \end{aligned}$$

Based on this calculation, we call $w_f := H(z)I\,[w]$ the *filtered regressor*. ◁

Recalling that $d_f = e(k) - C\hat{z}_d(k)$, we complete the internal model for the *filtered disturbance* using

$$\hat{w}_f(k+1) = F\hat{w}_f(k) + G(e(k) - C\hat{z}_d(k))\,. \tag{8.1.11}$$

Define the estimation error $\widetilde{w}_f(k) = w_f(k) - \hat{w}_f(k)$. Using (8.1.11) and Lemma 8.1.3, we get $\widetilde{w}_f(k+1) = F\widetilde{w}_f(k)$. Since F is Schur stable, we have $\widetilde{w}_f(k) \longrightarrow 0$ exponentially. To show that (8.1.8) and (8.1.11) form an internal model of d, we require the following.

Lemma 8.1.4. Consider a discrete-time signal d generated by the exosystem (8.1.6). Define the *filtered signal* $d_f := H(z)\,[d]$ with respective state w_f, where $H(z)$ is a stable transfer function. Suppose that no zero of $H(z)$ is an eigenvalue of $S' = F+G\psi$. Then there exists a nonsingular matrix $T \in \mathbb{R}^{q\times q}$ such that

$$w_f = Tw + \varepsilon$$

and $d = \psi_f w_f + \varepsilon$ with $\psi_f = \psi T^{-1}$.

Proof. By Remark 8.2, $w_f = H(z)I[w]+\varepsilon$. Let $H(z) = \frac{N(z)}{D(z)}$ with $N(z)$ and $D(z)$ coprime polynomials. Then

$$D(z)I\,[w_f] = N(z)I\,[w] + \varepsilon\,.$$

From (8.1.6) and (8.1.10), it follows that

$$D(S')w_f(k) = N(S')w(k) + \varepsilon(k)\,.$$

Since the roots of $N(z)$ do not coincide with the eigenvalues of S', then $N(S')$ is invertible. Similarly, $D(S')$ is invertible because $D(z)$ is Schur stable. Letting $T = D^{-1}(S')N(S')$ we have our result. □

We can apply the previous lemma by noting that because of (A4), no zero of $C(zI-A)^{-1}B$ is an eigenvalue of S'. Since state feedback does not move the zeros of a scalar transfer function (Brockett, 1965), then also $H_d(z)$ has the same property. Now we can write

$$d(k) = \psi_f w_f(k) + \varepsilon(k) = \psi_f \hat{w}_f(k) + \varepsilon(k)\,. \tag{8.1.12}$$

Finally, we define

$$u_{im}(k) = \hat{\psi}_f(k)\hat{w}_f(k)\,, \tag{8.1.13}$$

where $\hat{\psi}_f(k) \in \mathbb{R}^{1\times q}$ is an estimate of ψ_f.

Next we must design the parameter adaptation law. The error model (8.1.7) cannot be used for this purpose since in general A may be unstable. Instead, we use the observer (8.1.11) and invoke the discrete-time equivalent of the swapping lemma (Sastry and Bodson, 1989).

Lemma 8.1. Let $\psi : \mathbb{Z} \longrightarrow \mathbb{R}^{1\times q}$ and $w : \mathbb{Z} \longrightarrow \mathbb{R}^q$ be discrete signals. Let $H(z) := C(zI - A)^{-1}B$ be a stable scalar transfer function. Then

$$\begin{aligned}\psi H(z) I\left[w\right] - H(z)\left[\psi w\right] \\ = H_c(z)\left[zH_b(z)\left[w^{\mathrm{T}}\right](z-1)[\psi^{\mathrm{T}}]\right],\end{aligned}$$

where $H_b(z) = (zI - A)^{-1}B$, and $H_c(z) = C(zI - A)^{-1}$.

Proof. Consider the state space models

$$\begin{aligned}\eta_1(k+1) &= A\eta_1(k) + Bw(k)^{\mathrm{T}}, & y_1(k) &= C\eta_1(k)\psi(k)^{\mathrm{T}} \\ \eta_2(k+1) &= A\eta_2(k) + B(\psi(k)w(k)), & y_2(k) &= C\eta_2(k).\end{aligned}$$

Notice that $y_1(k) = \psi(k)H(z)I\left[w\right]$ and $y_2 = H(z)\left[\psi w\right]$, assuming zero initial conditions of all states. Define $\widetilde{\eta}(k) = \eta_1(k)\psi(k)^{\mathrm{T}} - \eta_2(k)$ and $\Delta\psi(k) := \psi(k+1) - \psi(k)$. Then we compute

$$\begin{aligned}\widetilde{\eta}(k+1) &= (A\eta_1(k) + Bw(k)^{\mathrm{T}})\psi(k+1)^{\mathrm{T}} - A\eta_2(k) - Bw(k)^{\mathrm{T}}\psi(k)^{\mathrm{T}} \\ &= A\widetilde{\eta}(k) + A\eta_1(k)\Delta\psi(k)^{\mathrm{T}} + Bw(k)^{\mathrm{T}}\Delta\psi(k)^{\mathrm{T}} \\ &= A\widetilde{\eta}(k) + \eta_1(k+1)\Delta\psi(k)^{\mathrm{T}}.\end{aligned}$$

Putting it all together,

$$\begin{aligned}y_1(k) - y_2(k) = C\widetilde{\eta}(k) &= H_c(z)\left[z\eta_1(z-1)\psi^{\mathrm{T}}\right] \\ &= H_c(z)\left[zH_b(z)[w^{\mathrm{T}}](z-1)\psi^{\mathrm{T}}\right].\end{aligned}$$

□

Using the discrete-time swapping lemma, we have

$$d_f = \psi_f\overline{w} + \varepsilon,$$

where $\overline{w} := H_d(z)I[\hat{w}_f]$. Hence we define the *augmented error*

$$\begin{aligned}\overline{e}(k) &:= e(k) - (C\hat{z}_d(k) + \hat{\psi}_f(k)\overline{w}(k)) \\ &= d_f(k) - \hat{\psi}_f(k)\overline{w}(k) \\ &= \widetilde{\psi}_f(k)\overline{w}(k) + \varepsilon(k),\end{aligned}$$

where $\widetilde{\psi}_f(k) := \psi_f - \hat{\psi}_f(k)$. Finally, we choose the parameter adaptation law

$$\hat{\psi}_f(k+1) = \hat{\psi}_f(k) + \gamma(k)\overline{e}(k)\overline{w}(k)^{\mathrm{T}} \tag{8.1.14a}$$

$$\gamma(k) = \frac{\overline{\gamma}}{1 + \overline{w}(k)^{\mathrm{T}}\overline{w}(k)}\,, \tag{8.1.14b}$$

where $\gamma(k) > 0$ is the adaptation rate and $\overline{\gamma} \in (0, 2)$.

We summarize the overall design:

$$\begin{aligned}
\hat{z}_s(k+1) &= (A+BK)\hat{z}_s(k) + L_s(e(k) - C\hat{z}_s(k)) && \text{(8.1.15a)}\\
\hat{z}_d(k+1) &= A\hat{z}_d(k) + Bu(k) + L_d(e(k) - C\hat{z}_d(k)) && \text{(8.1.15b)}\\
\hat{w}_f(k+1) &= F\hat{w}_f(k) + G(e(k) - C\hat{z}_d(k)) && \text{(8.1.15c)}\\
\overline{w}(k) &= H_d(z)I\,[\hat{w}_f] && \text{(8.1.15d)}\\
\overline{e}(k) &= e(k) - C\hat{z}_d(k) - \hat{\psi}_f(k)\overline{w}(k) && \text{(8.1.15e)}\\
\hat{\psi}_f(k+1) &= \hat{\psi}_f(k) + \gamma(k)\overline{e}(k)\overline{w}(k)^{\mathrm{T}} && \text{(8.1.15f)}\\
u(k) &= K\hat{z}_s(k) + \hat{\psi}_f(k)\hat{w}_f(k)\,. && \text{(8.1.15g)}
\end{aligned}$$

8.1.1 Stability Analysis

To analyze stability we require several discrete-time analogues of continuous-time results in Chapters 4 on persistency of excitation.

Definition 8.1.5. A discrete signal $w : \mathbb{N} \to \mathbb{R}^q$ is said to be *stationary* if the following limit exists, uniformly in k_0:

$$R_w(k) := \lim_{T\to\infty} \frac{1}{T} \sum_{\tau=k_0+1}^{k_0+T} w(\tau)w^{\mathrm{T}}(\tau+k)\,.$$

The limit, if it exists, is called the *autocovariance* of w.

Theorem 8.1.6. Consider an error $\overline{e}(k) = \widetilde{\psi}_r(k)\overline{w}_r(k)$, where $\overline{w}_r$ is bounded. Suppose $\widetilde{\psi}_r(k)\overline{w}_r(k) \longrightarrow 0$ and $\Delta\widetilde{\psi}_r(k) = \widetilde{\psi}_r(k+1) - \widetilde{\psi}_r(k) \longrightarrow 0$. If $\overline{w}_r$ is stationary and $R_w(0) > 0$, then $\widetilde{\psi}_r(k) \longrightarrow 0$.

Proof. Since $\overline{w}_r$ is stationary it has an autocovariance $R_w(k)$. We will show that $\widetilde{\psi}_r(k)R_w(0)\widetilde{\psi}_r^T(k) \longrightarrow 0$. By assumption $R_w(0) > 0$, which implies $\widetilde{\psi}_r(k) \to 0$ as required.

Since $\widetilde{\psi}_r$ and $\overline{w}_r$ are bounded, there exists $\kappa > 0$ such that

$$\|\widetilde{\psi}_r(k)\|, \|\overline{w}_r(k)\| < \kappa, \quad \forall k \geq 0. \tag{8.1.16}$$

Fix $\epsilon > 0$. We will show there exists $T_1 > 0$ such that for all $k \geq T_1$, $\widetilde{\psi}_r(k) R_w(0) \widetilde{\psi}_r^{\mathrm{T}}(k) < \epsilon$. Since $\overline{w}_r$ has an autocovariance, there exists $T > 0$ such that for all $k_0 \geq 0$

$$\left\| R_w(0) - \frac{1}{T} \sum_{\tau=k_0+1}^{k_0+T} \overline{w}_r(\tau) \overline{w}_r^T(\tau) \right\| \leq \frac{\epsilon}{3\kappa^2}. \tag{8.1.17}$$

Then using (8.1.16), we have

$$\left\| \widetilde{\psi}_r(k) R_w(0) \widetilde{\psi}_r^{\mathrm{T}}(k) - \widetilde{\psi}_r(k) \frac{1}{T} \sum_{\tau=k_0+1}^{k_0+T} \overline{w}_r(\tau) \overline{w}_r^{\mathrm{T}}(\tau) \widetilde{\psi}_r^{\mathrm{T}}(k) \right\| \leq \frac{\epsilon}{3}. \tag{8.1.18}$$

Since $\widetilde{\psi}_r(k) \overline{w}_r(k) \longrightarrow 0$ and $\Delta\widetilde{\psi}_r(k) \longrightarrow 0$, there exists $T_1 > 0$ such that for all $k > T_1$

$$\|\widetilde{\psi}_r(k) \overline{w}_r(k)\|^2 \leq \frac{\epsilon}{3}, \tag{8.1.19}$$

and

$$\|\Delta\widetilde{\psi}_r(k)\| \leq \frac{\epsilon}{6\kappa^3 T}. \tag{8.1.20}$$

Using (8.1.20), we have

$$\|\widetilde{\psi}_r(k) - \widetilde{\psi}_r(\tau)\| \leq \frac{\epsilon(\tau - k)}{6\kappa^3 T},$$

for all $\tau > k > T_1$. Then, using (8.1.16) we have for all $k > T_1$

$$\begin{aligned}
&\left\| \widetilde{\psi}_r(k) \frac{1}{T} \sum_{\tau=k+1}^{k+T} \overline{w}_r(\tau) \overline{w}_r^{\mathrm{T}}(\tau) \widetilde{\psi}_r^{\mathrm{T}}(k) - \frac{1}{T} \sum_{\tau=k+1}^{k+T} \widetilde{\psi}_r(\tau) \overline{w}_r(\tau) \overline{w}_r^{\mathrm{T}}(\tau) \widetilde{\psi}_r^{\mathrm{T}}(\tau) \right\| \\
&= \left\| \frac{1}{T} \sum_{\tau=k+1}^{k+T} \overline{w}_r^{\mathrm{T}}(\tau) (\widetilde{\psi}_r^{\mathrm{T}}(k) - \widetilde{\psi}_r^{\mathrm{T}}(\tau)) \overline{w}_r^{\mathrm{T}}(\tau) (\widetilde{\psi}_r^{\mathrm{T}}(k) + \widetilde{\psi}_r^{\mathrm{T}}(\tau)) \right\| \\
&\leq \frac{\epsilon}{3}.
\end{aligned} \tag{8.1.21}$$

Using (8.1.19), we have for all $k > T_1$

$$\left\| \frac{1}{T} \sum_{\tau=k+1}^{k+T} \widetilde{\psi}_r(\tau) \overline{w}_r(\tau) \overline{w}_r^{\mathrm{T}}(\tau) \widetilde{\psi}_r^{\mathrm{T}}(\tau) \right\| \leq \frac{\epsilon}{3}. \tag{8.1.22}$$

Finally, using (4.3.4), (4.3.7), and (4.3.8) we have for all $k > T_1$,

$$\widetilde{\psi}_r(k) R_w(0) \widetilde{\psi}_r(k)^{\mathrm{T}} \leq \epsilon \,.$$

This proves the result. □

The following is the main result on stability.

Theorem 8.2. Consider the system (8.1.1) satisfying Assumptions (A1)-(A8), and consider the regulator given in (8.1.3), (8.1.5), (8.1.8), (8.1.11), (8.1.13), and (8.1.14). Suppose $A_{cl} := A + BK$, $A_s := A - L_s C$, and $A_d := A - L_d C$ are Schur stable. Then $\hat{\psi}_f(k)$ is bounded, $\widetilde{\psi}_f(k)\hat{w}_f(k) \longrightarrow 0$, and $e(k) \longrightarrow 0$.

Proof. We study the adaptive subsystem consisting of

$$\begin{aligned} \overline{e}(k) &= \widetilde{\psi}_f(k)\overline{w}(k) + \varepsilon(k) \\ \widetilde{\psi}_f(k+1) &= \widetilde{\psi}_f(k) - \gamma(k)\overline{e}(k)\overline{w}(k)^{\mathrm{T}} \,. \end{aligned}$$

To deal with the exponentially stable term $\varepsilon(k)$, we note that there exists a pair $(C_\varepsilon, A_\varepsilon)$ with A_ε Schur stable such that $\overline{\varepsilon}(k+1) = A_\varepsilon \overline{\varepsilon}(k)$ and $|\varepsilon(k)| \leq |C_\varepsilon \overline{\varepsilon}(k)|$. For $\alpha > 0$, let P_ε be positive definite and solve the discrete-time Lyapunov equation

$$A_\varepsilon^{\mathrm{T}} P_\varepsilon A_\varepsilon - P_\varepsilon = -\alpha I \,.$$

Define the Lyapunov function

$$V(k) := ||\widetilde{\psi}_f(k)||^2 + \overline{\varepsilon}(k)^{\mathrm{T}} P_\varepsilon \overline{\varepsilon}(k) \,.$$

Then we compute

$$\begin{aligned} \Delta V(k) &= V(k+1) - V(k) \\ &= -2\gamma(k)\overline{e}(k)\big[\overline{e}(k) + \varepsilon(k)\big] + \gamma(k)^2 \overline{e}(k)^2 \overline{w}(k)^{\mathrm{T}} \overline{w}(k) - \alpha \|\overline{\varepsilon}(k)\|^2 \,. \end{aligned}$$

Noting that $-2\gamma(k)\overline{e}(k)\varepsilon(k) \leq \gamma(k)^2 \overline{e}(k)^2 + \varepsilon(k)^2$, we have

$$\begin{aligned} \Delta V(k) &\leq -\gamma'(k)\overline{e}(k)^2 - (\alpha - ||C_\varepsilon||^2)||\overline{\varepsilon}(k)||^2 \\ \gamma'(k) &:= (2 - \overline{\gamma})\gamma(k) \,, \end{aligned}$$

where $\gamma'(k) > 0$ and α is selected so that $\alpha > ||C_\varepsilon||^2$. We conclude $\Delta V(k) \leq 0$ and so $\hat{\psi}_f(k)$ is bounded. By the monotone convergence theorem,

$$V(k) = V(0) + \sum_{j=1}^{k} \Delta V(j)$$

converges and thus the divergence test tells us that $\Delta V(k) \longrightarrow 0$. Now we also know by (A3) that $w(k)$ and therefore $\hat{w}_f(k)$ are bounded. Since $H_d(z)$ is stable, $\overline{w}(k)$ is also bounded. In turn, for any $\overline{\gamma} \in (0, 2)$, $\gamma'(k)$ is bounded away from zero, and so it must be that $\overline{e}(k) \longrightarrow 0$.

By (A3) and (8.1.10), there exist matrix $M_r \in \mathbb{R}^{q \times (2s+1)}$ and vector $\hat{w}_r(k)$ such that $\hat{w}_f(k) = M_r \hat{w}_r(k) + \varepsilon(k)$ and

$$\hat{w}_r(k) = (1, \cos(\omega_1 k), \sin(\omega_1 k), \ldots, \cos(\omega_s k), \sin(\omega_s k))$$

with $0 < \omega_i < \pi$, $\omega_i \neq \omega_j$ for $i \neq j$, and $2s + 1 \leq q$. Then we have

$$\overline{w} = H_d(z) I\left[M_r \hat{w}_r + \varepsilon\right] = M_r H_d(z) I\left[\hat{w}_r\right] + \varepsilon\,.$$

Since $H_d(z)$ is stable, $H_d(z) I\left[\hat{w}_r\right] = \overline{w}_r + \varepsilon$, where

$$\begin{aligned}\overline{w}_r = (&H_d(1), |H_d(\mathrm{e}^{j\omega_1})| \cos(\omega_1 k + \phi(\omega_1)), |H_d(\mathrm{e}^{j\omega_1})| \sin(\omega_1 k + \phi(\omega_1)), \ldots, \\ &|H_d(\mathrm{e}^{j\omega_s})| \cos(\omega_s k + \phi(\omega_s)), |H_d(\mathrm{e}^{j\omega_s})| \sin(\omega_s k + \phi(\omega_s)))\,,\end{aligned}$$

and $\phi(\omega_i) = \angle H_d(e^{j\omega_i})$. One can verify by direct calculation that $\overline{w}_r$ is stationary, i.e. its autocovariance $R_{\overline{w}_r}(k)$ exists. Moreover, it can be shown that

$$R_{\overline{w}_r}(0) = \operatorname{diag}\left(H_d(1)^2, \frac{|H_d(e^{j\omega_1})|^2}{2}, \cdots, \frac{|H_d(e^{j\omega_s})|^2}{2}\right).$$

The zeros of $H_d(z)$ are the same as those of the plant $C(zI - A)^{-1}B$ (Brockett, 1965), and by (A4), $H_d(1) \neq 0$ and $|H_d(\mathrm{e}^{j\omega_i})| \neq 0$, for $i = 1, \ldots, s$. Then $R_{\overline{w}_r}(0)$ is positive definite.

The augmented error becomes

$$\overline{e}(k) = \widetilde{\psi}_f(k) M_r \overline{w}_r(k) + \varepsilon(k) =: \widetilde{\psi}_r(k) \overline{w}_r(k) + \varepsilon(k)\,.$$

We have established that $\widetilde{\psi}_r(k)\overline{w}_r(k) \longrightarrow 0$, $\Delta\widetilde{\psi}_r(k) = \Delta\widetilde{\psi}_f(k) M_r \longrightarrow 0$, and $R_{\overline{w}_r}(0) > 0$. Then we can apply Theorem 8.1.6 to conclude that $\widetilde{\psi}_r(k) \longrightarrow 0$. This implies $\widetilde{\psi}_f(k)\hat{w}_f(k) = \widetilde{\psi}_r(k)\hat{w}_r(k) \longrightarrow 0$.

Recalling that $\widetilde{z}_s(k) = z(k) - \hat{z}_s(k)$, one has

$$\begin{aligned} z(k+1) &= A_{cl} z(k) - B\widetilde{\psi}_f(k)\hat{w}_f(k) - BK\widetilde{z}_s(k) + \varepsilon(k) \\ \widetilde{z}_s(k+1) &= A_s \widetilde{z}_s(k) - B\widetilde{\psi}_f(k)\hat{w}_f(k) + \varepsilon(k)\,. \end{aligned}$$

Hence, $\widetilde{z}_s(k) \longrightarrow 0$ which implies $z(k) \longrightarrow 0$. Finally, $e(k) \longrightarrow 0$ as desired. □

9

Saccadic System and Visuomotor Adaptation

The *saccadic eye movement system* is responsible for generating *saccades*, a fast reset of eye position either back to the central position or to a visual target of interest. Saccades are among the fastest movements of the body, with a typical duration of $20-30$ms during reading and a peak velocity of $900^\circ/$s.

The saccadic system is equipped with a capability called *sensorimotor adaptation*, which has been described as follows: "an error-driven process of movement modification characterized, firstly, by a specific repeated pattern of muscle activation with changes only in certain variables (e.g. endpoint position); second, the change occurs gradually over repetitive trials; and third, once adapted, subjects are unable to retrieve the prior behaviour except by re-adapting with the same gradual process" (Martin *et al.*, 1996). Motor adaptation is termed *short-term* when it occurs over minutes or hours, contrasting with *long-term adaptation* that takes place over days or weeks (Robinson *et al.*, 2006). A special case of sensorimotor adaptation is *visuomotor adaptation*, in which adaptation is elicited by a *visual error* closely following the execution of a movement.

In saccade adaptation experiments, a visual error can be artificially introduced by inserting an *intersaccadic step* in the target position while the saccade is underway. The subject perceives that the target is misaligned with the fovea at the end of the saccade, thus triggering the adaptation process (Kojima *et al.*, 2004). In the *visuomotor rotation experiment*, a subject experiences a visual error at the end of a fast arm reach when a cursor on a computer screen representing the hand position is rotated from the true hand position (Krakauer *et al.*, 2005; Shadmehr and Wise, 2005).

This chapter presents a model of visuomotor adaptation based on adaptive internal models. Because we are working with event driven processes that take place almost instantaneously, a different modeling approach is required compared to the differential equations-based approach of prior chapters, in order to capture, within a reasonably simple model, the main characteristics of adaptation over successive movements. Neuroscientists have adopted discrete-time models for this purpose.

9.1 Visuomotor Adaptation Experiments

Visuomotor adaptation experiments consist of repetitive trials of a certain movement such as a saccade or arm reach, and each trial corresponds to an update of an associated discrete-time model. The trials are classified by type, and sequences of blocks of trials of specific types are utilized to elicit so-called dynamic behaviors of adaptation. The types of blocks most commonly include:

1. **Baseline** (B). An initial block of trials when the subject is being familiarized with the experiment.
2. **Learning** (L). The first block of trials after the baseline block when a disturbance or perturbation is introduced in the visual error at the end of each trial.
3. **Washout** (W). A block of trials following a learning block when the disturbance is removed.

4. **Unlearning** (U). A block of trials following a learning block in which the sign of the disturbance is reversed.
5. **Relearning** (R). A second learning block using the same disturbance as in the first learning block. Typically, a washout or unlearning block is inserted between the first and second learning blocks.
6. **Downscaling** (D). A second learning block in which the disturbance is set to a fraction of its value in the first learning block.

A typical experiment proceeds in blocks of a prespecified order. For example, a BLUW experiment consists of a baseline block, a learning block, an unlearning block, and a washout block, in this order. The number of trials in each block may also be important. For example, a $B_{50}L_{100}U_{30}W_{100}$ experiment consists of 50 trials in the baseline block, 100 trials in the learning block, 30 trials in the unlearning block, and 100 trials in the washout block.

When blocks of trials are sequenced in a particular order and with a particular number of trials in each block, then several phenomena emerge in experiments:

- *Savings* is a behavior in which learning is sped up in the second learning block relative to the first one. Two experiments in which savings can be exhibited are BLUR or BLWR.
- *Reduced savings* is a behavior in which savings is reduced by inserting a washout block of trials after the unlearning block. After the washout block, relearning does not proceed as rapidly as in the savings experiment. An experiment in which reduced savings may be exhibited is BLUWR.
- *Anterograde interference* is a behavior in which a previously learned task reduces the rate of subsequent learning of a different (and usually opposite) task. An experiment in which anterograde interference may be exhibited is BLU.
- *Rapid unlearning* is a behavior in which the rate of unlearning is faster than the rate of initial learning, if the number of trials in the learning block is small. An experiment in which rapid unlearning may be exhibited is a BLW experiment.

- *Rapid downscaling* is a behavior in which the rate of learning in a secondary learning block is faster when the rotation is set to a fraction of its value in the initial learning block. An experiment in which rapid downscaling may be exhibited is a $B_{50}L_{50}D_{50}$ experiment, with the disturbance during the D block set to half its value in the L learning block.
- *Spontaneous recovery* is a behavior observed during the washout block of a BLUW experiment in which the response partially "rebounds" to its value at the end of the learning block rather than converging monotonically to zero.

9.2 Dynamic Properties of Adaptation

It is possible to formalize the dynamic properties of visuomotor adaptation in terms of the transient response of a stable forced linear system. We make three simplifying assumptions. First, we focus on motor adaptation tasks involving a single output. That is, we restrict our attention to one degree of freedom of movement; for instance, horizontal movement of the eye, hand angle relative to a reference angle in a horizontal plane, forward (coronal) inclination of the body relative to a vertical reference, the horizontal angle of a dart thrown by a subject, and so forth. Second, we assume the model is linear time-invariant, as such models have promise to explain motor adaptation (Smith *et al.*, 2006). Third, we focus on disturbances that are constant within a block of trials (but can change instantaneously between different blocks), as currently there is a dearth of experiments with non-constant disturbances (Cassanello *et al.*, 2016).

Consider the discrete-time system

$$\begin{aligned} \xi(k+1) &= A\xi(k) + Ew(k) && \text{(9.2.1a)} \\ y(k) &= C\xi(k) + Dw(k)\,, && \text{(9.2.1b)} \end{aligned}$$

where $\xi(k) \in \mathbb{R}^n$ is the state, $w(k) \in \mathbb{R}^q$ is a disturbance, and $y(k) \in \mathbb{R}$ is the scalar measurement or output. Suppose that the unforced system (when $w(k) \equiv 0$) is asymptotically stable, i.e. $\sigma(A) \subset \mathbb{C}_1$, the open unit disk in the complex plane. In all definitions below, let $d_0 \in \mathbb{R}^q$ and

$y_0 \in \mathbb{R}$ be constants and let $k_0 \geq 0$ be an integer. We assume that the disturbance is a constant vector $w(k) \equiv d_0$. Since the system is stable, we can define y_{ss} to be the steady-state value of y when $w(k) \equiv d_0$. Also $-y_{ss}$ is the steady state value of y when $w(k) \equiv -d_0$.

Definition 9.2.1 (Savings)**.** Suppose we have discrete times $k_3 \geq k_2 > k_1 > k_0$ such that: $w(k) = d_0$ for $k \in [k_0, k_1) \cup [k_2, \infty)$, and $y(k_3) = y(k_0) = y_0$. Let T_{r0} and T_{r3} be the rise times starting at k_0 and k_3, respectively. We say (9.2.1a) - (9.2.1b) exhibits *savings* if $T_{r0} > T_{r3}$. Additionally, if $w(k) = -d_0$ for $k \in [k_1, k_2)$, then we say (9.2.1a) - (9.2.1b) exhibits *savings with counter perturbation (CP)*. If $w(k) = 0$ for $k \in [k_1, k_2)$, then we say (9.2.1a) - (9.2.1b) exhibits *savings with washout (WO)*. ◁

Remark 9.1. The rise time is the number of trials for $y(k)$ to reach 90% of its steady-state value. However, it need not be the case that $y(k)$ has already reached 90% of its steady-state value y_{ss} at discrete time k_1 when the first learning block ends. The rise time is computed by extending forward in time the solution curve of the relevant block of trials. ◁

Definition 9.2.2 (Reduced Savings)**.** Suppose we have a duration $T_{wo} > 0$ and times $k_2 > k_{wo} + T_{wo} > k_{wo} > k_1 > k_0$ such that: $w(k) = d_0$ for $k \in [k_0, k_1) \cup [k_{wo} + T_{wo}, \infty)$, $w(k) = -d_0$ for $k \in [k_1, k_{wo})$, $w(k) = 0$ for $k \in [k_{wo}, k_{wo} + T_{wo})$, and $y(k_2) = y(k_0) = y_0$. Let T_{r0} and T_{r2} be the rise times starting at k_0 and k_2, respectively. We say (9.2.1a) - (9.2.1b) exhibits *reduced savings* if $T_{r0} \geq T_{r2}$ and $\lim_{T_{wo} \to \infty} T_{r2} = T_{r0}$. ◁

Definition 9.2.3 (Anterograde Interference)**.** Suppose there exist discrete times $k_2 > k_1 > k_0$ such that: $w(k) = d_0$ for $k \in [k_0, k_1)$, $w(k) = -d_0$ for $k \in [k_1, \infty)$, and $y(k_2) = -y(k_0)$. Let T_{r0} and T_{r2} be the rise times starting at k_0 and k_2, respectively. We say (9.2.1a) - (9.2.1b) exhibits *anterograde interference* if $T_{r0} < T_{r2}$. Moreover T_{r2} increases as the number of trials in the first learning block increases. ◁

Definition 9.2.4 (Rapid Unlearning)**.** Suppose there exist discrete times $k_2 > k_1 > k_0$ such that: $w(k) = d_0$ for $k \in [k_0, k_2)$, $w(k) = 0$ for

$k \in [k_2, \infty)$, and $y(k_1) = y_{ss} - y(k_2)$. Let T_{r1} and T_{r2} be the rise times starting at k_1 and k_2, respectively. We say (9.2.1a) - (9.2.1b) exhibits *rapid unlearning* if $T_{r1} > T_{r2}$. Moreover T_{r2} decreases as the number of trials in the first learning block decreases. ◁

Definition 9.2.5 (Rapid Downscaling)**.** Suppose there exist $\alpha \in (0, 1)$ and discrete times $k_2 > k_1 > k_0$ such that: $w(k) = d_0$ for $k \in [k_0, k_2)$, $w(k) = \alpha d_0$ for $k \in [k_2, \infty)$, and $y(k_1) = (1 + \alpha)y_{ss} - y(k_2)$. Also, we assume that the steady-state value of $y(k)$ for $k \geq k_2$ is αy_{ss}, and $|y(k_2)| > \alpha |y_{ss}|$. Let T_{r1} and T_{r2} be the rise times starting at k_1 and k_2, respectively. We say (9.2.1a) - (9.2.1b) exhibits *rapid downscaling* if $T_{r1} > T_{r2}$. Moreover T_{r2} decreases as the number of trials in the first learning block $k_2 - k_0$ decreases. ◁

Remark 9.2. The justification for the expression $y(k_1) = (1 + \alpha)y_{ss} - y(k_2)$ in the previous definition is as follows. To make a fair comparison between the rise times for the learning block and the downscaling block, the output $y(k)$ must vary over the same range of values. If the initial time for the measurement of rise time in the learning block is selected to be k_1, then the total variation of $y(k)$ from this time to steady-state is $y_{ss} - y(k_1)$. Similarly, for the downscaling block, the total variation of $y(k)$ is $y(k_2) - \alpha y_{ss}$. Equating these two expressions and solving for $y(k_1)$, we obtain the expression above. ◁

Definition 9.2.6 (Spontaneous Recovery)**.** Suppose there exist discrete times $k_2 > k_1 > k_0$ such that $w(k) = d_0$ for $k \in [k_0, k_1)$, $w(k) = -d_0$ for $k \in [k_1, k_2)$, $w(k) = 0$ for $k \in [k_2, \infty)$, and $y(k_2) = y(k_0)$. We say (9.2.1a) - (9.2.1b) exhibits *spontaneous recovery* if the percent overshoot starting from $y(k_2) = y_0$ satisfies: $OS\% > 0$. ◁

The most important observation regarding the dynamic properties of visuomotor adaptation, also confirmed experimentally (Kojima *et al.*, 2004), is that they cannot arise from a first-order LTI model.

Lemma 9.2.7. Consider the stable system (9.2.1a)-(9.2.1b). If the system is first-order, then it does not exhibit savings, anterograde interference, rapid unlearning, rapid downscaling, or spontaneous recovery.

9.3 Visuomotor Adaptation Model

Consider the scalar open-loop system

$$x(k+1) = Ax(k) + Bu(k) \tag{9.3.1a}$$
$$e(k) = r(k) - x(k) - \overline{d}\,. \tag{9.3.1b}$$

This model provides a high-level, abstract description of the quantitative change in movement over successive trials of a single degree of freedom of the body. Integer k is the trial number; $x(k)$ is the state of that single degree of freedom at the end of the k-th trial; $u(k)$ captures the overall motor command; $r(k)$ is the desired target position for the k-th trial; $\overline{d}$ models a constant additive visual disturbance at the k-th trial; and $e(k)$ is a visual error observed by the subject shortly following the completion of the k-th trial. The term $Ax(k)$ models a retention or memory mechanism of the state in the previous trial. Since we assume disturbances are constant, $q = 1$ and $S = 1$. Also, we assume w.l.o.g. that $r(k) = 0$.

To obtain a model of visuomotor adaptation, we follow the design steps in Section 8.1. These steps include selecting the stabilizing controller u_s, the adaptive internal model, and the parameter adaptation law. To this end, it is helpful to consider the error model, derived from (9.3.1b):

$$e(k+1) = Ae(k) - Bu(k) + (A-1)\overline{d} \tag{9.3.2}$$
$$= Ae(k) - Bu(k) + B\psi w(k)\,. \tag{9.3.3}$$

Since $e(k)$ is available for measurement, the stabilizing observer (8.1.5) that generates $\hat{z}_s$ is not required. We take $u_s(k) = Ke(k)$ where K is such that $|A - BK| < 1$. The adaptive internal model is given in (8.1.8) and (8.1.11), where $z(k) = e(k)$, and we take note of the minus sign multiplying B. We define $\hat{e}(k) = \hat{z}_d(k)$ in (8.1.8). This notation suggests that $d_f(k) = e(k) - \hat{e}(k)$ may be interpreted as a *prediction error* (Slotine and Li, 1991). Using this notation, (8.1.8) and (8.1.11) become:

$$\hat{e}(k+1) = A\hat{e}(k) - Bu(k) + L_d(e(k) - \hat{e}(k))$$
$$\hat{w}_f(k+1) = F\hat{w}_f(k) + G(e(k) - \hat{e}(k))\,.$$

Finally, we must specify the parameter adaptation law. Visuomotor adaptation can be differentiated as *short-term adaptation* taking place over minutes, and *long-term adaptation* taking place over days and weeks (Robinson *et al.*, 2006). We interpret short-term adaptation in terms of disturbance rejection, with the dominant behavior arising from the dynamics of $\hat{w}_f$. Long-term adaptation is known to regard adaptation to changes in plant parameters (Robinson *et al.*, 2006). Because we only model short-term adaptation, we assume (8.1.8) already utilizes the correct values of A and B.

The last assumption is that because we restrict the model to constant disturbances, we assume that $\hat{\psi}_f$ has already adapted to its correct value. To derive this expression, define $\widetilde{e}(k) := e(k) - \hat{e}(k)$. Then

$$\widetilde{e}(k+1) = A_d\widetilde{e}(k) + B\psi w(k)\,,$$

where $A_d = A - L_d$. In steady-state we have

$$d_f(k) = \frac{B}{1-A_d}\psi w(k) = \psi w_f(k)\,.$$

Therefore,

$$d(k) = \psi w(k) = \frac{1-A_d}{B}\psi w_f(k) = \psi_f w_f(k)\,,$$

so $\psi_f = \frac{1-A_d}{B}\psi$. Then we take $u_{im}(k) = \psi_f\hat{w}_f(k)$.

In summary, our model of visuomotor adaptation is

$$x(k+1) = Ax(k) + Bu(k) \tag{9.3.4a}$$
$$e(k) = -x(k) - \overline{d} \tag{9.3.4b}$$
$$\hat{e}(k+1) = A\hat{e}(k) - Bu(k) + L_d(e(k) - \hat{e}(k)) \tag{9.3.4c}$$
$$\hat{w}_f(k+1) = F\hat{w}_f(k) + G(e(k) - \hat{e}(k)) \tag{9.3.4d}$$
$$u(k) = Ke(k) + \psi_f\hat{w}_f(k)\,. \tag{9.3.4e}$$

9.4 Simulations

Consider the *visuomotor rotation experiment* (Krakauer *et al.*, 2005; Shadmehr and Wise, 2005), in which a human subject makes rapid

reaches with a mouse or manipulandum from a start position to a target position on a computer screen. The hand is occluded from view, but its position at the end of each reach is momentarily presented by a cursor on the screen. In this scenario, $x(k)$ is the angle (in degrees) of the final hand position at the k-th reach relative to a reference line and measured at a predetermined radius from the start position; $\overline{d}$ is an experimentally imposed disturbance (in degrees) in the observed cursor angle on the k-th reach. The disturbance $\overline{d}$ is constant within a particular block of trials, while it instantaneously jumps in value between blocks of trials. The cursor angle within a block of trials at the k-th reach observed by the subject is $y(k) = x(k) + \overline{d}$. We assume w.l.o.g. that $r(k) = 0$ is the constant reference angle of the target disk. If we assume only constant disturbances, no proprioception of the hand position ($A = 0$), and $B = 1$, the error model within a block of trials is:

$$e(k+1) = -u(k) - \overline{d}\,.$$

Next consider a different behavior called *saccade adaptation*. It is known that proprioception plays no role in saccade adaptation, so $A = 0$. Also w.l.o.g. let $B = 1$. The reference $r(k)$ represents the desired change in eye position (the desired saccade size) for the k-th saccade; $x(k)$ represents the change in eye position during the k-th saccade; and $e(k)$ represents the error between the final eye position and the target position at the end of the k-th primary saccade. The disturbance $\overline{d}$ represents an experimentally imposed displacement of the target position introduced while the saccade is underway. The error is therefore given by $e(k) = r(k) + \overline{d} - x(k)$. Now the error model within a block of trials (with constant disturbance) is:

$$e(k+1) = -u(k) + r(k+1) + \overline{d}\,.$$

This error model seems not to be amenable to our analysis since the desired saccade size $r(k)$ varies from saccade to saccade in a possibly random manner. This contrasts with the visuomotor rotation experiment where the target position is assumed to be fixed throughout the experiment. Therefore, we cannot regard $r(k+1) + \overline{d}$ to be a constant disturbance. However, it is known that saccade adaptation occurs over

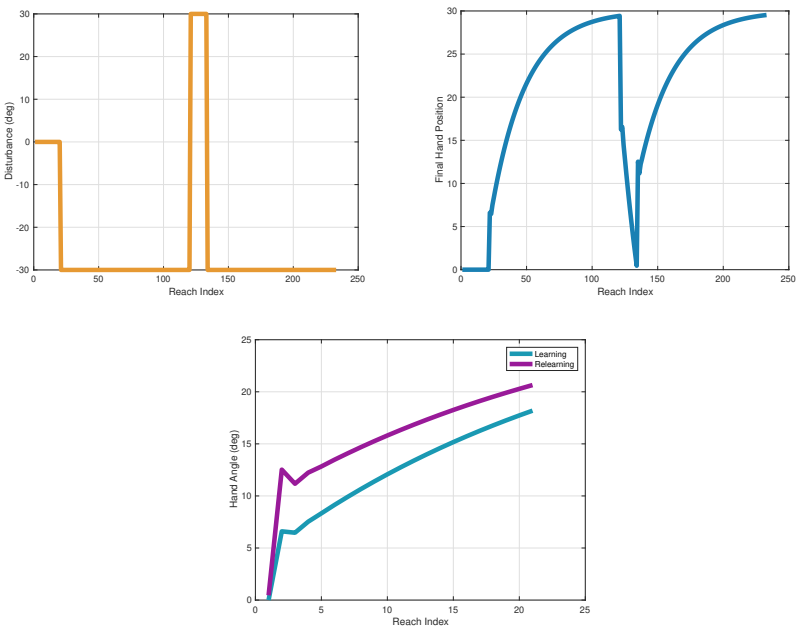

Figure 9.1: Savings with CP in a BLUR experiment. The top left figure shows the disturbance angle (yellow) and the top right figure shows the hand angle (blue). During the two learning blocks, the disturbance has a value -30°. The bottom figure demonstrates that learning has occurred in the second learning block. In the figure, $x(k)$ during the learning block is plotted in blue superimposed with a horizontally shifted version of $x(k)$ during the relearning block in purple. The purple curve is larger than the blue curve corresponding to faster learning in the relearning block.

adaptation fields (Frens and Opstal, 1994), where each adaptation field corresponds to saccades of roughly the same size and direction. This means that for a given adaptation field, $r(k)$ may be regarded once again to be a constant $\overline{r}$. Thus, the error model within a block of trials becomes

$$e(k+1) = -u(k) + \overline{r} + \overline{d}\,.$$

In sum, we can study either the saccadic system or the visuomotor rotation experiment with the same parameters: $A = 0$, $B = 1$, and $S = 1$.

Figures 9.1-9.6 present simulation results for the visuomotor rotation experiment. As discussed above, we assume that $A = 0$ (no proprio-

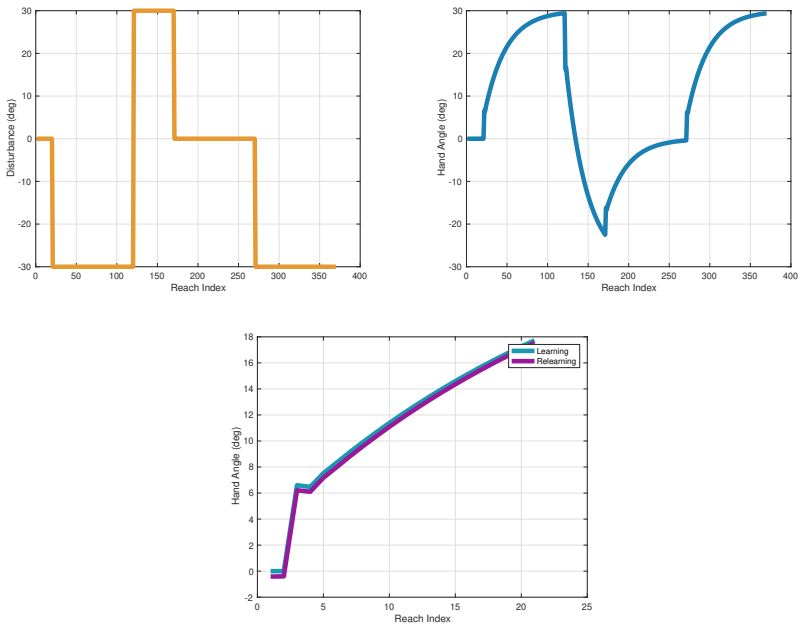

Figure 9.2: Reduced savings in a BLUWR experiment. The top left figure shows the disturbance angle (yellow) and the top right figure shows the hand angle (blue). During the two learning blocks, the disturbance has a value $-30°$. An intervening unlearning block with the opposite disturbance and a washout block with no disturbance are inserted between the two learning blocks. The bottom figure demonstrates that learning is reduced in the second learning block. In the figure, $x(k)$ during the learning block is plotted in blue superimposed with a horizontally shifted version of $x(k)$ during the relearning block in purple. The purple curve is no longer larger than the blue curve, meaning faster learning does not take place in the relearning block.

ception), $B = 1$, and $S = 1$ (all reference and disturbance signals are constant). Also, $K = 0.22$, $F = 0.8$, $G = 0.2$, $L_d = 0$, and $r(k) = 0$. In all figures, the left figure shows the disturbance as a function of the index k and the middle figure shows $x(k)$. For example, the left figure in Figure 9.1 shows that $\overline{d} = 0$ during the baseline block, $\overline{d} = -30$ during the learning block, $\overline{d} = 30$ during the counter-perturbation block, and $\overline{d} = -30$ during the relearning block. The center figure shows that $x(k)$ approaches its steady-state value $x_{ss} = 30$ during the learning block, and the steady-state value $-x_{ss} = 30$ during the unlearning block.

The right figure in Figure 9.1 verifies that savings has occurred in the

BLUR experiment. We plot $x(k)$ during the learning block superimposed with a horizontally shifted version of $x(k)$ during the relearning block. Precisely, $x(k)$ over the discrete time interval $k \in [k_0, k_0 + 20]$ is shown in blue, and $x(k + k_3)$ over the time interval $k \in [0, 20]$ is shown in purple. The time k_3 is the second time when $x(k_3)$ equals 0. We can see that the purple curve is larger than the blue curve, corresponding to faster learning in the relearning block.

In Figure 9.2 a washout block with $\overline{d} = 0$ has been inserted between the learning and relearning blocks. In the right figure $x(k+k_1)$ over the time interval of the learning block is shown in blue, and $x(k + k_2)$ over the time interval of the relearning block is shown in purple. The discrete time k_1 near the beginning of the learning block and the discrete time k_2 near the beginning of the relearning block are selected such that $x(k_1) = x(k_2)$. We can see that the purple curve is almost identical to the blue curve, corresponding to reduced savings.

The striking similarity between our simulation results and the experimental results reported in Figure 3A of (Kojima *et al.*, 2004) is noteworthy. Particularly, the *inflections* noted in (Kojima *et al.*, 2004) and observed on the right of Figure 9.1 following the fast rise of $x(k)$ seem to be an intrinsic feature of the adaptation response of the saccadic system.

Remark 9.3. The appearance of savings can be understood in terms of the two components of the input (6.4.6k). When there is a sudden change in the disturbance, as is the case between learning/unlearning blocks, the $Ke(k)$ term responds proportionally to this error with K relatively small. Then the change in hand angle from one trial to the next is $(K - 1)e(k)$, with $e(k)$ large, resulting in a fast change in the hand position at the start of each block. Instead, the change in $\hat{w}(k)$ is significantly slower. ◁

Figures 9.3-9.5 demonstrate anterograde interference, rapid unlearning, and rapid downscaling, with the interpretations of plots analogous to the interpretations for Figure 9.1. Figure 9.6 demonstrates spontaneous recovery. The right figure shows $x(k)$, particularly that $x(k)$ rebounds to a value greater than 0 during the washout block corresponding to

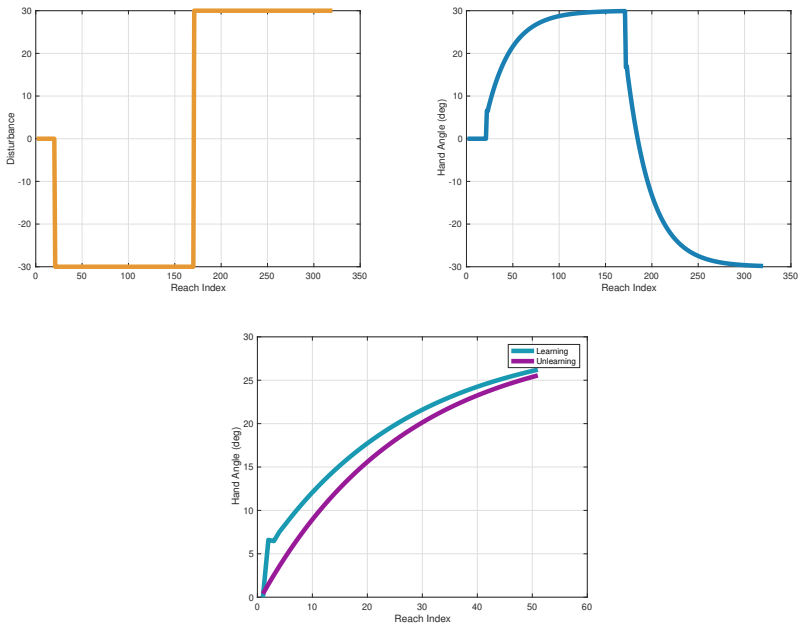

Figure 9.3: Anterograde interference in a BLU experiment. The top left figure shows the disturbance angle (yellow) and the top right figure shows the hand angle (blue). The bottom figure demonstrates that learning the first disturbance in the first learning block slows down learning of the second and opposite disturbance in the unlearning block. In the right figure $x(k)$ over the interval of the learning block is shown in blue, and $-x(k+k_2)$ over the interval of the unlearning block is shown in purple. The blue curve is larger than the purple curve indicating that the learning rate is reduced in the unlearning block.

$k \in [140, 240]$, even though the steady state value for the washout block is $x_{ss} = 0$.

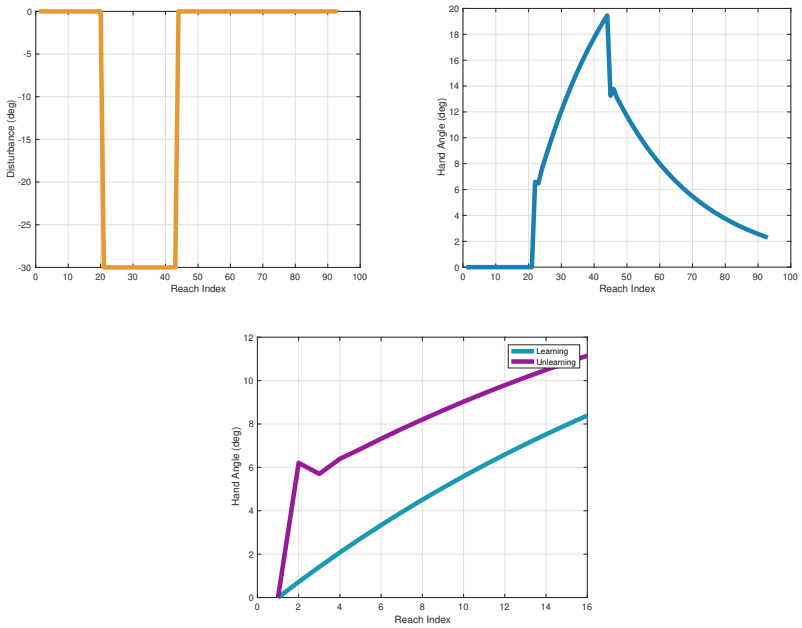

Figure 9.4: Rapid unlearning in a BLW experiment. The top left figure shows the disturbance angle (yellow) and the top right figure shows the hand angle (blue). The bottom figure demonstrates that due to the brevity of the learning block, the disturbance is rapidly unlearned. In the figure, $x(k)$ over the interval of the learning block is shown in blue, and $-x(k+k_2)$ over the interval of the washout block is shown in purple. The purple curve is larger than the blue curve indicating that the rate of unlearning the disturbance in the washout block is faster than the rate of learning in the learning block.

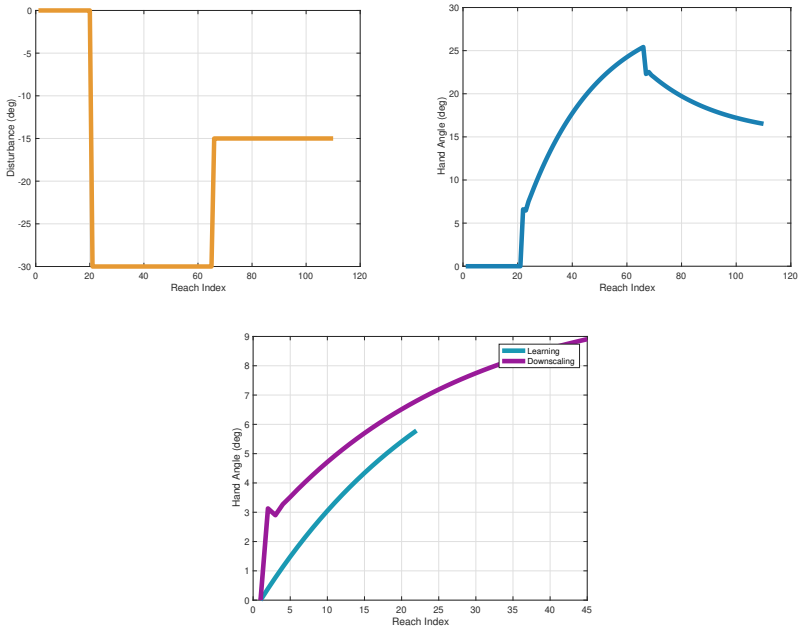

Figure 9.5: Rapid downscaling in a BLD experiment. The top left figure shows the disturbance angle (yellow) and the top right figure shows the hand angle (blue). The bottom figure demonstrates that learning a downscaled disturbance is sped up after first learning the full disturbance (here -30°). In the figure, $x(k)$ over the interval of the learning block is shown in blue, and a suitably scaled version of $-x(k+k_2)$ over the interval of the downscaling block is shown in purple. The purple curve is larger than the blue curve indicating that the learning rate is larger in the downscaling block.

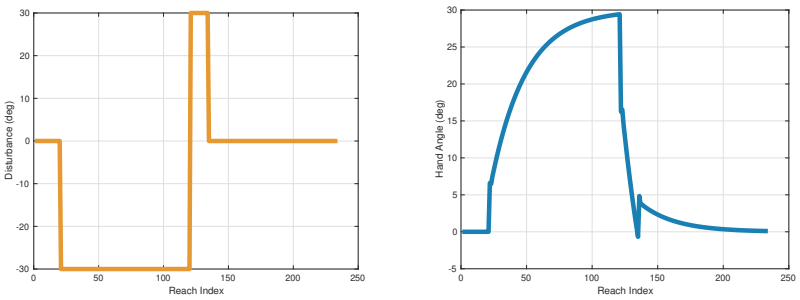

Figure 9.6: Spontaneous recovery in an LUW experiment. The top left figure shows the disturbance angle (yellow) and the top right figure shows the hand angle (blue). The right figure shows that the hand angle rebounds to a value greater than zero during the washout block, even though $x_{ss} = 0$.

10

Concluding Remarks

This monograph explores the idea that the brain, particularly the cerebellum, utilizes internal models in order to satisfy the requirements of the internal model principle of control theory. This interpretation of cerebellar function in terms of disturbance rejection of exogenous signals has brought into view results from control theory on the regulator problem, particularly recent progress on adaptive internal models.

We used adaptive internal models to model the contribution of the cerebellum to the eye movement systems: the vestibulo-ocular reflex, gaze holding, smooth pursuit, and the optokinetic system. We also jointly studied the saccadic system and visuomotor adaptation from the perspective of disturbance rejection. A modeling approach based on the internal model principle has the benefit to render a unified interpretation to seemingly disparate phenomena of motor systems. Nevertheless, many unsolved problems and open questions remain.

Linear regulator theory. We have initiated a discussion on linear regulator theory for neuroscience applications. A number of areas need to be further developed. First, we have not considered adaptation to changes in plant parameters. This subject is part of a general inquiry to

understand so-called *long-term adaptation*. Particularly, what are the mathematical processes underpinning long-term adaptation, and what is the involvement of the cerebellum? Second, it is likely necessary to revisit designs based on error feedback - Regulator Design V was inspired by currently available engineering designs, but it is not known to what extend the observers utilized in that design may be present in the brain. Third, we have used state feedback and observers to stabilize the closed-loop system, as these methods were expedient in the particular designs being considered. However, *robust stabilization methods*, *high gain feedback*, *high gain observers*, and *adaptive pole placement* are some methods that may be considered so that stabilization can be fully decoupled from processes associated with regulation and disturbance rejection. Such a modular approach is far more realistic in a neurological setting.

Intermittent Measurements. A mathematical framework that extends regulator theory to handle intermittent error measurements in neuroscience applications must be developed. Current frameworks for handling intermittent measures in regulator theory are generally based on engineering design principles that do not accord with experimental findings in neuroscience. Visuomotor adaptation is a specific case in point.

Time Delays. All of the models presented here made no special provisions for time delays in sensory measurements arriving at the cerebellum. An extension of the presented regulator designs is to include additional adaptive processes that cancel the effects of unknown time delays.

Robustness. More generally, the issue of robustness was not treated in any of the designs we presented. The primary issue we believe needs to be addressed is the presence of unmodeled, bounded disturbances. Modified parameter adaptation laws may need to be investigated, and assumptions about persistency of excitation may need to be revisited in the context of biological problems.

Nonlinear regulator theory. It will be necessary to extend nonlinear regulator theory for neuroscience appications, particularly to under-

stand the cerebellum's contribution to locomotion and limb movement. Adaptive control of robotic manipulators will no doubt provide inspiration for this development. The challenge for these motor systems is that they also involve a recurrent loop between the cerebellum and the motor cortex.

Parallel Adaptive Internal Models. So far we have only investigated two functional modules of the cerebellum: the part of the flocculus responsible for the slow eye movements and the part of the nodulus/uvula responsible for regulating the optokinetic system. Of great interest is to understand the combined behavior of the flocculus and the nodulus/uvula using the mathematical insights of control theory.

Cerebellar Micro-circuit. The models we are working with for the cerebellum are abstract and high level. A mapping from these high level models to the cerebellar microcircuit is required.

Visuomotor Adaptation Model. Complex nonlinear phenomena, such as saturation in the controller, have been discovered for visuomotor adaptation (Hafez *et al.*, 2021). A great deal more work is needed to complete the model of visuomotor adaptation. Of particular interest is the role played by the cerebral cortex. What are the mathematical processes underlying *consolidation* and *learning transfer*? What role does the cerebellum play in enabling these processes?

Discrete-time v.s. Continuous-time Models. We have worked both in discrete-time and ccontinuous-time to model processes in the brain. However, ultimately, all signals in the brain are continuous time. Our model of visuomotor adaptation is considerably more abstract than, say, our model of the slow eye movement systems, for which it has been possible to make concrete comparisons with signals recorded in the brain. The development of more realistic, continuous-time models of discrete-time, event-driven phenomena such as visuomotor adaptation provides an intriguing avenue to obtain deeper insight on the universal computations of the cerebellum.

References

Albus, J. S. (1971). "A theory of cerebellar function". *Mathematical Biosciences*. 10(1): 25–61.

Anderson, B. and R. B. et. al. (1986). *Stability of Adaptive Systems*. The MIT Press.

Apps, R., R. Hawkes, and S. A. et. al. (2018). "Cerebellar modules and their role as operational cerebellar processing units". *Cerebellum*. 17: 654–682.

Baarsma, E. and H. Collewijn. (1974). "Vestibulo-ocular and optokinetic reactions to rotation and their interaction in the rabbit". *Journal of Physiology*. 238: 603–625.

Bahill, A. and J. McDonald. (1983a). "Model emulates human smooth pursuit system producing zero-latency target tracking". *Biological Cybernetics*. 48: 213–222.

Bahill, A. and J. McDonald. (1983b). "Smooth pursuit eye movements in response to predictable target motions". *Vision Research*. 23(12): 1573–1583.

Barabasi, A.-L. and Z. Oltvai. (2004). "Network biology: understanding the cell's functional organization". *Nature Reviews Genetics*. 5(Feb.): 101–113.

Barlow, J. (2002). *The Cerebellum and Adaptive Control*. Cambridge University Press.

Barmack, N. (2006). "Inferior olive and oculomotor system". *Progress in Brain Research*. 151: 269–291.

Barmack, N., B. R., P. Errico, and H. Shojaku. (1993). "Vestibular primary afferent projection to the cerebellum of the rabbit". *J. Comp. Neurology*. 327: 521–534.

Barnes, G., S. Donnelly, and R. Eason. (1987). "Predictive velocity estimation in the pursuit reflex response to pseudo-random and step displacement stimuli in man". *Journal of Physiology*. 389: 111–136.

Barnes, G., S. Goodbody, and S. Collins. (1995). "Volitional control of anticipatory ocular pursuit responses under stabilized image conditions in humans". *Experimental Brain Research*. 106: 301–317.

Basturk, H. (2017). "Cancellation of unmatched biased sinusoidal disturbances for unknown LTI systems in the presence of state delay". *Automatica*. 76: 169–176.

Basturk, H. and M. Krstic. (2012). "Adaptive cancellation of matched unknown sinusoidal disturbances for unknown LTI systems by state derivative feedback". In: *2012 American Control Conference (ACC)*. 1149–1154.

Basturk, H. and M. Krstic. (2014). "State derivative feedback for adaptive cancellation of unmatched disturbances in unknown strict-feedback LTI systems". *Automatica*. 50(10): 2539–2545.

Basturk, H. and M. Krstic. (2015). "Adaptive sinusoidal disturbance cancellation for unknown LTI systems despite input delay". *Automatica*. 58: 131–138.

Battle, E. and M. Broucke. (2021). "Adaptive internal models in the optokinetic system". In: *IEEE Conference on Decision and Control*.

Berthoz, A. (1988). "The role of gaze in compensation of vestibular dysfunction: the gaze substitution hypothesis". *Progress Brain Research*. 76: 411–420.

Blohm, G., M. Missal, and P. Lefevre. (2005). "Direct evidence for a position input to the smooth pursuit system". *Journal of Neurophysiology*. 94: 712–721.

Bodson, M. and S. Douglas. (1997). "Adaptive algorithms for the rejection of sinusoidal disturbances with unknown frequency". *Automatica*. 33(12): 2213–2221.

Bodson, M., A. Sacks, and P. Khosla. (1994). "Harmonic generation in adaptive feedforward cancellation schemes". *IEEE Transactions on Automatic Control*. 39(9): 1939–1944.

Breakspear, M. (2017). "Dynamic models of large-scale brain activity". *Nature Neuroscience*. 20: 3.

Brockett, R. (1965). "Poles, zeros, and feedback: state space interpretation". *IEEE Transactions on Automatic Control*. 10(2): 129–135.

Broucke, M. (2020). "Model of the oculomotor system based on adaptive internal models". *IFAC World Congress*. 53(2): 16430–16437.

Broucke, M. (2021). "Adaptive internal model theory of the oculomotor system and the cerebellum". *IEEE Transactions on Automatic Control*.

Buettner, U. and U. U. Buttner. (1979). "Vestibular nuclei activity in the alert monkey during suppression of vestibular and optokinetic nystagmus". *Experimental Brain Research*. 37: 581–593.

Büttner, U. and J. Büttner-Ennever. (2006). "Present concepts of oculomotor organization". *Prog. Brain Research*. 151: 1–42.

Büttner, U. and W. Waespe. (1984). "Purkinje cell activity in the primate flocculus during optokinetic stimulation, smooth pursuit eye movements, and VOR-suppression". *Experimental Brain Research*. 55: 97–104.

Büttner, U., W. Waespe, and V. Henn. (1976). "Duration and direction of optokinetic after-nystagmus as a function of stimulus exposure time in the monkey". *Arch. Psychiat. Nervenkr.* 222: 281–291.

Büttner-Ennever, J. and A. Horn. (1997). "Anatomical substrates of oculomotor control". *Current Opinion in Neurobiology*. 7: 872–879.

Byrnes, C., F. D. Priscoli, and A. Isidori. (1997). *Output Regulation of Uncertain Nonlinear Systems*. Birkhauser.

Calvert, T. and F. Meno. (1972). "Neural Systems Modeling Applied to the Cerebellum". *IEEE Transactions on Systems, Man, and Cybernetics*. SMC-2(3): 363–374.

Cannon, S. and D. Robinson. (1987). "Loss of the neural integrator of the oculomotor system from brain stem lesions in monkey". *Journal of Neurophysiology*. 57(5): 1383–1409.

Carpenter, R. (1972). "Cerebellectomy and the transfer function of the vestibulo-ocular reflex in the decerebrate cat". *Proc. Royal Society of London, Series B, Biological Sciences*. 181(1065): 353–374.

Cassanello, C., S. Ohl, and M. Rolfs. (2016). "Saccadic adaptation to a systematically varying disturbance". *Journal of Neurophysiology*. 116: 336–350.

Cerminara, N., R. Apps, and D. Marple-Horvat. (2009). "An internal model of a moving visual target in the lateral cerebellum". *J. Physiology*. 587(2): 429–442.

Churchland, M., I. Chou, and S. Lisberger. (2003). "Evidence for object permanence in the smooth-pursuit eye movements of monkeys". *Journal of Neurophysiology*. 90: 2205–2218.

Cohen, B., V. Matsuo, and T. Raphan. (1977). "Quantitative analysis of the velocity characteristics of optokinetic mystagmus and optokinetic after-nystagmus". *J. Physiology*. 270: 321–344.

Collewijn, H. and E. Tamminga. (1984). "Human smooth and saccadic eye movements during voluntary pursuit of different target motions on different backgrounds". *J. Physiology*. 351: 217–250.

Dale, A. and K. Cullen. (2015). "Local population synchrony and the encoding of eye position in the primate neural integrator". *Journal of Neuroscience*. 35(10): 4287–4295.

Davison, E. (1972). "The output control of linear time-invariant multivariable systems with unmeasurable arbitrary disturbances". *IEEE Transactions on Automatic Control*. 17: 621–630.

Davison, E. (1975). "A generalization of the output control of linear time-invariant multivariable systems with unmeasurable arbitrary disturbances". *IEEE Transactions on Automatic Control*. 20: 788–792.

Davison, E. (1976). "The robust control of a servomechanism problem for linear time-invariant multivariable systems". *IEEE Transaction on Automatic Control*. 21(1): 25–35.

Dayan, P. and L. Abbott. (2001). *Theoretical Neuroscience: Computational and Mathematical Modeling of Neural Systems*. The MIT Press.

Dean, P. and J. Porrill. (2008). "Adaptive filter models of the cerebellum: computational analysis". *Cerebellum*. 7: 567–571.

Dean, P., J. Porrill, C.-F. Ekerot, and H. Jorntell. (2010). "The cerebellar microcircuit as an adaptive filter: experimental and computational evidence". *Nature Reviews: Neuroscience*. 11(Jan.): 30–45.

Dean, P., J. Porrill, and J. Stone. (2002). "Decorrelation control by the cerebellum achieves oculomotor plant compensation in simulated vestibulo-ocular reflex". *The Royal Society*. 269: 1895–1904.

Deno, D., W. Crandall, K. Sherman, and E. Keller. (1995). "Characterization of prediction in the primate visual smooth pursuit system". *BioSystems*. 34: 107–128.

Eccles, J., M. Ito, and J. Szentagothai. (1967). *The Cerebellum as a Neuronal Machine*. Springer.

Eggers, S., N. de Pennington, M. Walker, M. Shelhamer, and D. Zee. (2003). "Short-term adaptation of the VOR: non-retinal-slip error signals and saccade substitution". *Ann. N.Y. Academy of Sciences*. 1004: 94–110.

Fiorentini, L., A. Serrani, and S. Longhi. (2006). "A state-space approach to adaptive rejection of harmonic sensor disturbances in discrete-time systems". In: *2006 14th Mediterranean Conference on Control and Automation*. 1–6.

Francis, B. (1977). "The linear multivariable regulator problem". *SIAM Journal on Control and Optimization*. 15(3): 486–505.

Francis, B. and W. Wonham. (1975). "The internal model principle for linear multivariable regulators". *Applied Mathematics and Optimization*. 2(2): 170–194.

Francis, B. and W. Wonham. (1976). "The internal model principle of control theory". *Automatica*. 12: 457–465.

Frens, M. and A. van Opstal. (1994). "Transfer of short-term adaptation in human saccadic eye movements". *Exp. Brain Res.* 100: 293–306.

Fujita, M. (1982). "Adaptive filter model of the cerebellum". *Biological Cybernetics*. 45: 195–206.

Galiana, H. and J. Outerbridge. (1984). "A bilaternal model for central neural pathways in vestibuloocular reflex". *Journal of Neurophysiology*. 51(2): 210–241.

Gantmacher, F. (1959). *Matrix Theory. Vol 1.* Chelsea Press.

Gawad, A. and M. Broucke. (2020). "Visuomotor Adaptation is a Disturbance Rejection Problem". In: *IEEE Conference on Decision and Control*. 3895–3900.

Gerasimov, D., A. Miliushin, and V. Nikiforov. (2019a). "Algorithms of adaptive tracking of unknown multisinusoidal signals in linear systems with arbitrary input delay". *International Journal of Adaptive Control and Signal Processing*. 33(6): 900–912.

Gerasimov, D., A. Miliushin, A. Paramonov, and V. Nikiforov. (2019b). "Algorithms of Adaptive Tracking of Unknown Multi-Sinusoidal Signals in MIMO Linear Systems with Multiple Input Delay". In: *2019 American Control Conference (ACC)*. 3014–3019.

Gerasimov, D., A. Paramonov, and V. Nikiforov. (2020). "Algorithms of adaptive disturbance compensation in linear systems with arbitrary input delay". *International Journal of Control*. 93(7): 1596–1604.

Gernstner, W. and e. a. W. Kistler. (2014). *Neuronal Dynamics: From Single Neurons to Networks and Models of Cognition*. Cambridge University Press.

Gerrits, N., A. Epema, A. van Linge, and E. Dalm. (1989). "The primary vestibulocerebellar projection in the rabbit: absence of primary afferents in the flocculus." *Neuroscience Letters*. 105: 27–33.

Girard, B., N. Tabareau, Q. Pham, A. Berthoz, and J.-J. Slotine. (2008). "Where neuroscience and dynamic system theory meet autonomous robotics: a contracting basal ganglia model for action selection". *Neural Networks*. 21(4): 628–641.

Glasauer, S. (2003). "Cerebellar contribution to saccades and gaze holding". *Annals New York Academy of Sciences*. 1004(1): 206–219.

Goebel, R., R. Sanfelice, and A. Teel. (2009). "Hybrid dynamical systems". *IEEE Control Systems Magazine*. 29: 28–93.

Gomi, H. and M. Kawato. (1992). "Adaptive feedback control models of the vestibulocerebellum and spinocerebellum". *Biological Cybernetics*. 68: 105–114.

Green, A., Y. Hirata, H. Galiana, and S. Highstein. (2004). *Localizing sites for plasticity in the vestibular system*.

Green, A., H. Meng, and D. Angelaki. (2007). "A reevaluation of the inverse dynamic model for eye movements". *Journal of Neuroscience*. 27(6): 1346–1355.

Gu, S., R. Betzel, and M. M. et. al. (2017). "Optimal trajectories of brain state transitions". *NeuroImage*. 148: 305–317.

Gu, S., F. Pasqualetti, and M. C. et. al. (2015). "Controllability of structural brain networks". *Nature Communications*. 6(1): 1–10.

Guo, X. and M. Bodson. (2009). "Analysis and Implementation of an Adaptive Algorithm for the Rejection of Multiple Sinusoidal Disturbances". *IEEE Transactions on Control Systems Technology*. 17(1): 40–50.

Guthrie, B., J. Porter, and D. Sparks. (1983). "Corollary discharge provides accurate eye position information to the oculomotor system". *Science*. 221(Sept.): 1193–1195.

Hafez, M., E. Uzeda, and M. Broucke. (2021). "Discrete-time output regulation and visuomotor adaptation". *IEEE Conference on Decision and Control*.

Hassul, M. and P. D. Daniels. (1977). "Cerebellar Dynamics: The Mossy Fiber Input". *IEEE Transactions on Biomedical Engineering*. BME-24(5): 449–456.

Heinen, S. and E. Keller. (1996). "The function of the cerebellar uvula in monkey during optokinetic and pursuit eye movements: single-unit responses and lesion effects." *Experimental Brain Research*. 110: 1–14.

Hoagg, J., M. Santillo, and D. Bernstein. (2008). "Discrete-Time Adaptive Command Following and Disturbance Rejection With Unknown Exogenous Dynamics". *IEEE Transactions on Automatic Control*. 53(4): 912–928.

Houck, B. and A. Person. (2014). "Cerebellar loops: a review of the nucleocortical pathway". *Cerebellum*. 13: 378–385.

Houck, B. and A. Person. (2015). "Cerebellar premotor output neurons collateralize to innervate the cerebellar cortex". *Journal of Comparative Neurology*. 523(15): 2254–2271.

Huang, J., A. Isidori, L. Marconi, M. Mischiati, E. Sontag, and W. Wonham. (2018). "Internal models in control, biology, and neuroscience". In: *IEEE Conference on Decision and Control*. 5370–5390.

Iglesias, P. and B. Ingalls. (2009). *Control Theory and Systems Biology*. The MIT Press.

Ioannou, P. and J. Sun. (2012). *Robust Adaptive Control*. Dover.

Isidori, A. (2017). *Lectures in Feedback Design for Multivariable Systems*. Springer-Verlag.

Isidori, A., L. Marconi, and A. Serrani. (2003). *Robust Autonomous Guidance*. Springer London.

Ito, M. (1970). "Neurophysiological aspects of the cerebellar motor control system". *International Journal of Neurology*. 7(2): 162–167.

Ito, M. (1984). *The Cerebellum and Neural Control*. Raven Press.

Johnson, C. (1971). "Accommodation of external disturbances in linear regulator and servomechanism problems". *IEEE Transactions on Automatic Control*. 16: 535–644.

Jones, G. M. and G. Mandl. (1979). "Effects of strobe light on adaptation of vestibulo-ocular reflex (VOR) to vision reversal". *Brain Research*. 164: 300–303.

Jordan, M. and D. Rumelhart. (1992). "Forward models: supervised learning with a distal teacher". *Cognitive Science*. 16: 307–354.

Jordan, M. and E. Todorov. (2002). "Optimal feedback control as a theory of motor coordination". *Nature Neuroscience*. 5(11): 1226–1235.

Kaneko, C. (1999). "Eye movement deficits after ibotenic acid lesions of the nucleus prepositus hypoglossi in monkeys, II: pursuit, vestibular, and optokinetic responses". *Journal of Neurophysiology*. 81: 668–681.

Kassardjian, C., Y. Tan, J. Chung, R. Heskin, M. Peterson, and D. Broussard. (2005). "The site of a motor memory shifts with consolidation". *J. Neuroscience*. 25(35): 7979–7985.

Kawato, M. (1999). "Internal models for motor control and trajectory planning". *Current Opinion in Neurobiology*. 9(6): 718–727.

Kawato, M., K. Furukawa, and R. Suzuki. (1987). "A hierarchical neural-network model for control and learning of voluntary movement". *Biological Cybernetics*. 57: 169–185.

Kawato, M. and H. Gomi. (1992). "A computational model of four regions of the cerebellum based on feedback-error learning". *Biological Cybernetics*. 68: 95–103.

Keller, E. and P. Daniels. (1975). "Oculomotor related interaction of vestibular nucleus cells in alert monkey". *Exp. Neurology*. 46: 187–198.

Keller, E. and D. Robinson. (1971). "Absence of a stretch reflex in extraocular muscles of the monkey". *Journal of Neurophysiology*. 34(5): 908–919.

Khalil, H. (2001). *Nonlinear Systems, 3rd Ed.* Prentice-Hall.

Kim, S.-H., D. Zee, S. du Lac, H. Kim, and J.-S. Kim. (2016). "Nucleus prepositus hypoglossi lesions produce a unique ocular motor syndrome". *American Academy of Neurology*. 87(19): 2026–2033.

Koenig, E. and J. Dichgans. (1981). "Aftereffects of vestibular and optokinetic stimulation and their interaction". *Annals New York Academy of Sciences*. 374: 434–445.

Kojima, Y., Y. Iwamoto, and K. Yoshida. (2004). "Memory of learning facilitates saccadic adaptation in the monkey". *Journal of Neuroscience*. 24(34): 7531–7539.

Krakauer, J., C. Ghez, and M. Ghilardi. (2005). "Adaptation to visuomotor transformations: consolidation, interference, and forgetting". *Journal of Neuroscience*. 25(2): 473–478.

Krauzlis, R., M. Basso, and R. Wurtz. (1997). "Shared motor error for multiple eye movements". *Science*. 276(5319): 1693–1695.

Krauzlis, R. and F. Miles. (1996). "Transitions between pursuit eye movements and fixation in the monkey: dependence on context". *Journal of Neurophysiology*. 76(3): 1622–1638.

Langer, T., A. Fuchs, C. Scudder, and M. Chubb. (0185). "Afferents to the flocculus of the cerebellum in the rhesus macaque as revealed by retrograde transport of horseradish peroxidase". *Journal of Comparative Neurology*. 235: 1–25.

Leigh, R. and D. Zee. (2015). *The Neurology of Eye Movements*. Oxford University Press, 5th ed.

Lisberger, S. (1994). "Neural basis for motor learning in the vestibulooocular reflex of primates. III. Computational and behavioral analysis of the sites of learning". *Journal of Neurophysiology*. 72(2): 974–998.

Lisberger, S. (2009). "Internal models of eye movement in the floccular complex of the monkey cerebellum". *Neuroscience*. 162(3): 763–776.

Lisberger, S. (2015). "Visual guidance of smooth pursuit eye movements". *Annual Rev. Vis. Sci.* 1: 447–468.

Lisberger, S. and A. Fuchs. (1978a). "Role of primate flocculus during rapid behavioral modification of vestibular reflex I: Purkinje cell activity during visually guided horizontal smooth-pursuit eye movements and passive head rotation". *Journal of Neurophysiology*. 41(3): 764–777.

Lisberger, S. and A. Fuchs. (1978b). "Role of primate flocculus during rapid behavioral modification of vestibuloocular reflex. II. Mossy fiber firing patterns during horizontal head rotation and eye movement". *Journal of Neurophysiology*. 41(3): 764–777.

Lisberger, S. and T. Pavelko. (1986). "Vestibular signals carried by pathways subserving plasticity of the vestibulo-ocular reflex in monkeys". *Journal of Neuroscience*. 6(2): 346–354.

Liu, J., H. Khalil, and K. Oweiss. (2011). "Model-based analysis and control of a network of basal ganglia spiking neurons in the normal and Parkinsonian states". *Journal of Neural Engineering*. 8(4).

Liu, J., G. Owess, and H. Khalil. (2010). "Feedback control of spatiotemporal firing patterns of neural microcircuits". *IEEE Conference on Decision and Control*.

Luebke, A. and D. Robinson. (1988). "Transition dynamics between pursuit and fixation suggest different systems". *Vision Research*. 28(8): 941–946.

Madhav, M. and N. Cowan. (2020). "The synergy between neuroscience and control theory: the nervous system as inspiration for hard control problems". *Annual Review of Control, Robotics, and Autonomous Systems*. 3: 243–267.

Maioli, C. (1988). "Optokinetic nystagmus: modeling the velocity storage mechanism". *Journal of Neuroscience*. 8: 821–832.

Mandl, G., G. M. Jones, and M. Cynader. (1981). "Adaptability of the vestibulo-ocular reflex to vision reversal in strobe reared cats". *Brain Research*. 209(1): 35–45.

Marino, R. and P. Tomei. (2000). "Global adaptive compensation of noises with unknown frequency". In: *IEEE Conference on Decision and Control*. Vol. 5. 4926–4927.

Marino, R. and P. Tomei. (2003a). "Output regulation for linear systems via adaptive internal model". *IEEE Transactions on Automatic Control*. 48(12): 2199–2202.

Marino, R. and P. Tomei. (2003b). "Robust adaptive compensation of biased sinusoidal disturbances with unknown frequency". *Automatica*. 39(10): 1755–1761.

Marino, R. and P. Tomei. (2007). "Output Regulation for Linear Minimum Phase Systems With Unknown Order Exosystem". *IEEE Transactions on Automatic Control*. 52(10): 2000–2005.

Marino, R. and P. Tomei. (2011). "An adaptive learning regulator for uncertain minimum phase systems with undermodeled unknown exosystems". *Automatica*. 47(4): 739–747.

Marino, R. and P. Tomei. (2015). "Output Regulation for Unknown Stable Linear Systems". *IEEE Transactions on Automatic Control*. 60(8): 2213–2218.

Marino, R. and P. Tomei. (2016). "Adaptive disturbance rejection for unknown stable linear systems". *Transactions of the Institute of Measurement and Control*. 38(6): 640–647.

Marr, D. (1969). "A theory of the cerebellar cortex". *Journal of Physiology*. 202: 437–470.

Martin, T., J. Keating, H. Goodkin, A. Bastian, and W. Thach. (1996). "Throwing while looking through prisms II. Specificity and Storage of Multiple Gaze-Throw Calibrations". *Brain*. 119: 1199–1211.

Maxwell, J. C. (1868). "On governors". *Proc. Royal Soc. London*. 16.

Miall, R., D. Weir, D. Wolpert, and J. Stein. (1993). "Is the cerebellum a Smith predictor?" *Journal of Motor Behavior*. 25(3): 203–216.

Miall, R. and D. Wolpert. (1996). "Forward models for physiological motor control". *Neural Networks*. 9(8): 1265–1279.

Michael, J. and G. Jones. (1966). "Dependence of visual tracking capability upon stimulus predictability". *Vision Research*. 6(11-12): 707–716.

Miki, S., K. Urase, R. Baker, and Y. Hirata. (2020). "Velocity storage mechanism drives a cerebellar clock for predictive eye velocity control". *Nature Science Reports*. 10(6944).

Miles, F. and B. Eighmy. (1980). "Long-term adaptive changes in primate vestibuloocular reflex. I. Behavioral observations." *Journal of Neurophysiology*. 43(5): 1437–1476.

Montgomery, J. and D. Bodznick. (2016). *Evolution of the Cerebellar Sense of Self*. Oxford University Press.

Morris, E. and S. Lisberger. (1987). "Different responses to small visual errors during initiation and maintenance of smooth-pursuit eye movements in monkeys". *Journal of Neurophysiology*. 58(6): 1351–1369.

Narendra, K. and A. Annaswamy. (1989). *Stable Adaptive Systems*. Dover Publications.

Nikiforov, V. (1996). "Adaptive Servocompensation of Input Disturbances". *IFAC Proceedings Volumes*. 29(1): 5114–5119.

Nikiforov, V. (1997a). "Adaptive controller rejecting uncertain deterministic disturbances in SISO systems". In: *1997 European Control Conference (ECC)*. 1207–1212.

Nikiforov, V. (1997b). "Adaptive servomechanism controller with an implicit reference model". *International Journal of Control*. 68(2): 277–286.

Nikiforov, V. (2004a). "Observers of external deterministic disturbances I. Objects with known parameters". *Automation and Remote Control*. 65(10): 1531–1541.

Nikiforov, V. (2004b). "Observers of external deterministic disturbances II. Objects with unknown parameters". *Automation and Remote Control*. 65(11): 1724–1732.

Nikiforov, V., A. Paramonov, and D. Gerasimov. (2020). "Adaptive Output Servocontroller for MIMO System with Input Delay*". In: *2020 American Control Conference (ACC)*. 620–625.

Noda, H. and D. Suzuki. (1979). "The role of the flocculus of the monkey in fixation and smooth pursuit eye movements". *Journal of Physiology*. 294: 335–348.

Nozari, E. and J. Cortes. (2021a). "Hierarchical Selective Recruitment in Linear-Threshold Brain Networks Part I: Single-Layer Dynamics and Selective Inhibition". *IEEE Transactions on Automatic Control*.

Nozari, E. and J. Cortes. (2021b). "Hierarchical Selective Recruitment in Linear-Threshold Brain Networks Part II: Multi-Layer Dynamics and Top-Down Recruitment". *IEEE Transactions on Automatic Control*.

Ortega, R., V. Nikiforov, and D. Gerasimov. (2020). "On modified parameter estimators for identification and adaptive control". *Annual Reviews in Control*. 50: 278–293.

Ortega, R. and Y. Tang. (1989). "Robustness of adaptive controllers - a survey". *Automatica*. 25(5): 651–677.

Paulin, M. (1989). "A Kalman filter theory of the cerebellum". In: *Dynamic Interactions in Neural Networks: Models and Data*. Ed. by M. Arbib and S. Amari. Springer-Verlag.

Paulin, M. (2005). "Evolution of the cerebellum as a neuronal machine for Bayesian estimation". *Journal of Neural Engineering*. 2(3): 219–234.

Pettorossi, V., P. Errico, A. Ferraresi, and N. Barmack. (1999). "Optokinetic and vestibular stimulation determines the spatial orientation of negative optokinetic afternystagmus in the rabbit". *Journal of Neuroscience*. 19(4): 1524–1531.

Pola, J. (2002). "Models of the saccadic and smooth pursuit systems". In: *Models of the Visual System*. Springer. 385–429.

Pola, J. and H. Wyatt. (1980). "Target position and velocity: the stimulus for smooth pursuit eye movement". *Vision Research*. 20: 523–534.

Porrill, J., P. Dean, and J. Stone. (2004). "Recurrent cerebellar architecture solves the motor-error problem". *Proc. Royal Society of London. B*. 271: 789–796.

Ramanchandran, R. and S. Lisberger. (2008). "Neural substrate of modified and unmodified pathways for learning in monkey vestibulooocular reflex". *J. Neurophysiology*. 100: 1868–1878.

Raphan, T., V. Matsuo, and B. Cohen. (1979). "Velocity storage in the vestibulo-ocular reflex arc (VOR)". *Experimental Brain Research*. 35: 229–248.

Robinson, D. (1974). "The effect of cerebellectomy on the cat's vestibulo-ocular integrator". *Brain Research*. 71(2): 195–207.

Robinson, D. (1981). "The Use of Control Systems Analysis in the Neurophysiology of Eye Movements". *Annual Review of Neuroscience*. 4(1): 463–503.

Robinson, D., J. Gordon, and S. Gordon. (1986). "A model of the smooth pursuit eye movement system". *Biological Cybernetics*. 55: 43–57.

Robinson, F., R. Soetedjo, and C. Noto. (2006). "Distinct Short-Term and Long-Term Adaptation to Reduce Saccade Size in Monkey". *Journal of Neurophysiology*. 96(3): 1030–1041.

Rohrs, C., L. Valavani, M. Athans, and G. Stein. (1985). "Robustness of continuous-time adaptive control algorithms in the presence of unmodeled dynamics". *IEEE Trans. Automatic Control*. 30(9): 881–889.

Roy, J. and K. Cullen. (2003). "Brain Stem Pursuit Pathways: Dissociating Visual, Vestibular, and Proprioceptive Inputs During Combined Eye-Head Gaze Tracking". *Journal of Neurophysiology*. 90(1): 271–290.

Rudin, W. (1976). *Principles of Mathematical Analysis*. McGraw-Hill Education; 3rd edition.

Ruigrok, T. (2011). "Ins and outs of cerebellar modules". *Cerebellum*. 10: 464–474.

Saberi, A., A. Stoorvogel, and P. Sannuti. (2000). *Control of Linear Systems with Regulation and Input Constraints*. Springer.

Sastry, S. and M. Bodson. (1989). *Adaptive Control: Stability, Convergence, and Robustness*. Prentice-Hall.

Schiff, S. (2009). "Kalman meets neuron: the emerging intersection of control theory with neuroscience". *Conf. Proc. IEEE Eng. Med. Biol. Soc.*: 3318–3321.

Schiff, S. (2012). *Neural Control Engineering: The Emerging Intersection between Control Theory and Neuroscience*. The MIT Press.

Scott, S. (2004). "Optimal feedback control and the neural basis of volitional motor control". *Nature Reviews*. 5: 534–546.

Serrani, A. and A. Isidori. (2000). "Semiglobal nonlinear output regulation with adaptive internal model". *IEEE Conference on Decision and Control*. Dec.: 1649–1654.

Serrani, A., A. Isidori, and L. Marconi. (2001). "Semi-global nonlinear output regulation with adaptive internal model". *IEEE Transactions on Automatic Control*. 46(8): 1178–1194.

Shadmehr, R. and S. Wise. (2005). *The Computational Neurobiology of Reaching and Pointing*. MIT Press.

Shelhamer, M., B. Ravina, and P. Kramer. (1995). "Adaptation of the gain of the angular vestibulo-ocular reflex when retinal slip is zero". *Soc. Neuroscience Abstracts*. 21: 518.

Shelhamer, M., C. Tiliket, and D. Roberts. (1994). "Short-term vestibulo-ocular reflex adaptation in humans". *Experimental Brain Research*. 100: 328–336.

Shutoh, F., M. Ohki, H. Kitazawa, S. Itohara, and S. Nagao. (2006). "Memory trace of motor learning shifts transsynaptically from cerebellar cortex to nuclei for consolidation". *Neuroscience*. 139: 767–777.

Skavenski, A. and D. Robinson. (1973). "Role of abducens neurons in vestibuloocular reflex." *Journal of Neurophysiology*. 36(4): 724–738.

Slotine, J.-J. and W. Li. (1991). *Applied Nonlinear Control*. Prentice-Hall.

Smith, H. and E. Davison. (1972). "Design of industrial regulators: Integral feedback and feedforward control". *Proceedings of the IEE*. 199: 1210–1216.

Smith, M., A. Ghazizadeh, and R. Shadmehr. (2006). "Interacting adaptive processes with different timescales underlie short-term motor learning". *PLOS Computational Biology*. 4(6).

Smith, O. (1959). "A controller to overcome dead time". *ISA Journal*: 28–33.

Spong, M., S. Hutchinson, and M. Vidyasagar. (2005). *Robot Modeling and Control*. Wiley.

Stone, L. and S. Lisberger. (1990). "Visual responses of Purkinje cells in the cerebellar flocculus during smooth-pursuit eye movements in monkeys. I. Simple spikes". *Journal of Neurophysiology*. 63(5): 1241–1261.

Sylvestre, P. and K. Cullen. (1999). "Quantitative Analysis of Abducens Neuron Discharge Dynamics During Saccadic and Slow Eye Movements". *Journal of Neurophysiology*. 82(5): 2612–2632.

Tomei, P. (2017). "Multi-sinusoidal disturbance rejection for discrete-time uncertain stable systems". *Automatica*. 79: 144–151.

Waespe, W., B. Cohen, and T. Raphan. (1983). "Role of the flocculus and paraflocculus in optokinetic nystagmus and visual-vestibular interactions: effect of lesions". *Experimental Brain Research*. 50: 9–33.

Waespe, W., B. Cohen, and T. Raphan. (1984). "Dynamic modification of the vestibulo-ocular reflex by the nodulus and uvula". *Science*. 228: 199–202.

Waespe, W. and V. Henn. (1978a). "Conflicting visual-vestibular stimulation and vestibular nucleus activity in alert monkeys". *Experimental Brain Research*. 33: 203–211.

Waespe, W. and V. Henn. (1978b). "Reciprocal changes in primary and secondary optokinetic after-nystagmus (OKAN) produced by repetitive optokinetic stimulation in the monkey". *Archiv Psychiatrie und Nervenkrankheiten*. 225: 23–30.

Waespe, W. and U. Schwarz. (1986). "Characteristics of eye velocity storage during periods of suppression and reversal of eye velocity in monkeys". *Experimental Brain Research*. 65(1): 49–58.

Waterston, J., G. Barnes, M. Grealy, and L. Luxon. (1992). "Coordination of eye and head movements during smooth pursuit in patients with vestibular failure". *Journal of Neurology, Neurosurgery, and Psychiatry*. 55: 1125–1131.

Widrow, B. and S. Stearns. (1985). *Adaptive Signal Processing*. Prentice-Hall.

Wolpert, D. and M. Kawato. (1998). "Multiple paired forward and inverse models for motor control". *Neural Networks*. 11(7): 1317–1329.

Wolpert, D., C. Miall, and M. Kawato. (1998). "Internal models in the cerebellum". *Trends in Cognitive Sciences*. 2(9): 338–347.

Wonham, W. (1985). *Linear Multivariable Control: A Geometric Approach. 3rd Ed.* Springer-Verlag.

Wonham, W. and J. Pearson. (1974). "Regulation and internal stabilization in linear multivariable systems". *SIAM Journal on Control and Optimization*. 12: 5–18.

Wyatt, H. and J. Pola. (1981). "Slow eye movements to eccentric targets". *Investigative Ophthalmology and Visual Science*. 21(3): 477–483.

Wyatt, H. and J. Pola. (1983a). "Smooth eye movements with step-ramp stimuli: the influence of attention and stimulus extent". *Vision Research*. 27: 1121–1131.

Wyatt, H. and J. Pola. (1983b). "Smooth pursuit eye movements under open-loop and closed-loop conditions". *Vision Research*. 23(10): 1121–1131.

Wyatt, H. and J. Pola. (1988). "Predictive behavior of optokinetic eye movements". *Experimental Brain Research*. 73: 615–626.

Yi, T.-M., Y. Huang, M. Simon, and J. Doyle. (2000). "Robust perfect adaptation in bacterial chemotaxis through integral feedback control". *Proceedings of the National Academy of Sciences*. 97(9): 4649–4653.

Yilmaz, C. and H. Basturk. (2019). "Output feedback control for unknown LTI systems driven by unknown periodic disturbances". *Automatica*. 99: 112–119.

Zee, D. (2018). "A neurologist and ataxia: using eye movements to learn about the cerebellum". *Cerebellum Ataxias*. 5(2).

Zee, D., A. Yamazaki, P. Butler, and G. Gucer. (1981). "Effects of ablation of flocculus and paraflocculus on eye movements in primate". *J. Neurophysiology*. 46(4): 878–899.

Zee, D., R. Yee, D. Cogan, D. Robinson, and W. Engel. (1976). "Ocular motor abnormalities in hereditary cerebellar ataxia". *Brain*. 99(2): 207–234.